Dissertation

Unified description of vibronic transitions with coherent states

Dissertation
zur Erlangung der Doktorgrades
der Naturwissenschaften

vorgelegt beim Fachbereich Physik
der Johann Wolfgang Goethe-Universität
in Frankfurt am Main

von
Joonsuk Huh
aus
Seoul, Südkorea

Frankfurt am Main
2010

vom Fachbereich Physik der Johann Wolfgang Goethe-Universität
als Dissertation angenommen.

Dekan : Prof. Dr. Michael Huth

Gutachter : Prof. Dr. Robert Berger

Gutachter : Prof. Dr. Dieter Schuch

Datum der Disputation: 16.02.2011

Abstract   Vibronic (vibrational-electronic) transition is one of the fundamental processes in molecular physics. Indeed, vibronic transition is essential both in radiative and non-radiative photophysical or photochemical properties of molecules such as absorption, emission, Raman scattering, circular dichroism, electron transfer, internal conversion, etc. A detailed understanding of these transitions in varying systems, especially for (large) biomolecules, is thus of particular interest.

Describing vibronic transitions in polyatomic systems with hundreds of atoms is, however, a difficult task due to the large number of coupled degrees of freedom. Even within the relatively crude harmonic approximation, such as for Born-Oppenheimer harmonic potential energy surfaces, the brute-force evaluation of Franck-Condon intensity profiles in a time-independent sum-over-states approach is prohibitive for complex systems owing to the vast number of multi-dimensional Franck-Condon integrals.

The main goal of this thesis is to describe a variety of molecular vibronic transitions, with special focus on the development of approaches that are applicable to extended molecular systems. We use various representations of Fermi's golden rule in frequency, time and phase spaces via coherent states to reduce the computational complexity. Although each representation has benefits and shortcomings in its evaluation, they complement each other. Peak assignment of a spectrum can be made directly after calculation in the frequency domain but this sum-over-states route is usually slow. In contrast, computation is considerably faster in the time domain with Fourier transformation but the peak assignment is not directly available. The representation in phase space does not immediately provide physically-meaningful quantities but it can link frequency and time domains. This has been applied to, herein, for example (non-Condon) absorption spectra of benzene and electron transfer of bacteriochlorophyll in the photosynthetic reaction center at finite temperature.

This work is a significant step in the treatment of vibronic structure, allowing for the accurate and efficient treatment of complex systems, and provides a new analysis tool for molecular science.

Kurzfassung   Absorption von Licht und der darauf folgende Elektronentransfer in photosynthetischen Systemen sind entscheidende Prozesse in unserem Alltag. Die Verbesserung von Kontrolle und Effizienz dieser Prozesse ist eine Herausforderung im Hinblick auf die weltweite Nahrungs- und Energieversorgung. Diese Art von Prozessen wird jedoch dadurch kompliziert, dass Absorption, Emission und Lichtstreuung verschiedene strahlungslose molekulare Übergänge wie Ladungswanderung, innere Umwandlung und Interkombinationsübergänge nach sich ziehen können. Ein genaues Verständnis dieser Prozesse auf molekularer Ebene in verschiedenen Systemen ist daher von besonderem Interesse.

Molekulare Übergangsprozesse werden durch Wechselwirkungen zwischen Kernen, Elektronen, der Umgebung und äußeren Feldern (z. B. elektromagnetischen) bestimmt. Das Zusammenspiel von vibratorischen und elektronischen (vibronischen) Freiheitsgraden der Moleküle spielt typischerweise eine bedeutende Rolle in molekularen (vibronischen) Übergängen. Ein molekularer vibronischer Übergang wird für gewöhnlich durch Fermis goldene Regel (FGR), die sich aus der zeitabhängigen Störungstheorie ableitet, als eine das absolute Quadrat von Übergangsmomenten enthaltende Übergangsgeschwindigkeitskonstante beschrieben. Laut dem Ausdruck für die Übergangsgeschwindigkeitskonstante in der Basis der Born-Oppenheimer-Wellenfunktionen ist einer der Schlüsselbeiträge zu vibronischen Übergängen der Franck-Condon-Faktor (FCF). Der FCF ist definiert als das Absolutquadrat des Überlappungsintegrals zwischen zu verschiedenen elektronischen Zuständen gehörenden Schwingungswellenfunktionen.

Die theoretische Beschreibung vibronischer Übergänge großer polyatomarer Systeme (mehr als 100 Atome) ist jedoch wegen der hohen Dimensionalität eine schwierige Aufgabe. Sogar in einer relativ groben harmonischen Näherung wie den harmonischen Born-Oppenheimerschen Potentialhyperflächen ist die theoretische *brute-force*-Berechnung der FC-Intensitätsprofile durch eine Summenbildung über die zeitunabhängigen Zustände für komplexe Systeme wegen der gewaltig großen Zahl multi-dimensionaler FC-Integrale ungeeignet.

Das Hauptziel dieser Arbeit ist die Beschreibung einer Vielzahl molekularer vibronischer Übergänge, insbesondere der Entwicklung von Herangehensweisen, die auf ausgedehnte molekulare Systeme anwendbar sind. Wir haben verschiedene Darstellungen von FGR in Frequenz-, in Zeit- und, zur Verringerung des Rechenaufwandes über kohärente Zustände, in Phasenräumen verwendet. Jede Darstellung hat Vor- und Nachteile in ihrer Auswertung, aber alle ergänzen einander. Die Signalzuordnung des Spektrums zu verschiedenen Quantenzustandsübergängen kann direkt nach der Berechnung in der Frequenzdomäne vorgenommen werden, doch ist dieser Weg über die Summierung von Zuständen normalerweise zeitintensiv. Im Gegensatz dazu ist die Berechnung über Fouriertransformation in der Zeitdomäne schneller, aber eine Zuordnung der Signale zu verschiedenen Quantenzustandsübergängen ist nicht direkt möglich. Die Darstellung im Phasenraum liefert nicht sofort physikalisch bedeutsamen Größen, kann aber Frequenz- und Zeitdomäne verknüpfen. Folglich können wir die molekularen Übergangsspektren effizient berechnen, einschließlich thermischer und Nicht-Condon-Effekte. Zusätzlich zur Effizienzsteigerung sind wir in der Lage, die einzelnen Dynamiken der Schwingungsfreiheitsgrade während der elektronischen Übergänge für relativ große Systeme zu analysieren.

Unsere Methode ist nicht nur auf molekularer Übergänge anwendbar, sondern auf jedes physikalische Problem, das eine Näherung über harmonische Oszillatoren enthält, beispielsweise Nichtgleichgewichtsdynamiken dissipativer Systeme.

Contents

Acronyms

BO Born-Oppenheimer

CE cumulant expansion

cF coherent-Fock

CS coherent state

DFT density functional theory

DOF degrees of freedom

DOS density of states

ECD electronic circular dichroism

ET electron transfer

FC Franck-Condon

FCF Franck-Condon factor

FCW Franck-Condon factor weighted density of states

FC/HT Franck-Condon/Herzberg-Teller interference

FFT fast Fourier transform

FGR Fermi's golden rule

FT Fourier transform

FWHM full width at half maximum

GF generating function

HRF Huang-Rhys factor

HT Herzberg-Teller

IC internal conversion

ISC inter-system crossing

MHP multi-variate Hermite polynomial

MQM maximum excitation quantum number of modes

MSM maximum number of simultaneously excited modes

ONV occupation number vector

OPA one-photon absorption

OPE one-photon emission

PDF probability density function

PE photo-electron

PES potential energy surface

rR resonance Raman

SDF spectral density function

SVL single vibronic level

TCF time-correlation function

TD time-dependent

TDM transition dipole moment

TI time-independent

UV ultra-violet

Notation

- Underline is used for vectors, *i.e.* $\underline{v} = (v_1, \cdots, v_N)^{\mathrm{t}} = \begin{pmatrix} v_1 \\ \vdots \\ v_N \end{pmatrix}$ is an N-dimensional column vector. t is transpose.

- Special vectors are defined for $\underline{0} = (0, \cdots, 0)^{\mathrm{t}}$, $\underline{1} = (1, \cdots, 1)^{\mathrm{t}}$ and $\underline{\frac{1}{2}} = (\frac{1}{2}, \cdots, \frac{1}{2})^{\mathrm{t}}$

- Bold font is used for matrices, for example $\mathbf{A}$ is an N-dimensional (real or complex) square matrix.

- $\mathbf{I}$ is an identity matrix.

- $\mathbf{0}$ is a square zero matrix.

- "diag" transforms an N-dimensional vector to an N-dimensional diagonal square matrix which takes the diagonal elements from the vector, *i.e.* $\mathbf{v} = \mathrm{diag}(\underline{v})$.

- "bldiag" constructs a block diagonal square matrix from square matrices, *i.e.* $\mathbf{A} = \mathrm{bldiag}(\mathbf{a}, \mathbf{b}, \mathbf{c}, \mathbf{d})$.

- A notation is defined for products of vector elements with powers, *i.e.* $\overline{\prod}_{\underline{x}_1, \cdots, \underline{x}_N}^{\underline{n}_1, \cdots, \underline{n}_N} = \left(\prod_k x_{1,k}^{n_{1,k}} \right) \cdots \left(\prod_k x_{N,k}^{n_{N,k}} \right)$.

- A notation is defined for products of factorials of vector elements with powers, *i.e.* $\widetilde{\prod}_{\underline{x}_1, \cdots, \underline{x}_N}^{\underline{n}_1, \cdots, \underline{n}_N} = \left(\prod_k (x_{1,k}!)^{n_{1,k}} \right) \cdots \left(\prod_k (x_{N,k}!)^{n_{N,k}} \right)$.

- A notation is defined for multi-dimensional partial derivatives, *i.e.* $\hat{\partial}_{\underline{x}_1, \cdots, \underline{x}_N}^{\underline{n}_1, \cdots, \underline{n}_N} = \left(\frac{\partial^{\sum_k n_{1,k}}}{\prod_k \partial x_{1,k}^{n_{1,k}}} \right) \cdots \left(\frac{\partial^{\sum_k n_{N,k}}}{\prod_k \partial x_{N,k}^{n_{N,k}}} \right)$.

- An exponential functional is defined for $\mathcal{J}[\mathbf{A}, \underline{b}; \underline{x}] = \exp(-\frac{1}{2}\underline{x}^{\mathrm{t}}\mathbf{A}\underline{x} + \underline{b}^{\mathrm{t}}\underline{x})$.

List of Figures

List of Tables

1. Introduction

Theoretical molecular spectroscopy [1–8] plays a pivotal role in molecular physics and chemistry in complementing experimental techniques such as ultra-high resolution molecular spectroscopy and ultra-fast pump-probe laser spectroscopy [9–11]. Femto- and attosecond laser techniques can resolve fast processes like molecular vibration in the femtosecond regime or electron dynamics in the attosecond regime. Especially zero kinetic energy photo-electron (ZEKE-PE) spectroscopy in accompanying molecular beam techniques, *e.g.* supersonic molecular beams [9, 10] can provide high resolution ($1 \text{ cm}^{-1} = 1.2 \times 10^{-4}$ eV) molecular spectra in electronic regime. Structural information and energy levels can be obtained from vibronically (vibrational and electronic) or rovibronically (rotational, vibrational and electronic) resolved molecular spectra. Resonance frequencies are related to the molecular energy level differences. Such properties for large molecular systems can typically only be interpreted with the help of electronic structure calculations (see *e.g.* Ref. [12], for applications of density functional theory (DFT) [13–15] and its time-dependent (TD) counter-part TDDFT [16]) and corresponding vibrational analyses. In addition, line strengths (intensities of spectral band lines) and the corresponding peak widths provide information about the molecular transition probabilities and lifetimes of the corresponding molecular states, respectively. Spectra of large polyatomic systems (hundreds of atoms) are usually quite congested such that analyses of the spectra are demanding because of huge density of states (DOS). Therefore it is necessary to simulate the molecular spectra theoretically with proper molecular model systems (see *e.g.* [17–19]), especially for complex systems.

A simple theoretical model of molecular transitions between two electronic states, accompanied by vibrational motions (*i.e.* vibronic transitions), is commonly adopted to explain various molecular processes. This vibronic transition model has been used to explain molecular transition processes (see Fig. 1.1) such as[1] one-photon absorption (OPA) (see *e.g.* Refs. [12, 21–54]), one-photon emission (OPE) (see *e.g.* Refs. [55–59]), resonance Raman (rR) scattering (see *e.g.* Refs. [17, 60–76]), electron transfer (ET) (see *e.g.* Refs. [77–89]), internal conversion (IC) (see *e.g.* Refs. [90–95]) and inter-system crossing (ISC) (see *e.g.* Ref. [96]). The vibronic transition probabilities between two electronic states are proportional to the Franck-Condon factors (FCFs), the absolute square of overlap integrals between vibrational states of different electronic states. For the theoretical description of such vibronic transitions, the FCFs need to be computed. The calculation of vibronic transition spectra is, however, not an easy task because the number of Franck-Condon (FC) integrals to be evaluated for the spectra grows rapidly with increasing system size, temperature, energy window and coupling between vibronic states. In this thesis possible ways are suggested to reduce computational efforts to describe various molecular vibronic transitions of large molecular systems by bridging frequency and time domain

---

[1]*c.f.* One-photon infrared (IR) transition (see *e.g.* Refs. [1, 20]) can be considered as a vibronic transition within one electronic state.
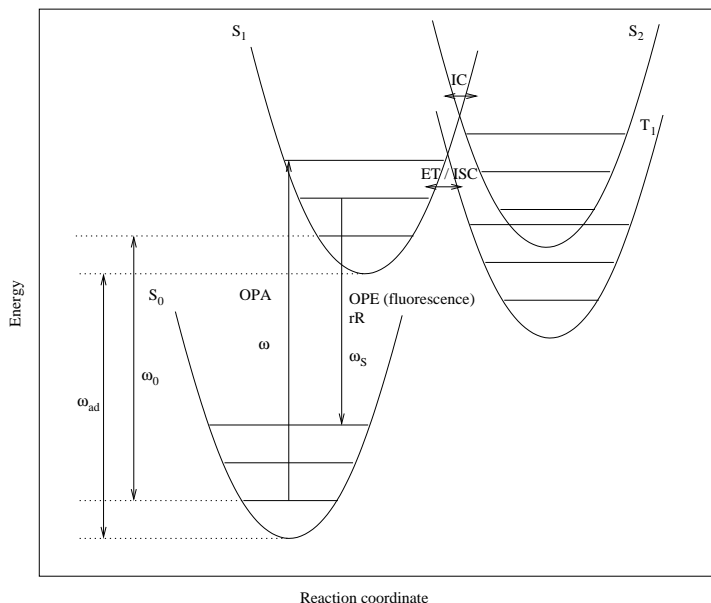
Figure 1.1.: Intramolecular transitions are illustrated in terms of reaction coordinate (internal nuclear coordinate) and BO PESs. Each parabola (S_0, S_1, S_2, T_1) represents electronic PES. The transitions are illustrated only between these parabolas for simplicity. One-photon absorption (OPA) is an optical transition from singlet ground state (S_0) to singlet excited state (S_1) with transition angular frequency (ω). One-photon emission (OPE) is a radiative transition from the singlet excited state (S_1) to the singlet ground state (S_0) with transition angular frequency (ω_S). Resonance Raman (rR) scattering is a two photon process invoking the incident light (ω) and scattering light (ω_S). ω_{ad} is the adiabatic electronic transition angular frequency and ω_0 is the adiabatic transition angular frequency including the vibrational zero-point energy difference between the two oscillators. Internal conversion (IC) and ISC are the radiationless transitions via nonadiabatic coupling without spin state change (S_1 to S_2) and with spin state change (S_1 to triplet T_1). Electron transfer (ET) is a radiationless transition as well to the charge transfered state.

representations of vibronic spectra via Glauber's coherent states (CSs) (complex Gaussian wavepackets) [97,98].

In the following subsection we review the two-electronic-state model system of vibronic transition between BO electronic PESs. Afterwards we indicate molecular transition problems treated in this thesis and outline possible solutions developed in the next four subsections. The achievements of this thesis are sketched in Sec. 1.1. This introduction chapter is summarized and the outline of this thesis is given in Sec. 1.2.

Vibronic transition The theoretical description of molecular electronic transitions is primarily based on the BO approximation [99] which involves a product ansatz of electronic and nuclear wavefunctions. The fast electronic degrees of freedom (DOF) ($\underline{r}_{el}$) and the slow DOF of the nuclei ($\underline{r}_{nu}$) are assumed to be separable within the BO approximation. The electrons are assumed to be moving so fast that nuclei appear to be stationary on that scale. The DOF of the nuclei therefore are treated as parametric variables for the electronic wavefunctions so that the motion of nuclei changes adiabatically on an electronic energy surface

without crossing[2] to other surfaces. With this approximation the molecular adiabatic wave-functions ($\langle \underline{r}_{\text{el}}, \underline{r}_{\text{nu}} | \psi_{i,n}^{\text{mol}} \rangle$) are expressed in a product form of i-th electronic ($\langle \underline{r}_{\text{el}}, \underline{r}_{\text{nu}} | \psi_i^{\text{el}} \rangle$) and n-th nuclear ($\langle \underline{r}_{\text{nu}} | \psi_{i,n}^{\text{nu}} \rangle$) wavefunctions, *i.e.* $\langle \underline{r}_{\text{el}}, \underline{r}_{\text{nu}} | \psi_{i,n}^{\text{mol}} \rangle = \langle \underline{r}_{\text{el}}, \underline{r}_{\text{nu}} | \psi_i^{\text{el}} \rangle \langle \underline{r}_{\text{nu}} | \psi_{i,n}^{\text{nu}} \rangle$. The nuclear wavefunctions are often further approximated as a product of rotational (ψ^{ro}) and vibrational (ψ^{vib}) wavefunctions. One should employ Eckart conditions [101] to min-imize the coupling between rotational and vibrational DOF (see also Sec. 2.2) to support this approximation. The molecular wavefunction is then expressed as products of three wavefunctions, *i.e.*

$$\langle \underline{r}_{\text{el}}, \underline{r}_{\text{nu}} | \psi_{i,n}^{\text{mol}} \rangle = \langle \underline{r}_{\text{el}}, \underline{Q} | \psi_i^{\text{el}} \rangle \langle \theta, \varphi, \chi | \psi_{i,n_{\text{r}}}^{\text{ro}} \rangle \langle \underline{Q} | \psi_{i,n_{\text{v}}}^{\text{vib}} \rangle, \tag{1.1}$$

where n_{r} and n_{v} are quantum numbers of rotational and vibrational wavefunctions respec-tively, and (θ, φ, χ) are Euler angles. $\underline{Q}$ is a normal coordinate vector with N-dimension which is three times the number of atoms minus six(five) trivial DOF, *i.e.* $N = 3N_{\text{atom}} - 6(5)$ for nonlinear molecules (for linear molecules). Coupling between distinct adiabatic PESs is in this picture induced by the nuclear kinetic energy operator. This is called diabatic (nonadiabatic) coupling beyond the BO approximation. Conventional electronic structure calculations provide the BO multi-dimensional PESs as a function of vibrational coordinates ($\underline{Q}$)[3]. The rovibrational wavefunctions are estimated from a rovibrational Hamiltonian con-strained to a specific BO (non-crossing) adiabatic PES.

The intramolecular (optical or radiationless) processes (see Fig. 1.1) are considered as electronic transitions between two distinct BO PESs. According to BO and FC the elec-tronic motion is so fast compared to the nuclei, that the nuclei do not move during the electronic transition. When a molecule undergoes an electronic transition, the molecular structure reorganizes and relaxes to the new equilibrium structure of the new BO PES while the molecule is vibrating to adjust to the new PES. Various molecular vibronic transitions are illustrated in Fig. 1.1. In addition to these, also other vibronic transitions like electronic circular dichroism (ECD) (see *e.g.* Ref. [102]) and two photon absorption and emission (see *e.g.* Ref. [3]) are usually described via Fermi's golden rule (FGR) [103, 104] resulting from TD perturbation theory within the BO picture. The FGR equation is originally a rate expres-sion. The rate is proportional to the absolute square of the matrix elements for a transition moment operator ($\hat{M}$) and the DOS (ρ), *i.e.* the transition rate from state $|i\rangle$ to $|f\rangle$ is

$$\Gamma_{fi} = \frac{2\pi}{\hbar} |\langle f | \hat{M} | i \rangle|^2 \rho. \tag{1.2}$$

To be specific, for instance the cross sections of OPA ($\sigma_{\text{OPA}}(\omega; T)$) and the rate of OPE ($\Gamma_{\text{OPE}}(\omega; T)$) between two electronic states, initial ($|i\rangle = |\psi_i^{\text{el}}\rangle$) and final ($|f\rangle = |\psi_f^{\text{el}}\rangle$) respectively, at a transition frequency ω and at a finite temperature (T) is proportional to a common[4] spectral density function (SDF) ($\rho_{\text{OP}}(\omega; T)$)[5]. The (isotropically averaged) SDF

---

[2]*cf.* Two PESs of the same irreducible representation can meet to form a conical intersection near crossing points, the BO approximation breaks down (see *e.g.* Ref. [2, 100]).

[3]*cf.* In crude adiabatic approximation, the electronic wavefunction has no nuclear coordinate dependence such that it includes only one specific nuclear structure as a parameter (see *e.g.* Ref. [2]).

[4]However, initial and final electronic states should be reversed for the emission process compared to the absorption process because emission process is from the excited state to the lower energy state.

[5]The dimension of $\rho_{\text{OP}}(\omega; T)$ is $\frac{[\text{Electric dipole moment}]^2}{[\text{Energy}]}$, *i.e.* $\frac{[\text{C·m}]^2}{[\text{J}]}$.

is obtained from FGR (see *e.g.* Refs. [51, 52, 54, 65, 70, 75, 95].), such that

$$\sigma_{\mathrm{OPA}}(\omega;T) = \frac{4\pi^2}{3}\left(\frac{\alpha_0}{e_0^2}\right)(\hbar\omega)\rho_{\mathrm{OP}}(\omega;T), \tag{1.3}$$

$$\Gamma_{\mathrm{OPE}}(\omega;T) = \frac{4}{3\hbar^3 c_0^2}\left(\frac{\alpha_0}{e_0^2}\right)(\hbar\omega)^4\rho_{\mathrm{OP}}(\omega;T), \tag{1.4}$$

where e_0, ε_0 and c_0 are the charge of a proton, the electric constant and the speed of light in vacuum, respectively, and $\alpha_0 = \frac{e_0^2}{(4\pi\varepsilon_0)\hbar c_0}$ is the fine-structure constant. Within the BO adiabatic approximation the (non-Hermitian) model Hamiltonian of a two-electronic-state system for the vibronic transitions would read [34]

$$\hat{H}_{fi}^{\mathrm{mol}} = |i\rangle\hat{H}_i^{\mathrm{vib}}\langle i| + |f\rangle(\hbar\omega_{\mathrm{ad}} + \hat{H}_f^{\mathrm{vib}} - \mathrm{i}\hbar\Gamma/2)\langle f|, \tag{1.5}$$

where ω_{ad} is the electronic adiabatic transition frequency (see Fig. 1.1) between electronic states $|f\rangle$ and $|i\rangle$. $\Gamma/2$ is related to the inverse lifetime[6] of the final electronic state and the initial state is assumed to have infinite lifetime. $\hat{H}_i^{\mathrm{vib}}$ and $\hat{H}_f^{\mathrm{vib}}$ are the vibrational Hamiltonians of initial and final electronic states respectively, *i.e.*

$$\hat{H}_i^{\mathrm{vib}} = -\tfrac{1}{2}\hat{\underline{P}}\cdot\hat{\underline{P}} + \hat{V}_i(\hat{\underline{Q}}),$$
$$\hat{H}_f^{\mathrm{vib}} = -\tfrac{1}{2}\hat{\underline{P}}'\cdot\hat{\underline{P}}' + \hat{V}_f(\hat{\underline{Q}}'), \tag{1.6}$$

where $\hat{\underline{Q}}$ and $\hat{\underline{Q}}'$ are the mass-weighted normal coordinates (hereafter normal coordinate refers to the mass-weighted one) of initial and final states respectively, and $\hat{\underline{P}}$ and $\hat{\underline{P}}'$ are the conjugate momenta. $\hat{V}_i$ and $\hat{V}_f$ are the corresponding potential energies[7]. The specific form of the approximate interaction Hamiltonian ($\hat{H}^{\mathrm{int}}$) at time t depends on the transition considered. For an electric dipole transition one commonly treats, for instance, the interaction between a transition dipole moment (TDM) ($\hat{\underline{\mu}}_{\mathrm{elec}}$) and a time-dependent electric field ($\underline{E}(t)$) as classical,

$$\hat{H}^{\mathrm{int}} = -\hat{\underline{\mu}}_{\mathrm{elec}}\cdot\underline{E}(t), \tag{1.7}$$

$$\hat{\underline{\mu}}_{\mathrm{elec}} = |f\rangle\hat{\underline{\mu}}(\underline{Q})\langle i| + |i\rangle\hat{\underline{\mu}}(\underline{Q})^\dagger\langle f|, \tag{1.8}$$

where $\hat{\underline{\mu}}(\underline{Q}) = \langle f|\hat{\underline{\mu}}_{\mathrm{elec}}|i\rangle$ is the electronic TDM which has been averaged over electronic DOF. For freely rotating molecules (*e.g.* in the gas phase) the isotropic approximation can be made to the polarization direction of light, *i.e.* the angular dependency of the electric transition dipole moment ($\hat{\underline{\mu}}_{\mathrm{elec}}\cdot\underline{E}(t)$) can be ignored after taking the isotropic rotational average over the polarization vector of light (see *e.g.* [3, 17]). The averaged factor ($\frac{1}{3}$) is included already in the prefactors of Eqs. (1.3) and (1.4). We can express the SDF in terms

---

[6] In principle the line widths of vibronic levels can vary, but we assume here that the line widths depend only on the electronic levels, *i.e.* the line widths of vibronic transitions $\Gamma_{\underline{v},\underline{v}'}/2$ are assumed to be constant ($\Gamma/2$) (see *e.g.* Ref. [17]). The assumption is related to the homogeneous line broadening arising from the (rapidly fluctuating) system-bath interaction (see *e.g.* Ref. [5]).

[7] The potential energy surfaces and the corresponding minima are usually different from each other for different electronic states. We allow for different normal coordinate systems with their origins shifted to the minimum of each electronic PES.

of electronic, rotational and vibrational wavefunctions via TD perturbation theory, *i.e.*

$$\rho_{\mathrm{OP,L}}(\omega;T) = \sum_{n_{\mathrm{v}},n_{\mathrm{v}}',n_{\mathrm{r}},n_{\mathrm{r}}'} p_{n_{\mathrm{v}}}(T)p_{n_{\mathrm{r}}}(T)|\langle\Psi_{f,n_{\mathrm{v}}'}^{\mathrm{vib}}|\langle\Psi_{f,n_{\mathrm{r}}'}^{\mathrm{ro}}|\langle f|\underline{\hat{\mu}}_{\mathrm{elec}}|i\rangle|\Psi_{i,n_{\mathrm{r}}}^{\mathrm{ro}}\rangle|\Psi_{i,n_{\mathrm{v}}}^{\mathrm{vib}}\rangle|^2$$

$$L(\omega,\omega_{\mathrm{ad}} + \omega_{n_{\mathrm{v}}',n_{\mathrm{v}}} + \omega_{n_{\mathrm{r}}',n_{\mathrm{r}}};\Gamma), \tag{1.9}$$

$$L(\omega,\overline{\omega};\Gamma) = \frac{1}{\pi}\cdot\frac{(\frac{\hbar}{2}\Gamma)}{[\hbar(\omega-\overline{\omega})]^2 + (\frac{\hbar}{2}\Gamma)^2}, \tag{1.10}$$

where $\omega_{n_{\mathrm{v}}',n_{\mathrm{v}}}$ and $\omega_{n_{\mathrm{r}}',n_{\mathrm{r}}}$ are the vibrational and rotational transition frequencies, respectively, between the two electronic states. $p_{n_{\mathrm{v}}}(T)$ and $p_{n_{\mathrm{r}}}(T)$ are the thermal populations of initial vibrational and rotational levels, respectively. In Eq. (1.9) a Lorentzian line shape function L defined in Eq. (1.10) with full width at half maximum (FWHM) of Γ is used as DOS for the two-state-model Hamiltonian (Eq. (1.5)) that accounts for a finite lifetime of the final state. L approaches to a Dirac δ-distribution for decreasing Γ and SDF corresponds in this limit to a stick representation. For spectra that are rotationally not-resolved, $\omega_{n_{\mathrm{r}}',n_{\mathrm{r}}}$ can be ignored in the distribution function of DOS with assumptions $(\omega_{n_{\mathrm{v}}',n_{\mathrm{v}}} \gg \omega_{n_{\mathrm{r}}',n_{\mathrm{r}}})$[8] and $(\Gamma \gg \omega_{n_{\mathrm{r}}',n_{\mathrm{r}}})$. Then the rotational part can be factored out from the SDF. Finally the vibronic transition problem is simplified to be a transition between two sets of vibrational wavefunctions with the transition moment operator $\underline{\hat{\mu}}(Q)$ (Eq. (1.11)), *i.e.*

$$\rho_{\mathrm{OP,L}}(\omega;T) \simeq \sum_{n_{\mathrm{v}}',n_{\mathrm{v}}} p_{n_{\mathrm{v}}}(T)|\langle\Psi_{f,n_{\mathrm{v}}'}^{\mathrm{vib}}|\underline{\hat{\mu}}(Q)|\Psi_{i,n_{\mathrm{v}}}^{\mathrm{vib}}\rangle|^2 L(\omega,\omega_{\mathrm{ad}} + \omega_{n_{\mathrm{v}}',n_{\mathrm{v}}};\Gamma),, \tag{1.11}$$

in which the sum rule $\sum_{n_{\mathrm{r}},n_{\mathrm{r}}'} p_{n_{\mathrm{r}}}(T)|\langle\Psi_{f,n_{\mathrm{r}}'}^{\mathrm{ro}}|\Psi_{i,n_{\mathrm{r}}}^{\mathrm{ro}}\rangle|^2 = 1$ is used. Neglecting rotational DOF would be still a reasonable approximation for large or randomly oriented condensed phase molecules because those molecules are mostly in a rotationless state (see *e.g.* Refs. [6, 17]) and the polarization directional vector of the electric field is fixed in space.

The vibrationally resolved ECD (see *e.g.* Ref. [102]) and rR (see *e.g.* Ref. [6]) cross sections can be expressed in a similar way. The major difference that appears in ECD is that it includes a coupling term of electronic and magnetic TDMs, *i.e.* the rotational strength (see *e.g.* Ref. [20]). And for rR the transition moment is frequency dependent (see Ch. 2). Radiationless processes (ET, IC and ISC) involving the nonadiabatic coupling operator (see *e.g.* Refs. [87,93–95,105]) are described by similar expressions to Eq. (1.11) with slight modifications. As mentioned already, many molecular transition processes are expressed via FGR in terms of a transition moment in the vibrational wavefunction basis. Thus, the overlap between two vibrational wavefunctions, the FC integrals, are important in understanding those molecular processes.

Evaluation of the sum-over-states expression (1.11) (also called time-independent (TI) frequency domain expression) is rather straightforward, if the vibrational wavefunctions as well as the nuclear coordinate dependence of the transition moments are known. The TI approach is beneficial in that it can provide information about individual peak intensities naturally from the direct evaluation of the integrals. The peak assignment is important for analyzing experimental spectral data and it is the main demand for the TI method. Even if

---

[8]The vibrational structure is then assumed to be embedded in the electronic structure and the rotational structure to be embedded in the vibrational structure.

the evaluation of the TI expression (1.11) is straightforward in the vibrational wavefunction basis, the application is restricted to small molecular (typically tri- or tetra-atomic) systems considering the full molecular (anharmonic) Hamiltonian (see *e.g.* Refs. [53, 106] and Sec. 7.4) within the Condon approximation ($\hat{\underline{\mu}}(Q) \simeq \underline{\mu}_0$ = a constant vector). Evaluating FCFs of anharmonic oscillators in the TI fashion for extended systems is computationally prohibitive because the anharmonic vibrational wavefunctions are typically expanded in a large number of basis functions (*e.g.* harmonic oscillator basis set). The harmonic approximation to the BO PESs gives satisfactory results (see *e.g.* Refs. [36, 43–46]) for molecules which have well separated initial and final BO surfaces and only small molecular structural changes[9] during the electronic transition. We may rewrite (approximate) the SDF (1.11) within the harmonic oscillator model,

$$\rho_{\mathrm{L}}(\omega; T) = \sum_{\underline{v}, \underline{v}'} p_{\underline{v}}(T) |\langle \underline{v}' | \hat{\underline{\mu}}(Q) | \underline{v} \rangle|^2 L(\omega, \omega_0 + \omega_{\underline{v}', \underline{v}}; \Gamma), \tag{1.12}$$

where $|\underline{v}\rangle$ and $|\underline{v}'\rangle$ are the N-dimensional harmonic oscillator eigenstates of initial and final electronic states, respectively, in the occupation number vector (ONV) representation. ω_0 is the adiabatic vibronic transition frequency (see Fig. 1.1) and $\omega_{\underline{v}', \underline{v}}$ corresponds to the vibrational frequency difference of two harmonic eigenstates excluding the harmonic zero-point frequency difference which has already been included in ω_0.

Within the validity of the FC approximation ($\hat{\underline{\mu}}(Q) \simeq \underline{\mu}_0$) and the harmonic oscillator approximation there still remains a challenging problem in evaluating Eq. (1.12) in the TI manner for two multi-dimensional harmonic oscillators being not only displaced and distorted but also rotated. When the molecule (multi-dimensional harmonic oscillators) undergoes an electronic transition, it experiences the equilibrium structural change (displacement), potential energy curvature change (distortion) and normal coordinate variation (rotation). The two sets of normal coordinates are related (approximately) by a linear transformation, the so called Duschinsky transformation (Ref. [107] and see also Sec. 2.2 for details),

$$\underline{Q}' = \mathbf{S}\underline{Q} + \underline{d}. \tag{1.13}$$

This linear equation implies that the final state N-dimensional normal coordinates $\underline{Q}'$ are expressed by a rotation (with $N \times N$ matrix $\mathbf{S}$) of the initial state normal coordinates $\underline{Q}$ with an N-dimensional displacement vector $\underline{d}$. The Duschinsky effect is one of the main reasons for asymmetry between absorption and emission spectra. It is responsible for the broadening of vibronic spectra and the effect is enhanced (for specific vibrational modes) when there are finite temperature effects (see *e.g.* Fig. 1.2). Small [108] pointed out that the Duschinsky effect is as important as the vibronic coupling effects because the mode mixing introduces a quadratic coupling between initial and final vibrational wavefunctions, *i.e.* the Duschinsky effects must be considered for vibronic coupling problems. The importance of Duschinsky mode mixing effect has been emphasized by many authors in various fields, such as absorption processes (see *e.g.* Refs. [19, 44–47, 49]), resonance Raman scattering (see *e.g.* Refs. [17, 56, 61, 64, 66, 67, 72, 73, 75, 109]), electron transfer processes (see *e.g.* Refs. [59, 82, 86, 87, 110]), radiationless transitions (see *e.g.* Ref. [91, 94]), in photoexcited state cooling processes (see *e.g.* Ref. [41]), vibronic coupling of electronic transitions (see

---

[9]*e.g.* the transitions from ground to the first excited states or first ionized states.

e.g. Refs. [80,108]) and molecular junction tunneling (see *e.g.* Ref. [111]).

When there is no Duschinsky rotation ($\mathbf{S} = \mathbf{I}$ = an identity matrix), the FC integrals can be separated into products of one-dimensional FC integrals, *i.e.*

$$\langle \underline{v}' | \underline{v} \rangle = \prod_{i=1}^{N} \langle v_i' | v_i \rangle, \tag{1.14}$$

which can be evaluated easily by one-dimensional Hermite polynomials (see Sec. 2.2). However if the Duschinsky effect is dominant ($\mathbf{S} \neq \mathbf{I}$) then the multi-dimensional FC integrals cannot be expressed as a simple product of one-dimensional FC integrals. Furthermore, the number of FC integrals to be evaluated grows steeply with increasing molecular system size, temperature and vibronic transition energy (see *e.g.* Ref. [112]). Evaluation of the huge number of multi-dimensional (inseparable) integrals make the TI description of the FC transition computationally a hard problem. Moreover, when the zero-th order of the TDM ($\underline{\mu}_0$) is not dominant one has to consider the coordinate dependence of the electronic TDM ($\hat{\underline{\mu}}(Q)$), *i.e.* the non-Condon effect. The computational problem becomes even harder. FC-forbidden ($|\underline{\mu}_0| = 0$) or weakly allowed FC ($|\underline{\mu}_0| \simeq 0$) transitions are usually described by a vibronic coupling intensity borrowing mechanism of Herzberg and Teller (see *e.g.* Refs. [2, 4, 20]). Herzberg and Teller [113] expanded $\hat{\underline{\mu}}(Q)$ with respect to the normal coordinates as follows,

$$\hat{\underline{\mu}}(Q) = \underline{\mu}_0 + \sum_{i=1}^{N} \underline{\mu}_i' \hat{Q}_i + \dots, \tag{1.15}$$

where $\underline{\mu}_i'$ is the first derivative with respect to the i-th normal coordinate (Q_i) at the equilibrium structure of the initial state ($Q = \underline{Q}_0$)[10]. This expansion is called Herzberg-Teller (HT) expansion. Usually the HT expansion contains only linear terms. In this case one refers to the linear order expansion. When the expansion includes also higher order terms it is called the nonlinear HT expansion. $\underline{\mu}_i'$ in Eq. (1.15) is a first derivative of a matrix element of a perturbed Hamiltonian, with respect to the i-th vibrational coordinate, between the ground and FC-allowed other excited electronic states (see *e.g.* Ref. [20] or Sec. 2.1). The SDF that is necessary for describing the non-Condon effects can be formulated as follows (in a general form)

$$\rho_{\mathrm{L}}(\omega; T)^{(\hat{f}, \hat{g})} = \sum_{\underline{v}, \underline{v}'} p_{\underline{v}}(T) \langle \underline{v} | \hat{g}^* | \underline{v}' \rangle \langle \underline{v}' | \hat{f} | \underline{v} \rangle L(\omega, \omega_0 + \omega_{\underline{v}', \underline{v}}; \Gamma), \tag{1.16}$$

which includes general operators $\hat{f}(\hat{\underline{P}}, \hat{\underline{Q}})$ and $\hat{g}(\hat{\underline{P}}, \hat{\underline{Q}})$, which are functions of momentum ($\hat{\underline{P}}$) and position ($\hat{\underline{Q}}$) operators. When $\hat{f} = \hat{g} = \underline{\mu}_0$ in Eq. (1.16) the FC SDF is recovered. Momentum operators, coupling terms between momentum and position operators and nonlinear operators could appear in the IC, ISC, anharmonic, rR and vibronic coupling problems. Therefore the ability to access the non-Condon SDF (1.16) is essential in describing those kinds of molecular transitions beyond the Condon approximation. The term "non-Condon" is, in this thesis, restricted to any transition problem involving polynomial

---

[10]The expansion can be made at any reference structure (see *e.g.* Ref. [49]).

expression of transition operators. Here, transition operators could be momentum and position operators. The term "non-Condon integral" refers to the corresponding matrix elements of non-Condon operators ($\hat{f}(\underline{\hat{P}}, \underline{\hat{Q}})$).

Franck-Condon integrals and beyond   A variety of methods to efficiently compute multi-dimensional FC integrals within the harmonic approximation that account Duschinsky mode mixing effects have been previously developed (see *e.g.* Ref. [46] and citations therein). Although the evaluation of FC integrals has a long history (see *e.g.* Ref. [114]), fast evaluation of FC integrals is still demanding and it attracted recent interest (see *e.g.* Refs. [115–121]). Especially for applications of large molecular systems the fast evaluation of FC integrals is important. In order to deal with large polyatomic systems and many other interesting quantum molecular problems like vibronic coupling effects involving these kind of overlap integrals, it is necessary to improve the existing (recursive or iterative) FC integral evaluation schemes. Usually the evaluation of linear HT-type integrals ($\langle \underline{v}' | \hat{Q}_i | \underline{v} \rangle$) is based on the FC integral evaluation schemes because the linear integrals can be decomposed into two FC integrals exploiting the second quantized expression of position operators [36, 49]. In chapter 3, we suggest a general non-Condon integral evaluation scheme by exploiting the CSs and the CS phase displacement operators [97, 98] in the form of multi-variate Hermite polynomials (MHPs) (see Ch. 3).

Franck-Condon factors and beyond   Even with fast integral evaluation schemes at hand, the brute-force evaluation of all inseparable integrals within a given transition energy window should be avoided due to the large vibrational DOS. It should be noticed that usually only a tiny fraction of integrals contributes significantly to a given photophysical quantity of interest (see *e.g.* Ref. [36]). There have been approaches to exploit this aspect (see *e.g.* Refs. [44–46]) which classifies the integrals into vibrational excitation patterns[11] (number of simultaneously excited vibrational modes[12] and maximum excitation quantum number of individual vibrational modes). They give satisfactory results with the reduced basis set for large systems (*e.g.* 156 atomic system in Ref. [46] for the FC transition at zero Kelvin). Santoro *et al.* [44, 45] have devised a method to restrict the vibrational excitation patterns according to the predefined total number of integrals. Therein the allowed number of simultaneously excited vibrational modes in the FC integrals increases until the convergence criteria are fulfilled (total number of FC integrals and total sum of FCFs). Similar to other types of convergence strategies (see *e.g.* Refs. [43, 122–124]) it is difficult to guess the quality of the calculation *a priori* before the evaluation of individual FC integrals is performed.

Jankowiak, Stuber and Berger [46] have solved this problem by introducing a CS-based generating function (GF) approach [24–29, 125] for FC transition processes at zero Kelvin where the initial vibrational state stays always to the vibrational ground state. It was shown that one can restrict the vibrational excitation patterns and estimate the error bounds of a corresponding calculation, before individual integrals are evaluated, via applying a threshold to the total FC intensity (summation of FCFs). This is called integral prescreening [46], because unimportant batches of integrals can be excluded before an individual integral is

---

[11] subset in vibrational ONV space
[12] number of non-zero vibrational quantum numbers in the FC integrals

calculated. One is able to simulate a FC transition spectrum at zero Kelvin for a relatively large system in frequency domain with this error bound control strategy within a reasonable computing time. This FCF GF approach is the foundation of this thesis. To illustrate the FC GF idea we consider an overlap integral of two identical ground state oscillators as an example,

$$\langle \underline{0}|\underline{0}\rangle = 1. \tag{1.17}$$

By expanding with the final vibrational eigenstates via a resolution of the identity, the overlap integral is expressed as a sum of FCFs and the integral value is conserved as long as the resolution of identity is retained,

$$\langle \underline{0}|\underline{0}\rangle = \sum_{\underline{v}'=\underline{0}}^{\infty} \langle \underline{0}|\underline{v}'\rangle\langle \underline{v}'|\underline{0}\rangle = \sum_{\underline{v}'=\underline{0}}^{\infty} |\langle \underline{v}'|\underline{0}\rangle|^2 = 1. \tag{1.18}$$

If one knows in advance a set of quantum numbers ($\in \mathcal{S}$) which makes the summation close to unity within a given tolerance before one computes a huge number of the individual FC integrals,

$$\sum_{\underline{v}'\in\mathcal{S}} |\langle \underline{v}'|\underline{0}\rangle|^2 \simeq 1, \tag{1.19}$$

one would be able to control the FC spectral calculation with the threshold. Then, the question is how we can find a set according to the predefined total intensity tolerance. We can exploits the GF idea to control the FCFs by introducing GF parameters $\underline{z}'$, *i.e.*

$$\widetilde{G}(\underline{z}';T=0) = \sum_{\underline{v}'=\underline{0}}^{\infty} |\langle \underline{v}'|\underline{0}\rangle|^2 \prod_{k}^{N} (z_k')^{2v_k'}. \tag{1.20}$$

Comparing to Eq. (1.12) the GF parameters in Eq. (1.20) are related to the DOS[13]. Exploiting the analytic expression (product of determinants and exponential functions) from the CS phase space integration corresponding to the series summation expression (1.20), the prescreening strategies can be constructed (Ref. [46] and see also Ch. 4). Using the summation (1.20) by assigning numbers to z_k', *e.g.* 0 for freezing the mode excitation and 1 for summing over all excitation, the precise integral patterns can be extracted.

The GF approach of Jankowiak *et al.* [46] has to be extended, for example, for finite temperature effects (Ch. 4) and for going beyond FC processes, *e.g.* for HT vibronic intensity borrowing effects (Ch. 6). The sum of FCFs ($|\langle \underline{v}'|\underline{v}\rangle|^2$) and the non-Condon factors ($\langle \underline{v}|\hat{g}^*|\underline{v}'\rangle\langle \underline{v}'|\hat{f}|\underline{v}\rangle$) over one set of states, at finite temperature and at zero Kelvin, converge to finite numbers. Integrating the Lorentzian line shape function (L) over all frequency range[14] in the non-Condon spectral density function of Eq. (1.16), in order to sum all non-Condon (or FCFs) factors, the summation converges to a finite number (Ch. 6).

One could exploit this sum rule to restrict the number of harmonic basis functions in the evaluation of the non-Condon (or FC) SDF. Hereafter this will simply be called sum

---

[13]It will be shown, later in chapter 4, that the GF parameters are related to the Dirac δ-distribution.
[14]It results 1.

rule. We derive a closed analytical functional form for the sum of non-Condon factors at finite temperature and use it for the sum rule in chapter 6. We apply the sum rule to the prototypical HT transition of benzene in chapter 6. To construct the non-Condon GF in an analytic form for the sum rule, we utilize the CS phase displacement operator. Similarly to the non-Condon integral evaluation schemes in Ch. 3, non-Condon effects can also be included by the MHP method (Ch. 6).

Franck-Condon time-correlation functions and beyond The direct evaluation of non-Condon (or FC) integrals with the sum rule explained above would improve the computational efficiency greatly but it still has limitations in applications to large molecules at high temperature. At high finite temperature the resulting spectra are typically highly congested, so that assignment of individual peaks from TI methods are of minor importance, if not even unnecessary. If we are interested only in the spectral shapes and not in individual peaks, we can compute the spectrum in the time domain [64] via Fourier transform (FT) techniques. The non-Condon SDF in Eq. (1.16) can be written alternatively by making use of the quantum mechanical trace formalism and the Fourier representation of the Lorentzian distribution in time (t) domain[15],

$$\rho_{\text{L}}(\omega; T)^{(\hat{f}, \hat{g})} = \hbar^{-1} \int_{-\infty}^{\infty} \mathrm{d}t \frac{\text{Tr}\left(\hat{g}^{\dagger} \mathrm{e}^{-\mathrm{i}\hat{H}'t/\hbar} \hat{f} \mathrm{e}^{\mathrm{i}\hat{H}(t/\hbar + \mathrm{i}\beta)}\right)}{\text{Tr}(\mathrm{e}^{-\beta\hat{H}})} \mathrm{e}^{\mathrm{i}(\omega-\omega_0)t - \frac{\Gamma}{2}|t|}, \qquad (1.21)$$

with $\beta = 1/(k_{\text{B}}T)$ (k_{B} is Boltzmann constant) and harmonic vibrational Hamiltonians ($\hat{H}$ and $\hat{H}'$, initial and final state ones, respectively)[16]. The vibrational eigenstates do not appear explicitly in the trace density matrix expression (1.21) in contrast to Eq. (1.16). In principle the traces can be evaluated over any complete basis set. It is well known for instance how to find an analytic functional form of the trace of the numerator in Eq. (1.21) (the denominator trace is just a vibration partition function of the initial state) within the Condon approximation in harmonic oscillator basis. For example it can be evaluated by the Feynman path integral [126] kernel of harmonic oscillators (see *e.g.* Refs. [34, 79, 86]) including the Duschinsky rotation. The trace part in Eq. (1.21) is usually called time-correlation function (TCF). This eigenstate-free TD method is widely used (within the Condon approximation) for the absorption spectrum and rR scattering (see *e.g.* Refs. [17, 23, 34, 64, 127]) because the eigenstate-free formulation helps to avoid the direct evaluation of the matrix elements by evaluating the (analytic) TCF at discrete times in contrast to the TI approach.

It is not, however, a trivial task to evaluate the non-Condon TCF including Duschinsky effects. There have been some approaches to compute the non-Condon TCF limiting Duschinsky effects (see *e.g.* Refs. [38, 47, 70, 91, 94]). Recently Islampour and Miralinaghi [93] devised a TCF for IC rate involving multi-promoting modes (which mediate the intramolecular transition) and vibrational mode mixing effects. They exploited second order multi-variate normal moments for the momentum operator matrix elements of the promoting modes. However their method is not generally applicable to other transition

---

[15]$L(\omega, \overline{\omega}; \Gamma) = \hbar^{-1} \int_{-\infty}^{\infty} \mathrm{d}t\, \mathrm{e}^{\mathrm{i}(\omega-\overline{\omega})t - \frac{\Gamma}{2}|t|}$, and as the FWHM $\Gamma \to 0$ the distribution approaches to the Dirac δ-distribution $\delta(\omega - \overline{\omega}) = \int_{-\infty}^{\infty} \mathrm{d}t\, \mathrm{e}^{\mathrm{i}(\omega-\overline{\omega})t}$.

[16]Zero-point harmonic energies are shifted to be 0. The zero-point energy differences of the two multi-dimensional harmonic oscillators are included already in ω_0.

problems and the method cannot handle nonlinear coupling problems. Peng *et al.* [94, 95] also have a similar TCF development to that of Islampour and Miralinaghi [93]. As one of the main results of this thesis, we overcome the shortcomings of Islampour and Mirali-naghi's method with the same CS-based GF approach which is exploited for the TI sum rule method to prescreen the integral basis set. Within the Duschinsky-rotated harmonic oscillator basis approximation we can use CSs easily for the phase space integration. It is convenient to express the phase space representation with the CS phase variables within the harmonic approximation because CS is a GF of harmonic oscillator eigenstates and as a result the overlap of two CS is a GF of harmonic FC integrals. The quantum mechanical trace is invariant in any complete basis set expansion. When we use the CSs as basis set for the numerator trace in Eq. (1.21) and introduce GF parameters related to the DOS in FGR which can absorb time dependence implicitly (Ch. 4), the same CS-based GF can be used both in frequency and time domains (Chs. 4 and 6). In this method, one only needs to introduce simply proper TD GF parameters to have the TCF without needing a complicated integration in position space. And the (complex) MHPs to arbitrary order can generate the non-Condon effects easily as well (Ch 6). The identical GF at $t = 0$ obeys the sum rule and at $t \neq 0$ provides the TCF at $t \neq 0$.

It has long been considered that the TI and TD approaches are independent of each other even if they are identical in principle [18]. The integral prescreening method can be compared consistently with the TD method because the TCF method can provide the upper bound of the TI method within the GFs developed in this thesis. The CS, together with GF parameters, in phase space can bridge the frequency and time domain representations of SDFs. The resulting expression is exploited for the GF (which can merge the TI and TD approaches) augmenting the thermal (Ch. 4) and non-Condon (Ch. 6) effects in its phase space via CSs. Similar idea is exploited for TI cumulant expansion (CE)[17] (Ch. 5), rR scattering [18] (Sec. 7.2), SVL transition[19] (Sec. 7.3) and anharmonic transition (Sec. 7.4).

Modifications to generating function approach   The CS-based GF of a molecular transition related to FGR is analogous to the partition function in statistical mechanics in the aspect that the GF is the fundamental functional of the molecular transition system (see Fig. 8.1). It contains the information about the transition, in frequency domain, in time domain and in phase space. As with partition functions it is possible to extract useful information via proper operation onto the GF. One is able to retrieve specific information or to invoke other quantum mechanical and environmental effects by introducing auxiliary parameters to the GF.

In some cases only the statistical quantities (*e.g.* mean and variance) are required, for example, for the Stokes shift, which corresponds to the peak maximum difference between absorption and emission spectra. This kind of information can be obtained without calculation of the entire spectrum, neither via the TI nor the TD approaches mentioned above. The cumulants[20] (or moments) of the FCF distribution in frequency domain are computed by the GF approach in chapter 5 with relatively low computational effort. An auxiliary GF parameter is used to evaluate cumulants in a TI way. The method is closely related to the

---

[17]For statistical quantities like mean, variance, skewness, kurtosis and so on for the FC transition.

[18]The rR excitation profile involves two single vibronic levels (SVLs).

[19]A fluorescence from a given vibrational level in the electronically excited state is called SVL fluorescence.

[20]mean, variance, skewness, kurtosis and so on.

TD CE method (see *e.g.* Refs. [5, 35, 87]). The TD CE, however, involves time-integration, which makes the algebra complicated even for second order cumulants (variance). The TI CE method developed in this thesis, instead, can compute cumulants to arbitrary order. The cumulants can provide useful information for other approaches, for instance about the time propagation of TCF, *i.e.* time step and time propagation length (Sec. 5.1.2).

The detailed control of vibronic levels is necessary for rR, SVL and anharmonic transitions. The GFs for these vibronic transitions are developed in chapter 7 with the help of a MHP technique. The MHP technique allows the manipulation of vibronic level excitations. It can provide more concrete information about the vibrational excitation patterns whereas the previous FC development [46] can support only a coarse-grained prescreening strategy[21]. The cross sections of rR and SVL take into account (non-thermally-averaged) excited SVLs which are not summed over in FGR [34, 58]. These developments are modifications to the thermal and non-Condon GFs in the aspects that they include SVLs of the fixed ONV states. The GF approach for anharmonic FC transition, which approximately takes into account a few anharmonic vibrational DOF (and the rests are harmonic), is also suggested in the same chapter for the possible integral prescreening strategies of this special case.
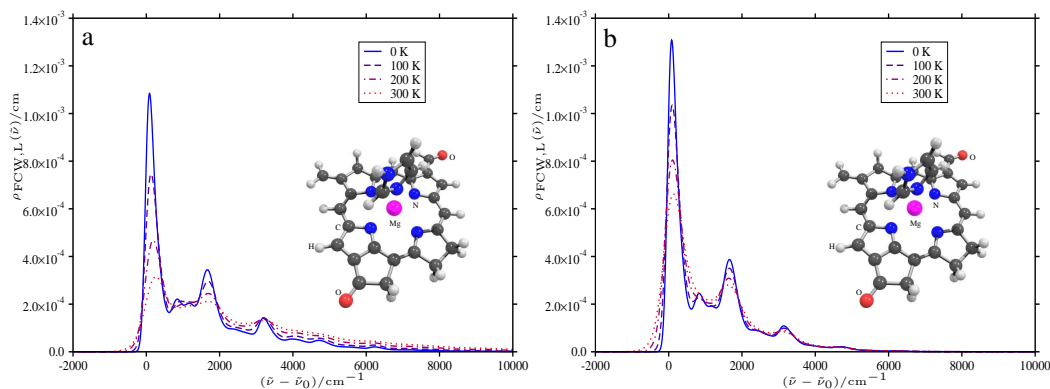
Figure 1.2.: Temperature dependence of FC profiles for electron transfer reaction of Bacteriochlorophyll (Bchl) in the photosynthetic reaction center, $Bchl^- \longrightarrow Bchl$. The FC SDFs are computed via TCF-FFT method at 0 K (solid), 100 K (dashed), 200 K (dot-dashed) and 300 K (dotted). a. Duschinsky mode mixing effect is considered. b. Duschinsky mode mixing effect is ignored. Instead of a Lorentzian line shape function, a Gaussian line shape function with FWHM of 200 cm^{-1} is used for the DOS in the FC profile calculation.

1.1. Achievements

The major goal of this thesis is to describe various molecular vibronic transitions theoretically and understand the transition mechanisms with the help of theoretical models, especially, for large molecular systems. For instance, we investigate an ET reaction of a Bacteriochlorophyll (Bchl) model in the photosynthetic reaction center (see *e.g.* Ref. [128])

---

[21]The maximum excitation quantum number of individual vibrational mode is computed with given intensity threshold neglecting correlation between other vibrational mode excitation pattern.

to study temperature dependence of the reaction and the corresponding effect of Duschinsky mode mixing. We compute the FC profiles at various temperature, switching on or off the Duschinsky mode mixing effects, via the TCF-FFT method (Fig. 1.2). Comparing the two figures in Fig. 1.2 one can notice significant Duschinsky effects at various temperatures. But it would be difficult to perform a detailed analysis of these highly congested spectra with the existing theoretical TD or TI tools. We need to have a unified TD and TI picture in one common language to analyze the individual vibrational mode contribution for the detailed analysis, *e.g.* thermal energy redistribution of initial state between the vibrational modes of final state in presence of Duschinsky mode mixing effect (see Sec. 5.3.2 for this specific example).

In this thesis we extend and modify the CS-based GF idea [29, 46] for the various vibronic transitions involving thermal excitation and non-Condon effects within the Duschinsky approximation. The methods of this thesis can provide TI and TD approaches with identical functionals. The sum rules of FCFs (used in the previous work [46][22] for devising prescreening criteria) are extended to the case of thermally excited Duschinsky rotated multi-dimensional harmonic oscillator states at finite temperature (see the illustration 1.3 for ultra-violet (UV) absorption of anthracene) as well as to the non-Condon effects. The GF approaches for rR scattering and SVL transition are developed to include the thermal and non-Condon effects in the Duschinsky rotated harmonic oscillator basis. The methods developed herein are general and can be applied to any kinds of transition processes via FGR with slight modifications either in frequency or time domains. Some developments (thermal, HT effects and TI CE) of this thesis are implemented in a development version of the vibronic structure program hotFCHT [36, 46, 129–131]. The CS-based GF approach, despite the achievements in this thesis, leaves still rooms for future developments, *e.g.* nonadiabatic coupling, full anharmonic, dissipative systems and non-equilibrium problems which are not treated in this thesis. To this end, we summarize the developments of this thesis as follows: The molecular transition and integral evaluation problems in the Duschinsky rotated harmonic oscillator basis can be translated into a MHP evaluation problem. The same mathematical machinery can be used for various other problems, either in TI or TD approach and either in Condon or non-Condon approximation (see Figs. 8.1 and 8.2 on pages 125 and 127, respectively).

Most of the developed methods and the results presented in this thesis have also appeared or will appear in:

Ref. [129][23]: *"Vibronic transitions in large molecular systems: Prescreening conditions for Franck-Condon factors at finite temperature and the thermal time-correlation function",*
J. Huh, H.-C. Jankowiak, J. L. Stuber and R. Berger, (to be published).

Ref. [130][24]: *"Vibronic transitions in large molecular systems: The thermal time-correlation*

---

[22]J. Huh was not involved in this work.

[23]J. Huh has contributed to this work with the thermal time-correlation function theory development and the implementation of the methods including the thermal prescreening to the vibronic structure program hot-FCHT.

[24]J. Huh has contributed to this work with the non-Condon thermal time-correlation function theory development, the Franck-Condon-Herzberg-Teller prescreening development and the implementation of the devel-

function and rigorous prescreening of Herzberg-Teller terms",
J. Huh, J. L. Stuber and R. Berger, (to be published).

Ref. [131][25]: *"Vibronic transitions in large molecular systems: Time-independent cumulant expansion for Franck-Condon profiles at finite temperature and at zero Kelvin",*
J. Huh, J. L. Stuber and R. Berger, (to be published).

Ref. [132][26]: *"Application of time-independent cumulant expansion to calculation of Franck-Condon profiles for large molecular systems",*
J. Huh and R. Berger, Faraday Discuss., (accepted).

Ref. [52][27]: *"An atomic-orbital based Lagrangian approach for calculating geometric gradients of linear response properties",*
S. Coriani, T. Kjærgaard, P. Jørgensen, K. Ruud, J. Huh and R. Berger, J. Chem. Theo. Comput. 6, 1028 (2010).

Ref. [53][28]: *"Franck–Condon profiles in photodetachment-photoelectron spectra of HS_2^- and DS_2^- based on vibrational configuration interaction wavefunctions",*
J. Huh, M. Neff, G. Rauhut and R. Berger, Mol. Phys. 108, 409 (2010).

1.2. Chapter summary and dissertation outline

In this chapter the FGR expression for the OPA in the vibrational wavefunction basis set within the BO approximation is introduced as an example for a vibronic transition process. The FCFs are the fundamental quantities in describing vibronic transitions. The FCF evaluation is a challenging problem even in the harmonic approximation because of the large number of FC/non-Condon integrals within the Duschinsky approximation. We suggest CS-based GF methods to describe theoretically molecular vibronic transition processes involving the finite temperature effects (Ch. 4) and the non-Condon (Ch. 6) effects. The GF can provide efficient numerical procedures with its representations in frequency and time domain be connected via the CS phase space. We modify the GFs for TI CE, rR scattering processes, SVL transitions and anharmonic transitions (Ch. 7) with the help of MHPs (see a summary diagram of this thesis in Fig. 8.1 on page 125).

The dissertation is organized as follows:

- The background knowledge related to the developments of this thesis is briefly pre-

---

oped methods to the vibronic structure program hotFCHT.

[25]J. Huh has contributed to this work with the time-independent cumulant theory development, the algorithm for the cumulant expansion and the implementation of the developed methods to the vibronic structure program hotFCHT.

[26]J. Huh has contributed to this work with an application of the time-independent cumulant theory development [131]. The method is applied for the UV/VIS absorption spectra of terrylene ($^1A_g \longrightarrow ^1B_{3u}$).

[27]J. Huh has contributed to this work by testing the analytical electronic TDM gradient by computing the Herzberg-Teller profiles of benzene with the method developed in Ref. [130] and implemented in hotFCHT.

[28]J. Huh has contributed to this work with the integral prescreening strategy development and the implementation of the anharmonic Franck-Condon computing routines to the vibronic structure program hotFCHT.
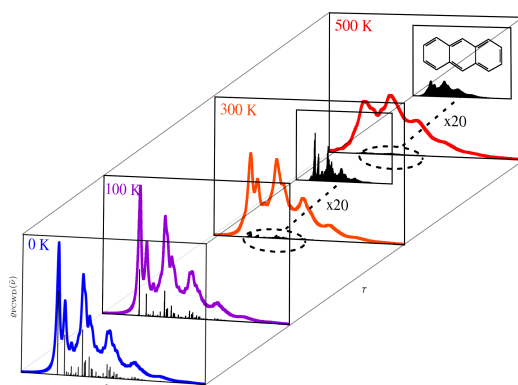
Figure 1.3.: Illustration of calculated Franck-Condon profiles for the $1\,^1A_g \rightarrow 1\,^1B_{2u}$ absorption spectra of anthracene at 0 K, 100 K, 300 K and 500 K. The stick representations have additionally been convoluted with Lorentzian line shapes. The figure is reproduced with permission from *Nachr. Chem.* 58, 331. Copyright 2010 WILEY-VCH Verlag GmbH & Co. KGaA, Weinheim."

sented in chapter 2. The OPA and rR scattering are described from the TI and TD perspectives. The basic properties of CSs and the Duschinsky relation are explained therein for the GF development. The zero Kelvin development [46][29], the foundation of the current work, is briefly explained.

- An iterative FC integral formula is suggested in chapter 3 with the help of multivariate normal moments based Hermite polynomial evaluation schemes [133,134]. A non-Condon integral evaluation scheme is suggested as well via the CS displacement operators.

- The following thermal FCF GF chapter 4 presents the CS-based GF approaches for the thermal effects both in TD and TI aspects. The integral prescreening strategy at finite temperature and thermal TCF are developed.

- Chapter 5 follows a slightly different route to obtain the FC profile from statistical quantities like mean, variance and higher order cumulants via the TI CE method.

- The non-Condon GF developments augmenting the TI and TD approaches are presented in chapter 6 and the HT transition of benzene is presented as an example.

- In the last method development chapter 7 we devise the coherent-Fock (cF)[30] GF via the MHP technique for the GFs for rR, SVL and anharmonic transitions in the TI and the TD pictures.

- Finally the conclusion of this dissertation follows in chapter 8.

---

[29]J. Huh was not involved in this work.
[30]the mixture of harmonic oscillator eigenstates and coherent states (Eq. (2.81)).

2. Background

The primary goal of this thesis is describing computationally vibronic transitions (see Fig. 1.1) such as one-photon absorption (OPA) (see *e.g.* Refs. [12, 21–54]), one-photon emission (OPE) (see *e.g.* Refs. [55–59]), resonance Raman (rR) scattering (see *e.g.* Refs. [17, 60–76]), electron transfer (ET) (see *e.g.* Refs. [77–89]), internal conversion (IC) (see *e.g.* Refs. [90–95]) and inter-system crossing (ISC) (see *e.g.* Ref. [96]). For the purpose, we devise (in this thesis) the computational frameworks for the Franck-Condon (FC) and non-FC[1] vibronic transitions within the (adiabatic) Born-Oppenheimer (BO) approximation [2, 99]. The inclusion of the Duschinsky vibrational mode mixing [107] together with the temperature and non-Condon effects make the computational complexity for the vibronic processes (prohibitively) high. Even in the harmonic oscillator approximation, the computational description of the vibronic transitions is still challenging. Herein we approximate molecular systems as N-dimensional harmonic oscillators. Accordingly, the (radiative) vibronic transition is considered as a transition between multi-dimensional harmonic oscillators.

The interaction between radiation and molecules is a fundamental time-dependent (TD) phenomenon. For that reason, the quantum mechanical description of such vibronic processes usually is based on TD perturbation theory. However, when the observables are not explicitly TD quantities and a radiation-matter interaction is weak, for example in the OPA process, it is sufficient to invoke Fermi's golden rule (FGR) [103, 104] from TD perturbation theory for describing the molecular transitions (see *e.g.* Refs. [3, 8, 66]). The various representations of FGR in frequency, time and phase spaces are exploited in this thesis via the coherent state (CS)-based generating function (GF) approach [46] to reduce the computational complexity. Each representation has benefits and shortcomings of its own in its evaluations, such that they are complementary to each other (see *e.g.* Ref. [18]). One of the main achievements of this thesis is that the different aspects of FGR can be combined in one GF based on CSs within the displaced-distorted-rotated harmonic oscillator (Duschinsky) approximation. The molecular vibronic transition spectra described by FGR are computed efficiently, including thermal (Ch. 4) and non-Condon (Ch. 6) effects with the CS-based GF.

In order to present the CS-based GF in some detail, we need to bear in mind the various representations of FGR and the relations among them (Sec. 2.1). As an example, the transformation between the time-independent (TI) and time-dependent expressions of the OPA and rR scattering cross sections are explained. We can apply slight modifications to the other vibronic transitions (see Fig. 1.1), such as OPE, ET, electronic circular dichroism (ECD), IC and ISC, so that they can be described similar to OPA and rR. The Duschinsky linear approximation and the corresponding unitary transformation (Sec. 2.2) as well as basic properties of CSs (Sec. 2.3), which are necessary for the CS-based GF method [46], are explained in the corresponding sections. The Franck-Condon factor (FCF) GF development

---

[1] non-Condon, *e.g.* linear and nonlinear Herzberg-Teller (HT) expansions (1.15)
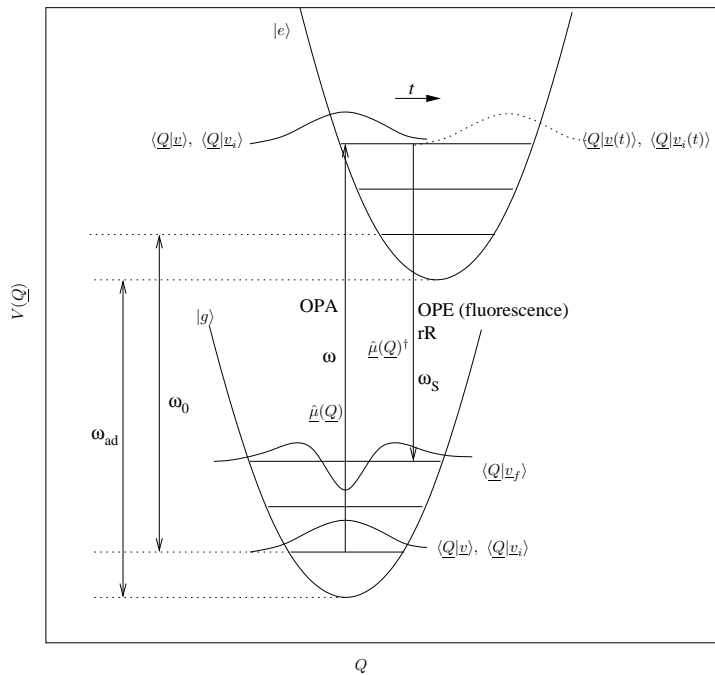
Figure 2.1.: One-photon absorption (OPA) and resonance Raman (rR) scattering in the time-dependent (TD) picture. OPA time-correlation function (TCF) is the overlap between the initial state $|\underline{v}\rangle$ and the time-propagating state $|\underline{v}(t)\rangle$ on the final potential energy surface. One-photon emission (OPE) is interpreted in the same way as OPA, the difference being that the initial and final states are reversed. rR scattering is a two photon process of the incident light (ω) and the scattered light (ω_S). ω_{ad} is defined to be the adiabatic electronic transition (angular) frequency between the electronic ground ($|g\rangle$) and excited ($|e\rangle$) states. ω_0 is defined to be the adiabatic transition (angular) frequency including the vibrational zero-point energy difference between the two oscillators. The time-dependent picture shows the rR scattering process. This process implies that the initial ground vibrational state $|\underline{v}_i\rangle$ propagates on the excited state $|\underline{v}_i(t)\rangle$ and return to the ground vibrational state $|\underline{v}_f\rangle$.

at zero Kelvin [46][2] for integral prescreening in the TI picture is briefly presented in section 2.4, which is based on the Duschinsky unitary transformation and the CSs. The zero Kelvin development serves as the basis for the method development within this thesis[3]. The mathematical machinery, notational convention and numerical schemes are employed, as far as possible, from the previous work [46].

2.1. One-photon absorption and resonance Raman scattering

In this section we transform the TI spectral density function (SDF) of the OPA and the rR scattering cross section from frequency domain to time domain via the density matrix

---

[2]J. Huh was not involved in this work.

[3]Thermal prescreening strategies, thermal time-correlation function (TCF), non-Condon effects, TI cumulant expansion (CE), anharmonicity, rR and single vibronic level (SVL)

trace formalism [135]. Herein the vibronic transition between N-dimensional harmonic oscillators are assumed to be the same as the ones introduced earlier (Eq. 1.5). The SDF of OPA (Eq. (1.12)) in frequency domain reads (again), with the Lorentzian line shape function ($L(\omega)$) of full width at half maximum (FWHM) of Γ,

$$\rho_{\mathrm{L}}(\omega; T) = \sum_{\underline{v},\underline{v}'=\underline{0}}^{\infty} p_{\underline{v}}(T)|\langle \underline{v}'|\hat{\underline{\mu}}(Q)|\underline{v}\rangle|^2 L(\omega, \omega_0 + \omega_{\underline{v}',\underline{v}}; \Gamma), \tag{2.1}$$

and the stick representation[4] with the Dirac δ-distribution is, accordingly,

$$\rho(\omega; T) = \sum_{\underline{v},\underline{v}'=\underline{0}}^{\infty} p_{\underline{v}}(T)|\langle \underline{v}'|\hat{\underline{\mu}}(Q)|\underline{v}\rangle|^2 \delta(\hbar\omega - \hbar(\omega_0 + \omega_{\underline{v}',\underline{v}})), \tag{2.2}$$

where the vibrational transition (angular) frequency is defined by the corresponding harmonic energies ($\underline{\epsilon}$ and $\underline{\epsilon}'$) of oscillators, *i.e.* ($\omega_{\underline{v}',\underline{v}} = (\underline{\epsilon}' \cdot \underline{v}' - \underline{\epsilon} \cdot \underline{v})/\hbar$). Prime "′" is used, conventionally, for specifying variables belonging to the final electronic state. Raman scattering is a two-photon process involving the incident (ω) and scattered light (ω_{S}) (see Fig. 2.1). From second order TD perturbation theory for the two-photon process, we can obtain the matrix elements of the polarizability tensor as the (vibronic) Raman scattering [60] amplitude in the frequency domain (see *e.g.* Refs. [3, 6, 17]).

The matrix element of the polarizability tensor $\boldsymbol{\alpha}$ in the molecular vibronic wavefunction basis[5] with polarization vectors, $\underline{e}^{\mathrm{L}}$ and $\underline{e}^{\mathrm{S}}$ of incident and scattered photons respectively, is the vibrational Raman scattering amplitude and corresponds to the vibrational Raman excitation profile ($\alpha_{\mathrm{R}}^{\underline{v}_i \rightarrow \underline{v}_f}$, see *e.g.* [17]), *i.e.*

$$\alpha_{\mathrm{R}}^{\underline{v}_i \rightarrow \underline{v}_f}(\omega, \omega_{\mathrm{S}}) = \langle \underline{v}_f|\langle g|\underline{e}^{\mathrm{S}} \cdot \boldsymbol{\alpha} \cdot \underline{e}^{\mathrm{L}}|g\rangle|\underline{v}_i\rangle = \sum_{\underline{v}'=\underline{0}}^{\infty} \frac{\langle \underline{v}_f|\hat{\mu}^{\mathrm{S}}(Q)^{\dagger}|\underline{v}'\rangle\langle \underline{v}'|\hat{\mu}^{\mathrm{L}}(Q)|\underline{v}_i\rangle}{\hbar(\omega - (\omega_{\underline{v}',\underline{v}_i} + \omega_0) + \frac{\mathrm{i}}{2}\Gamma_{\underline{v}_i,\underline{v}'})}$$
$$+ \sum_{\underline{v}'=\underline{0}}^{\infty} \frac{\langle \underline{v}_f|\hat{\mu}^{\mathrm{L}}(Q)^{\dagger}|\underline{v}'\rangle\langle \underline{v}'|\hat{\mu}^{\mathrm{S}}(Q)|\underline{v}_i\rangle}{\hbar(\omega_{\mathrm{S}} + (\omega_{\underline{v}',\underline{v}_i} + \omega_0) + \frac{\mathrm{i}}{2}\Gamma_{\underline{v}_i,\underline{v}'})}, \tag{2.3}$$

where we have used

$$\hat{\mu}^{\mathrm{L}}(Q) = \hat{\underline{\mu}}(Q) \cdot \underline{e}^{\mathrm{L}}, \quad \hat{\mu}^{\mathrm{S}}(Q) = \hat{\underline{\mu}}(Q) \cdot \underline{e}^{\mathrm{S}}. \tag{2.4}$$

In Eq. (2.3) $|\underline{v}_i\rangle$ and $|\underline{v}_f\rangle$ are the initial and the final vibrational states in the ground state ($|g\rangle$), $|\underline{v}'\rangle$ is the virtual (or intermediate) vibrational state in the excited electronic state ($|e\rangle$, see Fig. 2.1), and $\Gamma_{\underline{v}_i,\underline{v}'}$ is the line width of the initial to virtual state transition. The vibrational transition frequency from the initial state to the virtual vibrational state is given as $\omega_{\underline{v}',\underline{v}_i} = (\underline{\epsilon}' \cdot \underline{v}' - \underline{\epsilon} \cdot \underline{v}_i)/\hbar$.

At the resonance condition ($\omega \simeq (\omega_{\underline{v}',\underline{v}_i} + \omega_0)$), the non-resonance contribution of

---

[4]In practice, we evaluate the intensity profiles according to the stick representation and convolute the profiles in stick representation with the Lorentzian line shape function.

[5]We can ignore rotational wavefunctions for randomly oriented molecules (see *e.g.* Refs. [3, 6, 17] and Ch. 1).

$\alpha_{\mathrm{R}}^{\underline{v}_i \rightarrow \underline{v}_f}$, the second summation term in Eq. (2.3), can be neglected because the first summation (resonance) term in Eq. (2.3) is dominant. Therefore the vibrational rR scattering amplitude ($\alpha_{\mathrm{rR}}^{\underline{v}_i \rightarrow \underline{v}_f}$) is expressed in a reduced form,

$$\alpha_{\mathrm{rR}}^{\underline{v}_i \rightarrow \underline{v}_f}(\omega) = \sum_{\underline{v}'=\underline{0}}^{\infty} \frac{\langle \underline{v}_f | \hat{\mu}^{\mathrm{S}}(Q)^{\dagger} | \underline{v}' \rangle \langle \underline{v}' | \hat{\mu}^{\mathrm{L}}(Q) | \underline{v}_i \rangle}{\hbar(\omega - (\omega_{\underline{v}',\underline{v}_i} + \omega_0) + \frac{\mathrm{i}}{2}\Gamma)}, \tag{2.5}$$

where we have assumed a common homogeneous line broadening factor $\Gamma_{\underline{v}_i,\underline{v}'} = \Gamma$ for molecules in condensed phases (see *e.g.* [17, 65, 68, 70, 72, 136]).

The (differential) rR cross section is proportional (see *e.g.* Ref. [65]) to the SDF of rR from FGR similar to Eq. (2.1), *i.e.*

$$\frac{\mathrm{d}\sigma_{\mathrm{rR}}}{\mathrm{d}\omega_{\mathrm{S}}} = \frac{8\pi}{9\hbar c_0^2} \left(\frac{\alpha_0}{e_0^2}\right)^2 (\hbar\omega)(\hbar\omega_{\mathrm{S}})^3 \rho_{\mathrm{rR,L}}(\omega, \omega_{\mathrm{S}}). \tag{2.6}$$

The SDF of rR scattering is given with the Lorentzian line shape function[6] as in Eq. (2.1), *i.e.*

$$\rho_{\mathrm{rR,L}}(\omega, \omega_{\mathrm{S}}) = \sum_{\underline{v}_i,\underline{v}_f=\underline{0}}^{\infty} p_{\underline{v}_i}(T) |\alpha_{\mathrm{rR}}^{\underline{v}_i \rightarrow \underline{v}_f}(\omega)|^2 L(\omega - \omega_{\mathrm{S}}, \omega_{\underline{v}_f,\underline{v}_i}; \Gamma_{\mathrm{rR}}), \tag{2.7}$$

and the stick representation is obtained with the Dirac δ-distribution as in Eq. (2.2), accordingly,

$$\rho_{\mathrm{rR}}(\omega, \omega_{\mathrm{S}}) = \sum_{\underline{v}_i,\underline{v}_f=\underline{0}}^{\infty} p_{\underline{v}_i}(T) |\alpha_{\mathrm{rR}}^{\underline{v}_i \rightarrow \underline{v}_f}(\omega)|^2 \delta(\hbar(\omega - \omega_{\mathrm{S}}) - \hbar\omega_{\underline{v}_f,\underline{v}_i}), \tag{2.8}$$

where $\omega_{\underline{v}_f,\underline{v}_i} = (\underline{\epsilon} \cdot \underline{v}_f - \underline{\epsilon} \cdot \underline{v}_i)/\hbar$ is the rR Stokes scattering frequency.

Time-independent (TI) evaluation of equations (2.1) and (2.5) is limited to small molecular systems. For larger systems one would need efficient strategies, such as the integral prescreening [46] introduced in the previous chapter 1. The complementary TD approach for theoretical molecular spectroscopy has been used for several decades, in electron transfer theory [79,81,84,86,87], in Raman scattering theory [17,56,61,64,66,67,72,73,75,109], in FC absorption processes [33,34,55,137,138], in non-Condon processes [38,40,93–95] and in laser cooling theory [37,40–42,48]. The energy eigenstate-free TD approach (Eq. (1.21)) has long been appreciated for its computational efficiency and its wavepacket interpretation of the transition process. It describes the transition process via the time-propagation of initial wavepacket on the excited potential energy surface [64]. To express the absorption cross section (Eq. (2.1)) and the rR scattering amplitude (Eq. (2.5)) in time domain, one invokes the Fourier transformed representation of the Lorentzian line shape function[7] in Eq. (2.1) and the half-Fourier transformed representation of the frequency dependent weight func-

---

[6]with a line broadening factor Γ_{rR} within a single electronic state.

[7]$L(\omega, \overline{\omega}; \Gamma) = \hbar^{-1} \int_{-\infty}^{\infty} \mathrm{d}t\, \mathrm{e}^{\mathrm{i}(\omega-\overline{\omega})t - \frac{\Gamma}{2}|t|}$, and as the FWHM $\Gamma \rightarrow 0$ the distribution approaches to the Dirac δ-distribution $\delta(\omega - \overline{\omega}) = \int_{-\infty}^{\infty} \mathrm{d}t\, \mathrm{e}^{\mathrm{i}(\omega-\overline{\omega})t}$.

tion[8], the denominator in Eq. (2.5). That is for the absorption process [17, 64], *i.e.*

$$\rho_{\text{L}}(\omega;T) = \hbar^{-1} \int_{-\infty}^{\infty} dt \sum_{\underline{v},\underline{v}'=\underline{0}}^{\infty} p_{\underline{v}}(T) |\langle \underline{v}'|\hat{\underline{\mu}}(\underline{Q})|\underline{v}\rangle|^2 \exp[\text{i}(\omega - (\omega_{\underline{v}',\underline{v}} + \omega_0))t - \tfrac{\Gamma}{2}|t|] \,,$$
(2.9)

and for the scattering process [17, 64],

$$\alpha_{\text{rR}}^{\underline{v}_i \to \underline{v}_f}(\omega) = -\frac{\text{i}}{\hbar} \int_0^\infty d\tau \sum_{\underline{v}'=\underline{0}}^{\infty} \langle \underline{v}_f | \hat{\mu}^{\text{S}}(\underline{Q})^\dagger | \underline{v}'\rangle \langle \underline{v}'|\hat{\mu}^{\text{L}}(\underline{Q})|\underline{v}_i\rangle$$
$$\exp[\text{i}(\omega - (\omega_{\underline{v}',\underline{v}_i} + \omega_0))\tau - \tfrac{\Gamma}{2}\tau].$$
(2.10)

Now, one can recover the vibrational Hamiltonians corresponding to the expressions (2.9) and (2.10) from the vibrational frequencies, *e.g.* $e^{\text{i}\omega_{\underline{v}}t}|\underline{v}\rangle = e^{\text{i}\hat{H}t/\hbar}|\underline{v}\rangle$. The SDF of OPA is rewritten as follows (see *e.g.* Refs. [17, 64])

$$\rho_{\text{L}}(\omega;T) = Z_{\text{I}}^{-1}\hbar^{-1} \int_{-\infty}^{\infty} dt \sum_{\underline{v},\underline{v}'} \langle \underline{v}|\hat{\underline{\mu}}(\underline{Q})^\dagger \exp(-\text{i}\hat{H}'t/\hbar)|\underline{v}'\rangle$$

$$\langle \underline{v}'|\hat{\underline{\mu}}(\underline{Q}) \exp(\text{i}\hat{H}t/\hbar) \exp(-\beta\hat{H})|\underline{v}\rangle \exp[\text{i}(\omega - \omega_0)t - \tfrac{\Gamma}{2}|t|] \qquad (2.11)$$

$$= Z_{\text{I}}^{-1}\hbar^{-1} \sum_{\underline{v}} \int_{-\infty}^{\infty} dt \langle \underline{v}|\hat{\underline{\mu}}(\underline{Q})^\dagger \exp(-\text{i}\hat{H}'t/\hbar)\hat{\underline{\mu}}(\underline{Q}) \exp(\text{i}\hat{H}t/\hbar) \exp(-\beta\hat{H})|\underline{v}\rangle$$

$$\exp[\text{i}(\omega - \omega_0)t - \tfrac{\Gamma}{2}|t|] \qquad (2.12)$$

$$= \hbar^{-1} \int_{-\infty}^{\infty} dt \, \chi(t;\beta) \exp[\text{i}(\omega - \omega_0)t - \tfrac{\Gamma}{2}|t|] \,, \qquad (2.13)$$

where the vibrational partition function is $Z_{\text{I}} = \text{Tr}\left(\exp(-\beta\hat{H})\right)$ and the Boltzmann factor $p_{\underline{v}}(T)|\underline{v}\rangle = Z_{\text{I}}^{-1} \exp(-\beta\hbar\omega_{\underline{v}})|\underline{v}\rangle = Z_{\text{I}}^{-1} \exp(-\beta\hat{H})|\underline{v}\rangle$. From the expression (2.12), it is clear that the TCF[9] for the absorption spectral density can be defined within the density matrix formalism. Since equation (2.12) is just the trace over the initial vibrational states, $\chi(t;T)$ is the thermal TCF in a trace form as in Eq. (1.21), *i.e.*

$$\chi(t;T) = Z_{\text{I}}^{-1}\text{Tr}\left(\hat{\underline{\mu}}(\underline{Q})^\dagger \exp(-\text{i}\hat{H}'t/\hbar)\hat{\underline{\mu}}(\underline{Q}) \exp(\text{i}\hat{H}t/\hbar) \exp(-\beta\hat{H})\right). \qquad (2.14)$$

---

[8] $\frac{1}{\omega - \overline{\omega} + \text{i}\Gamma/2} = -\text{i}\int_0^\infty dt \, e^{\text{i}(\omega - \overline{\omega})t - \frac{\Gamma}{2}t}$, which is a special case of the Laplace transform.

[9] Here the time-correlation function includes the summation over initial vibrational occupation number vector (ONV) space.

Similarly, the rR amplitude is expressed in TD language as

$$
\alpha_{\mathrm{rR}}^{\underline{v}_i \to \underline{v}_f}(\omega) = -\frac{\mathrm{i}}{\hbar} \int_0^\infty \mathrm{d}\tau \sum_{\underline{v}'=\underline{0}}^\infty \langle \underline{v}_f | \hat{\mu}^{\mathrm{S}}(\underline{Q})^\dagger \exp(-\mathrm{i}\hat{H}'\tau/\hbar) | \underline{v}' \rangle \langle \underline{v}' | \hat{\mu}^{\mathrm{L}}(\underline{Q}) \exp(\mathrm{i}\hat{H}\tau/\hbar) | \underline{v}_i \rangle
$$
$$
\exp[\mathrm{i}(\omega - \omega_0)\tau - \tfrac{\Gamma}{2}\tau] \tag{2.15}
$$
$$
= -\frac{\mathrm{i}}{\hbar} \int_0^\infty \mathrm{d}\tau \langle \underline{v}_f | \hat{\mu}^{\mathrm{S}}(\underline{Q})^\dagger \exp(-\mathrm{i}\hat{H}'\tau/\hbar) \hat{\mu}(\underline{Q})^{\mathrm{L}} \exp(\mathrm{i}\hat{H}\tau/\hbar) | \underline{v}_i \rangle
$$
$$
\exp[\mathrm{i}(\omega - \omega_0)\tau - \tfrac{\Gamma}{2}\tau] \tag{2.16}
$$
$$
= -\frac{\mathrm{i}}{\hbar} \int_0^\infty \mathrm{d}\tau \, \chi_\alpha(\tau; \underline{v}_i, \underline{v}_f) \exp[\mathrm{i}(\omega - \omega_0)\tau - \tfrac{\Gamma}{2}\tau], \tag{2.17}
$$

where the rR amplitude TCF (χ_α) is defined with the vibrational transition operator $|\underline{v}_i\rangle\langle\underline{v}_f|$[10],

$$
\chi_\alpha(\tau; \underline{v}_i, \underline{v}_f) = \mathrm{Tr}\left(\hat{\mu}^{\mathrm{S}}(\underline{Q})^\dagger \exp(-\mathrm{i}\hat{H}'\tau/\hbar) \hat{\mu}^{\mathrm{L}}(\underline{Q}) \exp(\mathrm{i}\hat{H}\tau/\hbar) | \underline{v}_i \rangle\langle \underline{v}_f | \right). \tag{2.18}
$$

where we have used the resolution of identity $\sum_{\underline{v}'=\underline{0}}^\infty |\underline{v}'\rangle\langle\underline{v}'| = \hat{1}$. The matrix elements in the time integration of Eqs. (2.12) and (2.16), $\langle\underline{v}|\underline{v}(t)\rangle$ and $\langle\underline{v}_f|\underline{v}_i(\tau)\rangle$ respectively[11], are interpreted as follows [61, 64] (see Fig. 2.1). The initial wavepacket propagating on its ground potential energy surface (PES) is scattered on to the excited PES by the electronic transition dipole moment (TDM), and the scattered wavepacket propagates on the excited PES. Then the wavepacket returns to the vibronic state on the ground electronic state by the electronic TDM. The Fourier transform (FT) of the time correlations corresponds to a spectrum in the frequency domain.

The rR SDF can be expressed from Eqs. (2.7) and (2.17) in incident and scattered photon frequency domain with one Fourier $[-\infty, \infty]$ transformation for the function L in Eq. (2.7) and two half-Fourier $[0, \infty]$ transformations from Eq. (2.17), *i.e.*

$$
\rho_{\mathrm{rR,L}}(\omega, \omega_{\mathrm{S}}) = Z_{\mathrm{I}}^{-1} \hbar^{-3} \sum_{\underline{v}_i, \underline{v}_f = \underline{0}}^\infty \int_{-\infty}^\infty \mathrm{d}t \int_0^\infty \mathrm{d}\tau \int_0^\infty \mathrm{d}\tau' \chi_\alpha(\tau'; \underline{v}_i, \underline{v}_f)^* \chi_\alpha(\tau; \underline{v}_i, \underline{v}_f)
$$
$$
\exp[\mathrm{i}(\omega - \omega_0)(\tau - \tau') - \tfrac{\Gamma}{2}(\tau + \tau')] \exp[\mathrm{i}(\omega - \omega_{\mathrm{S}})t - \tfrac{\Gamma_{\mathrm{rR}}}{2}|t|] \tag{2.19}
$$
$$
= \hbar^{-3} \int_{-\infty}^\infty \mathrm{d}t \int_0^\infty \mathrm{d}\tau \int_0^\infty \mathrm{d}\tau' \chi_{\mathrm{rR}}(t, \tau, \tau'; T)
$$
$$
\exp[\mathrm{i}(\omega - \omega_0)(\tau - \tau') - \tfrac{\Gamma}{2}(\tau + \tau')] \exp[\mathrm{i}(\omega - \omega_{\mathrm{S}})t - \tfrac{\Gamma_{\mathrm{rR}}}{2}|t|], \tag{2.20}
$$

---

[10]One may consider the summation in Eq. (2.15) as trace over virtual vibrational states.

[11]$|\underline{v}(t)\rangle = \hat{\mu}(Q)^\dagger \exp(-\mathrm{i}\hat{H}'t/\hbar) \hat{\mu}(Q) \exp(\mathrm{i}\hat{H}t/\hbar) \exp(-\beta\hat{H}) |\underline{v}\rangle$ and

$|\underline{v}_i(\tau)\rangle = \hat{\mu}^{\mathrm{S}}(Q)^\dagger \exp(-\mathrm{i}\hat{H}'\tau/\hbar) \hat{\mu}^{\mathrm{L}}(Q) \exp(\mathrm{i}\hat{H}\tau/\hbar) |\underline{v}_i\rangle$

where we define a 3-point (t, τ, τ') thermal TCF in a trace form for rR intensity,

$$
\begin{aligned}
\chi_{\mathrm{rR}}(t, \tau, \tau'; T) = & Z_{\mathrm{I}}^{-1} \mathrm{Tr}\Big(\exp(-\mathrm{i}\hat{H}\tau'/\hbar)\hat{\mu}^{\mathrm{L}}(\underline{Q})^{\dagger} \exp(\mathrm{i}\hat{H}'\tau'/\hbar)\hat{\mu}^{\mathrm{S}}(\underline{Q}) \exp(-\mathrm{i}\hat{H}t/\hbar) \\
& \hat{\mu}^{\mathrm{S}}(\underline{Q})^{\dagger} \exp(-\mathrm{i}\hat{H}'\tau/\hbar)\hat{\mu}^{\mathrm{L}}(\underline{Q}) \exp(\mathrm{i}\hat{H}\tau/\hbar) \exp(\mathrm{i}\hat{H}t/\hbar) \exp(-\beta\hat{H})\Big).
\end{aligned}
\tag{2.21}
$$

Within the Condon approximation ($\hat{\underline{\mu}}(\underline{Q}) = \hat{\underline{\mu}}(\underline{Q} = \underline{Q}_0) = \underline{\mu}_0 = $ a constant vector, $\underline{Q}_0$ is the equilibrium molecular structure of the electronic ground state) the Rayleigh scattering ($\omega = \omega_{\mathrm{S}}$) intensity can be expressed in terms of a single Fourier transformation [66] from Eq. (2.20) [56, 66]. In Eq. (2.20), the integration over t with the Rayleigh scattering condition ($\delta(\omega - \omega_{\mathrm{S}})$) gives $\frac{4}{\Gamma_{\mathrm{rR}}}$ and the two half-Fourier integrations over τ and τ' are merged to be a (full) Fourier transformation with newly defined integral variables $\tau^+ = \tau + \tau'$ and $\tau^- = \tau - \tau'$. The integration over τ^- results in a factor Γ^{-1} and the remaining integration is the FT in τ^+, *i.e.*

$$
\rho_{\mathrm{rR,L}}^{\mathrm{Condon-Rayleigh}}(\omega) = \frac{4}{\hbar^2 \Gamma_{\mathrm{rR}}\Gamma} \int_{-\infty}^{\infty} \mathrm{d}\tau^+ \chi(\tau^+; T)\Big|_{\underline{Q}=\underline{Q}_0} \exp[\mathrm{i}(\omega - \omega_0)\tau - \tfrac{\Gamma}{2}|\tau|].
\tag{2.22}
$$

Note that the thermal TCF for the Rayleigh scattering intensity in the Condon approximation is expressed as the TCF of OPA in Eq. (2.14) in the Condon approximation, *i.e.*

$$
\chi(\tau^+; T)\Big|_{\underline{Q}=\underline{Q}_0} = \frac{|\underline{\mu}_0|^4}{Z_{\mathrm{I}}} \mathrm{Tr}\Big(\exp(-\mathrm{i}\hat{H}'\tau/\hbar) \exp(\mathrm{i}\hat{H}\tau/\hbar) \exp(-\beta\hat{H})\Big).
\tag{2.23}
$$

The Condon-Rayleigh scattering is interpreted as the total fluorescence emission [66]. Therefore the FCF can be viewed in two different ways: (i) For the absorption process the transition amplitude is $\langle \underline{v}'|\underline{v}\rangle$ and the corresponding transition probability is the absolute square, $|\langle \underline{v}'|\underline{v}\rangle|^2$. (ii) For the total fluorescence process, the initial vibrational state $|\underline{v}\rangle$ is excited to the final vibrational state $|\underline{v}'\rangle$, *i.e.* after the transition the system stays in the vibrational state $|\underline{v}'\rangle\langle \underline{v}'|\underline{v}\rangle$. When the system returns to the initial vibrational state, the corresponding amplitude is $\langle \underline{v}|\underline{v}'\rangle\langle \underline{v}'|\underline{v}\rangle = |\langle \underline{v}'|\underline{v}\rangle|^2$, while this amplitude is the transition probability (FCF) in the absorption process.

For the treatment of FC-forbidden or weakly FC-allowed transitions ($|\underline{\mu}_0| = 0$ or $|\underline{\mu}_0| \simeq 0$, respectively), one must go beyond the FC approximation (*i.e.* beyond the assumption of $\hat{\underline{\mu}}(\underline{Q}) = \underline{\mu}_0$) and incorporate the dependence of $\hat{\underline{\mu}}$ on the vibrational degrees of freedom (DOF) (*e.g.* Eq. (1.15)). Conventionally this expansion is provided in terms of the initial state coordinates $\underline{Q}$. In this case the electronic TDM is expanded at least to the linear order, *i.e.* the HT expansion (Eq. (1.15)).

$$
\begin{aligned}
\hat{\underline{\mu}}(\underline{Q}) &= \langle e|\hat{\underline{\mu}}_{\mathrm{elec}}|g\rangle \\
&= \underline{\mu}_0 + \sum_k \underline{\mu}_k' \hat{Q}_k + \cdots,
\end{aligned}
\tag{2.24}
$$

where the zero-th order ($\underline{\mu}_0$) and the first order ($\underline{\mu}'$) expansion vectors are determined by the first order perturbation of electron and nuclear Coulombic interaction ($V_{\mathrm{e-n}}$) relative to the

nuclear coordinate change. The electric TDM ($\underline{\hat{\mu}}_{\text{elec}}$) is given by the electronic DOF ($\underline{r}_{\text{el}}$), nuclear DOF ($\underline{r}_{\text{nu}}$) and the charge of the proton e_0 and nucleus $Z_a e_0$, *i.e.*

$$\underline{\hat{\mu}}_{\text{elec}} = -e_0 \sum_i \underline{\hat{r}}_{\text{el};i} + e_0 \sum_a Z_a \underline{\hat{r}}_{\text{nu};a}, \tag{2.25}$$

which is a general expression for the electric TDM. The definition in Eq. (1.8) only applies to the two electronic state model. Evaluating the matrix element in the BO electronic wavefunction basis ($|g\rangle$, $|e\rangle$ and $|l\rangle$) the nuclear contribution of the electronic TDM vanishes due to the orthogonality of different BO electronic wavefunctions. The expansion vectors are given as

$$\underline{\mu}_0 = \langle e|\underline{\hat{\mu}}_{\text{elec}}|g\rangle\Big|_{\underline{Q}=\underline{Q}_0}, \tag{2.26}$$

$$\underline{\mu}_k' = \frac{\partial}{\partial Q_k}\langle e|\underline{\hat{\mu}}_{\text{elec}}|g\rangle\Big|_{\underline{Q}=\underline{Q}_0} = \langle \frac{\partial e}{\partial Q_k}|\underline{\hat{\mu}}_{\text{elec}}|g\rangle\Big|_{\underline{Q}=\underline{Q}_0} + \langle e|\underline{\hat{\mu}}_{\text{elec}}|\frac{\partial g}{\partial Q_k}\rangle\Big|_{\underline{Q}=\underline{Q}_0}. \tag{2.27}$$

The first order derivative of electronic TDM with respect to the k-th normal mode Q_k at the equilibrium structure ($\underline{Q} = \underline{Q}_0$), *i.e.* $\underline{\mu}_k'$ can be calculated analytically either via the traditional perturbation theory formulation (see *e.g.* Refs. [2, 21, 42, 139]) or the linear response approach (see *e.g.* Ref. [52]). The perturbation expression of the electronic Hamiltonian with respect to the nuclear coordinate change shows the explicit coupling between BO electronic eigenstates, for example according to Ref. [42] Eq. (2.27) is expressed as the first order perturbation expansion,

$$\underline{\mu}_k' = \left[\sum_{l\neq e}^{L'} \frac{\langle e|\frac{\partial V_{\text{e-n}}}{\partial Q_k}|l\rangle}{E_l^0 - E_e^0}\langle l|\underline{\hat{\mu}}_{\text{elec}}|g\rangle + \sum_{l\neq g}^{L} \frac{\langle l|\frac{\partial V_{\text{e-n}}}{\partial Q_k}|g\rangle}{E_l^0 - E_g^0}\langle e|\underline{\hat{\mu}}_{\text{elec}}|l\rangle \right]_{\underline{Q}=\underline{Q}_0}, \tag{2.28}$$

where L and L' are the number of intermediate electronic states ($|l\rangle$) which are allowed by electronic state couplings ($\langle l|\underline{\hat{\mu}}_{\text{elec}}|g\rangle|_{\underline{Q}=\underline{Q}_0} \neq \underline{0}$ or $\langle e|\underline{\hat{\mu}}_{\text{elec}}|l\rangle|_{\underline{Q}=\underline{Q}_0} \neq \underline{0}$) with respect to the ground state ($|g\rangle$) and excited state ($|e\rangle$), respectively. The energy differences in the denominators are defined to be electronic transition energies in the unperturbed electronic BO eigenstate basis. Due to the coupling between BO electronic eigenstates, the HT electronic transition mechanism is usually called a vibronic intensity borrowing mechanism (see *e.g.* Refs. [2, 21, 42, 108, 139]). The sum-over-states perturbation expression (2.28) is, however, not practical because of its convergence problems (see *e.g.* Refs. [2, 36]). Recently a linear response formulation for analytic derivatives of the electronic wavefunctions (Eq. (2.27)) with respect to displacements of the nuclei was developed and exploited for calculations within the HT framework in Ref. [52]. The HT vibronic transition GF developed in chapter 6 is tested successfully in Ref. [52] (Sec. 6.3.2). Usually, the gradient of the electronic TDM was evaluated numerically by shifting the molecular equilibrium structure along the normal modes (see *e.g.* Refs. [2, 36]), which leads, however, to difficulties due to the phase of the electronic TDM.

The time-independent representation for the absorption spectrum of Eq. (2.1), the SDF, can then be decomposed into the FC and higher order non-Condon contributions, respec-

tively. This term-wise expansion yields[12]

$$\rho_{\text{FC,L}}(\omega;T) = |\underline{\mu}_0|^2 \sum_{\underline{v},\underline{v}'=\underline{0}}^{\infty} p_{\underline{v}}(T)|\langle \underline{v}'|\underline{v}\rangle|^2 L(\omega,\omega_0 + \omega_{\underline{v}',\underline{v}};\Gamma)\,, \tag{2.29}$$

for the FC contribution and

$$\rho_{\text{FC/HT,L}}(\omega;T) = 2\sum_{i=1}^{N} \underline{\mu}_0 \cdot \underline{\mu}'_i \Big[\sum_{\underline{v},\underline{v}'=\underline{0}}^{\infty} p_{\underline{v}}(T)\langle \underline{v}'|\hat{Q}_i|\underline{v}\rangle\langle \underline{v}|\underline{v}'\rangle L(\omega,\omega_0 + \omega_{\underline{v}',\underline{v}};\Gamma)\Big], \tag{2.30}$$

$$\rho_{\text{HT,L}}(\omega;T) = \sum_{i,j=1}^{N} \underline{\mu}'_i \cdot \underline{\mu}'_j \Big[\sum_{\underline{v},\underline{v}'=\underline{0}}^{\infty} p_{\underline{v}}(T)\langle \underline{v}'|\hat{Q}_i|\underline{v}\rangle\langle \underline{v}|\hat{Q}_j|\underline{v}'\rangle L(\omega,\omega_0 + \omega_{\underline{v}',\underline{v}};\Gamma)\Big], \tag{2.31}$$

for the Franck-Condon/Herzberg-Teller interference (FC/HT) and HT contributions. The FCHT term weighted density of states (FCHTW) is then defined as,

$$\begin{aligned}\rho_{\text{L}}(\omega;T) &\simeq \rho_{\text{FCHTW,L}}(\omega;T) \\ &= \rho_{\text{FC,L}}(\omega;T) + \rho_{\text{FC/HT,L}}(\omega;T) + \rho_{\text{HT,L}}(\omega;T)\,. \end{aligned} \tag{2.32}$$

Those term-wise expressions and the corresponding TCFs are exploited for the HT GF developments of the TI and TD approaches in chapter 6. The rR scattering SDF can also be expressed in the term-wise fashion with the HT expansion. But the explicit expansions will not be exploited in this thesis. The HT expansion expression for rR can be found in many books and articles (see *e.g.* Refs. [6, 60]).

For the evaluation of the SDFs and TCFs in two sets of harmonic oscillator basis, we need to consider, in which coordinate system the two sets of harmonic oscillators are defined. The matrix elements in the TI and TD approach are typically evaluated by integration in position space. When the vibronic wavefunctions in the initial and final electronic states are expressed in the corresponding normal coordinate systems, the relation between the two coordinate systems has to be defined for the integral evaluation. This will be discussed in the following section.

2.2. Duschinsky rotation

In evaluating overlap integrals and matrix elements in the vibrational wavefunction basis of two electronic states within the BO approximation, the choice of the coordinate system (in which the vibrational wavefunctions of two different BO surfaces are defined) is crucial.

If the two BO surfaces can be approximated as two harmonic potential surfaces, it appears beneficial to approximate the vibrational wavefunctions with harmonic oscillators centered at the corresponding equilibrium molecular structures instead of using one common set. One has to evaluate, therefore in the most general case, inseparable multi-dimensional over-lap integrals for FCFs. When the vibrational wavefunctions of the two electronic states were expressed in one center basis set (*e.g.* harmonic oscillator basis set), it would be triv-

---

[12]The corresponding stick representations with the Dirac δ-distribution are simply obtained by replacing the Lorentzian line shape function L with the Dirac δ-distribution.

ial to evaluate the overlap integrals. However, at this point one would need a larger basis set to describe the vibrational wavefunction properly for both electronic states (where the local potential minima are shifted relative to each other) which increases the computational complexity.

Herein the two reference point approach is adopted within the harmonic and Duschinsky approximation. The corresponding matrix element of an operator $\hat{f}$ in the Duschinsky rotated harmonic oscillator basis set reads

$$\langle \underline{v}' | \hat{f} | \underline{v} \rangle. \tag{2.33}$$

When $\hat{f} = \hat{1}$, the matrix element simply becomes a FC integral, and when $\hat{f} = \hat{Q}_i$, the matrix element becomes a linear (first order) HT integral of the i-th position operator of the initial electronic state. The initial and final vibrational eigenstates are described in molecule fixed axis systems attached to each equilibrium molecular structure $\underline{r}_0$ and $\underline{r}_0'$. We choose particular molecule fixed axis systems which minimize the coupling between rotational and vibrational DOFs so that we can use the separation ansatz for rotational and vibrational wavefunctions. This assumption could be supported by the Eckart conditions [1, 101, 140], which minimizes, when fulfills the arrangements, the vibrational angular momentum and the Coriolis coupling in the molecular Hamiltonian (see *e.g.* Ref. [141]), for the initial and final molecular systems, *i.e.*

$$\sum_{a=1}^{N_{\text{atom}}} m_a \underline{r}_{0,a} \times \underline{r}_a = 0, \quad \sum_{a=1}^{N_{\text{atom}}} m_a \underline{r}_{0,a}' \times \underline{r}_a' = 0, \tag{2.34}$$

where N_{atom} is the number of atoms in the polyatomic system and the vectors with the additional index a indicates the (3-dimensional) Cartesian coordinates of the corresponding atoms and with m_a indicating the mass of atom a. The origins of these molecule fixed axis systems are assigned to the center of mass.

The coordinate space representations of the vibrational states can be obtained by projecting on the position operator eigenstates $|Q\rangle$ and $|Q'\rangle$, where Q and Q' are the mass-weighted normal coordinates, *i.e.* $\langle Q | \underline{v} \rangle$ and $\langle Q' | \underline{v}' \rangle$. The Cartesian displacements from each equilibrium structure of the initial and final electronic states are expressed in terms of the corresponding (mass-weighted) normal coordinates, *i.e.*

$$\underline{r} - \underline{r}_0 = \mathbf{M}^{-\frac{1}{2}} \mathbf{L} \underline{Q}, \tag{2.35}$$

$$\underline{r}' - \underline{r}_0' = \mathbf{M}^{-\frac{1}{2}} \mathbf{L}' \underline{Q}', \tag{2.36}$$

where $\mathbf{M}$ is the $N_{\text{nu}} \times N_{\text{nu}}$ diagonal matrix consisting of the masses of atoms, the $N_{\text{nu}} = 3N_{\text{atom}}$ is the number of nuclear DOF and $\mathbf{L}$ and $\mathbf{L}'$ are $N_{\text{nu}} \times (N_{\text{nu}} - 6)$ dimensional matrices for nonlinear molecules and $N_{\text{nu}} \times (N_{\text{nu}} - 5)$ dimensional matrices for linear molecules. The matrices $\mathbf{L}$ and $\mathbf{L}'$ are constructed from a normal mode analysis [1] of the corresponding harmonic force fields from electronic structure calculations.

Even if we could successfully separate the vibrational motions from the other DOF by the Eckart transformations [1, 101, 140] (which is, however, not possible), we would need to consider the alignment between the two coordinate systems carefully, because sudden

axis-switching [142] can cause artifacts in the vibronic spectrum calculations. When the equilibrium structures of the two electronic states are different, the axis systems ($\underline{r}$ and $\underline{r}'$) from the Eckart conditions (2.34) fixed on the equilibrium structures are typically differently oriented. We determine the alignment of the two axis system via finding the Eckart condition again but with respect to the initial equilibrium structure $\underline{r}_0$ as the reference structure. Then the two axis systems ($\underline{r}$ and $\underline{r}'$) are adjusted to the initial state Eckart axes. The Cartesian coordinates are related by a rotation matrix depending on the normal coordinate ($\underline{Q}$), *i.e.*

$$\underline{r}' = \mathbf{T}(\underline{Q})\underline{r}. \tag{2.37}$$

The rotation matrix is called Eckart transformation matrix (axis-switching matrix) [39,143] and it is a unitary transformation matrix, *i.e.*

$$\mathbf{T}(\underline{Q})^{\mathrm{t}}\mathbf{T}(\underline{Q}) = \mathbf{I}. \tag{2.38}$$

The corresponding Eckart condition is given as

$$\sum_{a=1}^{N_{\mathrm{atom}}} m_a \underline{r}_{0,a} \times (\mathbf{T}_a(\underline{Q})^{\mathrm{t}}\underline{r}'_a) = 0, \tag{2.39}$$

where $\mathbf{T}_a$ is a 3-dimensional subblock matrix of $\mathbf{T}$ corresponding to the atom a. Recently Kudin and Dymarsky [144] showed that the root-mean-square deviation minimization condition, another widely used conformation alignment condition in crystallography, leads to one arrangement fulfilling the Eckart condition (2.39), provided that, mass weighting is included

$$\min_{\mathbf{T}(\underline{Q})} \sum_a m_a |\underline{r}_{0,a} - (\mathbf{T}_a(\underline{Q})^{\mathrm{t}}\underline{r}'_a)|^2. \tag{2.40}$$

We can find an Eckart transition matrix $\mathbf{T}(\underline{Q})$ by searching for a symmetric matrix $\mathbf{V}(\underline{Q})$, which is a necessary condition for the vanishing vector product in the Eckart equation (2.39), *i.e.*

$$\mathbf{V}(\underline{Q}) = \underline{r}_0^{'\mathrm{t}}\mathbf{M}\underline{r}\mathbf{T}(\underline{Q})^{\mathrm{t}} = \underline{r}_0^{'\mathrm{t}}\left(\mathbf{M}\underline{r}_0 + \mathbf{M}^{\frac{1}{2}}\mathbf{L}\underline{Q}\right)\mathbf{T}(\underline{Q})^{\mathrm{t}} = \mathbf{V}(\underline{Q})^{\mathrm{t}}. \tag{2.41}$$

We can relate the normal coordinates $\underline{Q}$ and $\underline{Q}'$ in Eqs. (2.35) and (2.36) via the transformation (2.37) using the unitary relation (2.38),

$$\underline{Q}' = \mathbf{L}^{'\mathrm{t}}\mathbf{M}^{\frac{1}{2}}\mathbf{T}(\underline{Q})\left(\underline{r}_0 - \mathbf{T}(\underline{Q})^{\mathrm{t}}\underline{r}'_0\right) + \mathbf{L}^{'\mathrm{t}}\mathbf{T}(\underline{Q})\mathbf{L}\underline{Q}. \tag{2.42}$$

The coordinate dependent rotation matrix, however, is complicated to include because its coordinate dependence is not formally known in a closed analytic form. In order to handle it, we expand $\mathbf{T}(\underline{Q})$ with respect to the normal coordinate $\underline{Q}$. The zero-th order term $\mathbf{T}_0 = \mathbf{T}(\underline{Q} = \underline{Q}_0)$ can be found by the symmetry condition via the singular value decom-

position [140, 145]. From Eq. (2.41), we obtain

$$\mathbf{V}_0 = \mathbf{V}(\underline{Q}_0) = \underline{r}_0^{'\mathrm{t}} \mathbf{M} \underline{r}_0 \mathbf{T}_0^{\mathrm{t}} = \mathbf{V}_0^{\mathrm{t}}. \tag{2.43}$$

Then we have a linear transformation between the two sets of normal coordinates by introducing the coordinate expansion to the Eckart transformation matrices in Eq. (2.42) and neglecting nonlinear terms. The Duschinsky linear transformation relation is given as

$$\underline{Q}' = \underline{d} + \mathbf{S}\underline{Q} + \mathcal{O}(\underline{Q}^2), \tag{2.44}$$

which is already a good approximation for vibronic spectra [146]. Here $\mathbf{S}$ is the Duschinsky mode mixing matrix, which rotates the initial normal coordinates $\underline{Q}$, and the displacement vector $\underline{d}$ is associated to the molecular structural changes shifting the origin of the final harmonic oscillators to that of the initial ones,

$$\underline{d} = \mathbf{L}^{'\mathrm{t}} \mathbf{M}^{\frac{1}{2}} \mathbf{T}_0 \left(\underline{r}_0 - \mathbf{T}_0^{\mathrm{t}} \underline{r}_0' \right), \tag{2.45}$$

$$\mathbf{S} = \mathbf{L}^{'\mathrm{t}} \mathbf{T}_0 \mathbf{L} + \mathbf{L}^{'\mathrm{t}} \mathbf{T}_0 \mathbf{M}^{\frac{1}{2}} \underline{r}_0 \left(\mathrm{Tr}(\mathbf{V}_0) \mathbf{I} - \mathbf{V}_0 \right)^{-1} \mathbf{M}^{\frac{1}{2}} \underline{r}_0^{'\mathrm{t}} \mathbf{T}_0 \mathbf{L}. \tag{2.46}$$

When the molecular structural changes ($|\underline{d}|^2$) are small, the second term in the $\mathbf{S}$ matrix (2.46) can be ignored [39]. This will be assumed in this thesis. But the second term of the $\mathbf{S}$ matrix and even the nonlinear terms have to be considered when there is a large molecular structural deformation.

Ideally, for the N-dimensional harmonic oscillator (complete separation of the rotational and translational motions from the vibrational modes), the Duschinsky rotation matrix $\mathbf{S}$ is an orthogonal matrix and its determinant is unity. Then the Duschinsky relation (2.44) becomes exactly a linear unitary transformation and the higher order nonlinear expansion terms vanish. However, in polyatomic molecular systems this normal coordinate transformation is generally nonlinear (see *e.g.* Refs. [39, 110, 140, 142, 147–150]) because the Eckart axis transition matrix $\mathbf{T}(\underline{Q})$ depends nonlinearly on the instantaneous displacements dynamically from the equilibrium structures.

To evaluate overlap integrals of CSs, FC integrals and non-Condon integrals exploiting the coordinate space representations of CSs and harmonic oscillator eigenstates, we need to transform one coordinate representation to the other according to the Duschinsky relation (2.44). The Duschinsky linear equation (2.44) is translated into a unitary transformation operator for the coordinate systems appearing in the overlap integration.

The N-dimensional harmonic oscillator Hamiltonian is defined as for the initial electronic state

$$\begin{aligned} \hat{H} &= \frac{1}{2} \hat{\underline{P}} \cdot \hat{\underline{P}} + \frac{1}{2} \hat{\underline{Q}}^{\mathrm{t}} \mathbf{\Omega}^4 \hat{\underline{Q}} - E_{\mathrm{zp}} \\ &= \frac{\hbar}{2} \hat{\underline{a}}^{\dagger\mathrm{t}} \mathbf{\Omega}^2 \hat{\underline{a}}, \end{aligned} \tag{2.47}$$

in terms of the annihilation ($\{\hat{a}_i\}$) and the creation ($\{\hat{a}_i^{\dagger}\}$) operators corresponding to the harmonic oscillators with harmonic energies $\{\epsilon_i\}$. The diagonal matrix of the (square root)

harmonic angular frequencies is defined and used,

$$\mathbf{\Omega} = \hbar^{-\frac{1}{2}} \mathrm{diag}(\underline{\epsilon})^{\frac{1}{2}}, \tag{2.48}$$

where "diag" stands for diagonal. It transforms a vector to a square matrix with the diagonal elements being identical to the vector and off-diagonal elements being zero. In addition, the zero-point vibrational energy ($E_{\mathrm{zp}} = \frac{1}{2}\mathrm{Tr}(\mathrm{diag}(\underline{\epsilon}))$) is subtracted from the vibrational Hamiltonian for convenience. The operators satisfy the following relations,

$$\underline{\hat{Q}} = \sqrt{\tfrac{\hbar}{2}} \mathbf{\Omega}^{-1}(\underline{\hat{a}}^{\dagger} + \underline{\hat{a}}), \tag{2.49}$$

$$\underline{\hat{P}} = \mathrm{i}\sqrt{\tfrac{\hbar}{2}} \mathbf{\Omega}(\underline{\hat{a}}^{\dagger} - \underline{\hat{a}}), \tag{2.50}$$

corresponding to the (mass-weighted) position[13] operator and the conjugate momentum operator. The commutation relations of the annihilation and creation operators are

$$[\hat{a}_i, \hat{a}_j] = 0, \quad [\hat{a}_i^{\dagger}, \hat{a}_j^{\dagger}] = 0, \quad [\hat{a}_i, \hat{a}_j^{\dagger}] = \delta_{ij}. \tag{2.51}$$

The harmonic oscillator eigenfunctions in coordinate space are given as products of one-dimensional Hermite polynomials[14],

$$\langle \underline{Q}|\underline{v}\rangle = \prod_{i=1}^{N} \frac{1}{\sqrt{v_i!}} \left(\frac{\epsilon_i}{\pi\hbar^2}\right)^{\frac{1}{4}} \mathrm{e}^{-\frac{\epsilon_i Q_i^2}{2\hbar^2}} \mathcal{H}_{v_i}\left(\sqrt{\frac{2\epsilon_i}{\hbar^2}}Q_i\right), \tag{2.52}$$

where $|\underline{v}\rangle$ is an N-dimensional ONV representation of the N-dimensional harmonic oscillator eigenstates with corresponding vibrational energy $E_{\underline{v}} = \underline{v} \cdot \underline{\epsilon}$. The action of the annihilation and creation operators on the ONV follows

$$\hat{a}_i|\underline{v}\rangle = \sqrt{v_i}|v_1, \ldots, v_i - 1, \ldots, v_N\rangle, \quad \hat{a}_i^{\dagger}|\underline{v}\rangle = \sqrt{v_i + 1}|v_1, \ldots, v_i + 1, \ldots, v_N\rangle. \tag{2.53}$$

Similarly the N-dimensional harmonic oscillator Hamiltonian of the final electronic state is given by

$$\begin{aligned} \hat{H}' &= \frac{1}{2}\underline{\hat{P}}' \cdot \underline{\hat{P}}' + \frac{1}{2}\underline{\hat{Q}}^{'\mathrm{t}}\mathbf{\Omega}^{'4}\underline{\hat{Q}}' - E'_{\mathrm{zp}} \\ &= \frac{\hbar}{2}\underline{\hat{a}}^{'\dagger\mathrm{t}}\mathbf{\Omega}^{'2}\underline{\hat{a}}', \end{aligned} \tag{2.54}$$

in terms of the annihilation ($\{\hat{a}_i'\}$) and the creation ($\{\hat{a}_i^{'\dagger}\}$) operators corresponding to the harmonic oscillators of harmonic energies $\{\epsilon_i'\}$. The diagonal matrix of (square root) harmonic angular frequencies is

$$\mathbf{\Omega}' = \hbar^{-\frac{1}{2}} \mathrm{diag}(\underline{\epsilon}')^{\frac{1}{2}}. \tag{2.55}$$

---

[13] in a dimension of $\sqrt{\mathrm{Mass}} \times \mathrm{Length}$.

[14] $\mathcal{H}_v(x) = (-1)^v \mathrm{e}^{x^2/2} \frac{\mathrm{d}^v}{\mathrm{d}x^v} \mathrm{e}^{-x^2/2}$.

In addition, the zero-point vibrational energy ($E'_{\mathrm{zp}} = \frac{1}{2}\mathrm{Tr}(\mathrm{diag}(\underline{\epsilon}'))$) is subtracted from the vibrational Hamiltonian for convenience. The operators satisfy the corresponding relations of Eq. (2.49)-(2.53) in which the primes "'" shall be used to indicate operators belonging to the final states.

Doktorov *et al.* [24,26] defined a unitary operator ($\hat{U}_{\mathrm{Doktorov}}$) which performs the Duschinsky transformation. It is composed of a translation operator ($\hat{U}_{\mathrm{translation}}$), two distortion operators ($\hat{U}_{\mathrm{distortion}}$ and $\hat{U}'_{\mathrm{distortion}}$) and a rotation operator ($\hat{U}_{\mathrm{rotation}}$). The Doktorov and coworker's [24, 26] unitary operator is given as

$$\hat{U}_{\mathrm{Doktorov}} = \hat{U}_{\mathrm{translation}}\hat{U}'^{\dagger}_{\mathrm{distortion}}\hat{U}_{\mathrm{distortion}}\hat{U}_{\mathrm{rotation}}, \tag{2.56}$$

where

$$\hat{U}_{\mathrm{translation}} = \mathrm{e}^{\frac{1}{\sqrt{2\hbar}}\underline{d}^{\mathrm{t}}\boldsymbol{\Omega}'(\hat{\underline{a}}^{\dagger}-\hat{\underline{a}})} = \mathrm{e}^{-\frac{\mathrm{i}}{\hbar}\underline{d}^{\mathrm{t}}\boldsymbol{\Omega}'\boldsymbol{\Omega}^{-1}\hat{\underline{P}}}, \tag{2.57}$$

$$\hat{U}'_{\mathrm{distortion}} = \mathrm{e}^{-\frac{1}{2}(\hat{\underline{a}}^{\dagger}+\hat{\underline{a}})^{\mathrm{t}}\ln\boldsymbol{\Omega}'(\hat{\underline{a}}^{\dagger}-\hat{\underline{a}})+\frac{1}{2}\mathrm{Tr}(\ln\boldsymbol{\Omega}')} = \mathrm{e}^{\frac{\mathrm{i}}{\hbar}\hat{\underline{Q}}^{\mathrm{t}}\boldsymbol{\Omega}\ln\boldsymbol{\Omega}'\boldsymbol{\Omega}^{-1}\hat{\underline{P}}+\frac{1}{2}\mathrm{Tr}(\ln\boldsymbol{\Omega}')}, \tag{2.58}$$

$$\hat{U}_{\mathrm{distortion}} = \mathrm{e}^{-\frac{1}{2}(\hat{\underline{a}}^{\dagger}+\hat{\underline{a}})^{\mathrm{t}}\ln\boldsymbol{\Omega}(\hat{\underline{a}}^{\dagger}-\hat{\underline{a}})+\frac{1}{2}\mathrm{Tr}(\ln\boldsymbol{\Omega})} = \mathrm{e}^{\frac{\mathrm{i}}{\hbar}\hat{\underline{Q}}^{\mathrm{t}}\ln\boldsymbol{\Omega}\hat{\underline{P}}+\frac{1}{2}\mathrm{Tr}(\ln\boldsymbol{\Omega})}, \tag{2.59}$$

$$\hat{U}_{\mathrm{rotation}} = \mathrm{e}^{\frac{1}{2}(\hat{\underline{a}}^{\dagger\mathrm{t}}\ln\mathbf{S}\hat{\underline{a}}-\hat{\underline{a}}^{\mathrm{t}}\ln\mathbf{S}\hat{\underline{a}}^{\dagger})} = \mathrm{e}^{\frac{\mathrm{i}}{2\hbar}[\boldsymbol{\Omega}\hat{\underline{Q}},\ln\mathbf{S}\boldsymbol{\Omega}^{-1}\hat{\underline{P}}]}. \tag{2.60}$$

Instead, however, in this thesis a unitary operator $\hat{U}$ which also performs the Duschinsky transformation is defined in position space similarly to the squeezing operator (see *e.g.* Ref. [151]), *i.e.*

$$\hat{U} = \int \mathrm{d}\underline{Q}|\underline{Q}'\rangle\langle\underline{Q}|$$
$$= |\det(\mathbf{S})|^{\frac{1}{2}}\int\mathrm{d}\underline{Q}|\mathbf{S}\underline{Q}+\underline{d}\rangle\langle\underline{Q}|, \tag{2.61}$$

$$\hat{U}^{\dagger} = |\det(\mathbf{S})|^{\frac{1}{2}}\int\mathrm{d}\underline{Q}|\underline{Q}\rangle\langle\mathbf{S}\underline{Q}+\underline{d}|, \tag{2.62}$$

or equivalently in momentum space as

$$\hat{U} = \left(\int\mathrm{d}\widetilde{\underline{P}}|\widetilde{\underline{P}}\rangle\langle\widetilde{\underline{P}}|\right)\hat{U}\left(\int\mathrm{d}\underline{P}|\underline{P}\rangle\langle\underline{P}|\right)$$
$$= |\det(\mathbf{S})|^{\frac{1}{2}}\int\mathrm{d}\underline{P}|\underline{P}\rangle\langle\mathbf{S}^{\mathrm{t}}\underline{P}|\exp(-\mathrm{i}\underline{P}\cdot\underline{d}/\hbar), \tag{2.63}$$

$$\hat{U}^{\dagger} = |\det(\mathbf{S})|^{\frac{1}{2}}\int\mathrm{d}\underline{P}|\mathbf{S}^{\mathrm{t}}\underline{P}\rangle\langle\underline{P}|\exp(\mathrm{i}\underline{P}\cdot\underline{d}/\hbar), \tag{2.64}$$

where the prefactor $|\det(\mathbf{S})|^{\frac{1}{2}}$ is introduced to restore unitarity $\hat{U}^{\dagger}\hat{U} = \hat{1}$. For the ideal N-dimensional harmonic oscillators, $|\det(\mathbf{S})| = 1$ but for the polyatomic systems the quantity slightly deviates from one as discussed. The unitary operator transforms the initial state

operators to the final ones and *vice versa*, *i.e.*

$$\hat{\underline{Q}}' = \hat{U}^\dagger \hat{\underline{Q}} \hat{U} = \mathbf{S} \hat{\underline{Q}} + \underline{d}, \tag{2.65}$$

$$\hat{\underline{P}}' = \hat{U}^\dagger \hat{\underline{P}} \hat{U} = (\mathbf{S}^{-1})^{\mathrm{t}} \hat{\underline{P}} = \mathbf{S} \hat{\underline{P}}. \tag{2.66}$$

In which $\mathbf{SS}^{\mathrm{t}} = \mathbf{I}$ is assumed for the momentum operator transformation, which is true only for ideal N-dimensional oscillators ($|\det(\mathbf{S})| = 1$) but not quite true for polyatomic molecules which have a quasi-unitary rotation matrix ($|\det(\mathbf{S})| \simeq 1$). Accordingly we can see the following relations for the position operator eigenstates,

$$\hat{\underline{Q}}|\underline{Q}\rangle = \underline{Q}|\underline{Q}\rangle, \quad \hat{\underline{Q}}'|\underline{Q}'\rangle = \underline{Q}'|\underline{Q}'\rangle,$$

$$\hat{\underline{Q}}'|\underline{Q}\rangle = (\mathbf{S}\underline{Q} + \underline{d})|\underline{Q}\rangle, \quad \hat{\underline{Q}}|\underline{Q}'\rangle = \mathbf{S}^{-1}(\underline{Q}' - \underline{d})|\underline{Q}'\rangle, \tag{2.67}$$

and for the momentum operator eigenstates,

$$\hat{\underline{P}}|\underline{P}\rangle = \underline{P}|\underline{P}\rangle, \quad \hat{\underline{P}}'|\underline{P}'\rangle = \underline{P}'|\underline{P}'\rangle,$$

$$\hat{\underline{P}}'|\underline{P}\rangle = (\mathbf{S}^{-1})^{\mathrm{t}}\underline{P}|\underline{P}\rangle, \quad \hat{\underline{P}}|\underline{P}'\rangle = \mathbf{S}^{\mathrm{t}}\underline{P}'|\underline{P}'\rangle. \tag{2.68}$$

The annihilation and creation operators in the initial and the final states are related by a similar equation to the linear Duschinsky expression (2.44), *i.e.*

$$\begin{pmatrix} \hat{\underline{a}}' \\ \hat{\underline{a}}'^\dagger \end{pmatrix} = \frac{1}{2} \begin{pmatrix} \mathbf{J} + (\mathbf{J}^{-1})^{\mathrm{t}} & \mathbf{J} - (\mathbf{J}^{-1})^{\mathrm{t}} \\ \mathbf{J} - (\mathbf{J}^{-1})^{\mathrm{t}} & \mathbf{J} + (\mathbf{J}^{-1})^{\mathrm{t}} \end{pmatrix} \begin{pmatrix} \hat{\underline{a}} \\ \hat{\underline{a}}^\dagger \end{pmatrix} + \sqrt{2} \begin{pmatrix} \underline{\delta} \\ \underline{\delta} \end{pmatrix}, \tag{2.69}$$

where the N-dimensional square matrix $\mathbf{J}$ and the N-dimensional vector $\underline{\delta}$ are defined as

$$\mathbf{J} = \mathbf{\Omega}' \mathbf{S} \mathbf{\Omega}^{-1}, \quad \underline{\delta} = \hbar^{-\frac{1}{2}} \mathbf{\Omega}' \underline{d}. \tag{2.70}$$

Accordingly the vibrational Hamiltonians are mutually convertible with the Duschinsky unitary transformation, *i.e.*

$$\hat{H}' = \hat{U}^\dagger \hat{H} \hat{U}. \tag{2.71}$$

The primed and unprimed ONVs states ($|\underline{v}'\rangle$ and $|\underline{v}\rangle$, respectively) are the eigenstates of primed and unprimed Hamiltonians ($\hat{H}'$ and $\hat{H}$, respectively), otherwise it will be indicated with its corresponding Hamiltonian, for example $|\underline{v}\rangle_{\hat{H}'}$ is an eigenstate of the primed Hamiltonian but with the unprimed ONV and $|\underline{v}'\rangle_{\hat{H}}$ is the opposite case. As a result of the Duschinsky unitary operator $\hat{U}$ the harmonic eigenstates (ONV states) of each Hamiltonian described in the respective coordinate systems are transformed into each other,

$$\hat{H}\left(\hat{U}|\underline{v}'\rangle\right) = \hat{H}\left(|\underline{v}'\rangle_{\hat{H}}\right) = E_{\underline{v}'}\left(\hat{U}|\underline{v}'\rangle\right), \tag{2.72}$$

$$\hat{H}'\left(\hat{U}^\dagger|\underline{v}\rangle\right) = \hat{H}'\left(|\underline{v}\rangle_{\hat{H}'}\right) E_{\underline{v}}'\left(\hat{U}^\dagger|\underline{v}\rangle\right), \tag{2.73}$$

where the eigenvalues are given by ONVs belong to different electronic states, *i.e.* $E_{\underline{v}'} = \underline{v}' \cdot \underline{\epsilon}$ and $E_{\underline{v}}' = \underline{v} \cdot \underline{\epsilon}'$. Precisely the harmonic eigenstates of initial and final states in each

phase space are transformed to the other phase space by the unitary transformation, *i.e.*

$$\hat{U}|\underline{v}'\rangle = \hat{U}|\underline{v}'\rangle_{\hat{H}'} = |\underline{v}'\rangle_{\hat{H}}, \tag{2.74}$$

$$\hat{U}^{\dagger}|\underline{v}\rangle = \hat{U}^{\dagger}|\underline{v}\rangle_{\hat{H}} = |\underline{v}\rangle_{\hat{H}'}. \tag{2.75}$$

Then the FC integrals in different coordinate systems can be described in one coordinate systems via the Duschinsky unitary transformation operator,

$$\langle \underline{v}'|\underline{v}\rangle = {}_{\hat{H}'}\langle \underline{v}'|\underline{v}\rangle_{\hat{H}} = {}_{\hat{H}}\langle \underline{v}'|\hat{U}|\underline{v}\rangle_{\hat{H}} = {}_{\hat{H}'}\langle \underline{v}'|\hat{U}|\underline{v}\rangle_{\hat{H}}. \tag{2.76}$$

The CS overlap integral is exploited for the FC or non-Condon integrals because the CS is the GF of harmonic eigenstates.

2.3. Basic properties of coherent states

Glauber's coherent state [97] is a special type of quantum harmonic oscillator state which fulfills the minimal uncertainty relation of position and momentum operators. The mean values of position and momentum of a quantum mechanical Gaussian wavepacket [152], which is evolving in time without spreading over phase space, follow the motion of a classical harmonic oscillator in a given harmonic potential. The basic mathematical properties of CSs which are exploited throughout this thesis are briefly reviewed in this section. The Duschinsky unitary operator (2.62) is used for computing the CS overlap integral for Duschinsky related (Eq. (2.44)) CS. Most of the following relations of CSs can be found in Refs. [97, 98], and in many other articles and books (see *e.g.* Ref. [3]).

Coherent states (CSs) are defined in three different ways i) as an eigenstate of the annihilation operator of the quantum harmonic oscillator, ii) as a CS phase displacement operator and iii) as a state satisfying the minimum uncertainty relation. For simple harmonic oscillators all three definitions are equivalent. The minimum uncertainty relation definition of CSs is usually exploited for the CSs of general potentials, *i.e.* nonlinear CSs (see *e.g.* Ref. [153]). Only the definitions i) and ii) shall be exploited for the method developments in the later chapters.

The N-dimensional CS $|\underline{\alpha}\rangle$ is defined as an eigenstate of the N-dimensional annihilation vector operator $\underline{\hat{a}}$,

$$\underline{\hat{a}}|\underline{\alpha}\rangle = \underline{\alpha}|\underline{\alpha}\rangle, \tag{2.77}$$

where $\underline{\alpha} \in \mathbb{C}^{N}$ is a complex-valued N-dimensional vector. The CSs can be expanded in the basis of harmonic oscillator eigenstates,

$$|\underline{\alpha}\rangle = \exp(-\tfrac{1}{2}\underline{\alpha}^{\dagger}\underline{\alpha}) \exp(\underline{\alpha}^{\mathrm{t}}\underline{\hat{a}}^{\dagger})|\underline{0}\rangle \tag{2.78}$$

$$= \exp(-\tfrac{1}{2}\underline{\alpha}^{\dagger}\underline{\alpha}) \sum_{\underline{v}=\underline{0}}^{\infty} \widetilde{\prod_{\underline{v}}}^{-\frac{1}{2}} \overline{\prod_{\underline{\alpha}}}^{\underline{v}} |\underline{v}\rangle, \tag{2.79}$$

where we have defined and used the product notations for factorials and powers of vectors, *i.e.* $\widetilde{\prod}_{\underline{x}_{1},\cdots,\underline{x}_{N}}^{\underline{n}_{1},\cdots,\underline{n}_{N}} = (\prod_{k}(x_{1,k}!)^{n_{1,k}}) \cdots (\prod_{k}(x_{N,k}!)^{n_{N,k}})$ and $\overline{\prod}_{\underline{x}_{1},\cdots,\underline{x}_{N}}^{\underline{n}_{1},\cdots,\underline{n}_{N}} = \left(\prod_{k} x_{1,k}^{n_{1,k}}\right) \cdots \left(\prod_{k} x_{N,k}^{n_{N,k}}\right)$

respectively. The N-dimensional CSs can be partitioned into subspaces X and Y of dimension N_X and $N - N_X$ respectively, *i.e.* $|\underline{\alpha}\rangle = |\underline{\alpha}_X; \underline{\alpha}_Y\rangle$,

$$|\underline{\alpha}_X; \underline{\alpha}_Y\rangle = \exp(-\tfrac{1}{2}|\underline{\alpha}_X|^2 - \tfrac{1}{2}|\underline{\alpha}_Y|^2) \exp(\underline{\alpha}_X^t \underline{a}_X^\dagger + \underline{\alpha}_Y^t \underline{a}_Y^\dagger)|\underline{0}_X; \underline{0}_Y\rangle. \tag{2.80}$$

Then the coherent-Fock state [151] $|\underline{v}_X; \underline{\alpha}_Y\rangle$ can be constructed by partial derivatives with respect to $\{\alpha_{X;i}\}$, *i.e.*

$$|\underline{v}_X; \underline{\alpha}_Y\rangle = \widetilde{\prod}^{-\frac{1}{2}} \hat{\partial}_{\underline{\alpha}_X}^{\underline{v}_X} \left(\exp(\tfrac{1}{2}|\underline{\alpha}_X|^2)|\underline{\alpha}_X; \underline{\alpha}_Y\rangle \right)\Big|_{\underline{\alpha}_X = \underline{0}}, \tag{2.81}$$

where we have defined and used the multi-dimensional partial derivative notation, *i.e.* $\hat{\partial}_{\underline{x}_1, \cdots, \underline{x}_N}^{\underline{n}_1, \cdots, \underline{n}_N} = \left(\frac{\partial^{\sum_k n_{1,k}}}{\prod_k \partial x_{1,k}^{n_{1,k}}} \right) \cdots \left(\frac{\partial^{\sum_k n_{N,k}}}{\prod_k \partial x_{N,k}^{n_{N,k}}} \right)$.

The spatial representation of CSs is given in a normalized form

$$\langle \underline{Q}|\underline{\alpha}\rangle = \overline{\prod}_{(\pi\hbar^2)^{-1}\underline{\epsilon}}^{\frac{1}{4}} \exp\left(-\tfrac{1}{2}\underline{Q}^t\boldsymbol{\Omega}^2\underline{Q} + \sqrt{2}\underline{\alpha}^t\boldsymbol{\Omega}\underline{Q} - \tfrac{1}{2}\underline{\alpha}^t\underline{\alpha} - \tfrac{1}{2}|\underline{\alpha}|^2 \right). \tag{2.82}$$

The conjugate momentum space representation reads

$$\langle \underline{P}|\underline{\alpha}\rangle = \overline{\prod}_{\pi\underline{\epsilon}}^{-\frac{1}{4}} \exp\left[-\tfrac{1}{2}\underline{P}^t\boldsymbol{\Omega}^{-2}\underline{P} - i\sqrt{2}\underline{\alpha}^t\boldsymbol{\Omega}^{-1}\underline{P} + \tfrac{1}{2}\underline{\alpha}^t\underline{\alpha} - \tfrac{1}{2}|\underline{\alpha}|^2 \right], \tag{2.83}$$

which is in a normalized form as well.

Coherent states (CSs) can be defined with a unitary operator, the CS displacement operator, which is defined by

$$\begin{aligned}
\hat{D}(\underline{\alpha}) &= \exp(\underline{\alpha}^t\underline{\hat{a}}^\dagger - \underline{\alpha}^\dagger\underline{\hat{a}}) \\
&= \exp(-\tfrac{1}{2}\sum_k [\hat{a}_k^\dagger, -\hat{a}_k]|\alpha_k|^2) \exp(\underline{\alpha}^t\underline{\hat{a}}^\dagger) \exp(-\underline{\alpha}^\dagger\underline{\hat{a}}) \\
&= \exp(-\tfrac{1}{2}|\underline{\alpha}|^2) \exp(\underline{\alpha}^t\underline{\hat{a}}^\dagger) \exp(-\underline{\alpha}^\dagger\underline{\hat{a}}).
\end{aligned} \tag{2.84}$$

Under the action of $\hat{D}(\underline{\alpha})$ CSs are created from a ground state $|\underline{0}\rangle$ as

$$\hat{D}(\underline{\alpha})|\underline{0}\rangle = |\underline{\alpha}\rangle, \tag{2.85}$$

and the CS displacement operator satisfies the following phase operation rules,

$$\hat{D}^\dagger(\underline{\alpha}) = \hat{D}^{-1}(\underline{\alpha}) = \hat{D}(-\underline{\alpha}), \tag{2.86}$$

$$\hat{D}(\underline{\alpha})\hat{D}(\underline{\gamma}) = \hat{D}(\underline{\alpha} + \underline{\gamma}) \exp[\tfrac{1}{2}(\underline{\gamma}^\dagger\underline{\alpha} - \underline{\gamma}^t\underline{\alpha}^*)], \tag{2.87}$$

$$[\hat{D}(\underline{\alpha}), \hat{D}(\underline{\gamma})] = \hat{D}(\underline{\alpha} + \underline{\gamma})2i\text{Im}\left(\exp[\tfrac{1}{2}(\underline{\gamma}^\dagger\underline{\alpha} - \underline{\gamma}^t\underline{\alpha}^*)] \right), \tag{2.88}$$

The unitary operation on the annihilation and creation operators look like

$$\hat{D}(\underline{\gamma})^{\dagger}\underline{\hat{a}}\hat{D}(\underline{\gamma}) = \underline{\hat{a}} + \underline{\gamma},$$
$$\hat{D}(\underline{\gamma})^{\dagger}\underline{\hat{a}}^{\dagger}\hat{D}(\underline{\gamma}) = \underline{\hat{a}}^{\dagger} + \underline{\gamma}^{*}. \tag{2.89}$$

Using the phase composition rule of Eq. (2.87), one finds

$$\hat{D}(\underline{\alpha})\hat{D}(\underline{\gamma})|\underline{0}\rangle = \hat{D}(\underline{\alpha})|\underline{\gamma}\rangle$$
$$= \exp[\tfrac{1}{2}(\underline{\gamma}^{\dagger}\underline{\alpha} - \underline{\gamma}^{\mathrm{t}}\underline{\alpha}^{*})]\,|\underline{\alpha} + \underline{\gamma}\rangle\,, \tag{2.90}$$

the phase composition state from the vacuum state.

The operation of the harmonic vibrational Hamiltonian $\hat{H}$ (2.47) on a CS appears relatively trivial. A unitary (Eq. (2.91)) and the non-unitary (Eq. (2.92)) transformations of CSs can be shown easily by applying the transforming operators to the occupation representation of the CSs, Eq. (2.79). Under the exponential such operators simply shift the CS phase, *e.g.*

$$\mathrm{e}^{-\mathrm{i}\hat{H}t/2\hbar}|\underline{\alpha}\rangle = |\mathbf{z}(t)\underline{\alpha}\rangle, \tag{2.91}$$

where $\mathbf{z}(t) = \mathrm{diag}(\mathrm{e}^{-\mathrm{i}\epsilon_1 t/2\hbar}, \ldots, \mathrm{e}^{-\mathrm{i}\epsilon_N t/2\hbar})$. The unitary operation like above is called the phase-shifting operation. For non-unitary transformations with a diagonal Hamiltonian in the harmonic oscillator basis, such as for the thermal Boltzmann population of states, an additional factor appears, *i.e.*

$$\mathrm{e}^{-\beta\hat{H}/2}|\underline{\alpha}\rangle = \mathrm{e}^{-\frac{1}{2}\underline{\alpha}^{\dagger}(\mathbf{I}-\mathbf{\Gamma}^{\dagger}\mathbf{\Gamma})\underline{\alpha}}|\mathbf{\Gamma}\underline{\alpha}\rangle\,, \tag{2.92}$$

where $\mathbf{\Gamma} = \mathrm{diag}(\mathrm{e}^{-\beta\epsilon_1/2}, \ldots, \mathrm{e}^{-\beta\epsilon_N/2})$ with the reciprocal temperature $\beta = 1/(k_{\mathrm{B}}T)$ where T is the temperature and k_{B} is the Boltzmann constant. Comparing to the unitary operation (2.91) the CS phase factor is rescaled as well with the Boltzmann related factors ($\mathbf{\Gamma}$) and the non-unitary operation leaves a prefactor (the exponential factor in Eq. (2.92)) which is related to the vibrational partition function (see Sec. 6.1.2).

Coherent states (CSs) are over-complete basis sets satisfying the following resolution of identity [97],

$$\frac{1}{\pi^N}\int \mathrm{d}^2\underline{\alpha}|\underline{\alpha}\rangle\langle\underline{\alpha}| = \hat{1}. \tag{2.93}$$

Two CSs are not orthogonal [97],

$$\langle\underline{\gamma}|\underline{\alpha}\rangle = \exp(-\tfrac{1}{2}|\underline{\alpha}|^2 - \tfrac{1}{2}|\underline{\gamma}|^2)\exp(\underline{\gamma}^{\dagger}\underline{\alpha}). \tag{2.94}$$

The overlap integral of CSs $|\underline{\alpha}\rangle$ and $|\underline{\gamma}'\rangle$, described by the corresponding normal coordinates $\underline{Q}$ and $\underline{Q}'$ respectively in the Duschinsky relation (Eq. (2.44)), can be given in the occupation representation [27] exploiting the occupation representation of the coherent

states (Eq. (2.79)) such that

$$\langle\underline{\gamma}'|\underline{\alpha}\rangle = \exp(-\tfrac{1}{2}\underline{\alpha}^{\dagger}\underline{\alpha} - \tfrac{1}{2}\underline{\gamma}'^{\dagger}\underline{\gamma}') \sum_{\underline{v},\underline{v}'=\underline{0}}^{\infty} \langle\underline{v}'|\underline{v}\rangle \widetilde{\prod}_{\underline{v},\underline{v}'}^{-\frac{1}{2},-\frac{1}{2}} \overline{\prod}_{\underline{\alpha},\underline{\gamma}'^{*}}^{\underline{v},\underline{v}'}, \qquad (2.95)$$

where $|\underline{v}\rangle$ and $|\underline{v}'\rangle$ are the harmonic oscillator eigenstates corresponding to the CSs $|\underline{\alpha}\rangle$ and $|\underline{\gamma}'\rangle$ respectively. The occupation representation of the overlap integral of the CSs, Eq. (2.95) is the GF of the FC integrals[15] with the generating function parameters $\{\alpha_k\}$ and $\{\gamma_k'\}$. The CS overlap integral in the Duschinsky relation is then given by

$$\begin{aligned}
\langle\underline{\gamma}'|\underline{\alpha}\rangle &= \langle\underline{\gamma}'; \underline{Q}', \underline{P}'|\underline{\alpha}; \underline{Q}, \underline{P}\rangle = \langle\underline{\gamma}'; \underline{Q}, \underline{P}|\hat{U}|\underline{\alpha}; \underline{Q}, \underline{P}\rangle \\
&= |\det(\mathbf{S})|^{\frac{1}{2}} \int \mathrm{d}\underline{Q}\langle\underline{\gamma}'|\mathbf{S}\underline{Q} + \underline{d}\rangle\langle\underline{Q}|\underline{\alpha}\rangle \\
&= \langle\underline{0}'|\underline{0}\rangle \exp(-\tfrac{1}{2}\underline{\xi}^{\dagger}\underline{\xi})\mathcal{J}\left[\mathbf{W}, \underline{r}; \underline{\xi}\right] ,
\end{aligned} \qquad (2.96)$$

where the collective CS phase vector is used

$$\underline{\xi} = \begin{pmatrix} \underline{\alpha} \\ \underline{\gamma}'_{*} \end{pmatrix} , \qquad (2.97)$$

and the exponential function $\mathcal{J}$ is defined as $\mathcal{J}[\mathbf{A}, \underline{b}; \underline{x}] = \exp(-\tfrac{1}{2}\underline{x}^{\mathrm{t}}\mathbf{A}\underline{x} + \underline{b}^{\mathrm{t}}\underline{x})$. The overlap integral of CSs that is represented by the Duschinsky rotated harmonic oscillators can be integrated in a closed form by exploiting the spatial representation of CSs, with the corresponding spatial representation[16] Eq. (2.82) being expressed by exponential functions. The Duschinsky relation, Eq. (2.44), is taken into account with the help of Doktorov matrices and vectors [26] as parameters,

$$\mathbf{W} = \begin{pmatrix} \mathbf{I} - 2\mathbf{Q} & -2\mathbf{R} \\ -2\mathbf{R}^{\mathrm{t}} & \mathbf{I} - 2\mathbf{P} \end{pmatrix} , \quad \underline{r} = \sqrt{2}\begin{pmatrix} -\mathbf{R}\underline{\delta} \\ (\mathbf{I} - \mathbf{P})\underline{\delta} \end{pmatrix} . \qquad (2.98)$$

$\mathbf{W}$ is a self-inverse $2N \times 2N$ matrix [117] and the $2N$-dimensional vector $\underline{r}$ should not be confused with Cartesian coordinates in section 2.2. The N-dimensional symmetric positive-definite square matrices $\mathbf{Q}$ and $\mathbf{P}$, and the N-dimensional vector $\underline{\delta}$ are given as

$$\mathbf{Q} = (\mathbf{I} + \mathbf{J}^{\mathrm{t}}\mathbf{J})^{-1}, \quad \mathbf{P} = \mathbf{J}\mathbf{Q}\mathbf{J}^{\mathrm{t}}, \quad \mathbf{R} = \mathbf{Q}\mathbf{J}^{\mathrm{t}}. \qquad (2.99)$$

The Doktorov matrices are related to each other as [117]

$$\mathbf{R}\mathbf{R}^{\mathrm{t}} = \mathbf{Q} - \mathbf{Q}^2, \quad \mathbf{R}^{\mathrm{t}}\mathbf{R} = \mathbf{P} - \mathbf{P}^2, \qquad (2.100)$$

$$\mathbf{R}\mathbf{P}^{-1}\mathbf{R}^{\mathrm{t}} = \mathbf{Q}, \quad \mathbf{R}^{\mathrm{t}}\mathbf{Q}^{-1}\mathbf{R} = \mathbf{P}, \quad \mathbf{Q}\mathbf{R} + \mathbf{R}\mathbf{Q} = \mathbf{R}. \qquad (2.101)$$

The vibrational ground state overlap integral ($\langle\underline{0}'|\underline{0}\rangle$) is expressed with the Doktorov matri-

---

[15]$\langle\underline{v}'|\underline{v}\rangle$
[16]or with the corresponding momentum space representation Eq. (2.83)

ces and vector as well,

$$\langle \underline{0}'|\underline{0}\rangle = 2^{\frac{N}{2}} \left(\frac{\overline{\prod}_{\underline{\epsilon'}}^{\frac{1}{2}}}{\overline{\prod}_{\underline{\epsilon}}^{\frac{1}{2}}} \right)^{\frac{1}{4}} \det(\mathbf{Q})^{\frac{1}{2}} \exp\left(-\frac{1}{2}\underline{\delta}^{\mathrm{t}}(\mathbf{I} - \mathbf{P})\underline{\delta} \right) |\det(\mathbf{S})|^{\frac{1}{2}}$$

$$= 2^{\frac{N}{2}} |\det(\mathbf{R})|^{\frac{1}{2}} \exp\left(-\frac{1}{2}\underline{\delta}^{\mathrm{t}}(\mathbf{I} - \mathbf{P})\underline{\delta} \right) . \tag{2.102}$$

Equating the occupation representation (2.95) of CS overlap integral and the expanded spatial expression (2.96) with respect to the CS phase variables, and comparing CS phase variables to collect same orders we can find the FC integral evaluation scheme. The CS phase variables take a role as FC integral generating function parameters. For example the FC integral evaluation schemes are given in recursion relations (see *e.g.* Refs. [24, 26, 36]). The recursion relations given in Ref. [46] reads

$$\sqrt{v_i + 1}\langle \underline{v}'|v_1, \dots, v_i + 1, \dots, v_N\rangle =$$

$$2\sum_{k=1}^{N} R_{ik}\sqrt{v_k'}\langle v_1', \dots, v_k' - 1, \dots, v_N'|\underline{v}\rangle$$

$$+ \sum_{j=1}^{N} (2\mathbf{Q} - \mathbf{I})_{ij}\sqrt{v_j}\langle \underline{v}'|v_1, \dots, v_j - 1, \dots, v_N\rangle$$

$$- \sqrt{2}(\mathbf{R}\underline{\delta})_i\langle \underline{v}'|\underline{v}\rangle , \tag{2.103}$$

for the initial state, and for the final state

$$\sqrt{v_k' + 1}\langle v_1', \dots, v_k' + 1, \dots, v_N'|\underline{v}\rangle =$$

$$2\sum_{i=1}^{N} R_{ik}\sqrt{v_i}\langle \underline{v}'|v_1, \dots, v_i - 1, \dots, v_N\rangle$$

$$+ \sum_{\ell=1}^{N} (2\mathbf{P} - \mathbf{I})_{k\ell}\sqrt{v_\ell'}\langle v_1', \dots, v_\ell' - 1, \dots, v_N'|\underline{v}\rangle$$

$$+ \sqrt{2}[(\mathbf{I} - \mathbf{P})\underline{\delta}]_k\langle \underline{v}'|\underline{v}\rangle , \tag{2.104}$$

which are exploited in this thesis for the FC integral evaluation with thermal prescreening (Ch. 4) and linear HT prescreening (Ch. 6). The corresponding integral evaluation scheme can be brought into an iterative form (see *e.g.* Refs. [44, 46]). The iterative formula exploited in Ref. [46] is presented here, to show the complexity of the existing iterative formula in comparison of the iterative scheme developed in this thesis (see Ch. 3), *e.g.*

$$\langle \underline{v}'|\underline{v}\rangle = \langle \tilde{u}_1,\ldots,\tilde{u}_N|\tilde{u}_{N+1},\ldots,\tilde{u}_{2N}\rangle =$$

$$\langle \underline{0}'|\underline{0}\rangle \sqrt{\prod_i^{2N} \tilde{u}_i!} \sum_{l_{p,p-1}=0}^{g_{p,p-1}} \frac{A_{p,p-1}^{l_{p,p-1}}}{l_{p,p-1}!} \quad \cdots \quad \sum_{l_{p,j}=0}^{g_{p,j}} \frac{A_{p,j}^{l_{p,j}}}{l_{p,j}!} \sum_{l_{p,j-1}=0}^{g_{p,j-1}} \frac{A_{p,j-1}^{l_{p,j-1}}}{l_{p,j-1}!} \quad \cdots \quad \sum_{l_{p,k}=0}^{g_{p,k}} \frac{A_{p,k}^{l_{p,k}}}{l_{p,k}!} \quad \cdots \quad \sum_{l_{p,1}=0}^{g_{p,1}} \frac{A_{p,1}^{l_{p,1}}}{l_{p,1}!} \sum_{m_p=0}^{[g_p/2]} \frac{A_{p,p}^{m_p} r_p^{g_p-2m_p}}{2^{m_p} m_p! (g_p-2m_p)!}$$

$$\vdots \qquad \vdots$$

$$\times \sum_{l_{j,j-1}=0}^{g_{j,j-1}} \frac{A_{j,j-1}^{l_{j,j-1}}}{l_{j,j-1}!} \quad \cdots \quad \sum_{l_{j,k}=0}^{g_{j,k}} \frac{A_{j,k}^{l_{j,k}}}{l_{j,k}!} \quad \cdots \quad \sum_{l_{j,1}=0}^{g_{j,1}} \frac{A_{j,1}^{l_{j,1}}}{l_{j,1}!} \sum_{m_j=0}^{[g_j/2]} \frac{A_{j,j}^{m_j} r_j^{g_j-2m_j}}{2^{m_j} m_j! (g_j-2m_j)!}$$

$$\vdots \qquad \vdots$$

$$\times \sum_{l_{2,1}=0}^{g_{2,1}} \frac{A_{2,1}^{l_{2,1}}}{l_{2,1}!} \sum_{m_2=0}^{[g_2/2]} \frac{A_{2,2}^{m_2} r_2^{g_2-2m_2}}{2^{m_2} m_2! (g_2-2m_2)!}$$

$$\times \sum_{m_1=0}^{[g_1/2]} \frac{A_{1,1}^{m_1} r_1^{g_1-2m_1}}{2^{m_1} m_1! (g_1-2m_1)!},$$

$$(2.105)$$

with the collectively indexed vector for ONVs of final and initial states

$$\underline{\tilde{u}} = \begin{pmatrix} \underline{v}' \\ \underline{v} \end{pmatrix}, \tag{2.106}$$

and with the setting $\mathbf{A} = -\mathbf{W}$ and $p = 2N$, and

$$g_{p,p-1} = \min(\tilde{u}_p,\ \tilde{u}_{p-1}), \quad g_{p,k} = \min(\tilde{u}_p - \sum_{i=k+1}^{p-1} l_{p,i},\ \tilde{u}_k), \tag{2.107}$$

$$g_{j,k} = \min(\tilde{u}_j - \sum_{i=k+1}^{j-1} l_{j,i} - \sum_{i=j+1}^{p} l_{i,j},\ v_k - \sum_{i=j+1}^{p} l_{i,k}), \quad g_j = \tilde{u}_j - \sum_{i=1}^{j-1} l_{j,i} - \sum_{j+1}^{p} l_{i,j}, \tag{2.108}$$

and $[i]$ is the greatest integer less or equal to i.

2.4. Franck-Condon transition at zero Kelvin

In this section we summarize the FCF GF development and the prescreening strategies at zero Kelvin [46][17]. Based on this previous work, this thesis contributes to extending the existing techniques by taking the thermal effect, non-Condon effect and time-dependence into account. The key idea of this development is exploiting a GF for the FCFs obtained from the CS representations, *cf.* chapter 1. The resulting expressions are in the form of a series summation of polynomials and closed integrals. One can partition the integral spaces into summed-over vibrational states and frozen vibrational states with the proposed partitioning scheme [46]. With the partitioning scheme, the intensity sum rule is exploited for the prescreening strategies developed by Jankowiak *et al.* [46].

---

[17]J. Huh was not involved in this work.

2.4.1. Coherent state-based generating function

As mentioned, we would like to have a closed analytic expression for the FCF GF, which is given in the occupation representation by

$$G(\mathbf{z}';\mathbf{z}) = \sum_{\underline{v},\underline{v}'=\underline{0}}^{\infty} q(\underline{v}';\underline{v})\overline{\prod_{\underline{z},\underline{z}'}}^{2\underline{v},2\underline{v}'}, \tag{2.109}$$

where the fractional FCF ($q(\underline{v}';\underline{v}) = |\langle \underline{v}'|\underline{v}\rangle|^2/|\langle \underline{0}'|\underline{0}\rangle|^2$) is used, which is a normalized FCF with the FCF of vibrational ground states ($|\langle \underline{0}'|\underline{0}\rangle|^2$). The GF parameters $\{z_k\}$ and $\{z_k'\}$ belong to the initial and final states respectively and the corresponding diagonal matrices are $\mathbf{z} = \mathrm{diag}(\underline{z})$ and $\mathbf{z}' = \mathrm{diag}(\underline{z}')$. The FCF GF (2.109) corresponds to the SDF (2.2) at zero Kelvin ($p_{\underline{0}} = 1$ and $p_{\underline{v}} = 0$ for $\underline{v} \neq \underline{0}$) within the Condon approximation ($\hat{\mu}(Q) = \underline{\mu}_0 = $ a constant unit vector). Compared to the SDF expression, the GF (2.109) has GF parameters instead of a δ-distribution. The relation between the GF parameters and the δ-distribution in time domain is exploited in section 4.4 for the thermal FCF TCF development.

It was first shown by Malkin *et al.* [125] in non-symmetric form[18] that the CS phase space integral of a product of two CS overlap integrals gives the spatial representation of the series summation of the GF. The method was exploited by Doktorov *et al.* [29] for the transition statistics[19] and it was modified by Jankowiak *et al.* [46] in a symmetric form[20] which uses mathematically convenient symmetric matrices. Malkin's non-symmetric expression [125] reads [21]

$$G_{\mathrm{Malkin}}(\mathbf{Z}) = \pi^{-2N}|\langle \underline{0}'|\underline{0}\rangle|^{-2} \int \mathrm{d}^2\underline{\alpha}\, \mathrm{d}^2\underline{\gamma}'\, \langle \underline{\gamma}'|\underline{\alpha}\rangle\langle \mathbf{z}'\underline{\gamma}'|\mathbf{z}^*\underline{\alpha}\rangle^*, \tag{2.110}$$

in which a collective block diagonal matrix is introduced $\mathbf{Z} = \mathrm{bldiag}(\mathbf{z}, \mathbf{z}')$ where "bldiag" denotes a matrix in block diagonal form[22]. The integration variables are defined as

$$\mathrm{d}^2\underline{\alpha} = \prod_{k=1}^{N} \mathrm{d}^2\alpha_k, \quad \mathrm{d}^2\underline{\gamma}' = \prod_{k=1}^{N} \mathrm{d}^2\gamma_k', \tag{2.111}$$

where

$$\mathrm{d}^2\alpha_k = \mathrm{dRe}(\alpha_k)\mathrm{dIm}(\alpha_k) = \tfrac{1}{2\hbar}\mathrm{d}P_k\mathrm{d}Q_k, \tag{2.112}$$

$$\mathrm{d}^2\gamma_k' = \mathrm{dRe}(\gamma_k')\mathrm{dIm}(\gamma_k') = \tfrac{1}{2\hbar}\mathrm{d}P_k'\mathrm{d}Q_k', \tag{2.113}$$

---

[18]The orders of GF parameters in the series summation are given in v_k and v_k' not in even orders $2v_k$ and $2v_k'$ as in the Eq. (2.109).

[19]The moments of the distribution, mean and covariance for specific vibrational modes. The method is further developed in this thesis (Ch. 5).

[20]The orders of generating function parameters in the series summation are given in even orders $2v_k$ and $2v_k'$ as in the Eq. (2.109).

[21]This integral form is not surprising if one thinks about the trace formalism (2.14) which can be traced over in any complete basis set. In this case the over-complete basis set (2.93) is used to trace the identity operator (in Condon approximation) with the additional GF parameters. Setting the GF parameters to be 1, it is clear to see the trace formula but the integration diverges because it implies double summation over two ONV spaces one for initial and the other one for final vibrational states.

[22]*cf.* diag transforms a vector to a diagonal square matrix.

for all $k = 1, \ldots, N$. The FCF GF in integral form was suggested as a symmetric expression by Jankowiak *et al.* [46],

$$
\begin{aligned}
G(\mathbf{Z}) &= G(\mathbf{z}'; \mathbf{z}) \\
&= \pi^{-2N} |\langle \underline{0}' | \underline{0} \rangle|^{-2} \int \mathrm{d}^2 \underline{\alpha} \, \mathrm{d}^2 \underline{\gamma}' \, \langle \mathbf{z}'^* \underline{\gamma}' | \mathbf{z} \underline{\alpha} \rangle \langle \mathbf{z}' \underline{\gamma}' | \mathbf{z}^* \underline{\alpha} \rangle^* .
\end{aligned}
\tag{2.114}
$$

Exploiting the occupancy representation of the CSs (2.79) one finds the series summation formula of the CS phase space integrals after inserting the occupation representation Eq. (2.79) into (2.114),

$$
\begin{aligned}
G(\mathbf{Z}) = |\langle \underline{0}' | \underline{0} \rangle|^{-2} \sum_{\underline{u}, \underline{u}'} \sum_{\underline{v}, \underline{v}'=\underline{0}}^{\infty} \langle \underline{u}' | \underline{u} \rangle \langle \underline{v}' | \underline{v} \rangle^* \\
\prod_{k=1}^{N} \left[\frac{z_k^{u_k + v_k} (z_k')^{u_k' + v_k'}}{\sqrt{u_k! v_k! u_k'! v_k'!}} \left(\frac{1}{\pi} \int \mathrm{d}^2 \alpha_k \mathrm{e}^{-|\alpha_k|^2} \alpha_k^{u_k} (\alpha_k^*)^{v_k} \right) \right. \\
\left. \left(\frac{1}{\pi} \int \mathrm{d}^2 \gamma_k' \mathrm{e}^{-|\gamma_k'|^2} (\gamma_k'^*)^{u_k'} (\gamma_k')^{v_k'} \right) \right] ,
\end{aligned}
\tag{2.115}
$$

where the GF parameters are on the unit circle in phase space $|z_k| = 1$, $|z_k'| = 1$. Evaluating the CS phase integrals in the summation via polar coordinates gives [23]

$$
\frac{1}{\pi} \int \mathrm{d}^2 \alpha_k \mathrm{e}^{-|\alpha_k|^2} \alpha_k^{u_k} (\alpha_k^*)^{v_k} = \delta_{u_k, v_k} v_k! ,
\tag{2.116}
$$

which applies similarly for the γ_k' CS phase integration. Then the GF (2.115) in the series summation of CS phase space integrals recovers the occupation representation of the FCF GF (2.109). By replacing the GF parameters with phase parameters, *i. e.*

$$
z_k = \exp(\mathrm{i}\theta_k/2), \quad z_k' = \exp(\mathrm{i}\theta_k'/2), \quad \theta_k, \theta_k' \in \mathbb{R},
\tag{2.117}
$$

we can find the phase formulation of the FCF GF,

$$
G(\underline{\theta}'; \underline{\theta}) = \sum_{\underline{v}, \underline{v}'=\underline{0}}^{\infty} q(\underline{v}'; \underline{v}) \exp(\mathrm{i} \left[\underline{\theta} \cdot \underline{v} + \underline{\theta}' \cdot \underline{v}' \right]) ,
\tag{2.118}
$$

and thus $G(\underline{\theta}'; \underline{\theta})$ is the Fourier transformed FCF GF with the phase parameters $\{\theta_k\}$ and $\{\theta_k'\}$, which is closely related to the TCF development in this thesis (Chs. 4 and 6).

Returning to the evaluation of the phase space integral of the FCF GF (2.114), the corresponding spatial representation of the CS overlap integral is obtained[24] as

---

[23] $\frac{1}{2\pi} \int_0^{2\pi} d\varphi \exp(\mathrm{i}(m-n)\varphi) = \delta_{mn}$ and $\int_0^{\infty} dx \exp(-x) x^n = n!$.
[24] exploiting the unit modulus properties of z_k, z_k' and the spatial representation of the CS overlap integral Eq. (2.96).

$$G(\mathbf{Z}) = \pi^{-2N} \int \mathrm{d}^2\underline{\alpha}\, \mathrm{d}^2\underline{\gamma}' \exp(-\underline{\xi}^\dagger \underline{\xi})$$
$$\exp(-\tfrac{1}{2}\underline{\xi}^\mathrm{t}\mathbf{ZWZ}\underline{\xi} - \tfrac{1}{2}\underline{\xi}^\dagger \mathbf{ZWZ}\underline{\xi}^* + \underline{r}^\mathrm{t}\mathbf{Z}(\underline{\xi} + \underline{\xi}^*)). \tag{2.119}$$

Partitioning $\underline{\xi}$ into real and imaginary parts,

$$\underline{\xi}_\mathrm{R} = \frac{1}{2}(\underline{\xi} + \underline{\xi}^*), \quad \underline{\xi}_\mathrm{I} = \frac{1}{2\,\mathrm{i}}(\underline{\xi} - \underline{\xi}^*), \tag{2.120}$$

we can separate the integration into two multi-variate Gaussian integrals. This leads after recasting the integration over the imaginary part, $\underline{\gamma}'_\mathrm{I} \to -\underline{\gamma}'_\mathrm{I}$ [25] to a FCF GF of the form

$$G(\mathbf{Z}) = \mathcal{I}_{2N}[\mathbf{I} + \mathbf{ZWZ}, \mathbf{Z}\underline{r}]\mathcal{I}_{2N}[\mathbf{I} - \mathbf{ZWZ}, \underline{0}]. \tag{2.121}$$

The M-dimensional multi-variate Gaussian integral is defined,

$$\mathcal{I}_M[\mathbf{A}, \mathbf{b}] = \pi^{-M/2} \int \mathrm{d}\underline{x} \exp(-\underline{x}^\mathrm{t}\mathbf{A}\underline{x} + 2\underline{b}^\mathrm{t}\underline{x})$$
$$= \det(\mathbf{A})^{-\frac{1}{2}} \exp(\underline{b}^\mathrm{t}\mathbf{A}^{-1}\underline{b}), \tag{2.122}$$

which converges when the matrix $\mathbf{A}$ is a complex symmetric matrix with positive-definite real part (see *e.g.* chapter 1 of Ref. [154]). Then the integration leads to a closed analytic form,

$$G(\mathbf{Z}) = \det(\mathbf{I} - \mathbf{ZWZ})^{-\frac{1}{2}} \det(\mathbf{I} + \mathbf{ZWZ})^{-\frac{1}{2}}$$
$$\exp(\underline{r}^\mathrm{t}\mathbf{Z}(\mathbf{I} + \mathbf{ZWZ})^{-1}\mathbf{Z}\underline{r}). \tag{2.123}$$

2.4.2. Partitioning integral spaces

The purpose of having the Franck-Condon factor generating function in the occupation and the spatial representation is to control the vibrational excitation via the GF parameters and to obtain useful information about the transition patterns. Keeping in mind the occupation representation (Eq. (2.109)) one can control the vibrational excitation in the summation by assigning the GF parameters ($\{z_k\}$ and $\{z'_k\}$) to 0 or 1. When 0 is assigned to a vibrational mode, the mode excitation contribution to the total intensity, which can be calculated from the GF, is excluded and the only surviving term of the mode is the ground state[26] contribution. If 1 is assigned to a vibrational mode then the mode excitation contribution to the summation is fully included in the total intensity. It is like on '1' and off '0' of the excitation. For the zero Kelvin case the initial state GF parameter $\underline{z}$ is set to $\underline{0}$ because all vibrational modes in the initial state are frozen to the vibrational ground state. By freezing[27] some vibrational modes in the final state we can figure out the mode contributions to the total intensity. In practice, however, a partitioning scheme in the Gaussian integral steps is invoked

---

[25] $\int_{-\infty}^{\infty} \mathrm{d}x f(x) = \int_{-\infty}^{\infty} \mathrm{d}(-x) f(-x)$
[26] $0^{2n} = \delta_{n0}$.
[27] by setting to 0

rather than switching the GF parameters directly on or off. With the partitioning, $G(\mathbf{Z})$ (Eq. (2.123)) is decomposed into products of contributions in the orthogonal subspaces X and Y. The subspaces X and Y have dimensions N_X and $N_Y = 2N - N_X$ respectively. The subspace X corresponds to the vibrational modes with fixed quantum numbers. The vibrational modes in subspace Y can be excited infinitely and stay in the CS phase integral space as a result[28]. The corresponding orthogonal projection operators $\hat{\pi}_X$ and $\hat{\pi}_Y$ satisfy the usual conditions for projection operators. Applying the projection operators to matrices and vectors indicates the corresponding projection labels, *e.g.*

$$\hat{\pi}_X \underline{\xi} = \underline{\xi}_X, \quad \hat{\pi}_Y \underline{\xi} = \underline{\xi}_Y,$$
$$\hat{\pi}_X \mathbf{A} \hat{\pi}_X = \mathbf{A}_{XX}, \quad \hat{\pi}_X \mathbf{A} \hat{\pi}_Y = \mathbf{A}_{XY}, \quad \hat{\pi}_Y \mathbf{A} \hat{\pi}_X = \mathbf{A}_{YX}, \quad \hat{\pi}_Y \mathbf{A} \hat{\pi}_Y = \mathbf{A}_{YY}. \tag{2.124}$$

Assigning Y on both initial and final state modes leads the FCF GF to divergence unless the modes are in subspaces mutually exclusive or weighted by some normalized distribution such as the Boltzmann distribution for thermal weight (see Ch. 4).

The partitioning scheme can be applied to the Gaussian integral (2.122) so that the integral is decomposed into an L-dimensional space X and an $(M - L)$ dimensional space Y with the corresponding integration variables $\underline{x}$ and $\underline{y}$ [46]

$$\mathcal{I}_M[\mathbf{A}, \mathbf{b}] = \pi^{-M/2} \int d\underline{x} \exp(-\underline{x}^{\mathrm{t}} \mathbf{A}_{XX} \underline{x} + 2\underline{b}_X^{\mathrm{t}} \underline{x})$$
$$\int d\underline{y} \exp(-\underline{y}^{\mathrm{t}} \mathbf{A}_{YY} \underline{y} + 2[\underline{b}_Y - \mathbf{A}_{YX} \underline{x}]^{\mathrm{t}} \underline{y}). \tag{2.125}$$

Then the space partitioned Gaussian integral is given by

$$\mathcal{I}_M[\mathbf{A}, \mathbf{b}] = \det(\mathbf{A}_{YY})^{-\frac{1}{2}} \det(\mathbf{A}_{XX} - \mathbf{A}_{XY}(\mathbf{A}_{YY})^{-1} \mathbf{A}_{YX})^{-\frac{1}{2}} \exp(\underline{b}_Y^{\mathrm{t}}(\mathbf{A}_{YY})^{-1} \underline{b}_Y)$$
$$\exp([\underline{b}_X - \mathbf{A}_{XY}(\mathbf{A}_{YY})^{-1} \underline{b}_Y]^{\mathrm{t}} (\mathbf{A}_{XX} - \mathbf{A}_{XY}(\mathbf{A}_{YY})^{-1} \mathbf{A}_{YX})^{-1} [\underline{b}_X - \mathbf{A}_{XY}(\mathbf{A}_{YY})^{-1} \underline{b}_Y]). \tag{2.126}$$

The Gaussian integral decomposition (Eqs. (2.125) and (2.126)) makes the FCF GF a product of two Gaussian integrals (Eq. (2.121)), which is decomposed into two subspaces, *i.e.*

$$G(\mathbf{Z}) = G(\mathbf{Z}_{XX}, \mathbf{Z}_{YY}) = G_{X|Y}(\mathbf{Z}_{XX}, \mathbf{Z}_{YY}) G_Y(\mathbf{Z}_{YY}), \tag{2.127}$$

where

$$G_Y(\mathbf{Z}_{YY}) = \mathcal{I}_{N_Y}[(\mathbf{I} + \mathbf{ZWZ})_{YY}, \mathbf{Z}_{YY} \underline{r}_Y]$$
$$= \det((\mathbf{I} + \mathbf{ZWZ})_{YY})^{-\frac{1}{2}} \det((\mathbf{I} - \mathbf{ZWZ})_{YY})^{-\frac{1}{2}}$$
$$\exp(\underline{r}_Y^{\mathrm{t}} \mathbf{Z}_{YY}((\mathbf{I} + \mathbf{ZWZ})_{YY})^{-1} \mathbf{Z}_{YY} \underline{r}_Y), \tag{2.128}$$

---

[28]Integration over one phase variable belonging to one vibrational mode corresponds to complete summation of the individual vibrational mode contributions to the total intensity.

and

$$G_{X|Y}(\mathbf{Z}_{XX}, \mathbf{Z}_{YY})$$
$$= \mathcal{I}_{N_X}[\mathbf{I}_{XX} - \mathbf{Z}_{XX}\widetilde{\mathbf{W}}_{XX}^{-}(\mathbf{Z}_{YY})\mathbf{Z}_{XX}, \underline{0}_X]$$
$$\quad \mathcal{I}_{N_X}[\mathbf{I}_{XX} + \mathbf{Z}_{XX}\widetilde{\mathbf{W}}_{XX}^{+}(\mathbf{Z}_{YY})\mathbf{Z}_{XX}, \mathbf{Z}_{XX}\widetilde{\underline{r}}_X^{+}(\mathbf{Z}_{YY})]$$
$$= \det(\mathbf{I}_{XX} + \mathbf{Z}_{XX}\widetilde{\mathbf{W}}_{XX}^{+}\mathbf{Z}_{XX})^{-\frac{1}{2}} \det(\mathbf{I}_{XX} - \mathbf{Z}_{XX}\widetilde{\mathbf{W}}_{XX}^{-}\mathbf{Z}_{XX})^{-\frac{1}{2}}$$
$$\exp((\widetilde{\underline{r}}_X^{+})^{\mathrm{t}}\mathbf{Z}_{XX}(\mathbf{I}_{XX} + \mathbf{Z}_{XX}\widetilde{\mathbf{W}}_{XX}^{+}\mathbf{Z}_{XX})^{-1}\mathbf{Z}_{XX}\widetilde{\underline{r}}_X^{+}) . \tag{2.129}$$

The symbol $X|Y$ indicates the conditional exclusion of Y space from X space, the integral space X is separated from the space Y but the GF concerning space X ($G_{X|Y}(\mathbf{Z}_{XX}, \mathbf{Z}_{YY})$) still depends on the GF parameter in Y space $\mathbf{Z}_{YY}$. Here the quantities for the fixed quantum number space are defined as,

$$\widetilde{\mathbf{W}}_{XX}^{\pm}(\mathbf{Z}_{YY}) = \mathbf{W}_{XX} \mp \mathbf{W}_{XY}\mathbf{Z}_{YY}((\mathbf{I} \pm \mathbf{ZWZ})_{YY})^{-1}\mathbf{Z}_{YY}\mathbf{W}_{YX}, \tag{2.130}$$

$$\widetilde{\underline{r}}_X^{+}(\mathbf{Z}_{YY}) = \underline{r}_X - \mathbf{W}_{XY}\mathbf{Z}_{YY}((\mathbf{I} + \mathbf{ZWZ})_{YY})^{-1}\mathbf{Z}_{YY}\underline{r}_Y . \tag{2.131}$$

The partitioning scheme of the FCF GF is exploited, in practical calculations of FC profiles, to find the maximum quantum numbers for the individual vibrational modes and the maximum number of simultaneously excited modes for given intensity threshold. This rigorous prescreening scheme is crucial to reduce the number of integrals to be computed in the subsequent steps. The output of the neglected integrals on the integrated SDF is here by known in advance. The numerical schemes for the rigorous prescreening strategies are generalized to include the thermal effect and presented in the thermal FCF GF chapter 4. In chapter 6 the thermal prescreening strategy is generalized to include non-Condon effects.

2.5. Chapter summary and conclusion

In this chapter we reviewed the basic background for the theoretical contributions of the thesis. The FGR can be expressed in frequency and time domain. We presented the transformation of the SDFs, for OPA and rR cross sections, from frequency to time domain via Fourier integration. For the evaluation of SDFs with Duschinsky mode mixing effect, a unitary transformation was introduced such that it transforms the coordinates according to the Duschinsky relation. This Duschinsky unitary operation was exploited to compute CS overlap integral and the overlap integral was used for the FC integral prescreening method at zero Kelvin [46].

Throughout the following chapters of this thesis the concepts introduced herein are exploited for thermal effect (Ch. 4), non-Condon effect (Chs. 3 and 6) and time-independent cumulant expansion (Ch. 5). In the next chapter 3 the FC/non-Condon integral evaluation schemes are developed for the efficient evaluation of SDFs in TI manner. The integral evaluation schemes are generalized to complex numbers for the TCF evaluation of rR, SVL and anharmonic GFs in chapter 7.

3. Franck-Condon integrals and beyond

In this chapter we develop integral evaluation schemes for Franck-Condon (FC) and non-Condon integrals. The efficient FC and non-Condon integral evaluation schemes are shown to be important not only for the time-independent (TI) method but also for the time-dependent (TD) approach (see *e.g.* Ref. [71]) of resonance Raman (rR) scattering and single vibronic level (SVL) transition (Ch. 7). We review first the history of the integral evaluation schemes. Afterwards, we suggest an iterative integral evaluation scheme for the FC integrals, which is different from the traditional iterative method (see *e.g.* Ref. [155]) in the aspect that it includes only a single uni-variate Hermite polynomial whereas the traditional approach contains multiple products of one-dimensional Hermite polynomials in the iterative summation. Our iterative FC integral expression, which is represented as multi-variate Hermite polynomials (MHPs), is shown to be in a simpler form than the traditional expression. Usually the non-Condon integrals in the Duschinsky relation (2.44), *e.g.* the Herzberg-Teller (HT) integrals $\langle \underline{v}'|\hat{Q}_i|\underline{v}\rangle$, are evaluated via linear combination of FC integrals (see *e.g.* Refs. [36, 49]) resulting from the second quantized expression of position operators (2.49). Thus the non-Condon integral evaluation is more expensive than FC integrals. Introducing the coherent state (CS) phase displacement operators to the CS overlap integral we can translate the non-Condon integral evaluation problem into a MHP evaluation problem even for nonlinear operators. As a result we can use the same integral evaluation scheme for the FC and non-Condon integrals, which are expressed as MHPs. In this chapter a unified approach for the FC/non-Condon integrals is developed.

A brief history Sharp and Rosenstock [114] developed the multi-dimensional Franck-Condon integral evaluation scheme in the displaced-distorted-rotated harmonic oscillator (from here on we refer to this as Duschinsky oscillator) basis. By using the Hermite polynomial generating function[1] (see *e.g.* Refs. [133, 134]), they found an equivalent series summation formula in expansion with the generating function (GF) parameters. Many other authors (see *e.g.* Refs. [149, 155–160]) modified the GF approach to iterative and recursive integral evaluation schemes. Doktorov *et al.* [24, 26] exploited the coherent state position space representation (2.82) to derive the recursion relations (Eqs. (2.103) and (2.104)) for the FC integrals with the Duschinsky oscillators. Recursion relations, identical to these obtained by Doktorov and coworker's [24, 26] CS approaches, were formulated by Kupka *et al.* [161] using the Hermite polynomial GF as well and were exploited by many others (see *e.g.* Refs. [80, 162–166]). The two approaches (Sharp and Rosenstock [114] and Doktorov *et al.* [24, 26]) exploit different kinds of GFs (Hermite polynomial and CS), however, end up in a common mathematical problem, namely *how to evaluate the multi-variate Hermite polynomials* (see *e.g.* Refs. [133, 134] for the mathematical works), which can be performed either iteratively or recursively.

---

[1] *e.g.* the one-dimensional Hermite polynomial generating function is $e^{xt-t^2/2} = \sum_{v=0}^{\infty} \mathcal{H}_v(x)\frac{t^v}{v!}$

The recursive approach is usually faster than the iterative one. But the former has an integral storage problem which can easily cause impractical memory requirements for large systems and FC integrals with high excitations in vibrational levels. To deal with the memory size problem of the recursion relation, there have been various computational strategic advances, *e.g.* binary tree [43, 124, 167–169] and hash tables [170–172] to store the integrals efficiently. The iterative scheme has been modified until recently (see *e.g.* Refs. [117, 118, 120, 121]). The new versions deviate only slightly from the initial development of Sharp and Rosenstock [114], for instance the usage of the summations of multiple products of one-dimensional Hermite polynomials. For the summations of one-dimensional Hermite polynomial products, one has to sum over many terms which can slow down the integral evaluation. An iterative method was developed for the one-dimensional non-Condon integrals [173], however, it has to be extended for multi-dimensional non-Condon integrals which is essential for larger system applications, anharmonic and vibronic coupling problems.

Malmquist and Forsberg [115] proposed a different approach, the so called LU method, expanding the initial and final harmonic oscillator eigenstates with a set of harmonic oscillator eigenstates which can mediate the initial and final vibrational states so that the Duschinsky mode mixing problem (2.44) can be avoided in the evaluation. A similar idea was used in Refs. [42, 84] for an iterative method explicitly expressing the integrals in series summation with the Duschinsky parameters for three dimensional case. These approaches can in principle be extended for the non-Condon integral evaluation of Duschinsky oscillators. In the LU approach, however, non-Condon integrals in the parallel harmonic oscillator basis have to be evaluated additionally even for the FC integrals.

Perturbation approaches [26, 57, 119, 174] were proposed to overcome the integral storage problem of the recursion relations and the complicated implementation of the iterative summation formulas (see *e.g.* Eq. (2.105)). In these perturbation approaches, the Duschinsky rotations are approximately taken into account by effective parameters of the non-interacting oscillators [175] even in the zero-th order. In zero-th order the multi-dimensional integrals separate into products of one-dimensional integrals. Borrelli and Peluso [119] claim that their perturbation method with second order expansion shows quantitative agreement with the exact calculations for small systems having small Duschinsky effects. The higher order terms, however, should be taken into account for larger systems, which is shown to be a computationally difficult task. The perturbation approach is useful for large systems having small Duschinsky mode mixing effects, if one can further approximate the Duschinsky rotation matrix to a block diagonal form by grouping the significantly mixed vibrational modes [43].

Svendsen *et al.* [71] suggested a TD recursion relation for the one-photon absorption (OPA) and rR time-correlation functions (TCFs) including the non-Condon effects. The recursion relation is similar to those of Doktorov *et al.* [24, 26] (Eqs. (2.103) and (2.104)) but it includes a time-propagation operator ($\exp(-\mathrm{i}\hat{H}'t/\hbar)$) and a position operator ($\hat{Q}_i$). Svendsen *et al.* could construct TCFs ($\langle v|v(t)\rangle$, see Sec. 2.1) for the OPA and rR processes with the recursion relation including a non-Condon operator of nonlinear one-dimensional position operator ($\hat{Q}_i^n$). We develop, instead, a similar TD generating function evaluation method for SVL transitions in this thesis using the complex MHPs which can be evaluated iteratively or recursively with arbitrary polynomial non-Condon operators. Later on we apply this method to SVL and rR TCF evaluation including non-Condon effects in chapter 7.

Throughout the work in this thesis, we utilize the coherent state recursion relation reported in Ref. [46] (Eqs. (2.103) and (2.104)) for the TI approach with integral prescreening methods for the finite temperature effect (Ch. 4) and the HT effect (Ch. 6). The CS formalism is physically intuitive and can easily be extended to the Franck-Condon factor (FCF) sum rule at finite temperature (Ch. 4), the FCF thermal TCF (Ch. 4), the non-Condon integral scheme (Sec. 3.2), the non-Condon thermal TCF and the corresponding sum rule (Ch. 6), the TI cumulant expansion (CE) to FC transition (Ch. 5), the SVL GF which is closely related to the rR and anharmonic developments (Ch. 7).

3.1. Franck-Condon integrals

One can evaluate the multi-dimensional FC integrals including the Duschinsky effect [107] by relating expressions (2.95) and (2.96) via the partial derivatives with respect to the CS phase parameters. With the collective indexed vector for occupation number vectors (ONVs) of initial and final states [2]

$$\underline{\tilde{v}} = \begin{pmatrix} \underline{v} \\ \underline{v}' \end{pmatrix} , \tag{3.1}$$

the FC integral reads

$$
\begin{aligned}
\langle \underline{\tilde{v}} \rangle_{\mathrm{FC}} &= \langle \underline{v}' | \underline{v} \rangle = \langle \tilde{v}_{N+1}, \dots, \tilde{v}_{2N} | \tilde{v}_1, \dots, \tilde{v}_N \rangle \\
&= \langle \underline{0}' | \underline{0} \rangle \widetilde{\prod_{\underline{\tilde{v}}}}^{-\frac{1}{2}} \hat{\partial}_{\underline{\xi}}^{\underline{\tilde{v}}} \exp\left(-\tfrac{1}{2} \underline{\xi}^{\mathrm{t}} \mathbf{W} \underline{\xi} + \underline{r}^{\mathrm{t}} \underline{\xi} \right) \Big|_{\underline{\xi} = \underline{0}},
\end{aligned} \tag{3.2}
$$

where [3] one can notice that the FC integral is nothing but a MHP [24, 26]. The MHP, $\mathcal{H}_{\underline{\tilde{v}}}$, is defined as,

$$\mathcal{H}_{\underline{\tilde{v}}}(\underline{x}; \mathbf{\Lambda}_{\mathrm{c}}) = (-1)^{\tilde{v}} \exp(\tfrac{1}{2} \underline{x}^{\mathrm{t}} \mathbf{\Lambda}_{\mathrm{c}}^{-1} \underline{x}) \hat{\partial}_{\underline{x}}^{\underline{\tilde{v}}} \exp(-\tfrac{1}{2} \underline{x}^{\mathrm{t}} \mathbf{\Lambda}_{\mathrm{c}}^{-1} \underline{x}), \tag{3.3}$$

where $\tilde{v} = \sum_k \tilde{v}_k$ and $\mathbf{\Lambda}_{\mathrm{c}}$ is a complex symmetric matrix with a symmetric positive definite real part. The overlap integrals of multi-dimensional harmonic oscillators (multi-variate Hermite-Gaussian function (2.52)) are expressed as MHPs, that is,

$$
\begin{aligned}
\langle \underline{\tilde{v}} \rangle_{\mathrm{FC}} &= \langle \underline{0}' | \underline{0} \rangle \widetilde{\prod_{\underline{\tilde{v}}}}^{-\frac{1}{2}} (-1)^{\tilde{v}} \mathcal{H}_{\underline{\tilde{v}}}(\underline{\xi} - \mathbf{W}^{-1} \underline{r}; \mathbf{W}^{-1}) \Big|_{\underline{\xi} = \underline{0}} \\
&= \langle \underline{0}' | \underline{0} \rangle \widetilde{\prod_{\underline{\tilde{v}}}}^{-\frac{1}{2}} \mathcal{H}_{\underline{\tilde{v}}}(\mathbf{W}^{-1} \underline{r}; \mathbf{W}^{-1}).
\end{aligned} \tag{3.4}
$$

---

[2] Note that the order of vectors is reversed comparing to Eq. (2.106).

[3] $\hat{\partial}_{\underline{x}_1, \cdots, \underline{x}_N}^{\underline{n}_1, \cdots, \underline{n}_N} = \left(\frac{\partial^{\sum_k n_{1,k}}}{\prod_k \partial x_{1,k}^{n_{1,k}}} \right) \cdots \left(\frac{\partial^{\sum_k n_{N,k}}}{\prod_k \partial x_{N,k}^{n_{N,k}}} \right)$ and $\widetilde{\prod}_{\underline{x}_1, \cdots, \underline{x}_N}^{\underline{n}_1, \cdots, \underline{n}_N} = \left(\prod_k (x_{1,k}!)^{n_{1,k}} \right) \cdots \left(\prod_k (x_{N,k}!)^{n_{N,k}} \right)$.

We can evaluate the MHPs by using the following recursion relation,

$$
\mathcal{H}_{\tilde{v}_1,\cdots,\tilde{v}_k+1,\cdots,\tilde{v}_{2N}}(\underline{x}; \boldsymbol{\Lambda}_{\mathrm{c}}) = \Big(\sum_{j=1}^{2N} (\boldsymbol{\Lambda}_{\mathrm{c}}^{-1})_{kj} x_j \Big) \mathcal{H}_{\tilde{v}_1,\cdots,\tilde{v}_{2N}}(\underline{x}; \boldsymbol{\Lambda}_{\mathrm{c}})
$$
$$
- \sum_{j=1}^{2N} (\boldsymbol{\Lambda}_{\mathrm{c}}^{-1})_{kj} \tilde{v}_j \mathcal{H}_{\tilde{v}_1,\cdots,\tilde{v}_j-1,\cdots,\tilde{v}_{2N}}(\underline{x}; \boldsymbol{\Lambda}_{\mathrm{c}}), \qquad (3.5)
$$

which was derived by Willink [134] in a similar form of Eqs. (2.103) and (2.104) (see Refs. [24, 26, 114]) for FC integrals. Together with Eq. (3.4) we can rewrite the recursion relation of Eqs. (2.103) and (2.104) in a single expression,

$$
\sqrt{\tilde{v}_k + 1} \langle \tilde{v}_1, \cdots, \tilde{v}_k + 1, \cdots, \tilde{v}_{2N} \rangle_{\mathrm{FC}} = r_k \langle \tilde{v}_1, \cdots, \tilde{v}_{2N} \rangle_{\mathrm{FC}}
$$
$$
- \sum_{j=1} \mathbf{W}_{kj} \sqrt{\tilde{v}_j} \langle \tilde{v}_1, \cdots, \tilde{v}_j - 1, \cdots, \tilde{v}_{2N} \rangle_{\mathrm{FC}}.
$$
$$
(3.6)
$$

Willink [134] suggested the recursion relation, Eq. (3.5), for the MHPs, which is a general form of the one by Doktorov and coworker's [24, 27]. The author found also the recursion relation of multi-variate normal moments from the recursion relation of the MHPs via the relation between the multi-variate normal moments $\mathcal{E}$ and the MHPs $\mathcal{H}$, *i.e.*

$$
\mathcal{E}\left(\overline{\prod}_{\underline{y}}^{\tilde{v}} \right) = \mathrm{i}^{-\tilde{v}} \mathcal{H}_{\underline{\tilde{v}}}(\mathrm{i}\boldsymbol{\Lambda}_{\mathrm{c}}\underline{\mu}_{\mathrm{m}}; \boldsymbol{\Lambda}_{\mathrm{c}}), \qquad (3.7)
$$

where $\underline{y}$ is a random variable vector in a normal distribution, $\mathcal{N}_{\mathrm{normal}}(\underline{\mu}_{\mathrm{m}}, \boldsymbol{\Lambda}_{\mathrm{c}}^{-1})$ [4]. Exploiting the Magnus series expansion, which shall not be confused with the multi-dimensional time integral expansion for the TD Schrödinger equation, for products of variables[5] Kan [176] developed an efficient algorithm to evaluate the multi-variate normal moments,

$$
\mathcal{E}\left(\overline{\prod}_{\underline{y}}^{\tilde{v}} \right) = \sum_{l_1=0}^{\tilde{v}_1} \cdots \sum_{l_{2N}=0}^{\tilde{v}_{2N}} \sum_{s=0}^{[\tilde{v}/2]} (-1)^{\sum_k^{2N} l_k} \binom{\tilde{v}_1}{l_1} \cdots \binom{\tilde{v}_{2N}}{l_{2N}} \frac{\left(\frac{\underline{h}^{\mathrm{t}} \boldsymbol{\Lambda}_{\mathrm{c}}^{-1} \underline{h}}{2} \right)^s (\underline{h}^{\mathrm{t}} \underline{\mu}_{\mathrm{m}})^{\tilde{v}-2s}}{s!(\tilde{v}-2s)!},
$$
$$
(3.8)
$$

where $\underline{h} = (\tilde{v}_1/2 - l_1, \cdots, \tilde{v}_{2N}/2 - l_{2N})^{\mathrm{t}}$ and $[\tilde{v}/2]$ is the greatest integer less or equal to $\tilde{v}/2$. Herein we propose an (alternative) iterative evaluation scheme of the MHPs, which can possibly be evaluated efficiently by identifying $\underline{\mu}_{\mathrm{m}} = -\mathrm{i}\underline{r}$ and $\boldsymbol{\Lambda}_{\mathrm{c}} = \mathbf{W}^{-1}$ in Eqs. (3.7) and (3.8), *i.e.*

---

[4]The normal distribution is defined as $p(\underline{y}) = \frac{1}{\sqrt{\det(2\pi\boldsymbol{\Lambda}_{\mathrm{c}}^{-1})}} \exp\left[-\frac{1}{2}(\underline{y}-\underline{\mu}_{\mathrm{m}})^{\mathrm{t}} \boldsymbol{\Lambda}_{\mathrm{c}}(\underline{y}-\underline{\mu}_{\mathrm{m}}) \right]$ with its mean vector $\underline{\mu}_{\mathrm{m}}$ and covariance matrix $\boldsymbol{\Lambda}_{\mathrm{c}}^{-1}$.

[5]$\overline{\prod}_{\underline{y}}^{\tilde{v}} = \prod_k^{2N} y_k^{\tilde{v}_k} = \sum_{l_1=0}^{\tilde{v}_1} \cdots \sum_{l_{2N}=0}^{\tilde{v}_{2N}} (-1)^{\sum_k^{2N} l_k} \binom{\tilde{v}_1}{l_1} \cdots \binom{\tilde{v}_{2N}}{l_{2N}} (\underline{h}^{\mathrm{t}}\underline{y})^{\tilde{v}}$ where $\underline{h} = \underline{\tilde{v}} - \underline{l}$.

$$\mathcal{H}_{\underline{\tilde{v}}}(\mathbf{W}^{-1}\underline{r};\mathbf{W}^{-1}) = \sum_{l_1=0}^{\tilde{v}_1} \cdots \sum_{l_{2N}=0}^{\tilde{v}_{2N}} \sum_{s=0}^{[\tilde{v}/2]} (-1)^{\sum_k^{2N} l_k+s} \binom{\tilde{v}_1}{l_1} \cdots \binom{\tilde{v}_{2N}}{l_{2N}} \frac{\left(\frac{\underline{h}^{\mathrm{t}}\mathbf{W}\underline{h}}{2}\right)^s (\underline{h}^{\mathrm{t}}\underline{r})^{\tilde{v}-2s}}{s!(\tilde{v}-2s)!}.$$

(3.9)

Then we can evaluate the multi-dimensional FC integral in Eq. (3.4) with the relation (3.9) involving the summation of uni-variate Hermite polynomials[6]. This iterative formula has simpler summation indices than the expression (2.105) used in Ref. [46] which is a generalized expression of Refs. [116, 149, 155, 157]. The summation indices and the corresponding summation bounds in the iterative equation (2.105) are dependent on each other, whereas the summation indices and the bounds in Eq. (3.9) are independent. We can further simplify the expression for a special case, when $\underline{r} = \underline{0}$ (when there is no molecular structural changes), only one term ($\tilde{v} = 2s$) in the summation over s survives.

3.2. Beyond Franck-Condon integrals

When the Condon approximation, in which one computes the FCFs as the transition probabilities, is not sufficient, it is necessary to take the transition moment as a function of vibrational normal coordinates. Beyond the Condon approximation, we need to evaluate the HT (non-Condon) integrals which are the matrix elements of the position operators. Usually the HT approximation is adopted for weakly FC-allowed or FC-forbidden transition within the Born-Oppenheimer (BO) ansatz. In the HT expansion of the electronic transition dipole moment (TDM), typically, at most the linear terms or the quadratic terms are considered (see Sec. 2.1). Usually the (linear) HT integrals are evaluated with a linear combination of FC integrals via the second quantized position operators (Eq. (2.49) and see *e.g.* Refs. [36, 49]). We propose, in this section, a general integral evaluation scheme for non-Condon operators so that it can be used within the MHP evaluation routes in the previous section 3.1.

Rather than solving for the specific HT-type-integrals $\langle \underline{v}'|\hat{Q}_i|\underline{v}\rangle$, we instead can generate such matrix elements from an arbitrary polynomial operator[7] $\hat{f} = \hat{f}(\underline{\hat{P}},\underline{\hat{Q}})$, cast as a function of momentum and position operators. In the CS basis the matrix elements of $\hat{f}$ are given in a series expansion, *i.e.*[8]

$$\langle \underline{\gamma}'|\hat{f}|\underline{\alpha}\rangle = \exp(-\tfrac{1}{2}\underline{\alpha}^\dagger\underline{\alpha} - \tfrac{1}{2}\underline{\gamma}'^\dagger\underline{\gamma}')$$

$$\sum_{\underline{v},\underline{v}'} \langle \underline{v}'|\hat{f}|\underline{v}\rangle \widetilde{\prod}_{\underline{v},\underline{v}'}^{-\frac{1}{2},-\frac{1}{2}} \overline{\prod}_{\underline{\alpha},\underline{\gamma}'^*}^{v,v'}.$$

(3.10)

Like for FC integrals, the analytic expression of $\langle \underline{\gamma}'|\hat{f}|\underline{\alpha}\rangle$ and the series expansion will be

---

[6]The summation over the s part in Eq. (3.9) is the iterative expression of the uni-variate Hermite polynomials.

[7]Herein we restrict polynomials of momentum and position operators to integer powers. But we can possibly consider non-integer powers such as $\sqrt{\hat{Q}_i}$ via *fractional calculus* (see *e.g.* Ref. [177]).

[8]$\overline{\prod}_{\underline{x}_1,\cdots,\underline{x}_N}^{\underline{n}_1,\cdots,\underline{n}_N} = \left(\prod_k x_{1,k}^{n_{1,k}}\right) \cdots \left(\prod_k x_{N,k}^{n_{N,k}}\right).$

compared to formulate the non-Condon integral evaluation scheme. A similar idea [173] was previously exploited to compute the matrix elements of the position operator in a one-dimensional harmonic oscillator basis. Herein we consider arbitrary polynomial operators rather than only a linear position operator for the generalization of the development and the possible expansions of the method to nonlinear HT terms, vibronic couplings and anharmonic oscillators.

It is precisely this action on the CS labels which is exploited for the HT operations, by making an identification between the CS displacement operator and the momentum and position operators. By introducing auxiliary parameters $\underline{\eta_P}$ and $\underline{\eta_Q}$, connected to the momentum and the position operators respectively, we can apply the general operator expansions by taking partial derivatives with respect to these auxiliary parameters. This relationship utilizes the product of CS displacement operators (Eqs. (2.87) and (2.90))

$$
\hat{D}(\underline{\eta_P})\hat{D}(\mathrm{i}\underline{\eta_Q})|\underline{\alpha}\rangle = |\underline{\alpha} + \underline{\eta_P} + \mathrm{i}\underline{\eta_Q}\rangle
$$
$$
\exp\left[\tfrac{1}{2}(\underline{\alpha}^\dagger - \underline{\alpha}^\mathrm{t})\underline{\eta_P} + \tfrac{\mathrm{i}}{2}(\underline{\alpha}^\dagger + \underline{\alpha}^\mathrm{t})\underline{\eta_Q} - \mathrm{i}\underline{\eta_Q}^\mathrm{t}\underline{\eta_P}\right], \tag{3.11}
$$

where

$$
\underline{\eta_Q} = (\eta_{Q_1}, \ldots, \eta_{Q_N})^\mathrm{t}, \; \eta_{Q_i} \in \mathbb{R},
$$
$$
\underline{\eta_P} = (\eta_{P_1}, \ldots, \eta_{P_N})^\mathrm{t}, \; \eta_{P_i} \in \mathbb{R}. \tag{3.12}
$$

Differentiating the CSs, Eq. (3.11), with respect to the auxiliary parameters one can extract the momentum and position operators from the corresponding CS displacement operators, for example

$$
\overline{\prod}_{\hat{P},\hat{Q}}^{l,m} = \prod_{k=1}^{N} \left[\mathrm{i}\sqrt{\tfrac{\epsilon_k}{2}}\right]^{l_k} \left[\tfrac{1}{\mathrm{i}}\sqrt{\tfrac{\hbar^2}{2\epsilon_k}}\right]^{m_k} \hat{\partial}_{\underline{\eta_P},\underline{\eta_Q}}^{l,m} \hat{D}(\underline{\eta_P})\hat{D}(\mathrm{i}\underline{\eta_Q})\Big|_{\underline{\eta_P},\underline{\eta_Q}=\underline{0}}, \tag{3.13}
$$

which has been placed into a momentum and position operator ordering. Other orderings, such as the reverse ordered form, can be made in a similar manner by exchanging the placement of the CS displacement operators in Eq. (3.11) and more complicated orderings are possible by introducing more CS displacement operators.

Returning to the central problem of evaluating CS matrix elements for the (arbitrary) polynomial operators[9] $\hat{f}(\hat{P}, \hat{Q})$, we make the identification between Eq. (3.10) and the overlap integral exploiting Eq. (3.11)

$$
\langle \underline{\gamma'}|\hat{D}_{\mathrm{NC}}(\underline{\eta})|\underline{\alpha}\rangle = \langle \underline{\gamma'} + (\underline{\eta_{P'}} + \mathrm{i}\underline{\eta_{Q'}})^* |\underline{\alpha} + (\underline{\eta_P} + \mathrm{i}\underline{\eta_Q})\rangle \exp\left[\tfrac{1}{2}\underline{\xi}^\dagger\underline{\eta} - \tfrac{1}{2}\underline{\eta}^\dagger\underline{\xi} - \mathrm{i}\underline{\tilde{\eta}_P}^\mathrm{t}\underline{\tilde{\eta}_Q}\right],
$$
$$
\tag{3.14}
$$

---

[9] Strictly speaking, this is not an arbitrary polynomial because one has to introduce many CS displacement operators with different auxiliary parameters for more arbitrariness.

where

$$\hat{D}_{\mathrm{NC}}(\underline{\eta}) = \hat{D}^{-1}((\mathrm{i}\underline{\eta}_{Q'})^*)\hat{D}^{-1}(\underline{\eta}_{P'})\hat{D}(\underline{\eta}_P)\hat{D}(\mathrm{i}\underline{\eta}_Q), \tag{3.15}$$

$$\tilde{\underline{\eta}}_P = \left(\frac{\eta_P}{\underline{\eta}_{P'}}\right), \quad \tilde{\underline{\eta}}_Q = \left(\frac{\eta_Q}{\underline{\eta}_{Q'}}\right), \tag{3.16}$$

$$\underline{\eta} = \tilde{\underline{\eta}}_P + \mathrm{i}\tilde{\underline{\eta}}_Q. \tag{3.17}$$

For computational convenience we use $(\mathrm{i}\eta_{Q'})^*$ instead of $(\mathrm{i}\underline{\eta}_{Q'})$ in Eq. (3.14) when we multiply prefactors of the position operators as in Eq. (3.13) to the corresponding partial derivatives[10]. The CS overlap integral in Eq. (3.14) can be further simplified by factoring the CS overlap integral ($\langle\underline{\gamma}'|\underline{\alpha}\rangle$) out, *i.e.*[11]

$$\langle\underline{\gamma}' + (\underline{\eta}_{P'} + \mathrm{i}\underline{\eta}_{Q'})^*|\underline{\alpha} + (\underline{\eta}_P + \mathrm{i}\underline{\eta}_Q)\rangle$$
$$= \langle\underline{\gamma}'|\underline{\alpha}\rangle\exp\left(-\tfrac{1}{2}\underline{\eta}^\dagger\underline{\eta}\right)\mathcal{J}\left[\mathbf{W},\underline{r};\underline{\eta}\right]$$
$$\exp(-\tfrac{1}{2}\underline{\xi}^\dagger\underline{\eta} - \tfrac{1}{2}\underline{\eta}^\dagger\underline{\xi} - \underline{\eta}^{\mathrm{t}}\mathbf{W}\underline{\xi}). \tag{3.18}$$

The occupation representation of the matrix elements (Eq. (3.10)) of the displacement operators (Eq. (3.14)) reads

$$\langle\underline{\gamma}'|\hat{D}_{\mathrm{NC}}(\underline{\eta})|\underline{\alpha}\rangle = \exp(-\tfrac{1}{2}\underline{\xi}^\dagger\underline{\xi})\sum_{\underline{v},\underline{v}'}\langle\underline{v}'|\hat{D}_{\mathrm{NC}}(\underline{\eta})|\underline{v}\rangle\widetilde{\prod}_{\underline{v},\underline{v}'}^{-\frac{1}{2},-\frac{1}{2}}\overline{\prod}_{\underline{\alpha},\underline{\gamma}'^*}^{\underline{v},\underline{v}'}. \tag{3.19}$$

To restore the matrix elements in the harmonic oscillator ONV basis from the CS matrix element (3.19) we take partial derivatives as follows

$$\langle\underline{v}'|\hat{D}_{\mathrm{NC}}(\underline{\eta})|\underline{v}\rangle = \widetilde{\prod}_{\tilde{\underline{v}}}^{-\frac{1}{2}}\hat{\partial}_{\underline{\xi}}^{\tilde{\underline{v}}}\exp(\tfrac{1}{2}\underline{\xi}^\dagger\underline{\xi})\langle\underline{\gamma}'|\hat{D}_{\mathrm{NC}}(\underline{\eta})|\underline{\alpha}\rangle\Big|_{\underline{\xi}=\underline{0}}. \tag{3.20}$$

We can, finally, arrive at the non-Condon integral evaluation formula by taking partial derivatives on Eq. (3.20) with respect to the auxiliary phase parameters to restore the momentum and position operators (Eq. (3.13)),

---

[10]We simply can multiply the position operator prefactor, $\frac{1}{\mathrm{i}}\sqrt{\frac{\hbar^2}{2\epsilon_k}}$ in Eq. (3.13), without considering whether a position operator belongs to the initial or final electronic state regarding for the sign change of the prefactor. Otherwise (if we use $(\mathrm{i}\eta_{Q'})$ instead of $(\mathrm{i}\eta_{Q'})^*$) we need to take the complex conjugate of the prefactor for the corresponding position operator belonging to the final electronic state.

[11]$\mathcal{J}[\mathbf{A},\underline{b};\underline{x}] = \exp(-\tfrac{1}{2}\underline{x}^{\mathrm{t}}\mathbf{A}\underline{x} + \underline{b}^{\mathrm{t}}\underline{x})$.

$$\langle \underline{v}'| \overline{\overline{\prod_{\hat{\underline{Q}}',\hat{\underline{P}}',\hat{\underline{P}},\hat{\underline{Q}}}^{m',l',l,m}}} |\underline{v}\rangle$$

$$= \prod_{k=1}^{N} \left[i\sqrt{\frac{\epsilon_k}{2}} \right]^{l_k} \left[i\sqrt{\frac{\epsilon'_k}{2}} \right]^{l'_k} \left[\frac{1}{i}\sqrt{\frac{\hbar^2}{2\epsilon_k}} \right]^{m_k} \left[\frac{1}{i}\sqrt{\frac{\hbar^2}{2\epsilon'_k}} \right]^{m'_k} \hat{\partial}_{\tilde{\eta}_P,\tilde{\eta}_{P'},\tilde{\eta}_Q,\underline{\tilde{\eta}}_{Q'}}^{l,l',m,m'} \langle \underline{v}'|\hat{D}_{\mathrm{NC}}(\underline{\eta})|\underline{v}\rangle \Big|_{\underline{\eta}=\underline{0}}$$

$$= \prod_{k=1}^{N} \left[i\sqrt{\frac{\epsilon_k}{2}} \right]^{l_k} \left[i\sqrt{\frac{\epsilon'_k}{2}} \right]^{l'_k} \left[\frac{1}{i}\sqrt{\frac{\hbar^2}{2\epsilon_k}} \right]^{m_k} \left[\frac{1}{i}\sqrt{\frac{\hbar^2}{2\epsilon'_k}} \right]^{m'_k}$$

$$\langle \underline{0}'|\underline{0}\rangle \widetilde{\prod_{\tilde{v}}}^{-\frac{1}{2}} \mathcal{H}_{\underline{v},\underline{v}',\underline{l},\underline{l}',\underline{m},\underline{m}'}(\widetilde{\mathbf{W}}_{\mathrm{NCI}}^{-1}\tilde{\underline{r}}_{\mathrm{NCI}}; \widetilde{\mathbf{W}}_{\mathrm{NCI}}^{-1}), \tag{3.21}$$

where the MHP dimensional order is $(\underline{v}, \underline{v}', \underline{l}, \underline{l}', \underline{m}, \underline{m}')$, and the collective matrix $\widetilde{\mathbf{W}}_{\mathrm{NCI}}$ and the vector $\tilde{\underline{r}}_{\mathrm{NCI}}$ are defined as

$$\widetilde{\mathbf{W}}_{\mathrm{NCI}} = \begin{pmatrix} \mathbf{W} & \mathbf{I}+\mathbf{W} & -i(\mathbf{I}-\mathbf{W}) \\ \mathbf{I}+\mathbf{W} & \mathbf{I}+\mathbf{W} & i(\mathbf{I}+\mathbf{W}) \\ -i(\mathbf{I}-\mathbf{W}) & i(\mathbf{I}+\mathbf{W}) & \mathbf{I}-\mathbf{W} \end{pmatrix}, \tag{3.22}$$

$$\tilde{\underline{r}}_{\mathrm{NCI}} = \begin{pmatrix} \underline{r} \\ \underline{r} \\ i\underline{r} \end{pmatrix}. \tag{3.23}$$

Note that the ordering of operators in Eq. (3.21) is symmetric, *i.e.* position-momentum-momentum-position such that the first position-momentum operators belong to the final state and the other belongs to the initial state. Other operator orderings are possible by placing the CS displacement operators of auxiliary parameters differently. Now we can evaluate the non-Condon integrals for arbitrary polynomial operators with the MHP evaluation schemes either in recursive (Eq. (3.5)) or iterative (Eq. (3.9)) way. Even if the parametric matrix ($\widetilde{\mathbf{W}}_{\mathrm{NCI}}$, Eq. (3.22)) and vector ($\tilde{\underline{r}}_{\mathrm{NCI}}$, Eq. (3.22)) are composed of complex numbers, the implementation of the integral formula can be made easily in real number arithmetic because only the off diagonal block matrices contain purely imaginary numbers. Normally the dimensionality of the integral can be reduced[12] because usually the dimensions of momentum operators ($N_P \leq 2N$) and position operators ($N_Q \leq 2N$) are smaller than the dimension of Duschinsky oscillators ($2N$). This non-Condon integral formula has not been implemented in software, but in this thesis the general framework has been successfully applied to the linear HT GF development in chapter 6 in time-independent and time-dependent approaches.

3.3. Chapter summary and conclusion

The integral evaluation schemes for the Franck-Condon and non-Condon factors in the Duschinsky oscillator basis were developed. First, the iterative integral strategy of the col-

---

[12]$\widetilde{\mathbf{W}}_{\mathrm{NCI}}$ and $\tilde{\underline{r}}_{\mathrm{NCI}}$ can be reduced in smaller ones.

lective feature in a uni-variate Hermite polynomial summation (see *e.g.* Eq. (3.9)) was shown to be of much simpler form than the existing multiple products of one-dimensional Hermite polynomial summation formulas (see *e.g.* Eq. (2.105)). The non-Condon integrals were transformed into the MHPs via the CS phase displacement operators like the FC integrals. As a result the FC and non-Condon integrals can be evaluated by MHP evaluation schemes either recursively (Eq. (3.5)) or iteratively (Eq. (3.9)). Numerical tests have not been made yet, but the key idea herein to transform every overlap integral in the Duschin-sky oscillator basis to the MHP problems is valuable for opening up new integral evaluation schemes. We apply the key idea to the later chapter developments, *i.e.* thermal FCF GF (Ch. 4), thermal non-Condon GF (Ch. 6). The complex number MHPs allow the evaluation of the TCFs for single vibronic level transition, anharmonic transition, rR scattering (Ch. 7). The CS displacement operator technique is numerically applied in the thermal FCHT GF chapter 6. Now we have evaluation schemes for the FC and non-Condon integrals, we will try in the next chapter to reduce the number of FC integrals for the thermally excited FC transition system based on the FC integral prescreening development at zero Kelvin [46] (see Sec. 2.4).

4. Thermal distribution of Franck-Condon factors

In this chapter we introduce techniques to take into account the thermally excited initial or final vibrational states with the Boltzmann distribution at finite temperature by including an integral kernel into the Franck-Condon factor (FCF) generating function (GF) (Sec. 2.4). In the time-independent (TI) approach, the corresponding Franck-Condon (FC) integral pre-screening schemes at finite temperature are rigorously developed with the GF. The FCF sum rule is used in the previous work [46][1] for searching prescreening conditions at zero Kelvin[2]. This method is extended to the case of thermalized Duschinsky oscillators (Ch. 2.2). By devising temperature-dependent Doktorov matrices and vectors (Eq. (2.98)), we derive the thermal FCF GF similar to the zero Kelvin development [46] (Eq. (2.123)) so that we can use similar integral prescreening steps at zero Kelvin. The only differences between the functional structure of the resulting thermal FCF GF (2.123) and that of the zero Kelvin is manifested in the former as an additional normalizing factor (the reciprocal vibrational partition function). The sum rules and integral prescreening strategy (Eq. (4.16) and (4.20)) at finite temperature can directly be translated from the zero Kelvin development with the (thermal) integral kernel.

Additionally, the GF approach is directly applicable to the computation of the thermal time-correlation function (TCF) (Eq. 2.14). It is shown that the prescreening parameter matrix $\mathbf{Z}$ in a FCF GF can play a role as a Dirac δ-distribution in the frequency domain. After applying Fourier transform (FT) in time domain, the GF gives rise to the corresponding (thermal) TCF. Our formulation of the coherent state (CS)-based TCF and its FT also provides convenient access to the spectral contribution of individual modes unlike other time-dependent (TD) approaches (see *e.g.* Refs. [17, 34, 35, 37, 64, 137]). The validity of the prescreening conditions at finite temperature has been verified by comparison of the TI and TCF approaches. As first applications of the thermal prescreening, the FC profiles of the $1\,^1A' \rightarrow 1\,^2A'$ band in the photo-electron (PE) spectrum of formic acid and the FC contribution to the lowest energy ultra-violet (UV) absorption band ($1\,^1A_g \rightarrow 1\,^1B_{2u}$) for anthracene at elevated temperatures are presented.

This chapter is presented as follows. In section 4.1 the thermal integral kernel is introduced to the coherent state-based GF with thermal weights on FCFs. The FC integral prescreening strategies for the TI method that also includes thermal effects are developed in sections 4.3 and 4.2 exploiting the GF at finite temperature and the corresponding integral space partition (Sec. 2.4.2). We derive the thermal TCF from the same GF for the TD approach. The results from the two different approaches (TI and TD) via the identical GF are compared in section 4.5. The chapter is concluded in section 4.6.

---

[1] J. Huh was not involved in this work.
[2] See *cf.* Refs. [44, 45] the FC intensity convergence methods.

4.1. Thermal integral kernel

Boltzmann distributed vibrational states corresponding to a thermally averaged initial state is required for the description of FC transition at finite temperature. For this reason, a parameterized integral kernel $K(\mathbf{\Lambda}; \underline{\xi})$ is introduced to the CS GF for the FCFs (Eq. (2.114)). This leads to

$$G^K(\mathbf{Z}; \mathbf{\Lambda}) = \pi^{-2N} |\langle \underline{0}' | \underline{0} \rangle|^{-2} \int \mathrm{d}^2 \underline{\alpha} \mathrm{d}^2 \underline{\gamma}' K(\mathbf{\Lambda}; \underline{\xi}) \langle \mathbf{z}'^* \underline{\gamma}' | \mathbf{z} \underline{\alpha} \rangle \langle \mathbf{z}' \underline{\gamma}' | \mathbf{z}^* \underline{\alpha} \rangle^* , \qquad (4.1)$$

with an ansatz for the thermal integral kernel[3],

$$K(\mathbf{\Lambda}; \underline{\xi}) = \mathcal{N} \det(\mathbf{I} + \mathbf{\Lambda}) \exp(-\underline{\xi}^\dagger \mathbf{\Lambda} \underline{\xi}) . \qquad (4.2)$$

Here the parameter matrix $\mathbf{\Lambda}$ is assumed to be diagonal (diag) with real-valued entries $\boldsymbol{\lambda} = \mathrm{diag}(\underline{\lambda})$ and $\boldsymbol{\lambda}' = \mathrm{diag}(\underline{\lambda}')$, so that $\mathbf{\Lambda} = \mathrm{bldiag}(\boldsymbol{\lambda}, \boldsymbol{\lambda}')$. This matrix will be associated with the Boltzmann factors. $\mathcal{N}$ is a normalization factor which turns out, later, to be a reciprocal vibrational partition function.

We evaluate the GF (Eq. 4.1) in the occupancy representation expression (2.79) with the CSs[4] and find

$$G^K(\mathbf{Z}; \mathbf{\Lambda}) = \mathcal{N} |\langle \underline{0}' | \underline{0} \rangle|^{-2} \sum_{\underline{u}, \underline{u}'} \sum_{\underline{v}, \underline{v}'} \langle \underline{u}' | \underline{u} \rangle \langle \underline{v}' | \underline{v} \rangle^*$$

$$\det(\mathbf{I} + \mathbf{\Lambda}) \prod_{k=1}^N \left[\frac{z_k^{u_k + v_k} (z_k')^{u_k' + v_k'}}{\sqrt{u_k! v_k! u_k'! v_k'!}} \right.$$

$$\left. \left(\frac{1}{\pi} \int \mathrm{d}^2 \alpha_k e^{-|\alpha_k|^2(1+\lambda_k)} \alpha_k^{u_k} (\alpha_k^*)^{v_k} \right) \left(\frac{1}{\pi} \int \mathrm{d}^2 \gamma_k' e^{-|\gamma_k'|^2(1+\lambda_k')} (\gamma_k'^*)^{u_k'} (\gamma_k')^{v_k'} \right) \right] . \quad (4.3)$$

Rescaling of the integration variables reduces to the conventional GF expression (2.109) with a scaling factor. Consequently

$$G^K(\mathbf{Z}; \mathbf{\Lambda}) = \mathcal{N} \sum_{\underline{v}, \underline{v}' = \underline{0}}^{\infty} q(\underline{v}'; \underline{v}) \prod_{k=1}^N \left[\left(\frac{z_k^2}{1+\lambda_k} \right)^{v_k} \left(\frac{(z_k')^2}{1+\lambda_k'} \right)^{v_k'} \right]$$

$$= \mathcal{N} \sum_{\underline{v}, \underline{v}' = \underline{0}}^{\infty} q(\underline{v}'; \underline{v}) \prod_{k=1}^N [z_k^{2v_k} (z_k')^{2v_k'}] e^{-(\underline{v}^\mathrm{t} \mathbf{B} \underline{\epsilon} + \underline{v}'^\mathrm{t} \mathbf{B}' \underline{\epsilon}')} , \qquad (4.4)$$

where the parameters $\mathbf{\Lambda}$, which are related to the Boltzmann factors, are used both for the initial and final states for the sake of generality to cope with the absorption and emission processes and their possible thermal integral prescreening scheme. Making this relationship more explicit, they are connected via

$$(1 + \lambda_k)^{-1} = \exp(-\beta_k \epsilon_k), \qquad (4.5)$$

$$(1 + \lambda_k')^{-1} = \exp(-\beta_k' \epsilon_k'), \qquad (4.6)$$

---

[3]Contribution by J. L. Stuber to J. Huh *et al.* [129].
[4]See Eq. (2.115) for the corresponding expression at zero kelvin.

where $\beta_k = 1/(k_B T_k)$ (with Boltzmann constant k_B and temperature T_k). These parameters are combined in the matrix $\mathbf{B} = \mathrm{diag}(\beta_1, \ldots, \beta_k)$ with analogous expressions holding for primed quantities. All energy parameters ϵ_k and ϵ_k' are assumed to be positive real quantities. Having a β_k for each mode rather than a common value allows to select specific modes. Choosing $\beta_k = 0$, for example, keeps mode k from being Boltzmann weighted which is analogous to the integral space partitioning in section 2.4.2 for the fully integrated space (Y). Our choice of the integral kernel (4.2) thus leads to precisely the required expression (4.4) for the thermally weighted FCFs.

Utilizing the spatial representation of the CS (2.96) for the thermal GF expression of Eq. (4.1) we have then

$$
\begin{aligned}
G^K(\mathbf{Z}; \boldsymbol{\Lambda}) = &\mathcal{N} \pi^{-2N} \det(\mathbf{I} + \boldsymbol{\Lambda}) \\
&\int d^2\underline{\alpha} d^2\underline{\gamma}' \exp(-\underline{\xi}^\dagger (\mathbf{I} + \boldsymbol{\Lambda})\underline{\xi}) \exp(-\tfrac{1}{2}\underline{\xi}^t \mathbf{ZWZ}\underline{\xi} - \tfrac{1}{2}\underline{\xi}^\dagger \mathbf{ZWZ}\underline{\xi}^* + \underline{r}^t \mathbf{Z}(\underline{\xi} + \underline{\xi}^*)),
\end{aligned}
\tag{4.7}
$$

which differs from the zero-temperature formulation (2.119) only in the normalization factor and the prefactor of the first exponential. After a rescaling of variables $\underline{\xi} \to (\mathbf{I} + \boldsymbol{\Lambda})^{\frac{1}{2}}\underline{\xi}$, this again becomes the conventional GF expression (2.119),

$$
\begin{aligned}
G^K(\mathbf{Z}; \boldsymbol{\Lambda}) = &\mathcal{N} \pi^{-2N} \int d^2\underline{\alpha} d^2\underline{\gamma}' \exp(-\underline{\xi}^\dagger \underline{\xi}) \\
&\exp(-\tfrac{1}{2}\underline{\xi}^t \mathbf{ZW}_T\mathbf{Z}\underline{\xi} - \tfrac{1}{2}\underline{\xi}^\dagger \mathbf{ZW}_T\mathbf{Z}\underline{\xi}^* + \underline{r}_T^t \mathbf{Z}(\underline{\xi} + \underline{\xi}^*)),
\end{aligned}
\tag{4.8}
$$

however the quantities $\mathbf{W}_T = \mathbf{W}(T)$ and $\underline{r}_T = \underline{r}(T)$ are now temperature dependent. Specifically,

$$
\mathbf{W}_T = (\mathbf{I} + \boldsymbol{\Lambda})^{-\frac{1}{2}}\mathbf{W}(\mathbf{I} + \boldsymbol{\Lambda})^{-\frac{1}{2}}, \quad \underline{r}_T = (\mathbf{I} + \boldsymbol{\Lambda})^{-\frac{1}{2}}\underline{r},
\tag{4.9}
$$

and the temperature dependence enters via the association made previously in Eqs. (4.5) and (4.6) with the Boltzmann factors. After formal integration, this leads to

$$
\begin{aligned}
G^K(\mathbf{Z}; \boldsymbol{\Lambda}) = &\mathcal{N} \det(\mathbf{I} - \mathbf{ZW}_T\mathbf{Z})^{-\frac{1}{2}} \det(\mathbf{I} + \mathbf{ZW}_T\mathbf{Z})^{-\frac{1}{2}} \\
&\exp(\underline{r}_T^t \mathbf{Z}(\mathbf{I} + \mathbf{ZW}_T\mathbf{Z})^{-1}\mathbf{Z}\underline{r}_T),
\end{aligned}
\tag{4.10}
$$

in the same functional form of zero-temperature GF (2.123) with temperature dependent parameters and a normalizing factor.

Evaluating the normalization constant $\mathcal{N}$, the reciprocal vibrational partition function, is necessary for subsequent interpretation of the entries forming thermal FCF sum rules and FC transition probabilities, and for the subsequent application of the sum rules on the FC integral prescreening. As indicated previously, we can select the states which participate in the Boltzmann weighting scheme by choosing $\beta_k > 0$ and prevent thermalization of selected modes by fixing $\beta_k = 0$, corresponding to $\lambda_k = 0$. Using the polynomial expression for the GF in Eq. (4.4) together with the formal integral of the spatial representation (Eq. (4.10)),

$$1 = |\langle \underline{0}'|\underline{0}\rangle|^2 G^K(\mathbf{I}; \mathbf{\Lambda})$$

$$= \mathcal{N} \sum_{\underline{v},\underline{v}'=\underline{0}}^{\infty} |\langle \underline{v}'|\underline{v}\rangle|^2 \exp(-\underline{v}^{\mathrm{t}}\mathbf{B}\underline{\epsilon}) \exp(-\underline{v}'^{\mathrm{t}}\mathbf{B}'\underline{\epsilon}') \tag{4.11}$$

$$= |\langle \underline{0}'|\underline{0}\rangle|^2 \mathcal{N} \det(\mathbf{I} - \mathbf{W}_T)^{-\frac{1}{2}} \det(\mathbf{I} + \mathbf{W}_T)^{-\frac{1}{2}}$$
$$\exp(\underline{r}_T^{\mathrm{t}}(\mathbf{I} + \mathbf{W}_T)^{-1}\underline{r}_T). \tag{4.12}$$

The choice of the normalization constant which must therefore be taken is

$$\mathcal{N} = |\langle \underline{0}'|\underline{0}\rangle|^{-2} \det(\mathbf{I} - \mathbf{W}_T)^{\frac{1}{2}} \det(\mathbf{I} + \mathbf{W}_T)^{\frac{1}{2}}$$
$$\exp(-\underline{r}_T^{\mathrm{t}}(\mathbf{I} + \mathbf{W}_T)^{-1}\underline{r}_T). \tag{4.13}$$

The factor $\mathcal{N}|\langle \underline{0}'|\underline{0}\rangle|^2$ can be viewed as the effective temperature dependence of the $\langle \underline{0}'|\underline{0}\rangle$ integral. The series summation in Eq. (4.11) can be rewritten in a density matrix form, if we invoke the (harmonic) vibrational Hamiltonians (Eqs. (2.47) and (2.54)),

$$1 = \mathcal{N} \mathrm{Tr}(\exp(-\underline{\beta} \cdot \hat{\underline{h}}) \exp(-\underline{\beta}' \cdot \hat{\underline{h}}')), \tag{4.14}$$

where the vibrational Hamiltonians are in mode separated form $\hat{H} = \sum_k^N \hat{h}_k$ and $\hat{H}' = \sum_k^N \hat{h}'_k$ for the initial and final state respectively. This shows that $\mathcal{N}$ is the reciprocal vibrational partition function.

For the special case $T_k = 0$ one has to substitute in Eq. (4.12) the term $\exp(-v_k \beta_k \epsilon_k)$ by $\delta_{v_k,0} = \lim_{\beta_k \epsilon_k \to \infty} e^{-v_k \beta_k \epsilon_k}$, which is unity for $v_k = 0$ and vanishes otherwise. With these changes, namely that of the normalization ($\mathcal{N}$) and coefficients ($\mathbf{W}_T$ and $\underline{r}_T$), the sum rules and prescreening conditions corresponding to the previous work [46] can be translated directly to the thermal case (Secs. 4.2 and 4.3).

4.2. Sum rules

Analogously to the integral partitioning scheme in section 2.4.2, we can decompose the GF $G^K(\mathbf{Z}; \mathbf{\Lambda})$ into terms depending on variables belonging to the orthogonal subspaces X and Y. The space X is associated with modes for which quantum numbers are kept fixed, while Y contains modes which involve summation over all harmonic oscillator states, possibly weighted by a Boltzmann factor at finite temperature. The partitioned expression for the thermal FCF GF is[5]

$$G^K(\mathbf{Z}_{XX}, \mathbf{Z}_{YY}; \mathbf{\Lambda}) = G^K_{X|Y}(\mathbf{Z}_{XX}, \mathbf{Z}_{YY}; \mathbf{\Lambda}) G^K_Y(\mathbf{Z}_{YY}; \mathbf{\Lambda}). \tag{4.15}$$

We can apply the sum rules arising from this partitioned expression to prescreen FCFs at finite temperatures. And we can obtain rigorous bounds on the integrated FC profile according to the maximum number of simultaneously excited modes (MSM) and the maximum

---

[5]See Eq. (2.127) for zero Kelvin development.

excitation quantum number of modes (MQM), which are required to achieve a given tolerance level. Specifics of the prescreening strategy are given in the following subsections.

4.2.1. No excited modes in the X space

When all vibrational modes in the the fixed quantum number space X (see Sec. 2.4.2 for the integral space partitioning convention in this thesis) are frozen in their vibrationless ground states, the generating function component in X space $G_{X|Y}^K$ is factored out as a value of unity so that one only needs to care about the component in Y space, *i.e.* G_Y^K. A specific example of practical use is setting the GF parameter matrix in Y space to the identity matrix ($\mathbf{Z}_{YY} = \mathbf{I}_{YY}$), the parameters of X space to the zero matrix ($\mathbf{Z}_{XX} = \mathbf{0}_{XX}$), so that the Boltzmann factor weighted partitioned GF reads

$$G^K(\mathbf{0}_{XX}, \mathbf{I}_{YY}; \mathbf{\Lambda}) = G_Y^K(\mathbf{I}_{YY}; \mathbf{\Lambda}) = \mathcal{N} \sum_{\underline{v}_Y, \underline{v}_Y' = \underline{0}}^{\infty} q(\underline{v}_Y'; \underline{v}_Y) \mathrm{e}^{-\underline{v}_Y^{\mathrm{t}} \mathbf{B}_{YY} \underline{\epsilon}_Y} \mathrm{e}^{-\underline{v}_Y'^{\mathrm{t}} \mathbf{B}_{YY}' \underline{\epsilon}_Y'}$$

$$= \mathcal{N} \det((\mathbf{I} + \mathbf{W}_T)_{YY})^{-\frac{1}{2}} \det((\mathbf{I} - \mathbf{W}_T)_{YY})^{-\frac{1}{2}}$$
$$\exp(\underline{r}_{T;Y}^{\mathrm{t}} ((\mathbf{I} + \mathbf{W}_T)_{YY})^{-1} \underline{r}_{T;Y}). \tag{4.16}$$

Usually only the initial states are thermally excited and the temperature dependent Doktorov quantities (Eqs. (4.9)) are given precisely for this case,

$$\mathbf{W}_T = \begin{pmatrix} (\mathbf{I} + \boldsymbol{\lambda})^{-\frac{1}{2}} (\mathbf{I} - 2\mathbf{Q}) (\mathbf{I} + \boldsymbol{\lambda})^{-\frac{1}{2}} & -2(\mathbf{I} + \boldsymbol{\lambda})^{-\frac{1}{2}} \mathbf{R} \\ -2\mathbf{R}^{\mathrm{t}} (\mathbf{I} + \boldsymbol{\lambda})^{-\frac{1}{2}} & \mathbf{I} - 2\mathbf{P} \end{pmatrix}, \tag{4.17}$$

$$\underline{r}_T = \sqrt{2} \begin{pmatrix} -(\mathbf{I} + \boldsymbol{\lambda})^{-\frac{1}{2}} \mathbf{R} \underline{\delta} \\ (\mathbf{I} - \mathbf{P}) \underline{\delta} \end{pmatrix}, \tag{4.18}$$

in which the thermal factors are weighted only on the initial degrees of freedom (DOF).

4.2.2. One excited mode in the X space

When a mode in the space X is excited to a certain vibrational state, say the mode k is excited to n-th vibrational excited state, the GF component $G_{X|Y}^K$ in X space is no longer factored out as unity but a portion of $G_{X|Y}^K$ is weighted on the GF [6]. This provides a criterion for the MQM required in each mode. The resulting expression for the GF Eq. (4.15) in this case is given by

$$G^K(\mathbf{Z}_{XX}, \mathbf{I}_{YY}; \mathbf{\Lambda}) = G_{X|Y}^K(\mathbf{Z}_{XX}, \mathbf{I}_{YY}; \mathbf{\Lambda}) G_Y^K(\mathbf{I}_{YY}; \mathbf{\Lambda}). \tag{4.19}$$

The mode k under consideration corresponds with v_k'' the vibrational quantum number constrained to n, the expression for the factor of interest is obtained via a power series expan-

---

[6]This number, the partial summation of $G_{X|Y}^K$, can be considered as a contribution of an n-fold excitation on the k-th mode to the total intensity.

sion of $G_{X|Y}^K$ with $v_k'' = n$,

$$
\mathcal{N} \sum_{\underline{v}_Y, \underline{v}_Y' | v_k'' = n} q(\underline{v}_Y'; \underline{v}_Y) \mathrm{e}^{-\underline{v}_Y^{\mathrm{t}} \mathbf{B}_{YY} \underline{\epsilon}_Y} \mathrm{e}^{-\underline{v}_Y^{\prime\mathrm{t}} \mathbf{B}_{YY}' \underline{\epsilon}_Y'}
$$
$$
= G_Y^K(I_{YY}; \boldsymbol{\Lambda}) \mathcal{G}(\widetilde{\mathbf{W}}_T^{\pm}(\mathbf{I}_{YY}); \underline{\tilde{r}}_T^+(\mathbf{I}_{YY}); k; n; 0, \tfrac{1}{2}, 0, 0), \tag{4.20}
$$

where

$$
\widetilde{\mathbf{W}}_{T;XX}^{\pm}(\mathbf{Z}_{YY}) = \mathbf{W}_{T;XX} \mp \mathbf{W}_{T;XY} \mathbf{Z}_{YY}((\mathbf{I} \pm \mathbf{Z} \mathbf{W}_T \mathbf{Z})_{YY})^{-1} \mathbf{Z}_{YY} \mathbf{W}_{T;YX}, \tag{4.21}
$$
$$
\underline{\tilde{r}}_{T;X}^+(\mathbf{Z}_{YY}) = \underline{r}_{T;X} - \mathbf{W}_{T;XY} \mathbf{Z}_{YY}((\mathbf{I} + \mathbf{Z} \mathbf{W}_T \mathbf{Z})_{YY})^{-1} \mathbf{Z}_{YY} \underline{r}_{T;Y}, \tag{4.22}
$$

with the GF parameter matrix $\mathbf{Z}_{YY} = \mathbf{I}_{YY}$, corresponding to the zero-temperature quantities (2.130) and (2.131), respectively, and the power series expansion functional,

$$
\mathcal{G}(\widetilde{\mathbf{W}}_T^{\pm}; \underline{\tilde{r}}_T^+; k; n; a_0, b_0, c_0, d_0) =
$$
$$
\pi^{-1} \sum_{l=0}^{n-d_0} \sum_{m=0}^{n-l-d_0} \frac{(-\widetilde{W}_{T;kk}^+)^l (2\tilde{r}_{T;k}^+)^{2m+a_0} (\widetilde{W}_{T;kk}^-)^{n-l-m-d_0}}{l!(2m+a_0)!(n-l-m-d_0+c_0)!}
$$
$$
\Gamma(l+m+b_0)\Gamma(n-l-m-d_0+c_0). \tag{4.23}
$$

4.3. Integral prescreening

The prescreening strategies taken by the previous work [46] and the current thesis invoke several subspaces in vibrational occupation number vector (ONV) space classified by the MQM and the MSM. The goal of this numerical scheme is to determine restriction on the vibrational quantum excitations such that the partial sum over fractional FCFs reaches a desired threshold, before we calculate individual FC integrals, *i.e.* finding MQM and MSM according to the intensity threshold. For a given error tolerance $\epsilon_{\max}^{\mathrm{tol}}$ in the FC total intensity[7] (the integrated FC profile), the vibrational ONV subspace $\mathcal{S}$ (in which FC integrals are evaluated later) is systematically expanded until the calculated total FC intensity error[8] ϵ_{tot} drops below the desired intensity error $\epsilon_{\max}^{\mathrm{tol}}$ such that

$$
\epsilon_{\mathrm{tot}} = 1 - F_{\mathrm{FC}}^{\mathrm{tot}} \le \epsilon_{\max}^{\mathrm{tol}}, \tag{4.24}
$$

where the total intensity in the ONV subspace is

$$
F_{\mathrm{FC}}^{\mathrm{tot}} = \mathcal{N} \sum_{\underline{v}, \underline{v}' \in S} \left| \langle \underline{v}' | \underline{v} \rangle \right|^2 \mathrm{e}^{-\underline{v}^{\mathrm{t}} \mathbf{B} \underline{\epsilon}} \mathrm{e}^{-\underline{v}'^{\mathrm{t}} \mathbf{B}' \underline{\epsilon}'}. \tag{4.25}
$$

A coarse-grained FC integral prescreening strategy determines for instance a maximum harmonic oscillator quantum number in each normal mode as well as a MSM, such that all FCFs in line with these restrictions yield an integrated FC profile that deviates at most by

---

[7]The FC spectral density function (Eq. (2.29)) is normalized with the absolute square of electronic transition dipole moment (TDM) in Condon approximation ($|\underline{\mu}_0|^2$) to make the total intensity unity when all FCFs are summed.

[8]Error is defined as the remaining intensity summation of the rest of vibrational ONV space ($\not\subseteq \mathcal{S}$).

the user defined threshold $\epsilon_{\max}^{\mathrm{tol}}$ from the complete integrated FC profile. Instead of utilizing $\epsilon_{\max}^{\mathrm{tol}}$ directly, it is convenient to employ auxiliary parameters [46] t_m and t_c satisfying

$$\epsilon_{\max}^{\mathrm{tol}} = 1 - \prod_{\gamma}\left[1 - (t_{\mathrm{c}} + N_\gamma t_{\mathrm{m}})\right],\ 0 \le t_{\mathrm{c}} + N_\gamma t_{\mathrm{m}} \le 1\,, \tag{4.26}$$

where t_{m} and t_{c} are associated to the mode and coupling tolerances, respectively, and γ is a index over all irreducible representations in the molecular system. N_γ is the number of vibrational modes belonging to the irreducible representation γ.

4.3.1. Vibrational mode coupling error

We can obtain the minimum number of simultaneously excited modes that are required to reach the threshold t_{c} by repeated application of Eq. (4.16). All integrals involving a large number of simultaneously excited modes are then neglected. For the different modes belonging to the X and Y spaces, the MSM M is increased from $M = 0$ until the desired vibrational mode coupling error[9] is achieved for the coupling tolerance t_c, *i.e.* according to Ref. [46]

$$\epsilon_{\mathrm{c}} = 1 - \sum_{m=0}^{M} F_{\mathrm{FC;c}}^{(m)} = 1 - \widetilde{F}_{\mathrm{FC;c}}^{(M)} < t_c\,, \tag{4.27}$$

where $F_{\mathrm{FC;c}}^{(m)}$ is an increment for the contribution of m simultaneously excited modes to the total intensity and $\widetilde{F}_{\mathrm{FC;c}}^{(M)} = \sum_{m=0}^{M} F_{\mathrm{FC;c}}^{(m)}$. Each increment can be determined from the intermediate quantity,

$$B_{\mathrm{FC}}^{(m)} = \sum_{Y \in C_m^{2N}} |\langle \underline{0}'|\underline{0}\rangle|^2 G_Y^K(\mathbf{I}_{YY}; \boldsymbol{\Lambda})\,, \tag{4.28}$$

where C_m^{2N} is the set from the space Y given by choosing m modes for summation out of possible $2N$, via the relation

$$F_{\mathrm{FC;c}}^{(m)} = B_{\mathrm{FC}}^{(m)} - \sum_{i=1}^{m} \binom{2N - m + i}{i} F_{\mathrm{FC;c}}^{(m-i)}\,. \tag{4.29}$$

Here we have used $F_{\mathrm{FC;c}}^{(0)} = \mathcal{N} |\langle \underline{0}'|\underline{0}\rangle|^2$.

---

[9]This quantity is directly related to the Duschinsky mode mixing effects. When there is no Duschinsky mode mixing the error is already zero at $M = 1$. When the Duschinsky mode mixing is significant, M is increased to make the error drop below the requested tolerance.

4.3.2. Vibrational mode excitation error

We define a mode contribution $F_{\text{FC;m}}^{(k)}(n)$ associated with a fixed vibrational quantum number $v_k'' = n$ for mode k while other modes are summed over, *i.e.*

$$F_{\text{FC;m}}^{(k)}(n) = \mathcal{N} \sum_{\underline{v}, \underline{v}' | v_k'' = n} |\langle \underline{v}' | \underline{v} \rangle|^2 e^{-\underline{v}^{\text{t}} \mathbf{B} \underline{\epsilon}} e^{-\underline{v}'^{\text{t}} \mathbf{B}' \underline{\epsilon}'}. \tag{4.30}$$

The total mode contribution of mode k to the total intensity can be given by Eq. (4.16) summing over the quantum numbers of all other modes while leaving the mode k at $v_k'' = 0$, *i.e.* the partial contribution $F_{\text{FC;m}}^{(k)}(0)$ is the contribution excluding excitations of mode k. We determine the contribution $F_{\text{FC;m}}^{(k)}(n)$ with the finite series summation for a fixed quantum number Eq. (4.20). To obtain the maximum quantum number for a specific vibrational mode, we determine a minimum quantum number $v_k''^{\max}$ satisfying

$$\epsilon_{\text{m}}^{(k)} = \left(1 - F_{\text{FC};v_k''^{\max}} \right) < t_{\text{m}}, \tag{4.31}$$

where $\epsilon_{\text{m}}^{(k)}$ is the corresponding vibrational mode excitation error and

$$F_{\text{FC};v_k''^{\max}} = \sum_{n=0}^{v_k''^{\max}} F_{\text{FC;m}}^{(k)}(n). \tag{4.32}$$

4.3.3. Error bound condition

The error bound can be deduced from the intensity errors of the irreducible representations (γ) of the corresponding molecular symmetry group. The Duschinsky rotational matrix $\mathbf{S}$ is in a block diagonal form for a symmetric molecule. The blocks are separated by the irreducible representation of the molecular point group symmetry. This separation feature can reduce the effort to evaluate the multi-dimensional FC integrals and the FC integral prescreening conditions can be made accordingly with the separated from of the GF,

$$G^K(\mathbf{Z}; \mathbf{\Lambda}) = \prod_{\gamma} G_{(\gamma)}^K(\mathbf{Z}_{(\gamma)(\gamma)}; \mathbf{\Lambda}), \tag{4.33}$$

where γ indicates the irreducible representations and $\mathbf{Z}_{(\gamma)(\gamma)}$ is the corresponding parameter matrix. The quantities of $\epsilon_{\text{m}}^{(k)}$ and ϵ_{c} are written as $\epsilon_{\text{m}}^{(k,\gamma)}$ and $\epsilon_{\text{c}}^{(\gamma)}$ respectively corresponding to the irreducible representations. With the following quantities defined as follow,

$$\epsilon_{\min}^{(\gamma)} = \max(\epsilon_{\text{m}}^{(\gamma)}, \epsilon_{\text{c}}^{(\gamma)}), \tag{4.34}$$

and

$$\epsilon_{\max}^{(\gamma)} = \epsilon_{\text{c}}^{(\gamma)} + \sum_{k \in \gamma} \epsilon_k^{(m,\gamma)}, \tag{4.35}$$

where

$$\epsilon_{\mathrm{m}}^{(\gamma)} = \max_k \epsilon_{\mathrm{m}}^{(k,\gamma)}, \qquad (4.36)$$

it is found [46] that the following bound condition is satisfied,

$$\epsilon_{\min} \le \epsilon_{\mathrm{tot}} \le \epsilon_{\max} \le \epsilon_{\max}^{\mathrm{tol}}. \qquad (4.37)$$

Here the lower and upper bounds are given in terms of irreducible representation contributions,

$$\epsilon_{\min} = 1 - \prod_{\gamma} \left(1 - \epsilon_{\min}^{(\gamma)} \right), \qquad (4.38)$$

$$\epsilon_{\max} = 1 - \prod_{\gamma} \left(1 - \epsilon_{\max}^{(\gamma)} \right). \qquad (4.39)$$

4.4. Thermal time-correlation function

The Franck-Condon factor weighted density of states (FCW) in a stick representation $\varrho_{\mathrm{FCW}}(\omega; T) = \lim_{\Gamma \to 0} |\underline{\mu_0}|^{-2} \rho_{\mathrm{FC,L}}(\omega; T)$ at a given transition frequency ω is given by

$$\varrho_{\mathrm{FCW}}(\omega; T) = \mathcal{N} \sum_{\underline{v}, \underline{v}' = \underline{0}}^{\infty} |\langle \underline{v}' | \underline{v} \rangle|^2 \delta((\underline{v}' \cdot \underline{\epsilon}' - \underline{v} \cdot \underline{\epsilon}) - \hbar(\omega - \omega_0)) \mathrm{e}^{-(\underline{v}^{\mathrm{t}} \mathbf{B} \underline{\epsilon} + \underline{v}'^{\mathrm{t}} \mathbf{B}' \underline{\epsilon}')}, \quad (4.40)$$

with ω_0 corresponding to the frequency of the $0' - 0$ transition. Bearing in mind the Fourier representation of the Dirac δ-distribution, $\delta(\omega - \overline{\omega}) = \int_{-\infty}^{\infty} \mathrm{d}t \, \mathrm{e}^{\mathrm{i}(\omega - \overline{\omega})t}$ and $\delta(\hbar(\omega - \overline{\omega})) = \hbar^{-1}\delta(\omega - \overline{\omega})$, we can express $\varrho_{\mathrm{FCW}}(\omega)$ according to Eq. (4.4) with the help of the GF via

$$\varrho_{\mathrm{FCW}}(\omega; T) = \mathcal{N} |\langle \underline{0}' | \underline{0} \rangle|^2 \hbar^{-1} \int_{-\infty}^{\infty} \mathrm{d}t \, G^K(\mathbf{Z}(t); \mathbf{\Lambda}) \mathrm{e}^{\mathrm{i}(\omega - \omega_0)t}, \qquad (4.41)$$

where we choose $\mathbf{Z}(t) = \mathrm{bldiag}(\mathbf{z}(t), \mathbf{z}'(t))$ as with

$$\mathbf{z}(t) = \mathrm{diag}(\mathrm{e}^{\mathrm{i}\epsilon_1 t/(2\hbar)}, \dots, \mathrm{e}^{\mathrm{i}\epsilon_N t/(2\hbar)}), \qquad (4.42)$$

$$\mathbf{z}'(t) = \mathrm{diag}(\mathrm{e}^{-\mathrm{i}\epsilon_1' t/(2\hbar)}, \dots, \mathrm{e}^{-\mathrm{i}\epsilon_N' t/(2\hbar)}), \qquad (4.43)$$

introduced in Eqs. (4.42) and (4.43) respectively. The expression $|\underline{\mu_0}|^2 \mathcal{N} |\langle \underline{0}' | \underline{0} \rangle|^2 G^K(\mathbf{Z}(t); \mathbf{\Lambda})$ corresponds to the TCF in Eq. (2.14) within the Condon approximation. A convolution of $\varrho_{\mathrm{FCW}}(\omega; T)$ with a Lorentzian line shape function of full width at half maximum (FWHM) Γ can be achieved by introducing $L(t) = \exp(-\Gamma |t|/2)$ in the expression for the TCF (4.41) via

$$\varrho_{\mathrm{FCW,L}}(\omega; T) = \mathcal{N} |\langle \underline{0}' | \underline{0} \rangle|^2 \hbar^{-1} \int_{-\infty}^{\infty} \mathrm{d}t \, G^K(\mathbf{Z}(t); \mathbf{\Lambda}) L(t) \mathrm{e}^{\mathrm{i}(\omega - \omega_0)t}. \qquad (4.44)$$

If only the initial states are thermally excited in the mode excitation active space Y, as required in many practical applications, the explicit working equation is given by

$$\varrho_{\text{FCW,L}}(\omega) = \mathcal{N}|\langle \underline{0}'|\underline{0}\rangle|^2 \hbar^{-1} \int_{-\infty}^{\infty} \mathrm{d}t \det(\mathbf{I} - \mathbf{Z}(t)\mathbf{W}_T\mathbf{Z}(t))^{-\frac{1}{2}}$$

$$\det(\mathbf{I} + \mathbf{Z}(t)\mathbf{W}_T\mathbf{Z}(t))^{-\frac{1}{2}}$$

$$\exp(\underline{r}_T^{\text{t}}\mathbf{Z}(t)(\mathbf{I} + \mathbf{Z}(t)\mathbf{W}_T\mathbf{Z}(t))^{-1}\mathbf{Z}(t)\underline{r}_T)L(t)\mathrm{e}^{\mathrm{i}(\omega-\omega_0)t},$$

$$(4.45)$$

with the Doktorov quantities in Eqs. (4.17) and (4.18). Other types of line shape functions such as the Gaussian line shape function can also be used or can be used together with the Lorentzian line shape function. Therefore, the FC profile can be obtained with the help of the fast Fourier transform (FFT) technique as in Eq. (4.45). In contrast to the TI approach, this does not facilitate the direct assignment of individual vibronic transitions which contribute to the FC profile. With different sets of $\mathbf{Z}(t)$, however, it is possible to extract further useful information by exploiting the FFT of the resulting TCF. Contributions of individual normal modes may be filtered, for instance, by preventing time-propagation of some vibrational modes assigning some of the diagonal elements in $\mathbf{z}(t)$ and $\mathbf{z}'(t)$ to 1 ($t = 0$), similar to the TI prescreening approaches in the previous work [46] and this work. Furthermore, if one sets all ϵ_i to 1 and all ϵ'_i to 1 in Eq. (4.42), one can obtain the FC contributions of sums of quantum number difference ($\sum_i v'_i - v_i$) and one may also obtain further useful prescreening criteria for the TI approach on this basis. In the present work, however, such additional prescreening conditions are not exploited. The TCF can also be expressed in a product form of irreducible representation group TCFs as in Eq. (4.33), *i.e.*

$$G^K(\mathbf{Z}(t); \mathbf{\Lambda}) = \prod_\gamma G^K_{(\gamma)}(\mathbf{Z}_{(\gamma)(\gamma)}(t); \mathbf{\Lambda}), \qquad (4.46)$$

which is useful in fast TCF evaluation.

The important aspect of our time-dependent development is that our TCF is constructed from the generating function in the time-independent approach (Eq. (4.4)). The identical generating function can be used for the FC intensity sum rule and TCF calculation. The extension to the non-Condon application is shown in chapter 6. The link between the TD and TI approaches are made via the GF parameters (Eqs. (4.42) and (4.43)), which are related to the Dirac δ-distribution. The GF derivation from the time-dependent perspective in the trace formalism is presented in section 6.1.2 for the non-Condon effects.

4.5. Results and discussion

The Franck-Condon profiles of the photo-electron and ultra-violet absorption spectra reported herein have been calculated with the vibronic structure program hotFCHT [36, 46, 129–131] [10] using the FC integral prescreening conditions developed in the previous section for FCFs, and the finite temperature TCF method. The FC integrals are evaluated with the recurrence relations of Eqs. (2.103) and (2.104). For prescreening steps before FC integral

---

[10]The thermal prescreening routine and thermal TCF method are implemented by J. Huh.

calculations, one first selects thresholds t_{m} and t_{c} for the mode and coupling tolerances to determine a first error estimate $\epsilon_{\mathrm{max}}^{\mathrm{tol}}$ via Eq. (4.26) for the integrated FC profile. Tighter error bounds ϵ_{min} and ϵ_{max} at a given finite temperature are then calculated in the prescreening stage (Sec. 4.3). The FC profile is then obtained for the batch of FC integrals selected at the prescreening stage and the resulting total error ϵ_{tot} is compared to the rigorous prescreening error bounds, satisfying the inequality Eq. (4.37).

One difference between the integral prescreening at finite temperatures and the integral prescreening at zero Kelvin is that the Y space in the latter case includes only modes from the final electronic state, whereas in the former case the modes of the initial electronic state also belong to this space. Consequently, the number of vibrational DOF N_γ in Eq. (4.26) is twice as large for finite temperatures as compared to 0 K, so that $\epsilon_{\mathrm{max}}^{\mathrm{tol}}$ values differ even for the same tolerance sets. For formic acid and anthracene, two of the application examples for the previous 0 K development [46], the influence of different threshold choices on the accuracy of the calculation at different finite temperatures are investigated (see Table 4.1 and Table 4.2).

In the evaluation of Eq. (4.45), corresponding to the FT of the Lorentzian weighted TCF, the FFTW [178] library (version 3.1.2) for the FFT is used with a grid size of 2^{16} and a time increment of $\Delta t = 0.51$ fs, and the time interval [-16.7 ps, 16.7 ps]. The time reversal symmetry relation of the TCF, $G^K(\mathbf{Z}(-t); \mathbf{\Lambda}) = G^K(\mathbf{Z}(t); \mathbf{\Lambda})^*$ is also exploited. The real part of the FT is taken for the FC profile. For these plots (Figs. 4.1 and 4.3) the relation between the frequency and the wavenumber representations $\varrho_{\mathrm{FCW,L}}(\tilde{\nu}) = hc_0 \varrho_{\mathrm{FCW,L}}(\omega)$ have been exploited.

Equilibrium structures and harmonic force fields of formic acid and anthracene have been taken from the previous work [46] and molecular symmetry (point groups of the equilibrium structures are C_{s} for formic acid and $D_{2\mathrm{h}}$ for anthracene) is exploited at the prescreening stage. Symmetry leads to a block diagonal Duschinsky matrix $\mathbf{S}$ and allows us to treat modes according to different irreducible representations independently.

The M_{max} in Tables 4.1 and 4.2 represents a maximum of the MSMs among all symmetry blocks that is necessary to achieve the tolerance t_c. Additionally, in the tables the individual $M_{\mathrm{max}}^{(\gamma)}$ of each symmetry block is given, such that $M_{\mathrm{max}} = \max_\gamma M_{\mathrm{max}}^{(\gamma)}$. The behaviour of the resulting coupling error $\epsilon_{\mathrm{c}} = 1 - \widetilde{F}_{\mathrm{c}}^{(M)}$ with increasing number of simultaneously excited modes M in formic acid and anthracene is displayed in Figs. 4.2 and 4.4. To obtain plots in accordance with the results given in Table III of Ref. [46] and Table I of Ref. [44] $\epsilon_{\mathrm{c}}^{(\gamma)}(M^{(\gamma)})$ are combined for different values of $M^{(\gamma)}$ such that a value of $\epsilon_{\mathrm{c}}(M)$ for each distinct $M = \sum_\gamma M^{(\gamma)}$ is obtained. The coupling error obtained in this way corresponds to prescreening without exploiting the point group symmetry. A direct comparison between Table 4.1 and Figure 4.2 as well as between Table 4.2 and Figure 4.4 for the mode coupling errors cannot be made due to the symmetry argument and the different tolerance settings. In the TCF method calculation, the molecular symmetry is not exploited, even if it is straightforward in Eq. (4.46), due to the relatively low computational cost of this method for the small size of molecules (formic acid and anthracene).

The supplementary data (harmonic wavenumbers, integral prescreening data, etc.) for this chapter are given in appendix A.

4.5.1. Formic acid

Leach *et al.* [179] measured PE spectra of various formic acid isotopologues for the $1\,^1\mathrm{A}' \to 1\,^2\mathrm{A}'$ transition from the electronic ground state of the neutral to the electronic ground state of the formic acid cation. The authors assigned most of their vibrationally resolved spectral peaks, with the help of vibrational frequencies obtained with harmonic force fields from *ab initio* quantum chemical calculations, leaving a few peaks unassigned. Rudberg *et al.* [180] simulated the vibronic spectra of the formic acid isotopologues with zero Kelvin assumption by computing FCFs with molecular structures and harmonic force fields from density functional theory (DFT) calculations, and completed the peak assignments. Jankowiak *et al.* [46] computed the vibronic spectrum of formic acid (HCOOH) at zero Kelvin with FCF calculation to test their FC integral prescreening technique. The equilibrium molecular structures and harmonic force fields in Ref. [46] were obtained from CCSD(T) quantum chemical calculations.

The results obtained for zero Kelvin for formic acid (HCOOH) are also presented herein (see Table 4.1 and Fig. 4.1) to see the finite temperature effects. The time-independent FC calculations at zero Kelvin are identical to those of Ref. [46] with the integral prescreening technique. The experimental PE spectrum of Leach *et al.* [179] is compared with our FC profile at zero Kelvin in Fig. 4.1(c). The overlay of the experimental curve to the theoretical one is based on the peak assignments in Ref. [179] and the curve height is rescaled to fit its $0'-0$ peak to our computed one. The most prominent feature of the spectrum is a progression on the C=O stretching mode, because the C=O bond length increases when an electron is removed from the corresponding π-orbital. The experimental spectrum and the theoretical one from harmonic approximation agrees well even if the theoretical calculation of C=O stretching mode ($\tilde{\nu}_3 = 1566\ \mathrm{cm}^{-1}$) shows a longer progression in the computed spectrum. This is due to a slightly overestimated C=O bond length in the ionized ground state. The corresponding experimental fundamental wavenumber is $1495\ \mathrm{cm}^{-1}$. The unassigned peak in Ref. [179], the 7-th peak (at $2890\ \mathrm{cm}^{-1}$) in Fig. 4.1(c), is assigned as[11] $3_0^1 4_0^1$ with the corresponding theoretical wavenumber $\tilde{\nu}_3 + \tilde{\nu}_4 = 2966\ \mathrm{cm}^{-1}$. In spite of the overestimation of the C=O bond length the theoretical study [46] could confirm the previous peak assignments of Refs. [179, 180] for the 16 peaks of Leach *et al.* [179] in Fig. 4.1(c).

We compute, herein, the FC profiles of the PE spectra formic acid (HCOOH) at given finite temperatures for different choices of tolerance settings (Table 4.1). For all tolerance sets and temperatures the error bound condition Eq. (4.37) is numerically satisfied. Looser tolerance settings naturally give rise to a larger number of prescreened FCFs as indicated in the Table 4.1 with larger total intensity error ϵ_{tot}. The FC profile is, even with the coarse-grained prescreening employed herein, available for temperatures as high as $1000\ \mathrm{K}$, with a value of ϵ_{tot} on the order of 0.7%. Fig. 4.1 displays the temperature dependence of the FC profile. The temperature effect on the profile at $300\ \mathrm{K}$ is barely visible on the scale given here, whereas a much more congested FC structure within the same energy range is obtained for $1000\ \mathrm{K}$.

If it were not for the finite accuracy of the numerical FT, the spectra from the TCF approach should always be an upper bound to the spectra from the prescreening FCF calculation, as the FC profile from the TCF should integrate to 1, whereas it approaches the

---

[11]The peaks are denoted with a_b^c which indicates a vibronic transition from a-th vibrational mode in b-th vibrationally excited initial state to a-th vibrational mode in c-th vibrationally excited final state.
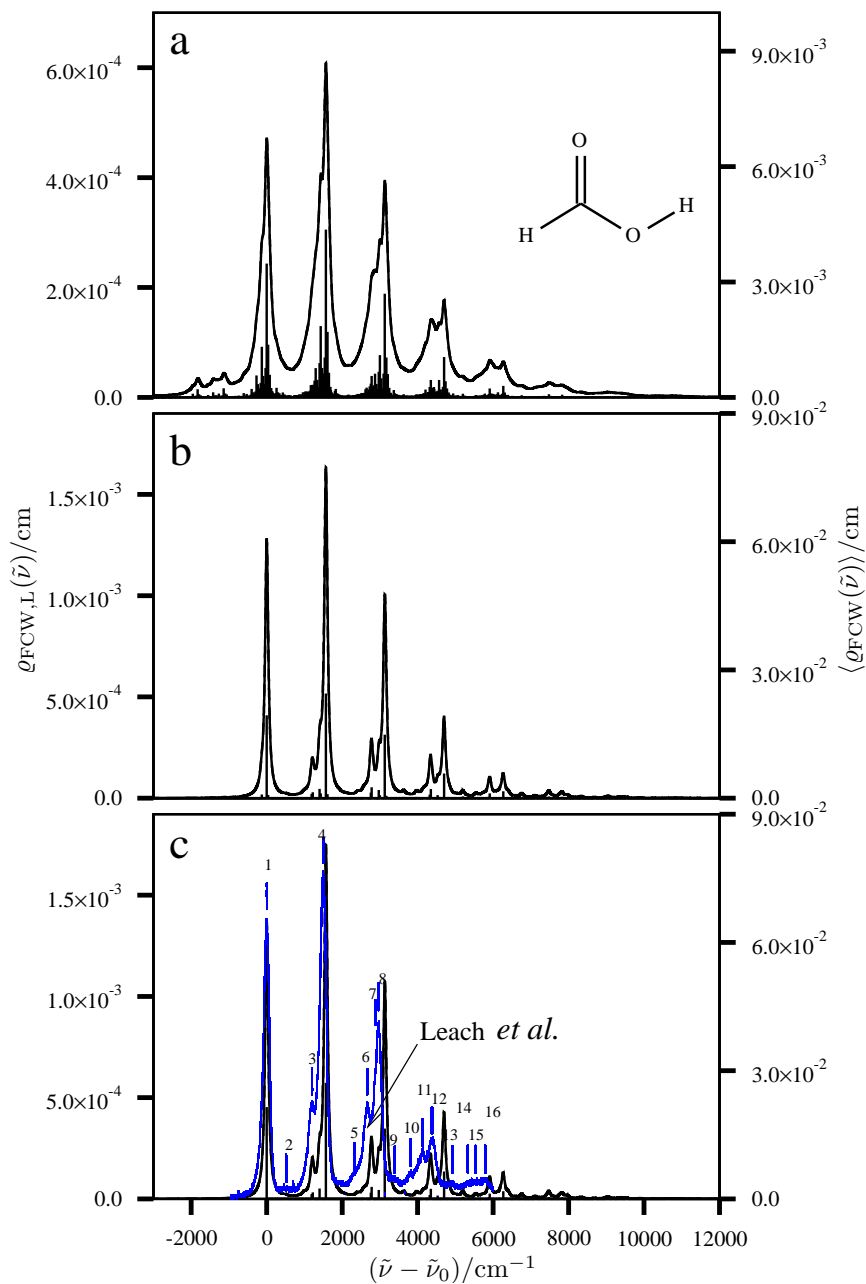
Figure 4.1.: Calculated FC profiles for the $1\,^1A'\,\rightarrow\,1\,^2A'$ PE transition band of formic acid at (a) 1000 K with tolerance set III, (b) 300 K with tolerance set I and (c) 0 K with tolerance set I. Tolerance set descriptions are provided in Table 4.1. Each line in the stick spectra [right axis, $\langle\varrho_{\mathrm{FCW}}(\tilde{\nu})\rangle$] represents the averaged FC weighted density of states in a wavenumber interval $\Delta\tilde{\nu} = 10\ \mathrm{cm}^{-1}$. The $\langle\varrho_{\mathrm{FCW}}(\tilde{\nu})\rangle$ of all intervals sums to $(1 - \epsilon_{\mathrm{tot}})/\Delta\tilde{\nu}$ for a given temperature. The stick representations have additionally been convoluted with Lorentzian line shapes with full width at half maximum (half-width) of $100\ \mathrm{cm}^{-1}$ [solid, left axis, $\varrho_{\mathrm{FCW,L}}(\tilde{\nu})$] and compared to the results obtained from the TCF approach [dashed, left axis, $\varrho_{\mathrm{FCW,L}}(\tilde{\nu})$]. Differences are, however, barely visible on the current scale. Here $\tilde{\nu}_0$ corresponds to the wavenumber of the $0'-0$ transition for this band. The experimental PE spectrum of Leach *et al.* [179] is additionally compared with the FC profile at 0 K in (c).

Table 4.1.: Prescreening and error bound performance for formic acid at 0 K and at finite temperatures (300 K and 1000 K). For a given tolerance set (Tol. Set), the associated error tolerance ($\epsilon_{\max}^{\text{tol}}$), prescreening stage rigorous error bounds ($\epsilon_{\max}$ and $\epsilon_{\min}$), maximum value for the maximum number of simultaneously excited modes of all irreducible representations and maximum number of simultaneously excited modes $M_{\max}^{(\gamma)}$ of each symmetry block ($M_{\max}(M_{\max}^{(a')}; M_{\max}^{(a'')})$) as well as the error of the integrated FC profile (ϵ_{tot}) are provided.

| T	Tol. Set $(t_{\text{m}}, t_{\text{c}})$	$\epsilon_{\max}^{\text{tol}}$	$\epsilon_{\max}$	ϵ_{tot}	$\epsilon_{\min}$	$M_{\max}(M_{\max}^{(\gamma)})$
0 K	I($10^{-5}, 10^{-5}$)	1.1×10^{-4}	0.29×10^{-4}	0.29×10^{-4}	0.10×10^{-4}	6(6;2)
	II($10^{-4}, 10^{-4}$)	1.1×10^{-3}	0.17×10^{-3}	0.17×10^{-3}	0.09×10^{-3}	5(5;2)
	III($10^{-3}, 10^{-3}$)	1.1×10^{-2}	0.38×10^{-2}	0.30×10^{-2}	0.13×10^{-2}	4(4;1)
300 K	I($10^{-5}, 10^{-5}$)	2.0×10^{-4}	0.42×10^{-4}	0.39×10^{-4}	0.15×10^{-4}	7(7;4)
	II($10^{-4}, 10^{-4}$)	2.0×10^{-3}	0.41×10^{-3}	0.35×10^{-3}	0.15×10^{-3}	6(6;4)
	III($10^{-3}, 10^{-3}$)	2.0×10^{-2}	0.28×10^{-2}	0.26×10^{-2}	0.08×10^{-2}	5(5;2)
1000 K	III($10^{-3}, 10^{-3}$)	2.0×10^{-2}	0.80×10^{-2}	0.66×10^{-2}	0.14×10^{-2}	8(8;4)
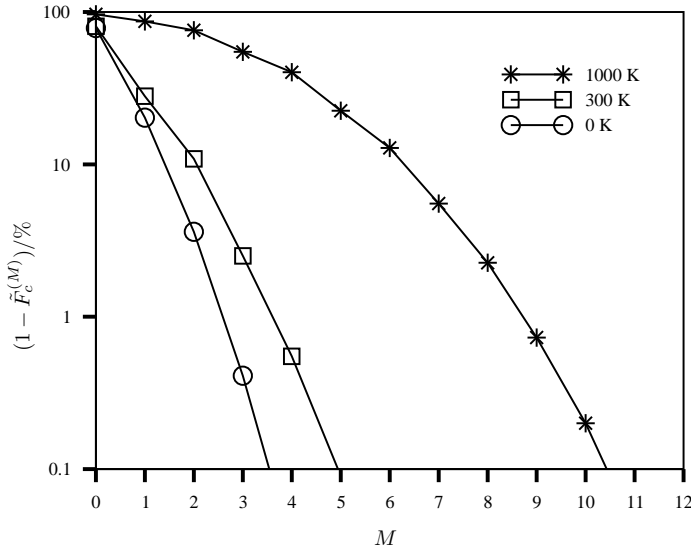
Figure 4.2.: Dependence of the coupling error $\epsilon_{\text{c}} = 1 - \widetilde{F}_{\text{FC;c}}^{(M)}$ on the largest number of simultaneously excited modes M for the FC profile of the $1\,^1\text{A}' \rightarrow 1\,^2\text{A}'$ PE transition band of formic acid. The coupling error is shown on a logarithmic scale for temperatures of 0 K, 300 K and 1000 K. Lines are drawn only to guide the eye. M is different from $M_{\max}$ in Table 4.1, these are identical only when we use C_1 symmetry in the caculation.

integral value of 1 from below in the latter case. In Fig. 4.1 the spectra of the two methods are almost identical. It is difficult to see the 0.7% difference in Fig.4.1(a) at this scale and the ϵ_{tot} is even smaller in Figs. 4.1(b) and (c).

As shown in Fig. 4.2, we require up to 4 simultaneously excited modes (of the final electronic state only) in the coarse-grained prescreening step to achieve a value of ϵ_c smaller than 0.1% at 0 K. At 300 K and 1000 K we need up to 5 and 11 simultaneously excited modes respectively (out of the total 18 modes composed of 9 initial and 9 final state modes) to achieve a similar target value of the coupling error. In Fig. 4.2 M is different from M_{max} in Table 4.1, these are identical only when the C_1 symmetry is used for the calculation.

4.5.2. Anthracene

Ferguson *et al.* [181] measured a spectrum for the $1\,^1A_g \rightarrow 1\,^1B_{2u}$ UV transition ($S_0 \rightarrow S_1$) of anthracene. The spectrum is not vibrationally well-resolved but, at least, it shows major vibrational progressions. The reason of the low resolution could be the finite temperature effect because the measurement was made at 298-313 K. The main feature of the spectrum is a progression on the C–C stretching modes, because the lengths of C–C bonds having double bond nature increase and the lengths of C–C bonds having single bond nature decrease when an electron is excited from the ground to the first excited state [12]. In previous theoretical works of others [12,44,46] the experimental spectrum of Ferguson *et al.* was compared with the FC profile calculation at zero Kelvin. The FC profile calculations at zero Kelvin shows already good agreement with the experimental spectrum because the calculated spectrum at 300 K does not deviate much from the one at zero Kelvin (see Fig. 4.3(b)(d)).

We compute the FC profile of the $1\,^1A_g \rightarrow 1\,^1B_{2u}$ UV transition ($S_0 \rightarrow S_1$) of anthracene at given finite temperatures for different choices of tolerance settings in the prescreening step (see Table 4.2). Again, the error bound conditions of Eq. (4.37) are numerically satisfied. The resulting FC profiles are displayed in Fig. 4.3, which show a pronounced temperature dependence due to the number of normal modes with low harmonic frequency (low vibrational temperature). The experimental spectrum of Ferguson *et al.* [181] is compared with the FC profile calculation at 300 K in Fig. 4.3(b). The overlay is made according to the experimental energy scale[12] and the experimental spectrum height is rescaled to have the same $0' - 0$ peak height of the computed one. The calculated spectrum at 300 K fits to the experimental one better than the zero Kelvin one does. Especially, the thermal excitation part below 0 cm^{-1} fits well with the experimental one, which cannot be explained by the zero Kelvin calculation. The shoulder around 2000 cm^{-1} next to the second highest peak also agrees to the experiment better than the zero Kelvin calculation. The peak assignment at 300 K is difficult because the spectrum is highly congested. The spectrum, however, does not deviate sharply from the zero Kelvin one. According to the zero Kelvin calculation the major vibration progression is from the in-planar middle ring deformation totally symmetric vibrational mode ($\tilde{\nu}_6 = 1356$ cm^{-1}) belonging to irreducible representation a_g.

The FC profile computed for 500 K with an ϵ_{tot} of 4.0% is extremely congested and calculating it without integral selection requires a substantial effort. The coarse-grained prescreening employed here is not ideal for this case. As shown in Fig. 4.4, only up to 6 simultaneously excited modes (out of the final state alone) are sufficient at 0 K to reach a

---

[12]The second highest peaks are at 1327 cm^{-1} and 1423 cm^{-1} in the theoretical and the experimental spectrum, respectively

Table 4.2.: Prescreening and error bound performance for anthracene at 0 K and finite temperatures (100 K, 300 K and 500 K). For a given tolerance set, the associated error tolerance (ϵ_{max}^{tol}), prescreening stage rigorous error bounds (ϵ_{max} and ϵ_{min}), maximum value for the maximum number of simultaneously excited modes of all irreducible representations and maximum number of simultaneously excited modes $M_{max}^{(\gamma)}$ of each symmetry block ($M_{max}(M_{max}^{(a_g)}; M_{max}^{(b_{1g})}; M_{max}^{(b_{2g})}; M_{max}^{(b_{3g})}; M_{max}^{(a_u)}; M_{max}^{(b_{1u})}; M_{max}^{(b_{2u})}; M_{max}^{(b_{3u})})$), and the error of the integrated FC profile (ϵ_{tot}) are provided.

T	Tol. Set (t_m, t_c)	ϵ_{max}^{tol}	ϵ_{max}	ϵ_{tot}	ϵ_{min}	$M_{max}(M_{max}^{(\gamma)})$
0 K	I($10^{-5}, 10^{-5}$)	7.4×10^{-4}	1.6×10^{-4}	1.6×10^{-4}	0.6×10^{-4}	6(6;2;3;4;3;3;2;3)
	II($10^{-4}, 10^{-4}$)	7.4×10^{-3}	1.8×10^{-3}	1.7×10^{-3}	0.6×10^{-3}	5(5;2;2;4;2;2;2;2)
	III($10^{-3}, 10^{-3}$)	7.2×10^{-2}	2.2×10^{-2}	2.0×10^{-2}	0.7×10^{-2}	4(4;2;2;3;2;2;2;2)
100 K	I($10^{-5}, 10^{-5}$)	1.4×10^{-3}	0.23×10^{-3}	0.22×10^{-3}	0.05×10^{-3}	6(6;4;4;5;5;4;3)
	II($10^{-4}, 10^{-4}$)	1.4×10^{-2}	0.25×10^{-2}	0.23×10^{-2}	0.06×10^{-2}	5(5;2;4;4;4;4;3;2)
	III($10^{-3}, 10^{-3}$)	1.3×10^{-1}	0.26×10^{-1}	0.22×10^{-1}	0.06×10^{-1}	4(4;2;2;3;4;4;2;2)
300 K	II($10^{-4}, 10^{-4}$)	1.4×10^{-2}	0.35×10^{-2}	0.29×10^{-2}	0.06×10^{-2}	8(8;6;6;7;7;8;6;4)
	III($10^{-3}, 10^{-3}$)	1.3×10^{-1}	0.37×10^{-1}	0.30×10^{-1}	0.06×10^{-1}	7(6;4;6;6;6;7;4;4)
500 K	III($10^{-3}, 10^{-3}$)	1.3×10^{-1}	0.54×10^{-1}	0.39×10^{-1}	0.07×10^{-1}	10(9;8;7;8;8;10;8;6)

coupling error below 0.1%. At higher temperatures, however, up to 9, 20 and 32 simultaneously excited modes out of a total 132 modes composed of 66 initial and 66 final state modes are necessary to reach a similar threshold for ϵ_c at 100 K, 300 K and 500 K, respectively. In Fig. 4.4 M is different from M_{max} in Table 4.2. These are identical only when one uses C_1 symmetry in the calculation.

The resulting number of prescreened FCFs could be significantly increased in the finite temperature case by employing a finer-grained strategy instead of the coarse-grained prescreening approach reported herein. This is possible with the help of the equations reported herein in a straightforward manner. An alternative route would be to perform for each significantly populated pure initial state (or for collections thereof) the corresponding mode couplings and mode excitations in the final vibronic state. Such rigorous prescreening conditions for FC integrals are developed in the single vibronic level (SVL) transition chapter 7. Related ideas were reported in Ref. [44,45], where, however, a somewhat heuristic selection scheme rather than rigorous prescreening based on sum rules have been exploited.

In Fig. 4.3(a), one can see the difference (ϵ_{tot}=4.0%) between the results obtained from the prescreening method and the TCF method due to the relatively loose tolerance settings for the prescreening. As indicated for formic acid, the TCF based FC profiles should be an upper bound to those obtained from the prescreening FCF calculation. Looking closely at the two Lorentzian weighted spectra in Fig. 4.3(a), however, one is able to observe crossing points of these two spectra. This is attributed to the fact that the averaged Franck-Condon factor weighted density of states has been evaluated in finite wavenumber intervals. If finer wavenumber grids (< 10 cm^{-1}) were employed, such crossings should, in principle, vanish. In the present work, the finer wavenumber grids are not adopted due to the somewhat higher computational cost in the time-independent method. Utilizing the FCF prescreening and TCF methods together, analysis of the difference between these two spectra, can thus indicate the quality of the prescreening conditions and whether any significant peaks are still missing in the prescreening FCF calculation in the same framework of the generating function approach.
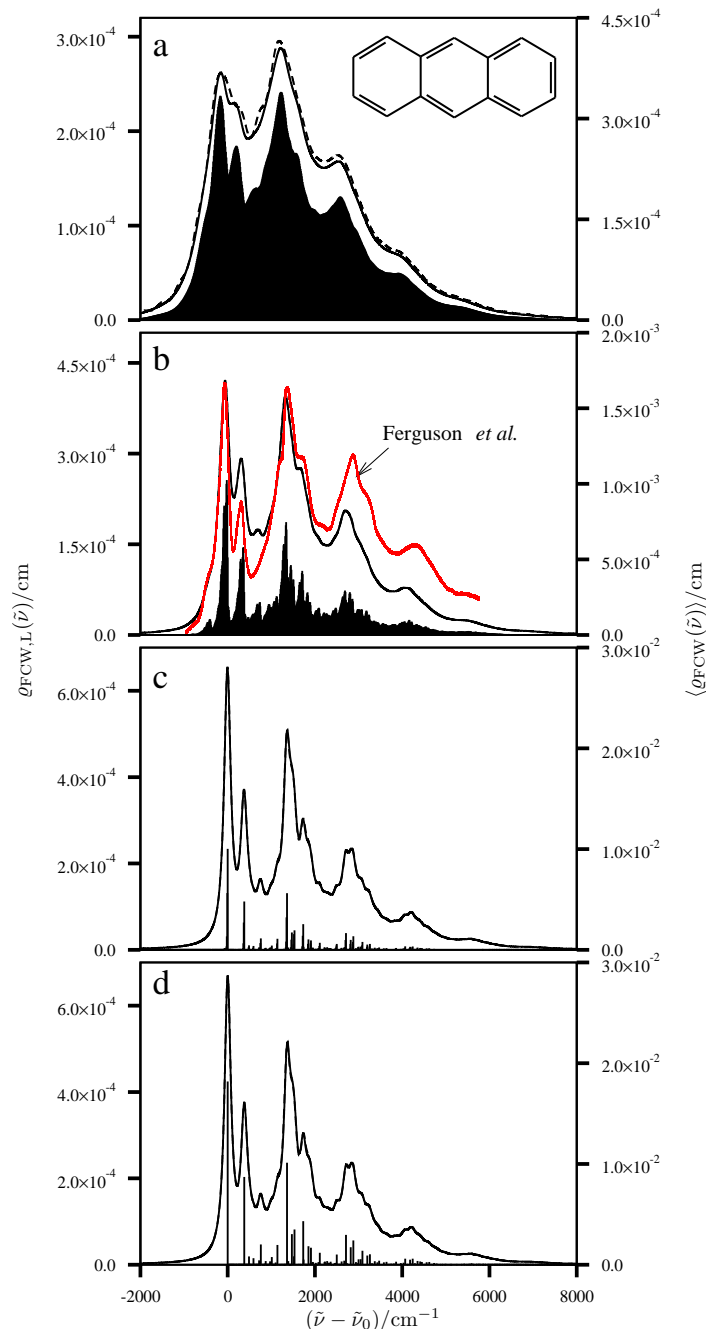
Figure 4.3.: Calculated FC profiles for the $1\,^1A_g \rightarrow 1\,^1B_{2u}$ absorption spectrum of anthracene at (a) 500 K with tolerance set III, (b) 300 K with tolerance set II, (c) 100 K with tolerance set I and (d) 0 K with tolerance set I. Tolerance set descriptions are provided in Table 4.2. Each line in the stick spectra [right axis, $\langle \varrho_{FCW}(\tilde{\nu}) \rangle$] represents the averaged FC weighted density of states in a wavenumber interval $\Delta\tilde{\nu} = 10$ cm^{-1}. The $\langle \varrho_{FCW}(\tilde{\nu}) \rangle$ of all intervals sums to $(1-\epsilon_{tot})/\Delta\tilde{\nu}$ for a given temperature. The stick representations have additionally been convoluted with Lorentzian line shapes with FWHM of 180 cm^{-1} [solid, left axis, $\varrho_{FCW,L}(\tilde{\nu})$] and compared to the results obtained from the TCF approach [dashed, left axis, $\varrho_{FCW,L}(\tilde{\nu})$]. Differences are, however, barely visible on the current scale. Here $\tilde{\nu}_0$ corresponds to the wavenumber of the $0' - 0$ transition for this UV absorption band. The experimental UV spectrum of Ferguson *et al.* [181] is additionally compared with the FC profile at 300 K in (b).
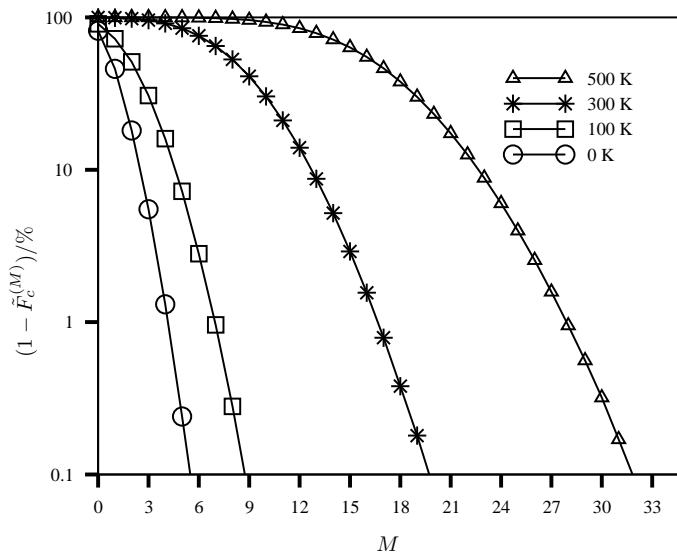
Figure 4.4.: Dependence of the coupling error $\epsilon_c = 1 - \widetilde{F}_{\mathrm{FC;c}}^{(M)}$ on the largest number of simultaneously excited modes M for the FC contribution to the $1\,^1\mathrm{A_g} \to 1\,^1\mathrm{B_{2u}}$ UV absorption spectrum of anthracene. The coupling error is shown on a logarithmic scale for temperatures of 0 K, 100 K, 300 K and 500 K. Lines are drawns only to guide the eye. M is different from M_{max} in Table 4.2, these are identical only when we use $\mathrm{C_1}$ symmetry in the calculation.

4.6. Chapter summary and conclusion

Herein we extended the rigorous prescreening criteria for the FCFs in the finite temperature case with Boltzmann weighted harmonic oscillator states. For this purpose, we have derived sum rules which provide upper and lower bounds for the integrated FC profile on the basis of selected FCF batches. We present only the results of the most coarse-grained version for prescreening, which already led to a significant reduction in the number of calculated FCFs, as explicitly demonstrated for the vibronic spectra of formic acid up to temperatures of 1000 K and that of anthracene with temperatures up to 500 K. Finer-grained prescreening can easily be facilitated (see *e.g.* Sec. 7.3 for multi-dimensional X space development), for instance by determining restrictions for the final state modes depending on a specific choice in the initial state. This demonstrates the particular strength of sum rule based prescreening in large-scale vibronic structure theory.

This GF approach is also directly applicable to the computation of the thermal TCF, which is of particularly advantageous at elevated temperatures. The two approaches, time-independent and time-dependent, show excellent agreement in the testing applications. The TCF method is computationally much cheaper than the TI method; 5 min. *vs* two weeks for anthracene on a 32 bit single processor machine, however at the expense that individual peak assignments are not directly possible. In contrast to other works [17,34,35,37,64,137], one can approach such peak assignments within the TCF method by exploiting similar techniques as those used in the prescreening. It appears, nevertheless, to be of advantage to combine both the time-dependent and TI approaches, the former to compute the full FC profile and the latter to assign specific vibronic contributions. To this end one would no-

tice that the prescreening step can be controlled by the thermal space related to the thermal integral kernel not only by the partitioned integral spaces. The differently assigned temperatures to the individual vibrational modes can provide useful information about the transition processes.

In the following chapter 5 we modify the FCF generating function at finite temperature to compute a probability density function (PDF) of FCFs[13] by extracting statistical quantities like mean, variance, skewness and higher order cumulants of PDF from the thermal FCF GF (neither by the direct TI integral calculation nor by TCF method). This comparatively cheap method provides useful information for the TI and TD methods in aspects of restricting the energy window in the TI calculation and fast time-propagation of TCF.

---

[13]Because FCF distribution is a PDF of which the integrated summation is normalized to be 1 in energy domain.

5. Probability density functions of Franck-Condon transitions

A good guess on the relevant time step (Δt) and length (T_{FFT}) corresponding to the highest frequency and resolution in the frequency domain, respectively is required in the evaluation of the time-correlation function (TCF) (see *e.g.* Sec. 4.4) and its Fourier transform (FT). Time scaling parameters (Δt and T_{FFT}) should be chosen carefully because of the large number of TCF evaluations ($T_{\text{FFT}}/\Delta t$) that involve the calculation of matrix inverse (Eq. (4.10)). These calculations can slow down the computation of the Franck-Condon (FC) profile.

We cannot just increase Δt to reduce the number of TCF evaluations because of the aliasing problem. This problem causes interferences between peaks of high frequency ($>\pi/\Delta t$) and those of lower frequency ($\leq \pi/\Delta t$), if significantly large peaks exist in the high frequency region. We need to perform long time propagations for high resolution. Because π/T_{FFT} corresponds to the resolution, T_{FFT} must be long enough to avoid the intensity leakage problem (see *e.g.* Ref. [182] for fast Fourier transform). Even though the relevant energy window (corresponding to $[-\pi/\Delta t, \pi/\Delta t]$) can be obtained as a result of the prescreening scheme (see Ref. [46] and Ch. 4), the associated computational cost is not negligible if not even prohibitively high.

Also in time-independent (TI) approach with the prescreening technique (Ref. [46] and Sec. 4) one would benefit if the energy window of interest were known before the FC integrals are calculated. When there is large structural deformation during the vibronic transition[1] or the vibronic transition occurs at a high finite temperature, the spectra could not be vibrationally resolved and the distribution would be close to a normal distribution. In these cases one would primarily be interested in quantities such as mean energy, variance of the distribution and peak maximum rather than a vibrationally resolved spectrum which has high computational cost. Thus, an approximate spectral shape, which is available at low computational cost, would be highly desirable.

So far, all of our concerns were about computing the FC spectral density function (SDF) in Eq. (4.40), which is simply a probability density function (PDF). A PDF is characterized by its mean, variance and higher order statistical quantities such as moments or cumulants. We can generate a PDF from the statistical quantities not only by computing the distribution at each transition frequency either by the time-independent or the time-dependent (TD) approaches (Ch. 4). We can obtain the statistical quantities instead from the Franck-Condon factor (FCF) generating function (4.10) directly.[2] The FCF generating function (GF) contains all the information of the corresponding FC distribution. We can extract the statistical

---

[1] The vibronic transition has a large reorganization energy (vibrational vertical transition energy), $\frac{1}{2}\underline{\delta}^{\text{t}}\text{diag}(\underline{\epsilon}')\underline{\delta}$, see Eq. (2.70)

[2] In principle it applies to non-Condon processes as well (see *e.g.* Ref. [40] for the development without Duschinsky effects).

quantities from the GF by taking partial derivatives with respect to GF parameters.

The idea can be realized by the cumulant expansion (CE) of the Franck-Condon factor weighted density of states (see *e.g.* Refs. [29, 183]) with the coherent state (CS)-based FCF GF [29, 46, 129]. The mean vibrationally excited quanta at zero Kelvin was exploited by Doktorov and his coworkers [29] for the absorption spectrum. Finite temperature effects and terms higher than 2-nd order were not taken into account. We note here in parsing that a complementary time-dependent CE method has been presented (see *e.g.* Refs. [5, 35, 37, 87]). The TD CE method approximates the TCF in an exponential function with exponents expanded in the order of time correlations. As a result, one has to evaluate multi-dimensional time integration to have the cumulants, thus the order of evaluation is usually limited to second order, which also includes Duschinsky effects (see *e.g.* Ref. [87]). The TI CE method developed herein computes the cumulants without multi-dimensional time integration, instead.

Cumulants offer a useful information for a PDF such as mean, variance, skewness and (excess) kurtosis corresponding or related to 1-st, 2-nd, 3-rd and 4-th order cumulants, respectively. Mean and variance are frequently used important quantities of a distribution, skewness provides the relative position of the peak maximum (deviation from normal distribution) to the mean value and (excess) kurtosis shows by its sign and magnitude how flat a peak is and how long progressions are, respectively.

Herein we develop an approach for computing arbitrary order of cumulants for vibronic transition energies [183], vibrationally excited quanta[3] [29] and approximating the Franck-Condon factor weighted density of states (FCW) of Duschinsky rotated multi-dimensional harmonic oscillators. As a first applications of the TI cumulant expansion for Franck-Condon factor weighted density of states, the FC profiles of the $1\,^1A' \rightarrow 1\,^2A'$ band in the photo-electron (PE) spectrum of formic acid and the FC contribution to the lowest energy ultra-violet (UV) absorption band ($1\,^1A_g \rightarrow 1\,^1B_{2u}$) for anthracene are presented (see also Sec. 5.3.1 for the corresponding FC profiles). In section 5.3.2 we analyze the FC profile of bacteriochlorophyll (Bchl) for the electron detachment process, $Bchl^- \longrightarrow Bchl$ (see Fig. 1.2), with the TI CE method. Temperature dependence of the FC profiles in presence of Duschinsky rotation is studied in this subsection, because Duschinsky rotation introduces the temperature dependence of electron transfer as can be seen in Fig. 1.2.

In addition to the cumulant GF of the vibrational transition energies, we present the corresponding moment GF of the vibrationally excited quanta [29] to arbitrary order including thermal effects. Additionally we propose a book keeping algorithm for multi-dimensional partial derivatives (Sec. 5.2.1). The moments of vibrationally excited quanta can provide detailed information about the molecular system such as molecular structural changes, potential energy distortions and normal coordinate rotations which can be obtained from either experiment or electronic structure calculations. Employing the thermal-moment integral kernel (see Sec. 4.1 for the thermal integral kernel) to the FCF GF we can explore the temperature effect of individual vibrational modes, which is an important topic in electron transfer theory (see *e.g.* Ref. [87]).

This chapter is constructed as follows. In section 5.1 the cumulant GF is developed by introducing a thermal-moment integral kernel that includes an auxiliary parameter for

---

[3]The corresponding cumulants are the correlation of vibrational excitation quantum numbers of various vibrational modes.

the vibronic transition energy. The algorithm calculating cumulants to arbitrary order is developed in the section. And a possible TCF estimation method with the TI CE is suggested. Then the complementary development for moments of vibrationally excited quanta is presented in section 5.2. For the efficient calculation of the moments, an algorithm for multi-dimensional partial derivatives is developed. Numerical applications of the cumulants are presented and discussed in section 5.3. This chapter is concluded in section 5.4.

5.1. Time-independent cumulant generating function

Using the ansatz of the thermal integral kernel K in equation (4.2) one can find the FCF GF $G^{(K)}$ in spatial representation (Eq. (4.10)). This GF has all information about the distribution of the corresponding vibronic transitions. With proper operations one can extract the information analogously to the partition function for the thermodynamic quantities. Similarly, we operate on the (cumulant) GF in order to obtain the cumulants of the vibronic transition energy distribution.

5.1.1. Cumultants of vibronic transition energies

The cumulants of the vibronic transition energies ($E_{\underline{\epsilon}',\underline{\epsilon}} = \underline{v}' \cdot \underline{\epsilon}' - \underline{v} \cdot \underline{\epsilon}$)[4] with respect to the $0' - 0$ transition energy (Fig. 2.1) are defined as (see *e.g.* Ref. [184])

$$\langle E_{\underline{\epsilon}',\underline{\epsilon}}^n \rangle^{\mathrm{c}} = \frac{\partial^n}{\partial \varepsilon^n} \ln \langle \mathrm{e}^{E_{\underline{\epsilon}',\underline{\epsilon}}\varepsilon} \rangle \Big|_{\varepsilon=0} = \frac{\partial^n}{\partial \varepsilon^n} \ln \frac{\langle \mathrm{e}^{E_{\underline{\epsilon}',\underline{\epsilon}}\varepsilon} \rangle}{|\langle \underline{0}'|\underline{0} \rangle|^2} \Big|_{\varepsilon=0}$$
$$= \frac{\partial^n}{\partial \varepsilon^n} \ln G^{K_{\mathrm{m}}}(\mathbf{I}; \mathbf{\Lambda}, \mathbf{\Lambda}_{\varepsilon}) \Big|_{\varepsilon=0}, \quad n \geq 1, \tag{5.1}$$

with ε playing the role of a cumulant generating parameter. $\langle x^n \rangle$ indicates the mean value of x^n in the FCW distribution and $\langle x^n \rangle^{\mathrm{c}}$ is the corresponding n-th order cumulant.

The vibronic transition energy moment generating function $G^{K_{\mathrm{m}}}(\mathbf{I}; \mathbf{\Lambda}, \mathbf{\Lambda}_{\varepsilon})$ can be expressed in terms of traces, *i.e.*

$$G^{K_{\mathrm{m}}}(\mathbf{I}; \mathbf{\Lambda}, \mathbf{\Lambda}_{\varepsilon}) = \frac{\mathrm{Tr}(\exp(\hat{H}'\varepsilon) \exp(-\hat{H}\varepsilon) \exp(-\beta\hat{H}))}{|\langle \underline{0}'|\underline{0} \rangle|^2 \mathrm{Tr}(\exp(-\beta\hat{H}))}, \tag{5.2}$$

which is in a form similar to that of the TCF in Eq. (2.14), where $\hat{H}$ and $\hat{H}'$ are the vibrational Hamiltonians defined in Eqs. (2.47) and (2.54) respectively.

We introduce our previous generating function parameters ($\mathbf{Z}$) also to the cumulant GF and take the logarithm of the moment GF, $\ln G^{K_{\mathrm{m}}}$, at finite temperature to control the individual vibrational mode excitation and to facilitate the possible incorporation of the TCF as in chapter 4. Thus, we employ

$$\langle E_{\underline{\epsilon}',\underline{\epsilon}}^n \rangle^{\mathrm{c}}(\mathbf{Z}; \mathbf{\Lambda}) = \frac{\partial^n}{\partial \varepsilon^n} \ln G^{K_{\mathrm{m}}}(\mathbf{Z}; \mathbf{\Lambda}, \mathbf{\Lambda}_{\varepsilon}) \Big|_{\varepsilon=0}, \quad n \geq 1, \tag{5.3}$$

---

[4]This is only the vibrational transition energy but we consider the electronic transition energy plus the zero point energy difference between two sets of harmonic oscillators (see Fig. 2.1) as the zero energy level.

such that $\langle E^n_{\underline{\epsilon}',\underline{\epsilon}}\rangle^c(\mathbf{I};\mathbf{\Lambda}) = \langle E^n_{\underline{\epsilon}',\underline{\epsilon}}\rangle^c$. The corresponding occupation representation of the moment GF $G^{K_{\mathrm{m}}}$ reads

$$G^{K_{\mathrm{m}}}(\mathbf{Z};\mathbf{\Lambda},\mathbf{\Lambda}_\varepsilon) = \mathcal{N}\sum_{\underline{v},\underline{v}'=\underline{0}}^{\infty} q(\underline{v}';\underline{v})\overline{\prod_{\underline{z},\underline{z}'}}^{2\underline{v},2\underline{v}'}\mathrm{e}^{-(\underline{v}^{\mathrm{t}}\mathbf{B}\underline{\epsilon}+\underline{v}'^{\mathrm{t}}\mathbf{B}'\underline{\epsilon}')}\mathrm{e}^{E_{\underline{\epsilon}',\underline{\epsilon}}\varepsilon},$$

where[5] the additional parameter ε is introduced for the Boltzmann weighted FCF GF G^K (4.4) as a formal order parameter.

Similarly to the ansatz of the thermal integral kernel K, Eq. (4.2), we invoke a thermal-moment integral kernel $K_{\mathrm{m}}(\mathbf{\Lambda},\mathbf{\Lambda}_\varepsilon;\underline{\xi})$ that constructs the moment GF $G^{K_{\mathrm{m}}}(\mathbf{I};\mathbf{\Lambda},\mathbf{\Lambda}_\varepsilon)$ in a closed analytic form,

$$K_{\mathrm{m}}(\mathbf{\Lambda},\mathbf{\Lambda}_\varepsilon;\underline{\xi}) = \mathcal{N}\det(\mathbf{I}+\mathbf{\Lambda})\det(\mathbf{I}+\mathbf{\Lambda}_\varepsilon)\exp(-\underline{\xi}^\dagger(\mathbf{\Lambda}+\mathbf{\Lambda}_\varepsilon+\mathbf{\Lambda}\mathbf{\Lambda}_\varepsilon)\underline{\xi}), \qquad (5.4)$$

where, $(\mathbf{I}+\mathbf{\Lambda}_\varepsilon) = \mathrm{diag}(\mathrm{e}^{\epsilon_1\varepsilon},\ldots,\mathrm{e}^{\epsilon_N\varepsilon},\mathrm{e}^{-\epsilon'_1\varepsilon},\ldots,\mathrm{e}^{-\epsilon'_N\varepsilon})$ and $(\mathbf{I}+\mathbf{\Lambda}_\varepsilon)\big|_{\varepsilon=0} = \mathbf{I}$. After formal integration of Eq. (4.1) with the kernel K being replaced by the thermal-moment integral kernel K_{m} the resulting GF is obtained, which reads

$$\begin{aligned}G^{K_{\mathrm{m}}}(\mathbf{Z};\mathbf{\Lambda},\mathbf{\Lambda}_\varepsilon) =\,&\mathcal{N}\det(\mathbf{I}+\mathbf{\Lambda}_\varepsilon)\det(\mathbf{I}+\mathbf{\Lambda}_\varepsilon-\mathbf{Z}\mathbf{W}_T\mathbf{Z})^{-\frac{1}{2}}\det(\mathbf{I}+\mathbf{\Lambda}_\varepsilon+\mathbf{Z}\mathbf{W}_T\mathbf{Z})^{-\frac{1}{2}}\\ &\exp(\underline{r}_T^{\mathrm{t}}\mathbf{Z}(\mathbf{I}+\mathbf{\Lambda}_\varepsilon+\mathbf{Z}\mathbf{W}_T\mathbf{Z})^{-1}\mathbf{Z}\underline{r}_T),\end{aligned} \qquad (5.5)$$

and we may restore[6]. Using the identities (see also Ref. [185]) $G^K=G^{K_{\mathrm{m}}}\big|_{\varepsilon=0}$,

$$\frac{\partial\det(\mathbf{Y})}{\partial x} = \det(\mathbf{Y})\mathrm{Tr}(\mathbf{Y}^{-1}\frac{\partial\mathbf{Y}}{\partial x}), \qquad (5.6)$$

$$\frac{\partial\mathrm{Tr}(\mathbf{Y})}{\partial x} = \mathrm{Tr}(\frac{\partial\mathbf{Y}}{\partial x}), \qquad (5.7)$$

$$\frac{\partial\mathbf{Y}^{-1}}{\partial x} = -\mathbf{Y}^{-1}\frac{\partial\mathbf{Y}}{\partial x}\mathbf{Y}^{-1}, \qquad (5.8)$$

the first derivative of $\ln G^{K_{\mathrm{m}}}(\mathbf{Z};\mathbf{\Lambda},\mathbf{\Lambda}_\varepsilon)$ with respect to ε, corresponding to the mean value, is given by,

$$\begin{aligned}\frac{\partial\ln G^{K_{\mathrm{m}}}(\mathbf{Z};\mathbf{\Lambda},\mathbf{\Lambda}_\varepsilon)}{\partial\varepsilon} =\,&\mathrm{Tr}[\mathbf{\Xi}]\\ &-\tfrac{1}{2}\mathrm{Tr}[(\mathbf{I}+\mathbf{\Lambda}_\varepsilon-\mathbf{Z}\mathbf{W}_T\mathbf{Z})^{-1}(\mathbf{I}+\mathbf{\Lambda}_\varepsilon)\mathbf{\Xi}]\\ &-\tfrac{1}{2}\mathrm{Tr}[(\mathbf{I}+\mathbf{\Lambda}_\varepsilon+\mathbf{Z}\mathbf{W}_T\mathbf{Z})^{-1}(\mathbf{I}+\mathbf{\Lambda}_\varepsilon)\mathbf{\Xi}]\\ &+\underline{r}_T^{\mathrm{t}}\mathbf{Z}\frac{\partial(\mathbf{I}+\mathbf{\Lambda}_\varepsilon+\mathbf{Z}\mathbf{W}_T\mathbf{Z})^{-1}}{\partial\varepsilon}\mathbf{Z}\underline{r}_T,\end{aligned} \qquad (5.9)$$

where, $\mathbf{\Xi} = \mathrm{diag}(\epsilon_1,\ldots,\epsilon_N,-\epsilon'_1,\ldots,-\epsilon'_N)$. The crucial part is how to evaluate the n-th order partial derivatives of the inverse matrices for higher order cumulants. We can compute

---

[5]$\overline{\prod}_{\underline{x}_1,\cdots,\underline{x}_N}^{\underline{n}_1,\cdots,\underline{n}_N} = \left(\prod_k x_{1,k}^{n_{1,k}}\right)\cdots\left(\prod_k x_{N,k}^{n_{N,k}}\right)$.

[6]See Eq. (4.10)

arbitrary orders of partial derivatives of the inverse matrix by defining a function $L_{\underline{n}}^{\underline{m}}$,

$$L_{\underline{n}}^{\underline{m}}(\mathbf{Y}) = \prod_{i=1}^{n} (\mathbf{Y}^{-1} \frac{\partial^{m_i} \mathbf{Y}}{\partial \varepsilon^{m_i}}), \tag{5.10}$$

where

$$\mathbf{Y} = (\mathbf{I} + \mathbf{\Lambda}_\varepsilon + \mathbf{A}), \tag{5.11}$$

$$\frac{\partial^{m_i} \mathbf{Y}}{\partial \varepsilon^{m_i}} = (\mathbf{I} + \mathbf{\Lambda}_\varepsilon) \mathbf{\Xi}^{m_i}, \ m_i \geq 1. \tag{5.12}$$

$\mathbf{A}$ is a matrix which does not depend on ε. $L_{\underline{n}}^{\underline{m}}$ satisfies the following recursion relation,

$$\frac{\partial L_{\underline{n}}^{\underline{m}}(\mathbf{Y})}{\partial \varepsilon} = \sum_{i=1}^{n} \left[L_{n}^{(m_1,\dots,m_i+1,\dots,m_n)}(\mathbf{Y}) - L_{n+1}^{(m_1,\dots,m_{i-1},1,m_i,\dots,m_n)}(\mathbf{Y}) \right]. \tag{5.13}$$

From this recursion relation we present the following expressions which will be used for the partial derivatives of the 2-nd and the 3-rd terms (traces) in Eq. (5.9),

$$\frac{\partial^n L_1^1(\mathbf{Y})}{\partial \varepsilon^n} = \sum_{k=1}^{n+1} (-1)^{k+1} \sum_{\{\underline{m}\}_k} \binom{n}{m_1,\dots,m_{k-1},m_k-1} L_{\underline{k}}^{\underline{m}}(\mathbf{Y}), \tag{5.14}$$

and of the last partial derivative term in Eq. (5.9),

$$\frac{\partial^n \mathbf{Y}^{-1}}{\partial \varepsilon^n} = \left[\sum_{k=1}^{n} (-1)^k \sum_{\{\underline{m}\}_k} \binom{n}{m_1,\dots,m_k} L_{\underline{k}}^{\underline{m}} \right] \mathbf{Y}^{-1}, \tag{5.15}$$

here the set $\{\underline{m}\}_k$ consists of all positive integer vectors $\underline{m}$ satisfying $n = \sum_i^k m_i$ where k is the dimension of $\underline{m}$. So far, the algorithm for computing the cumulants of the vibronic transition energies has been presented. The cumulant GF is proposed rather than the moment GF for algorithmic purposes, the logarithm separates the GF in summations[7] and the cumulants provide the statistically meaningful quantities directly unlike moments. One can, however, compute the moments from cumulants because cumulants and moments are mutually convertible via the following recursion relations (see *e.g.* Ref. [186]),

$$\langle E_{\underline{\varepsilon}',\underline{\varepsilon}}^{n+1} \rangle = \sum_{k=0}^{n} \binom{n}{k} \langle E_{\underline{\varepsilon}',\underline{\varepsilon}}^{n-k} \rangle \langle E_{\underline{\varepsilon}',\underline{\varepsilon}}^{k+1} \rangle^{\mathrm{c}}, \tag{5.16}$$

$$\langle E_{\underline{\varepsilon}',\underline{\varepsilon}}^{n+1} \rangle^{\mathrm{c}} = \langle E_{\underline{\varepsilon}',\underline{\varepsilon}}^{n+1} \rangle - \sum_{k=0}^{n-1} \binom{n}{k} \langle E_{\underline{\varepsilon}',\underline{\varepsilon}}^{n-k} \rangle \langle E_{\underline{\varepsilon}',\underline{\varepsilon}}^{k+1} \rangle^{\mathrm{c}}. \tag{5.17}$$

In principle the PDF can be reconstructed from the corresponding cumulants or moments, if cumulants or moments exist for the corresponding distribution, such that for the

---

[7]Otherwise, one has to carry many terms for the multiple partial derivatives of determinants and an exponential function in Eq. (5.5).

FC SDF (2.29),

$$\varrho_{\text{FCW}}(\omega; T) = \hbar^{-1} \int_{-\infty}^{\infty} dt \exp\left(\sum_{k=1}^{\infty} \frac{\langle E_{\underline{\epsilon}',\underline{\epsilon}}^k \rangle^{\text{c}}(T)}{k!} (\mathrm{i}t/\hbar)^k\right) e^{\mathrm{i}(\omega - \omega_0)t}. \tag{5.18}$$

If one could reconstruct the distribution for the transition from the cumulants then it would provide useful information with low computational cost. There have been, however, many attempts to produce the probability distribution from the corresponding cumulants or moments but they were mostly not too suitable because existing methods such as Edgeworth expansion and Gram-Charlier expansion produce non-positive-definite distributions[8]. In this work, nonetheless, the Edgeworth expansion algorithm is utilized in an arbitrary order for nearly Gaussian distributions [187]. This will provide at least rough pictures (*e.g.* normal distribution) of the distributions. The PDFs in figures 5.1 and 5.2, $\varrho_{\text{FCW}}^{(\text{c})}(\tilde{\nu})$ are generated by the following Edgeworth expansion to an arbitrary order (see Ref. [187]) n (≥ 3, $n = 2$ is simply for a Gaussian function),

$$\varrho_{\text{FCW}}^{(\text{c})}(\tilde{\nu} - \tilde{\nu}_0; n) = \frac{1}{\sqrt{2\pi \langle E_{\underline{\epsilon}',\underline{\epsilon}}^2 \rangle^{\text{c}}/(hc_0)^2}} \exp\left(-\frac{(\tilde{\nu} - \tilde{\nu}_0)^2}{2\langle E_{\underline{\epsilon}',\underline{\epsilon}}^2 \rangle^{\text{c}}/(hc_0)^2}\right)$$
$$\left[1 + \sum_{s=1}^{n} \left(\sqrt{\langle E_{\underline{\epsilon}',\underline{\epsilon}}^2 \rangle^{\text{c}}/(hc_0)^2}\right)^s \sum_{\{\underline{k}\}} \mathcal{H}_{s+2r}(\tilde{\nu} - \tilde{\nu}_0) \prod_{m=1}^{s} \frac{1}{k_m!}\left(\frac{S_{m+2}}{(m+2)!}\right)^{k_m}\right], \tag{5.19}$$

where $\{\underline{k}\}$ is a set of (non-negative integer) vectors satisfying $s = \sum_{m=1}^{s} mk_m$ and $r = \sum_{m=1}^{s} k_m$, in which the fractional quantity corresponding to the cumulants is used,

$$\mathcal{S}_n = \frac{\langle E_{\underline{\epsilon}',\underline{\epsilon}}^n \rangle^{\text{c}}/(hc_0)^n}{(\langle E_{\underline{\epsilon}',\underline{\epsilon}}^2 \rangle^{\text{c}}/(hc_0)^2)^{n-1}}. \tag{5.20}$$

The Edgeworth expansion with a finite number of cumulants in Eq. (5.19) is related to the FCW by

$$\lim_{n\to\infty} \varrho_{\text{FCW}}^{(\text{c})}(\tilde{\nu}; T; n) = \varrho_{\text{FCW}}(\tilde{\nu}; T) = hc_0 \varrho_{\text{FCW}}(\omega; T). \tag{5.21}$$

5.1.2. Time-propagation with time-independent cumulant expansion

In the evaluation of the TCF (Eq. (4.10)) for large system it is necessary to estimate the TCF value at a given time step from the values at previous time steps because the direct evaluation of the TCF becomes too expensive due to the repeated calculation of the inverse complex matrices. It is worth to note that Petrenko and Neese [75] devised a method to avoid the TCF evaluation. They found a recursion relation for the SDF in frequency domain by expanding the TCF, neglecting Duschinsky effect, in a power series and by performing partial integration on the expansion. When we need to consider Duschinsky effect, however, the method of Petrenko and Neese is not not directly applicable because the analytic time

---

[8]in the tails of PDFs with high order (≥ 3) cumulant expansion.

integration of the series expansion cannot be found in the presence of Duschinsky effect. Instead, the TCF can be estimated by short time expansion (herein 2-nd order) by expanding the TD cumulant GF[9] ($\ln G^{K_m}(\mathbf{Z}(t); \mathbf{\Lambda})$) in a Taylor series. The Taylor expansion of the cumulant GF with small time step Δt would look like

$$\ln G^K(\mathbf{Z}(t + \Delta t); \mathbf{\Lambda}) = \ln G^K(\mathbf{Z}(t); \mathbf{\Lambda}) + \sum_{k=1}^{\infty} \frac{\partial^k}{k! \partial \Delta t^k} \ln G^K(\mathbf{Z}(t + \Delta t); \mathbf{\Lambda})\Big|_{\Delta t=0} \Delta t^k,$$
(5.22)

where the TD GF parameter matrix $\mathbf{Z}(t)$ consists of Eqs. (4.42) and (4.43). After identifying the cumulant ordering parameter $\varepsilon = \mathrm{i}\Delta t/\hbar$ we can express the expansion in terms of TD cumulants, *i.e.*

$$\ln G^K(\mathbf{Z}(t + \Delta t); \mathbf{\Lambda}) = \ln G^K(\mathbf{Z}(t); \mathbf{\Lambda}) + \sum_{k=1}^{\infty} \frac{\partial^k}{k! \partial \varepsilon^k} \ln G^{K_m}(\mathbf{Z}(t); \mathbf{\Lambda}, \mathbf{\Lambda}_\varepsilon)\Big|_{\varepsilon=0} (\mathrm{i}\Delta t)^k$$

$$= \ln G^K(\mathbf{Z}(t); \mathbf{\Lambda}) + \sum_{k=1}^{\infty} \frac{\langle E_{\underline{\epsilon}', \underline{\epsilon}}^k \rangle^c(\mathbf{Z}(t); \mathbf{\Lambda})}{k!} (\mathrm{i}\Delta t/\hbar)^k. \qquad (5.23)$$

When we apply exponential to Eq. (5.23) we arrive at the following expression,

$$G^K(\mathbf{Z}(t + \Delta t); \mathbf{\Lambda}) = G^K(\mathbf{Z}(t); \mathbf{\Lambda}) \exp\Big(\sum_{k=1}^{\infty} \frac{\langle E_{\underline{\epsilon}', \underline{\epsilon}}^k \rangle^c(\mathbf{Z}(t); \mathbf{\Lambda})}{k!} (\mathrm{i}\Delta t/\hbar)^k\Big), \qquad (5.24)$$

such that the TCF at $t + \Delta t$ is expressed as a product of the TCF at t and a GF of TD cumulants at t in an exponential form. This expansion (5.24) at $t = 0$ and $\mathbf{Z} = \mathbf{I}$ is simply the TI cumulant GF. Accordingly if we rewrite the expression (5.24) for $n + 1$ time steps after t, we have

$$G^K(\mathbf{Z}(t + (n+1)\Delta t); \mathbf{\Lambda}) = G^K(\mathbf{Z}(t + n\Delta t); \mathbf{\Lambda})$$

$$\exp\Big(\sum_{k=1}^{\infty} \frac{\langle E_{\underline{\epsilon}', \underline{\epsilon}}^k \rangle^c(\mathbf{Z}(t + n\Delta t); \mathbf{\Lambda})}{k!} (\mathrm{i}\Delta t/\hbar)^k\Big). \qquad (5.25)$$

We can estimate this cumulant expansion expression by ignoring high order terms in Δt of the power series summation as a short time approximation. For example if we neglect Δt^k terms higher than 2-nd order, we obtain

$$G^K(\mathbf{Z}(t + (n+1)\Delta t); \mathbf{\Lambda})$$
$$\simeq G^K(\mathbf{Z}(t + n\Delta t); \mathbf{\Lambda}) \exp\Big(\mathrm{i}\langle E_{\underline{\epsilon}', \underline{\epsilon}}^1 \rangle^c(\mathbf{Z}(t); \mathbf{\Lambda})(\Delta t/\hbar) - (\tfrac{1}{2} + n)\langle E_{\underline{\epsilon}', \underline{\epsilon}}^2 \rangle^c(\mathbf{Z}(t); \mathbf{\Lambda})(\Delta t/\hbar)^2\Big).$$
(5.26)

This expression is in a form that its value can be estimated based on the TCF value from the previous time step. The numerical procedure for the fast evaluation of the TCF can be

---

[9]This should not be confused with the TD CE method which involves multi-dimensional time integration for the time correlation of potential energy difference for two electronic states (see *e.g.* Refs. [5, 35, 37, 87]).

made with the short time expansion approximation. For example, only in every n time step the exact TCF is evaluated and in between the TCF is estimated by Eq. (5.26). Namely we need to evaluate the complex inverse matrix only every n time steps which can speed up the TCF calculation.

5.1.3. Cumultants of vibrationally excited quanta

In addition to extracting statistical information about the vibronic transition energy (Sec. 5.1.1) one can perform detailed computations of the individual vibrational mode statistics are also possible. Cumulants of vibrationally excited quanta in FC distribution can be generated in a similar way for the order $n = \sum_{i=1}^{2N} k_i$, *i.e.*[10]

$$\langle \overline{\prod_{\underline{v}}^k} \rangle^{\mathrm{c}} = \hat{\partial}_{\underline{\tilde{\eta}}}^{\underline{k}} \ln G^{K_{\mathrm{m}}}(\mathbf{I}; \mathbf{\Lambda}, \mathbf{\Lambda}_{\underline{\tilde{\eta}}}) \Big|_{\underline{\tilde{\eta}}=\underline{0}}, \tag{5.27}$$

with $(\mathbf{I} + \mathbf{\Lambda}_{\tilde{\eta}}) = \mathrm{diag}(\mathrm{e}^{-\tilde{\eta}_1}, \ldots, \mathrm{e}^{-\tilde{\eta}_{2N}})$ where we have redefined the auxiliary parameters $\underline{\tilde{\eta}}^{\mathrm{t}} = (\eta_1, \ldots, \eta_N, \eta_1', \ldots, \eta_N') = (\tilde{\eta}_1, \ldots, \tilde{\eta}_{2N})$ to identify individual vibrational moments. The corresponding occupation representation is given as

$$G^{K_{\mathrm{m}}}(\mathbf{Z}; \mathbf{\Lambda}, \mathbf{\Lambda}_{\underline{\tilde{\eta}}}) = \mathcal{N} \sum_{\underline{v}, \underline{v}'=\underline{0}}^{\infty} q(\underline{v}'; \underline{v}) \overline{\prod_{\underline{z}, \underline{z}'}^{2v, 2v'}} \mathrm{e}^{-(\underline{v}^{\mathrm{t}} \mathbf{B} \underline{\epsilon} + \underline{v}'^{\mathrm{t}} \mathbf{B}' \underline{\epsilon}')} \mathrm{e}^{(\underline{v} \cdot \underline{\eta} + \underline{v}' \cdot \underline{\eta}')}, \tag{5.28}$$

Replacing $(\mathbf{I} + \mathbf{\Lambda}_{\varepsilon}) \rightarrow (\mathbf{I} + \mathbf{\Lambda}_{\tilde{\eta}})$ in Eq. (5.5), one obtains the GF in an analytic form,

$$
\begin{aligned}
G^{K_{\mathrm{m}}}(\mathbf{Z}; \mathbf{\Lambda}, \mathbf{\Lambda}_{\tilde{\eta}}) = & \mathcal{N} \det(\mathbf{I} + \mathbf{\Lambda}_{\tilde{\eta}}) \det(\mathbf{I} + \mathbf{\Lambda}_{\tilde{\eta}} - \mathbf{Z}\mathbf{W}_T\mathbf{Z})^{-\frac{1}{2}} \\
& \det(\mathbf{I} + \mathbf{\Lambda}_{\tilde{\eta}} + \mathbf{Z}\mathbf{W}_T\mathbf{Z})^{-\frac{1}{2}} \\
& \exp(\underline{r}_T^{\mathrm{t}} \mathbf{Z}(\mathbf{I} + \mathbf{\Lambda}_{\tilde{\eta}} + \mathbf{Z}\mathbf{W}_T\mathbf{Z})^{-1} \mathbf{Z}\underline{r}_T).
\end{aligned}
\tag{5.29}
$$

The recursive expressions (Eqs. (5.14) and (5.15)) can in principle be applied for an arbitrary order calculation as well, but require careful book keeping of vibrational mode indices. One can find the original idea of the cumulants of vibrationally excited quanta and explicit expressions up to 2-nd order (mean and covariance) in Doktorov *et al.* [29]. In this thesis, the numerical results obtained for the cumulants of vibrationally excited quanta are not shown, but we mention, that these can be useful for finer-grained prescreening strategies[11] suggested in Refs. [46, 129].

5.2. Moment generating function

Even if the moments of vibrationally excited quanta can be evaluated with the cumulant GF in section 5.1.3, the multi-dimensional partial derivative of inverse matrices is a complicated task. One- or two- dimensional partial derivatives could be easily done with the method

---

[10] $\hat{\partial}_{\underline{x}_1, \cdots, \underline{x}_N}^{\underline{n}_1, \cdots, \underline{n}_N} = \left(\frac{\partial^{\sum_k n_{1,k}}}{\prod_k \partial x_{1,k}^{n_{1,k}}} \right) \cdots \left(\frac{\partial^{\sum_k n_{N,k}}}{\prod_k \partial x_{N,k}^{n_{N,k}}} \right).$

[11] By exploiting the vibrational mode correlations, more restrictions on the vibrational basis set can be made.

in section 5.1.3 but for higher dimensional cases one would need an algorithm to keep the multi-dimensional orders of partial derivatives 5.1.3. In this section, a book keeping algorithm is developed to compute the moments of vibrational quanta to arbitrary order.

5.2.1. Book keeping algorithm

The vibrational quantum number moments of FCFs can be generated from partial derivatives of $G^{K_m}(\mathbf{Z}; \mathbf{\Lambda}, \mathbf{\Lambda}_{\tilde{\eta}})$ in Eq. (5.29) in the same manner as the cumulants, but without the logarithmic function,

$$
\begin{aligned}
\frac{\langle \overline{\prod}_{\tilde{v}}^{k} \rangle}{|\langle \underline{0}' | \underline{0} \rangle|^2} &= \sum_{\underline{v}, \underline{v}' = \underline{0}}^{\infty} q(\underline{v}'; \underline{v}) \overline{\prod}_{\tilde{v}}^{k} e^{-(\underline{v}^{\mathrm{t}} \mathbf{B} \underline{\epsilon} + \underline{v}'^{\mathrm{t}} \mathbf{B}' \underline{\epsilon}')} e^{-(\underline{v}^{\mathrm{t}} \underline{\eta} + \underline{v}'^{\mathrm{t}} \underline{\eta}')} \Big|_{\tilde{\underline{\eta}} = \underline{0}} \\
&= (-1)^{-\sum_i^{2N} k_i} \hat{\partial}_{\underline{\tilde{\eta}}}^{k} G^{K_m}(\mathbf{I}; \mathbf{\Lambda}, \mathbf{\Lambda}_{\underline{\tilde{\eta}}}) \Big|_{\underline{\tilde{\eta}} = \underline{0}}.
\end{aligned}
\tag{5.30}
$$

In the derivation of Eq. (5.29) we have already used a thermal-moment integral kernel which is mode-selective, similarly to the non-selective thermal-moment integral kernel in Eq. (5.4),

$$
K_m(\mathbf{\Lambda}, \mathbf{\Lambda}_{\tilde{\eta}}; \underline{\xi}) = \mathcal{N} \det(\mathbf{I} + \mathbf{\Lambda}) \det(\mathbf{I} + \mathbf{\Lambda}_{\tilde{\eta}}) \exp(-\underline{\xi}^{\dagger}(\mathbf{\Lambda} + \mathbf{\Lambda}_{\tilde{\eta}} + \mathbf{\Lambda}\mathbf{\Lambda}_{\tilde{\eta}})\underline{\xi}).
\tag{5.31}
$$

The integral form of the moment GF with the thermal-moment integral kernel $G^{K_m}(\mathbf{Z}; \mathbf{\Lambda}, \mathbf{\Lambda}_{\tilde{\eta}})$ is given in the CS integral form as in Eq. (4.7), *i.e.*

$$
\begin{aligned}
G^{K_m}(\mathbf{Z}; \mathbf{\Lambda}, \mathbf{\Lambda}_{\tilde{\eta}}) &= \mathcal{N} \pi^{-2N} \det(\mathbf{I} + \mathbf{\Lambda}) \det(\mathbf{I} + \mathbf{\Lambda}_{\tilde{\eta}}) \\
&\quad \int d^2\underline{\alpha} d^2\underline{\gamma}' \exp(-\underline{\xi}^{\dagger}(\mathbf{I} + \mathbf{\Lambda})(\mathbf{I} + \mathbf{\Lambda}_{\tilde{\eta}})\underline{\xi}) \\
&\quad \exp(-\tfrac{1}{2}\underline{\xi}^{\mathrm{t}} \mathbf{Z}\mathbf{W}\mathbf{Z}\underline{\xi} - \tfrac{1}{2}\underline{\xi}^{\dagger} \mathbf{Z}\mathbf{W}\mathbf{Z}\underline{\xi}^* + \underline{r}^{\mathrm{t}} \mathbf{Z}(\underline{\xi} + \underline{\xi}^*)),
\end{aligned}
\tag{5.32}
$$

which will be formally integrated to obtain Eq. (5.29). This integral expression is partitioned into two Gaussian integral functions (as in Eq. (2.122)), *i.e.*

$$
\begin{aligned}
&G^{K_m}(\mathbf{Z}; \mathbf{\Lambda}, \mathbf{\Lambda}_{\tilde{\eta}}) \\
&= \mathcal{N} \det(\mathbf{I} + \mathbf{\Lambda}_{\tilde{\eta}}) \, I_{2N}[\mathbf{I} + \mathbf{\Lambda}_{\tilde{\eta}} + \mathbf{Z}\mathbf{W}_T\mathbf{Z}, \mathbf{Z}\underline{r}_T] I_{2N}[\mathbf{I} + \mathbf{\Lambda}_{\tilde{\eta}} - \mathbf{Z}\mathbf{W}_T\mathbf{Z}, \underline{0}] \\
&= \mathcal{N} \det(\mathbf{I} + \mathbf{\Lambda}_{\tilde{\eta}}) G_1^{K_m}(\mathbf{Z}; \mathbf{\Lambda}, \mathbf{\Lambda}_{\tilde{\eta}}) G_2^{K_m}(\mathbf{Z}; \mathbf{\Lambda}, \mathbf{\Lambda}_{\tilde{\eta}}).
\end{aligned}
\tag{5.33}
$$

$G_1^{K_m}$ and $G_2^{K_m}$ are defined as

$$
\begin{aligned}
G_1^{K_m}(\mathbf{Z}; \mathbf{\Lambda}, \mathbf{\Lambda}_{\tilde{\eta}}) &= \det(\mathbf{I} + \mathbf{\Lambda}_{\tilde{\eta}})^{\frac{1}{2}} I_{2N}[\mathbf{I} + \mathbf{\Lambda}_{\tilde{\eta}} + \mathbf{Z}\mathbf{W}_T\mathbf{Z}, \mathbf{Z}\underline{r}_T] \\
&= \pi^{-N} \det(\mathbf{I} + \mathbf{\Lambda}_{\tilde{\eta}})^{\frac{1}{2}} \int d\underline{x} R_1(\mathbf{Z}; \mathbf{\Lambda}, \mathbf{\Lambda}_{\tilde{\eta}}),
\end{aligned}
\tag{5.34}
$$

$$
\begin{aligned}
G_2^{K_m}(\mathbf{Z}; \mathbf{\Lambda}, \mathbf{\Lambda}_{\tilde{\eta}}) &= \det(\mathbf{I} + \mathbf{\Lambda}_{\tilde{\eta}})^{\frac{1}{2}} I_{2N}[\mathbf{I} + \mathbf{\Lambda}_{\tilde{\eta}} - \mathbf{Z}\mathbf{W}_T\mathbf{Z}, \underline{0}] \\
&= \pi^{-N} \det(\mathbf{I} + \mathbf{\Lambda}_{\tilde{\eta}})^{\frac{1}{2}} \int d\underline{x} R_2(\mathbf{Z}; \mathbf{\Lambda}, \mathbf{\Lambda}_{\tilde{\eta}}),
\end{aligned}
\tag{5.35}
$$

where[12] $R_1 = \mathcal{J}[2(\mathbf{I}+\mathbf{\Lambda}_{\tilde{\eta}}+\mathbf{Z}\mathbf{W}_T\mathbf{Z}), 2\mathbf{Z}\underline{r}_T; \underline{x}]$ and $R_2 = \mathcal{J}[2(\mathbf{I}+\mathbf{\Lambda}_{\tilde{\eta}}-\mathbf{Z}\mathbf{W}_T\mathbf{Z}), 2\mathbf{Z}\underline{r}_T; \underline{x}]$ are the corresponding integrands of the Gaussian integrals (Eq. (2.122)). To derive a recursion relation of the partial derivatives of $G_1^{K_m}$ and $G_2^{K_m}$ we define a function B,

$$B\frac{m}{a,\tilde{\eta}} = \pi^{-N}e^{\underline{m}^t\eta}\det(\mathbf{I}+\mathbf{\Lambda}_{\tilde{\eta}})^{\frac{1}{2}}$$
$$\int d\underline{x}\overline{\prod_{\underline{x}}}^{2m}R_a(\mathbf{Z};\mathbf{\Lambda},\mathbf{\Lambda}_{\tilde{\eta}}),\ (a=1,2)\,, \tag{5.36}$$

where $\underline{m}$ is a vector of orders of moments. Eq. (5.36) gives the relations $G_1^{K_m} = B_{1,\tilde{\eta}}^0$ and $G_2^{K_m} = B_{2,\tilde{\eta}}^0$. Eq. (5.36) satisfies the following recursion relation of partial derivatives,

$$\frac{\partial B\frac{m}{a,\tilde{\eta}}}{\partial \tilde{\eta}_k} = (-\tfrac{1}{2}+m_k)B\frac{m}{a,\tilde{\eta}} + B_{a,\tilde{\eta}}^{(m_1,\ldots,m_k+1,\ldots,m_{2N})},\ (a=1,2)\,, \tag{5.37}$$

where we have used

$$\frac{\partial \det(\mathbf{I}+\mathbf{\Lambda}_{\tilde{\eta}})^{\frac{1}{2}}}{\partial \tilde{\eta}_k} = -\tfrac{1}{2}\det(\mathbf{I}+\mathbf{\Lambda}_{\tilde{\eta}})^{\frac{1}{2}}. \tag{5.38}$$

We can expand the partial derivatives in Eq. (5.30) using Eq. (5.33) and Eq. (5.36) in a combinatoric summation rule [188],

$$\frac{\langle \overline{\prod_{\tilde{v}}}^k \rangle}{|\langle \underline{0}'|\underline{0}\rangle|^2} = \mathcal{N}\sum_{l_1=0}^{k_1}\cdots\sum_{l_{2N}=0}^{k_{2N}}\binom{k_1}{l_1}\cdots\binom{k_{2N}}{l_{2N}}\hat{\partial}_{\tilde{\eta}}^l B_{1,\tilde{\eta}}^0\hat{\partial}_{\tilde{\eta}}^{(k-l)}B_{2,\tilde{\eta}}^0\Big|_{\tilde{\eta}=\underline{0}}. \tag{5.39}$$

Eq. (5.36) can be written in terms of the expectation value of a normal distribution[13]. B at $\tilde{\eta}=\underline{0}$ can be evaluated with multi-variate normal moments (3.7), *i.e.*

$$B\frac{m}{a,\tilde{\eta}}\Big|_{\tilde{\eta}=\underline{0}} = \sqrt{\det(2\mathbf{\Lambda}_c^{-1})}E_a(\overline{\prod_{\underline{x}}}^{2m}),\ (a=1,2)\,, \tag{5.40}$$

where E_1 is the expectation value of the normal distribution $\mathcal{N}_{\text{normal}}((\mathbf{I}+\mathbf{Z}\mathbf{W}_T\mathbf{Z})^{-1}\mathbf{Z}\underline{r}_T, \mathbf{I}+\mathbf{Z}\mathbf{W}_T\mathbf{Z})$ and E_2 is of $\mathcal{N}_{\text{normal}}(\underline{0}, \mathbf{I}-\mathbf{Z}\mathbf{W}_T\mathbf{Z})$. The expectation value E, the multi-variate normal moments, can be evaluated by the iterative formula in Eq. (3.9) or by the following recursion relation in Ref. [134],

$$E_a(x_1^{m_1}\cdots x_k^{m_k+1}\cdots x_{2N}^{m_{2N}}) = \mu_{m,k}E_a(x_1^{m_1}\cdots x_k^{m_k}\cdots x_{2N}^{m_{2N}})$$
$$+ \sum_{j=1}^{2N}(\mathbf{\Lambda}_c)_{kj}m_jE_a(x_1^{m_1}\cdots x_j^{m_j-1}\cdots x_{2N}^{m_{2N}}),\ m_j\geq 1. \tag{5.41}$$

---

[12] $\mathcal{J}[\mathbf{A},\underline{b};\underline{x}] = \exp(-\tfrac{1}{2}\underline{x}^t\mathbf{A}\underline{x}+\underline{b}^t\underline{x})$.

[13] The normal distribution $\mathcal{N}_{\text{normal}}(\underline{\mu}_m, \mathbf{\Lambda}_c^{-1})$ is defined as $p(\underline{y}) = \frac{1}{\sqrt{\det(2\pi\mathbf{\Lambda}_c^{-1})}}\exp\left[-\tfrac{1}{2}(\underline{y}-\underline{\mu}_m)^t\mathbf{\Lambda}_c(\underline{y}-\underline{\mu}_m)\right]$ with its mean vector $\underline{\mu}_m$ and covariance matrix $\mathbf{\Lambda}_c^{-1}$.

5.2.2. Algorithm for evaluating partial derivatives

We can evaluate the moments of vibrationally excited quanta via Eqs. (5.39) and (5.40). But the partial derivatives in Eq. (5.39) will give many $B_{a,\tilde{\eta}}^{m}$ functions in different multi-dimensional partial derivative orders ($\underline{m}$) according to the recursion relation in Eq. (5.37). For this reason, we need to book keeping the order ($\underline{m}$) of B functions for the corresponding coefficients to complete the calculation. The two sets of partial derivatives of B_1 and B_2 in Eq. (5.39) can be expanded by the recursion relation Eq. (5.37). When we consider a single mode partial derivative, the n-dimensional expansion coefficient vector of n-th partial derivative $\underline{c}_n$ is given by the recursion relation (5.37),

$$\underline{c}_n = \sum_{k=0}^{n-1} c_{n-1;k+1}[(-\tfrac{1}{2}+k)\underline{e}_k + \underline{e}_{k+1}], \qquad (5.42)$$

where $\underline{e}_k$ is a n-dimensional unit vector that represents the k-th order partial derivative. The multi-mode partial derivative coefficient space can be made with the help of the single mode expansion coefficient vectors, *i.e.* Consequently,

$$\hat{\partial}_{\underline{\tilde{\eta}}}^{l} B_{1,\tilde{\eta}}^{0}\Big|_{\tilde{\eta}=\underline{0}} = \det(2(\mathbf{I}+\mathbf{Z}\mathbf{W}_T\mathbf{Z}))^{-\frac{1}{2}} \sum_{\underline{s}=\underline{0}}^{l} \left(\prod_{i=1}^{2N} c_{l_i;s_i+1}\right) E_1(\overline{\prod_{\underline{x}}}^{2\underline{s}}), \qquad (5.43)$$

and

$$\hat{\partial}_{\underline{\tilde{\eta}}}^{(k-l)} B_{2,\tilde{\eta}}^{0}\Big|_{\tilde{\eta}=\underline{0}} = \det(2(\mathbf{I}-\mathbf{Z}\mathbf{W}_T\mathbf{Z}))^{-\frac{1}{2}} \sum_{\underline{s}=\underline{0}}^{l} \left(\prod_{i=1}^{2N} c_{k_i-l_i;s_i+1}\right) E_2(\overline{\prod_{\underline{x}}}^{2\underline{s}}). \qquad (5.44)$$

Finally from the equations (5.40), (5.41), (5.42), (5.43) and (5.44), we can evaluate the Eq. (5.39). It is possible to exploit the space decomposition, similar to the integral partitioning scheme (Sec. 2.4.2), for example X: moments space, Y: non-moments space, to reduce the dimension of the problem. The numerical results for the moments, however, are not presented in this thesis.

5.3. Results and discussion

In this section we test and discuss our TI CE method for vibronic transition energies. In the following subsection 5.3.1 we show the CE results of formic acid and anthracene for PE and UV transitions, respectively, which have been discussed already in the previous chapter 4 for the integral prescreening method at finite temperature. We analyze, in the second subsection 5.3.2, the electron transfer reaction of bacteriochlorophyll at finite temperature with the TI CE method. The detailed calculation data are available in appendix B.

5.3.1. Cumulants of Franck-Condon profiles

We have calculated the FC profiles of the PE and UV absorption spectra reported herein with the vibronic structure program hotFCHT [36, 46, 129–131]. Using the time-independent cumulant expansion developed in this chapter, FC intensity profiles are estimated with the

Edgeworth expansion algorithm for cumulants of arbitrary order (Eq. (5.19)). FC intensity profiles from the TI CE approach are compared with the results of the time-correlation function method developed in the previous chapter 4. Molecular equilibrium structures and harmonic force fields are taken form the previous work [46]. With the Edgeworth expansion algorithm, it is possible to construct a distribution constrained to the computed cumulants. The scheme employs Hermite-Gaussians as its expansion basis set and it is useful to evaluate the peak maximum. For lower order expansions the analytic solutions are available. A Gaussian line shape function with full width at half maximum (FWHM) of 500 cm^{-1} (the corresponding standard deviation $\sigma = 212.33 \ hc_0\text{cm}^{-1}$) is convoluted in the TCF evaluation. To include the Gaussian line shape function in the statistics we simply added σ^2 ($= 4.51\text{E}+04 \ (hc_0\text{cm}^{-1})^2$) to the second order cumulant (variance). This can be rationalized if one consider a convolution of the TCF with a Gaussian line shape function in time space ($\exp(-\frac{1}{2}\sigma^2(t/\hbar)^2)$) for the FT (Eq. (5.18)). The cumulants can be found in appendix B.

Fig. 5.1 compares the PE transition band of formic acid from TI CE and TCF (Ref. [129]) approaches at (a) 1000 K and (b) 0 K. The (vibrational) vertical transition energy (reorganization energy) of this vibronic transition is about $2329 \ hc_0\text{cm}^{-1}$ and one would expect to see the peak maximum of the spectrum at 0 K around this energy. As can be seen in Fig. 5.1(b) the peak maximum of TCF curve (solid line) is not at this vertical transition energy. The Gaussian approximation (dotted line) from the 2-nd TI CE expansion is much deviated from the TCF one. The discrepancy of vertical transition energy and mean energy ($= 2420\text{cm}^{-1}$) at 0 K is due to the effects of Duschinsky rotation and the harmonic frequency differences of the initial and final vibronic states. Peak maximum energy, vertical transition energy ($\frac{1}{2}\underline{\delta}^{\text{t}}\text{diag}(\underline{\epsilon}')\underline{\delta}$) and mean energy are generally not identical if the distribution deviates from a normal distribution. Even though the TI CE-Edgeworth cannot produce detailed FC profiles, the higher order TI CE calculation results (4-th and 8-th order expansions in dashed and dot-dashed lines, respectively) agree fairy well with the TCF curve especially for the peak maximum and the width of FC profile. When the distribution is closer to a normal distribution (at 1000 K, Fig. 5.1(a)), the two different approaches have better agreement. The mean energy (see the maximum of the Gaussian curve) is approaching the peak maximum energy as temperature is increasing, that is the distribution is approaching a normal distribution.

Fig. 5.2 compares the UV absorption spectra of anthracene obtained from the TI CE and the TCF approaches at (a) 500 K and (b) 0 K. The spectra of the TCF approach (solid lines in Fig. 5.2) with a Gaussian line shape with FWHM of 500 cm^{-1} are near to a normal distribution. The peak maximum energy of the two approaches are close to each other but the convolution of the TCF spectrum with a broader half-width line shape function would give better agreement. TI CE curves of anthracene agree TCF ones better than the formic acid calculations (see figures 5.1 and 5.2) because the distributions of FC profiles of anthracene at 0 K and 500 K are closer to a normal distribution. As one can see from the two examples, the TI CE approach can provide good guide lines already with 4-th order expansion for the full spectrum. If one is interested in the peak maximum or Stokes shift only, TI CE can provide the results quickly.

In principle the higher order TI CE should produce more detailed features of the distribution. But the Edgeworth expansion (5.19) can become numerically unstable. Oscillations of tails, furthermore, with negative values at high order CE can become unavoidable when
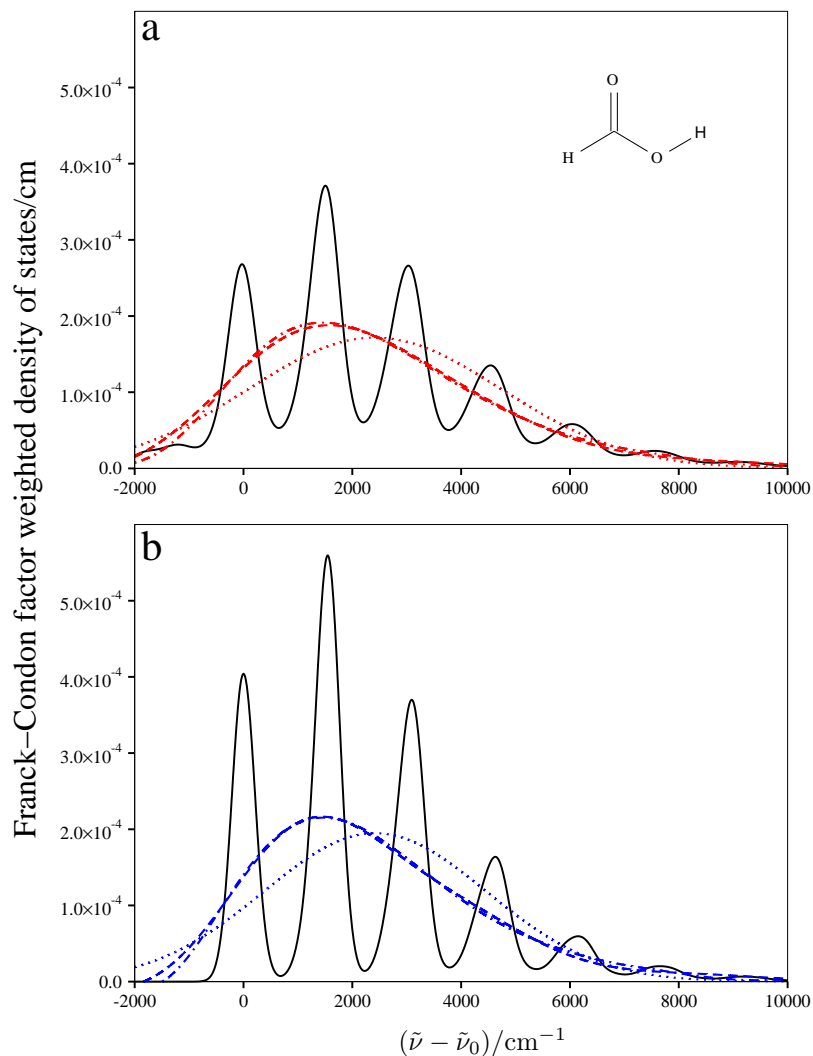
Figure 5.1.: Calculated FC profiles for the $1\ ^1A'\ \rightarrow\ 1\ ^2A'$ PE transition band of formic acid at (a) 1000 K and (b) 0 K. TCF-FFT [129] curves ($\varrho_{\mathrm{FCW,G}}(\tilde{\nu})$) are drawn as a solid line. The dotted, dashed and dot-dashed lines are for TICE-Edgeworth calculations ($\varrho_{\mathrm{FCW}}^{(c)}(\tilde{\nu})$) corresponding to the 2-nd, 4-th and 8-th order expansions, respectively. TCF-FFT curves are obtained with Gaussian line shapes with FWHM of 500 cm^{-1}. Here $\tilde{\nu}_0$ corresponds to the wavenumber of the $0'-0$ transition for this band.
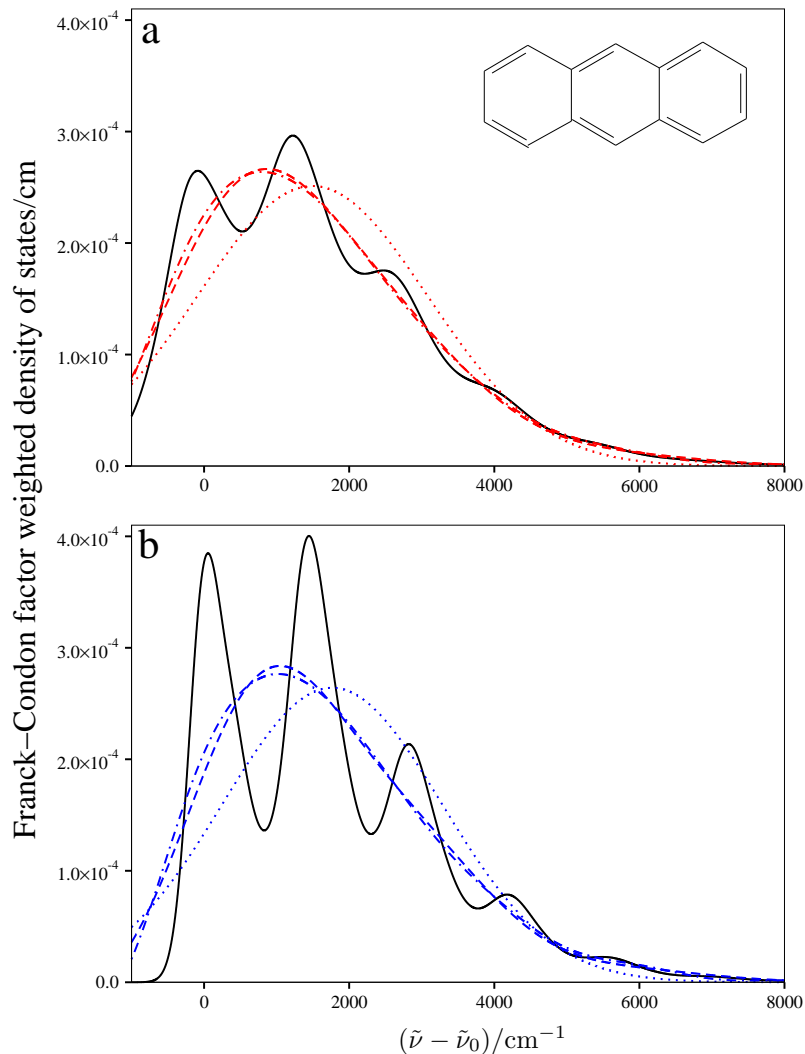
Figure 5.2.: Calculated FC profiles for the $1\,^1A_g \rightarrow 1\,^1B_{2u}$ absorption spectra of anthracene at (a) 500 K and (b) 0 K. TCF-FFT [129] curves ($\varrho_{FCW,G}(\tilde{\nu})$) are drawn as a solid line. The dotted, dashed and dot-dashed lines are for TICE-Edgeworth calculations ($\varrho_{FCW}^{(c)}(\tilde{\nu})$) corresponding to the 2-nd, 4-th and 8-th order expansions, respectively. TCF-FFT curves are obtained with Gaussian line shapes with FWHM of $500\,\text{cm}^{-1}$. $\tilde{\nu}_0$ corresponds to the wavenumber of the $0' - 0$ transition for this UV absorption band.

the distribution significantly deviates from the normal distribution because of the oscillatory nature of the Hermite-Gaussians as an expansion basis set. Thus the Edgeworth expansion renders the computed curve unsuitable as a PDF due to negative regions, but it provides a good overview of the overall spectrum (spectrum width) and peak maximum at virtually no computational cost, when compared to TI or even TCF-fast Fourier transform (FFT) FC profile calculations. If a more stable expansion method would be exploited, the higher order cumulants could be used as well.

The TI CE method developed herein is shown to be simple but it promises the following possible applications:

1. The 2-nd order (normal distribution) or higher order TI CE can possibly provide the confidence intervals which can serve to determine the relevant energy windows for FC profile calculations.

2. One can construct TCF of moments (cumulants and moments are mutually convertible) such as $\langle E_{\underline{\epsilon}',\underline{\epsilon}}\rangle(\mathbf{Z}(t))$ and $\langle E^4_{\underline{\epsilon}',\underline{\epsilon}}\rangle(\mathbf{Z}(t))$ at time t (see Ref. [129] and Sec. 4), then their FTs correspond to the absorption and emission (interchanging the initial and final states) spectrum, respectively. A similar approach of the frequency dependent mean transition energy has been exploited in Refs. [37, 40, 41, 48] for photoinduced cooling processes.

3. The TD CE described herein with the TD GF parameters can serve as an approximated time-propagator with the Taylor expansion of the TCF in terms of the TD cumulants (Sec. 5.1.2). This Taylor expansion allows a fast evaluation of the TCF by avoiding complex inverse matrix calculation at each time step.

4. We can define a parameter which is a function of molecular structural change, force field variation and temperature for individual vibrational modes with the mean excitation energy. This feature is useful in studying large molecular system to resolve individual vibrational mode contributions (see the following subsection 5.3.2).

5. The covariance [29] or higher order cumulants (multi-variance) of the vibrationally excited quanta can give the information about the coupling strength of the normal modes. This possibly offers an algorithm for grouping the coupled normal modes with a certain threshold for a large molecule, which has no symmetry, to approximate the Duschinsky rotation matrix as a block diagonal matrix so that one can reduce the dimensionality of the vibronic transition problem. One would argue that just looking at the Duschinsky rotation matrix is enough to see the coupling strength of normal modes [43] but this idea ignores molecular structural displacements and temperature effect, thus the TI CE approach would give better grouping strategies and results with more generality.

6. One can attempt to compute thermodynamic quantities of the vibronic transition such as specific heat by taking a partial derivative on the mean vibronic transition energy with respect to temperature, it is possible to have an arbitrary order partial derivatives on the mean vibronic transition energy with respect to reciprocal temperature (β) as well. This is precisely the method exploited for the molecular cooling applications [37, 40, 41, 48].

7. Exploiting the GF parameters (**Z**) in TI CE can possibly provide complementary pre-screening methods to the existing ones [46, 129] (see also Ch. 4).

5.3.2. Thermal energy redistribution via Duschinsky mode coupling

Electron transfer (ET) is one of the fundamental processes in chemistry and biology. Indeed, ET is essential both in photosynthesis as well as respiration and thus crucial for life as we know it. Therefore, a detailed understanding of this process in varying systems are interesting on the molecular level.

In the electron transfer theory the intramolecular vibrational relaxation process (see *e.g.* Ref. [85]) is the major mechanism of the charge migration. Nonadiabatic ET theory of Marcus [189] is based on the nuclear tunneling mechanism with the ET rate being proportional to the Franck-Condon factor weighted density of states and the absolute square of electronic coupling matrix element ($|V|^2$, within Condon approximation), *i.e.* the ET rate is defined as

$$\Gamma_{\mathrm{ET}}(\omega; T) = \tfrac{2\pi}{\hbar} |V|^2 \varrho_{\mathrm{FCW}}(\omega; T).$$
(5.45)

We can exploit the methods developed in the previous chapters for TI and TD approaches to compute the FCW. FC profiles are, however, typically highly congested at finite temperature, especially for large system such as bacteriochlorophyll (Bchl) in the photosynthetic reaction center (see *e.g.* Ref. [128] and Fig. 1.2)[14].

It has been emphasized by many researchers (see *e.g.* Ref. [82]) that the Duschinsky effect is important in electron transfer processes. In the presence of Duschinsky mode mixing effects a vibrational state-resolved analysis of the FC profile is thus prohibitive even in the harmonic approximation. Duschinsky rotations spoil the one to one correspondence between vibrational modes in the initial and final electronic states. As a result, FC profiles typically broaden and acquire a different temperature dependence as compared to systems without Duschinsky rotation as shown in Fig. 1.2. Thus it is difficult to analyze the individual vibrational mode contributions including the Duschinsky effects. It is more difficult at finite temperatures to see which of the vibrational modes are important in complex electron transferring systems. To analyze the individual vibrational mode contribution to an ET process, one uses in the absence of Duschinsky rotation and at zero Kelvin the reorganization energy ($\frac{1}{2}\epsilon_i' \delta_i^2$) or the Huang-Rhys factor ($\frac{1}{2}\delta_i^2$) as an electron-phonon coupling constant. In the presence of Duschinsky mode mixing, a similar parameter to characterize the mode contribution is required, which has to be a function of molecular structural change, harmonic force constant change, normal coordinate variation and temperature. The Huang-Rhys factor is identical to the mean vibrationally excited quanta of a particular vibrational mode and only depends on the molecular structural displacements when the displaced identical harmonic oscillator approximation is used. The primary solution we suggest for the Duschinsky rotated systems is to use the mean quantum number of the individual vibrational modes as the effective Huang-Rhys factor, the electron-phonon coupling constant. This fac-

---

[14]In Fig. 1.2, we present the FC profile of Bchl$^-$ $\longrightarrow$ Bchl. Each equilibrium structure and the corresponding harmonic force field of each electronic states are computed by electronic structure program package TURBOMOLE [190] at density functional theory (DFT) level calculation with density functional B3LYP and basis set TZVP. The equilibrium structures, harmonic wavenumbers and relevant data are provided in appendix B.

tor is temperature and potential energy surface dependent. The time-independent cumulant expansion method for FC profiles can provide a mode by mode analysis for the mean of the vibronic transition energy. The temperature dependent mean energy from Eq. (5.9) is given explicitly,

$$\langle E_{\underline{\epsilon}',\underline{\epsilon}}\rangle(T) = \text{Tr}[\boldsymbol{\Xi}] - \tfrac{1}{2}\text{Tr}[(\mathbf{I} - \mathbf{W}_T)^{-1}\boldsymbol{\Xi}] - \tfrac{1}{2}\text{Tr}[(\mathbf{I} + \mathbf{W}_T)^{-1}\boldsymbol{\Xi}]$$
$$- \underline{r}_T^{\text{t}}(\mathbf{I} + \mathbf{W}_T)^{-1}\boldsymbol{\Xi}(\mathbf{I} + \mathbf{W}_T)^{-1}\underline{r}_T\,. \tag{5.46}$$

By ignoring some modes in the statistics (setting some diagonal elements of Ξ to zero), we are able to compute the (effective) reorganization energy [82, 191–193] of a normal mode including the Duschinsky mode mixing and temperature effects with the mean energy and individual mode distributions. The mode-wise separable expression (5.46) can be obtained by choosing for example $\boldsymbol{\Xi} = \text{diag}(0,\dots,0,\,\dots,-\epsilon_i',\dots,0)$ for i-th vibrational mode in final state, *i.e.*

$$\langle E_{\underline{\epsilon}',\underline{\epsilon}}\rangle(T) = \sum_i \epsilon_i'\langle v_i'\rangle(T), \tag{5.47}$$

where $\epsilon_i'\langle v_i'\rangle(T)$ is the mode-wise effective reorganization energy and $\langle v_i'\rangle(T)$ is the corresponding effective Huang-Rhys factor (mean vibrationally excited quanta) of i-th mode in final state. We express explicitly the mean energies for displaced harmonic oscillators,

$$\langle E_{\underline{\epsilon}',\underline{\epsilon}}\rangle = \sum_i \tfrac{1}{2}\epsilon_i'\delta_i^2, \tag{5.48}$$

and for displaced-distorted harmonic oscillators,

$$\langle E_{\underline{\epsilon}',\underline{\epsilon}}\rangle(T) = \sum_i (\epsilon_i - \epsilon_i') - \frac{\epsilon_i - \epsilon_i' - \frac{(\epsilon_i - \epsilon_i')^2}{4\epsilon_i}(1 + \text{e}^{-\epsilon_i/k_{\text{B}}T})}{1 - \text{e}^{-\epsilon_i/k_{\text{B}}T}} + \tfrac{1}{2}\epsilon_i\delta_i^2. \tag{5.49}$$

The (traditional) reorganization energy $(\tfrac{1}{2}\epsilon_i'\delta_i^2)$, which is identical to the mean energy of displaced harmonic oscillator model, is temperature independent (see Eq. (5.48)), while the displaced-distorted harmonic oscillator system shows its temperature dependence in its mean energy expression (5.49). Here we learn that the temperature effect stems from the frequency change between two sets of harmonic oscillators. One could expect the harmonic frequency distortion can be enhanced via Duschinsky mode mixing effects because Duschinsky rotation is able to couple low frequency modes and high frequency modes such that it results a large effective harmonic frequency distortion.

In the figure 5.3(a) we approximate the FC profiles in figure 1.2 as Gaussian functions. The mean values and variances are computed from the method in Sec. 5.1.1 at 0 K, 100 K, 200 K and 300 K. The distortion (dotted lines) shows very little temperature dependence while the Duschinsky rotation (solid lines) induces a significant blue shift as temperature increases[15]. Figure 5.3(b) displays temperature dependence of mean energies corresponding to the peak maxima of Fig. 5.3(a) and it also indicates large Duschinsky effect on the temperature dependence. We have just showed that Duschinsky rotation can cause signifi-

---

[15]Because the displaced-distorted model usually includes small frequency changes.
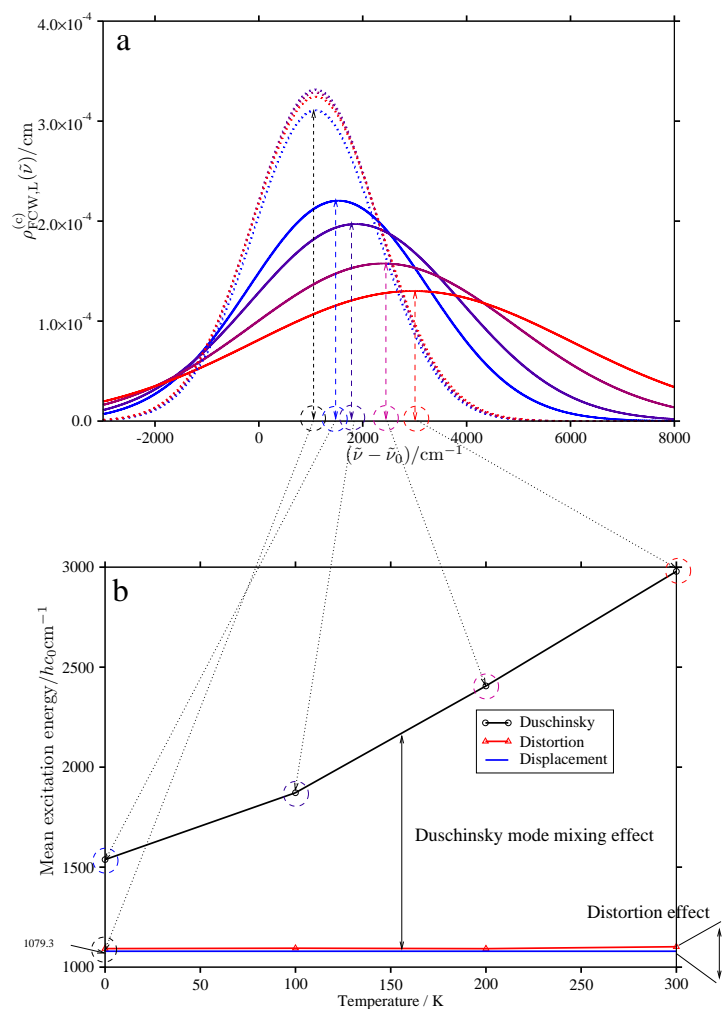
Figure 5.3.: a. The Gaussian approximated FCWs of (Bchl$^-$ $\longrightarrow$Bchl) from the TI CE method. The solid curves are obtained for a model with Duschinsky rotation and the dotted curves are obtained without Duschinsky rotation. In each set of curves the lines are calculated at 0 K, 100 K, 200 K and 300 K, and the intensities at the peak maxima decrease as temperature increases. b. The mean energies are plotted against temperature.

cant temperature dependence via total mean energy calculations (Fig. 5.3(b)). To quantify the relation between the Duschinsky rotation and the temperature dependence, we need to analyze the individual vibrational mode contributions to this process.

We compute the mean excitation energies of individual vibrational modes according to Eqs. (5.46) and (5.47). The cumulative sums of them at various temperatures are plotted in Fig. 5.4(a) for distortion (dotted lines) and rotation (solid lines) models. To see the Duschinsky rotation effect, we subtract dotted lines from solid lines at each temperature and plot the result in Fig. 5.4(b). According to Fig. 5.4(b), a C-C stretching mode ($\tilde{\nu}'_{79} = 997$ cm^{-1}) and a C-H stretching mode ($\tilde{\nu}'_{17} = 3038$ cm^{-1}) of the final (neutral) state show significant Duschinsky effect. These modes have little displacements compared to other modes and this indicates that displacements would not be important in the temperature dependence. The Duschinsky rotation matrix in Fig. 5.5 shows the reason why the two modes acquire significant amount of thermal excitation energies from the initial state. The two vibrational modes are coupled to the initial (anionic) vibrational modes, circled in Fig. 5.5, which give large effective frequency changes. The coupling strengths are not strong, only slightly above $\sin(\frac{\pi}{60}) \sim 0.05$. To check if this small coupling can cause large thermal energy redistribution among mixed modes, we investigate a 2-dimensional model system, $\underline{\epsilon} = hc_0(993 \text{ cm}^{-1}, 65 \text{ cm}^{-1})^{\text{t}}$, $\underline{\epsilon}' = hc_0(997 \text{ cm}^{-1}, 60 \text{ cm}^{-1})^{\text{t}}$, $\mathbf{S} = \begin{pmatrix} \cos(\frac{\pi}{60}) & -\sin(\frac{\pi}{60}) \\ \sin(\frac{\pi}{60}) & \cos(\frac{\pi}{60}) \end{pmatrix}$
and the (dimensionless) displacement vectors ($\underline{\delta}$) are chosen as $(0,0)^{\text{t}}$ and $(1,1)^{\text{t}}$ for nontotally symmetric and totally symmetric modes, respectively. We compute the mean excitation energy of individual vibrational modes of these 2-dimensional systems (see Fig. 5.6). The high wavenumber mode 993 cm^{-1} of initial state acquires little thermal excitation energy at increasing temperatures from 0 K to 300 K comparing to the low wavenumber mode 65 cm^{-1}. Without Duschinsky rotation ($\mathbf{S} = \mathbf{I}$) only a small amount of thermal energy would transfer to the high wavenumber mode 997 cm^{-1} of final state because only the thermal excitation energy of 993 cm^{-1} in initial state can transfer to the high wavenumber mode in the absence of Duschinsky rotation. But the result shows that the Duschinsky mode coupling can redistribute the thermal excitation energy of initial state by coupling modes. Displacement effect seems to be little according to the calculations (compare left and right plots in Fig. 5.6), the equal amount of thermal energies are transfered regardless of the displacements (see appendix B).

From our calculations and the 2-dimensional model system we can conclude and expect the followings:

1. Duschinsky rotation effect can induce different temperature dependence.

2. Mean excitation vibrational energy provides effective parameters which can characterize individual vibrational mode contribution including displacement, distortion, rotation and temperature effects.

3. Temperature dependence with Duschinsky effects can possibly be analyzed by the effective reorganization energy or Huang-Rhys factor obtained from the mean excitation quantum numbers.

4. Duschinsky mode mixing provides a mechanism for thermal vibrational energy transfer from low frequency modes to high frequency modes.
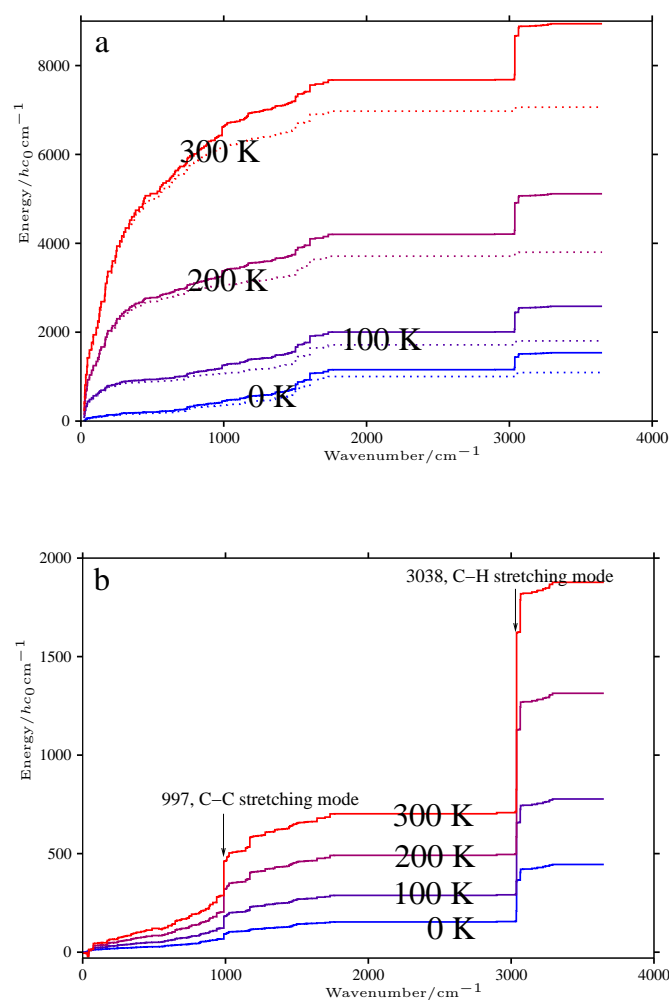
Figure 5.4.: a. Cumulative mean excitation energy of vibrational modes for Bchl$^-$ $\longrightarrow$Bchl. The solid lines are with Duschinsky effect and dotted lines are without Duschinsky effect. The temperatures are indicated on the lines. b. Duschinsky effect = (solid lines) - (dotted lines) at each temperature.
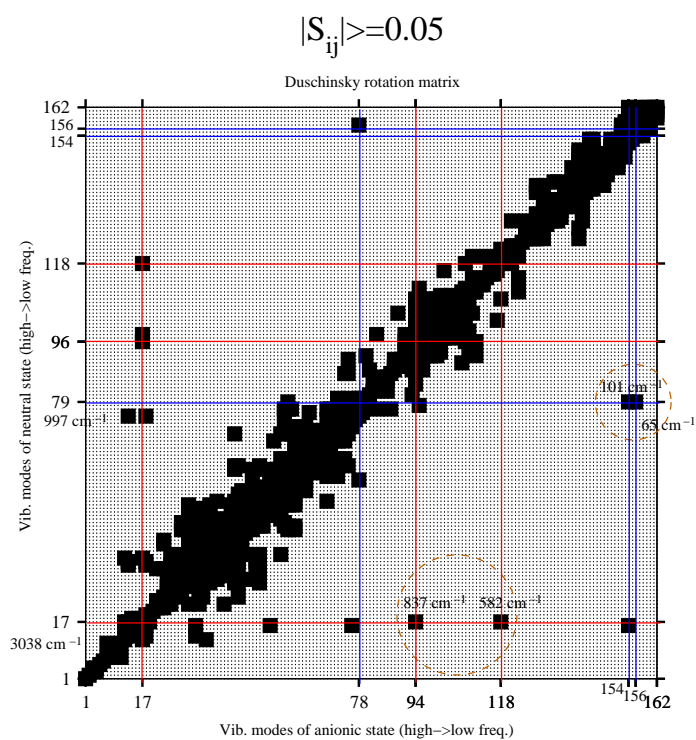
Figure 5.5.: Duschinsky rotation matrix (**S**) of Bchl$^-$ $\longrightarrow$Bchl. Only when the absolute value of a matrix element is greater or equal to 0.05 ($|S_{ij}| \geq 0.05$) a black square box is placed.
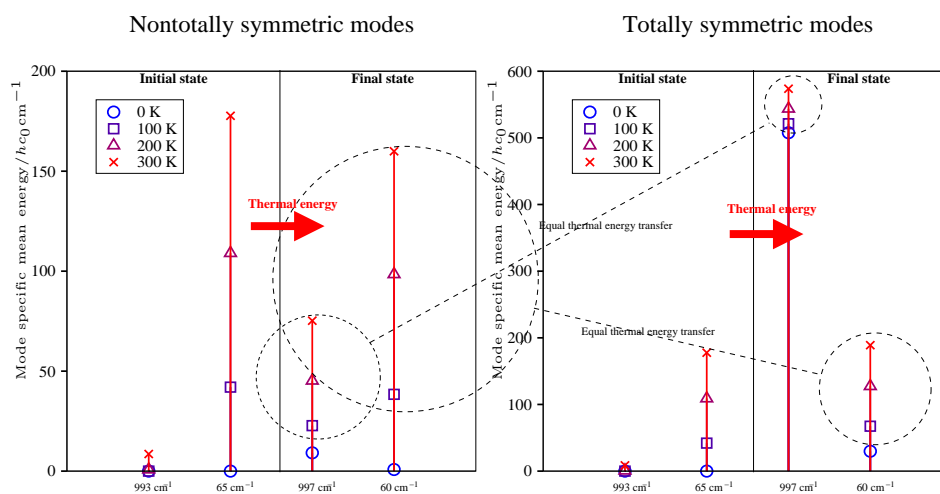
Figure 5.6.: Thermal energy transfer from low to high frequency modes via Duschinsky mode coupling. 2-dimensional model systems are studied for nontotally symmetric ($\underline{d} = \underline{0}$, left) and totally symmetric ($\underline{d} \neq \underline{0}$, right) mode mixing effects on temperature dependence. See text for details.

5. Displacements are not important for the temperature dependence.

6. Frequency change (distortion) is most important for the temperature dependence and the Duschinsky rotation enhances distortion effects.

7. TCF approach with mode screening could provide complementary information to the current approach.

8. Temperature effect on variances of FC profiles in presence of Duschinsky effect would be interesting to study.

5.4. Chapter summary and conclusion

We have proposed numerical schemes for computing cumulants of vibronic transition energies and moments of individual vibrationally excited quanta in an arbitrary order in this chapter. We have, also, presented the time propagation scheme with TD cumulants for the TCF approach. The cumulants and moments of the vibronic transition distribution can be exploited for many other application such as temperature dependent electron transfer processes. We have shown, with the electron transfer of bacteriochlorophyll in a photosynthetic system, that the thermal excitation energy of the initial state can be redistributed via the Duschinsky mode coupling mechanism. Duschinsky mode mixing effects can induce a different temperature dependence as a result. Currently the method is restricted to FC transitions but it can be extended to include also non-Condon effects. The TI cumulant expansion method can provide insights into the transition process with relatively low computational cost within the harmonic approximation. In the next chapter the non-Condon effects are considered. The development is a combination of the developments in section 3.2 and in chapter 4.

6. One-photon absorption with Herzberg-Teller effects

In order to describe weak or even Franck-Condon (FC)-forbidden transitions one needs to go beyond the Condon approximation (Sec. 2.1), which assumes a vibrational coordinate independent electronic transition moment, and take vibronic coupling effects [4, 30] into account. Within the adiabatic picture the Herzberg-Teller (HT) approach is perhaps the most natural extension (see *e.g.* Ref. [36] and Eq. (2.24)), where one incorporates the coordinate dependence of the electronic transition moment operator to linear or even higher order. This procedure requires calculation of additional integrals beyond the FC treatment (Ch. 3), involving the vibrational wavefunctions corresponding to different electronic states.

The focus of this chapter is on the direct calculation of HT and Franck-Condon/Herzberg-Teller interference (FC/HT) profiles at finite temperature utilizing the time-correlation function (TCF) and on the development of associated prescreening conditions within the time-independent (TI) formalism [36, 44–46, 49]. This is an anticipated extension of the previous FC pre-screening strategy at zero-temperature [46] and includes the finite-temperature FC transitions (Ch. 4). Herein, the formalism developed in Ref. [46] and in the previous chapter for the Franck-Condon factor (FCF) generating function (GF) (Ch. 4) is extended to the non-Condon effects via the incorporation of coherent state (CS) displacement operators (Eq. (2.84)) which were introduced in section 3.2 for the non-Condon integral evaluation scheme. At lowest order the resulting extended GF leads to analytical forms for the FC, FC/HT and HT GFs corresponding to the expressions (2.29), (2.30) and (2.31). These expressions are utilized within the previous prescreening and TCF strategy, providing rigorous error bounds for entire batches of HT integrals and the TCF for the integrated HT profile. These complementary approaches are applied to FC-forbidden vibronic transitions of benzene (ultra-violet (UV) absorption, $1\ ^1A_g \rightarrow 1\ ^1B_{2u}$) as a case study. In addition to the linear HT GF development, the extended GF detailed in this work can also be applied to go beyond the linear HT approximation and is connected to the nonadiabatic coupling effects beyond Born-Oppenheimer (BO) approximation and the inclusion of anharmonic corrections.

This chapter is organized as follows: Similar to the thermal FCF chapter 4, the method is developed in section 6.1 for non-Condon GFs and the prescreening strategies for FCHT profiles are constructed in section 6.2 on the basis of the FCHT GF. Then the methods are tested (Sec. 6.3) for benzene UV absorption profiles. The chapter is concluded in section 6.4.

6.1. Methodology

In the following subsections we develop the GFs for the FC/HT and HT contributions of Eq. (2.30) and Eq. (2.31) respectively, via the incorporation of CS displacement operators,

in correspondence with the previous FC developments at zero Kelvin [46] and at finite temperature (Ch. 4). We apply the CS displacement operator developments in section 3.2 to the non-Condon GF development. Exploiting the GF, we present the FCHT profile sum rules for integral prescreening strategies in section 6.1.3. Then the working equations (in TI and time-dependent (TD) approaches) for the spectral density functions (SDFs) and the summary of the current section developments follows in section 6.1.4.

6.1.1. Augmented generating function

To determine the explicit functional forms for the contributions corresponding to the FC, FC/HT and HT expressions of Eqs. (2.29)–(2.31), we now introduce a Boltzmann weighted GF G^K which has been augmented with the operators $\hat{f}(\underline{\hat{P}}, \underline{\hat{Q}})$ and $\hat{g}(\underline{\hat{P}}, \underline{\hat{Q}})$, that is[1]

$$G^K(\mathbf{Z};\mathbf{\Lambda})^{(\hat{f},\hat{g})} = \mathcal{N}|\langle\underline{0}'|\underline{0}\rangle|^{-2} \sum_{\underline{v},\underline{v}'=\underline{0}}^{\infty} \langle\underline{v}|(\hat{g})^*|\underline{v}'\rangle\langle\underline{v}'|\hat{f}|\underline{v}\rangle \overline{\prod}_{\underline{z},\underline{z}'}^{2\underline{v},2\underline{v}'} \mathrm{e}^{-(\underline{v}^{\mathrm{t}}\mathbf{B}\underline{\epsilon}+\underline{v}'^{\mathrm{t}}\mathbf{B}'\underline{\epsilon}')}, \quad (6.1)$$

where $\overline{\prod}_{\underline{x}_1,\cdots,\underline{x}_N}^{n_1,\cdots,n_N} = \left(\prod_k x_{1,k}^{n_{1,k}}\right)\cdots\left(\prod_k x_{N,k}^{n_{N,k}}\right)$ is used. After identification of $\hat{f}$ and $\hat{g}$ with products of CS displacement operators as introduced in Sec. 3.2, we can obtain an analytic expression for G^K and subsequently specialize to the desired FC, FC/HT and HT GF expressions (corresponding to Eqs. (2.29), (2.30) and (2.31) repectively) via partial derivatives with respect to CS parameters. In this section we derive these specific functional forms for the possible prescreening strategy and the non-Condon TCFs.

We can evaluate the non-Condon GF G^K, which is casted within the occupancy representation in Eq. (6.1), analytically through an integral formulation arising from a CS representation [46] (see also Ch. 4) with thermal integral kernel K in Eq. (4.2), so that[2]

$$G^K(\mathbf{Z};\mathbf{\Lambda})^{(\hat{f},\hat{g})} = \pi^{-2N}|\langle\underline{0}'|\underline{0}\rangle|^{-2} \int \mathrm{d}^2\underline{\alpha}\,\mathrm{d}^2\underline{\gamma}'\, K(\mathbf{\Lambda};\underline{\xi})\langle\mathbf{z}'^*\underline{\gamma}'|\hat{f}|\mathbf{z}\underline{\alpha}\rangle\langle\mathbf{z}'\underline{\gamma}'|\hat{g}|\mathbf{z}^*\underline{\alpha}\rangle^*. \quad (6.2)$$

Identifying $\hat{f}$ and $\hat{g}$ with the CS displacement operators (Eq. (2.84)) within the overlap integrals, as in Eq. (3.14), then the integral form of the GF Eq. (6.2) becomes[3]

$$G^K(\mathbf{Z};\mathbf{\Lambda};\underline{\eta},\underline{\eta}')$$
$$= \pi^{-2N}|\langle\underline{0}'|\underline{0}\rangle|^{-2} \int \mathrm{d}^2\underline{\alpha}\,\mathrm{d}^2\underline{\gamma}'\, K(\mathbf{\Lambda};\underline{\xi})\langle\mathbf{z}'^*\underline{\gamma}'|\hat{D}_{\mathrm{NC}}(\underline{\eta})|\mathbf{z}\underline{\alpha}\rangle\langle\mathbf{z}'\underline{\gamma}'|\hat{D}_{\mathrm{NC}}(\underline{\eta}')|\mathbf{z}^*\underline{\alpha}\rangle^*$$
$$= \pi^{-2N}|\langle\underline{0}'|\underline{0}\rangle|^{-2} \int \mathrm{d}^2\underline{\alpha}\,\mathrm{d}^2\underline{\gamma}'\, K(\mathbf{\Lambda};\underline{\xi})$$
$$\langle\mathbf{z}'^*\underline{\gamma}' + (\underline{\eta}_{P'}+\mathrm{i}\underline{\eta}_{Q'})^*|\mathbf{z}\underline{\alpha} + (\underline{\eta}_P+\mathrm{i}\underline{\eta}_Q)\rangle\langle\mathbf{z}'\underline{\gamma}' + (\underline{\eta}'_{P'}+\mathrm{i}\underline{\eta}'_{Q'})^*|\mathbf{z}^*\underline{\alpha} + (\underline{\eta}'_P+\mathrm{i}\underline{\eta}'_Q)\rangle^*$$
$$\exp\left[\tfrac{1}{2}\underline{\xi}^\dagger\mathbf{Z}\underline{\eta} - \tfrac{1}{2}\underline{\xi}^{\mathrm{t}}\mathbf{Z}\underline{\eta}^* + \tfrac{1}{2}\underline{\xi}^{\mathrm{t}}\mathbf{Z}\underline{\eta}'^* - \tfrac{1}{2}\underline{\xi}^\dagger\mathbf{Z}\underline{\eta}'\right]\exp\left[-\mathrm{i}\underline{\tilde{\eta}}_P^{\mathrm{t}}\underline{\tilde{\eta}}_Q + \mathrm{i}\underline{\tilde{\eta}}_P'^{\mathrm{t}}\underline{\tilde{\eta}}_Q'\right]. \quad (6.3)$$

This construction does include additional, often unnecessary, parametric flexibility, however restrictions can then be imposed on the resulting GF G^K for the specific cases of interest.

---

[1] *cf.* Eq. (2.109) for FCF GF at zero Kelvin and Eq. (4.4) for FCF GF at finite temperature.

[2] *cf.* Eq. (4.1) of thermal FCF GF

[3] See Eq. (4.1) of thermal FCF GF, Eq. (3.14) and the corresponding definitions on parameters and variables.

Exploiting the overlap integral of Eq. (3.18), then Eq. (6.3) reduces significantly to the analytic form

$$
\begin{aligned}
G^K(\mathbf{Z}; \mathbf{\Lambda}; \underline{\eta}, \underline{\eta}') =\ & \mathcal{N} \det(\mathbf{I} + \mathbf{Z}\mathbf{W}_T\mathbf{Z})^{-\frac{1}{2}} \det(\mathbf{I} - \mathbf{Z}\mathbf{W}_T\mathbf{Z})^{-\frac{1}{2}} R(\underline{\eta}, \underline{\eta}') \\
& \exp((\underline{b}^+)^{\mathrm{t}} \mathbf{Z}(\mathbf{I} + \mathbf{Z}\mathbf{W}_T\mathbf{Z})^{-1}\mathbf{Z}\underline{b}^+) \exp((\underline{b}^-)^{\mathrm{t}} \mathbf{Z}(\mathbf{I} - \mathbf{Z}\mathbf{W}_T\mathbf{Z})^{-1}\mathbf{Z}\underline{b}^-)\,.
\end{aligned}
\tag{6.4}
$$

This expression is achieved by a rescaling of the variables $\underline{\xi} \to (\mathbf{I} + \mathbf{\Lambda})^{-1}\underline{\xi}$ and then evaluating the resulting expression in terms of the real and imaginary parts of $\underline{\xi}$, as per Refs. [46] and chapters 2 and 4. Here the quantities in Eq. (6.4) are defined as

$$
\begin{aligned}
R(\underline{\eta}, \underline{\eta}') =\ & \exp(-\tfrac{1}{2}\underline{\eta}^{\dagger}\underline{\eta} - \tfrac{1}{2}\underline{\eta}'^{\dagger}\underline{\eta}') \exp(-\tfrac{1}{2}\underline{\eta}^{\mathrm{t}}\mathbf{W}\underline{\eta} - \tfrac{1}{2}\underline{\eta}'^{\dagger}\mathbf{W}\underline{\eta}'^* + \underline{r}^{\mathrm{t}}(\underline{\eta} + \underline{\eta}'^*)) \\
& \exp(-\mathrm{i}\underline{\tilde{\eta}}_P{}^{\mathrm{t}}\underline{\tilde{\eta}}_Q + \mathrm{i}\underline{\tilde{\eta}}'_P{}^{\mathrm{t}}\underline{\tilde{\eta}}'_Q)\,,
\end{aligned}
\tag{6.5}
$$

$$
(\underline{b}^+)^{\mathrm{t}}(\mathbf{\Lambda}; \underline{\eta}, \underline{\eta}') = \underline{r}_T^{\mathrm{t}} - \tfrac{1}{2}[\underline{\eta}^{\dagger} + \underline{\eta}'^{\mathrm{t}} + (\underline{\eta}^{\mathrm{t}} + \underline{\eta}'^{\dagger})\mathbf{W}](\mathbf{I} + \mathbf{\Lambda})^{-\frac{1}{2}},
\tag{6.6}
$$

$$
(\underline{b}^-)^{\mathrm{t}}(\mathbf{\Lambda}; \underline{\eta}, \underline{\eta}') = -\tfrac{\mathrm{i}}{2}[\underline{\eta}^{\dagger} - \underline{\eta}'^{\mathrm{t}} + (\underline{\eta}^{\mathrm{t}} - \underline{\eta}'^{\dagger})\mathbf{W}](\mathbf{I} + \mathbf{\Lambda})^{-\frac{1}{2}}.
\tag{6.7}
$$

We note that only the vector $\underline{r}_T$ in $\underline{b}^+$ is the temperature dependent Doktorov quantity (Eq. (4.9)), whereas $\mathbf{W}$ refers to the temperature independent Doktorov matrix.

Utilizing the relationship in Eq. (3.13) between the partial derivatives of CS parameters and the position and momentum operators we can straightforwardly construct the desired FC, FC/HT and HT GF expressions with Eq. (6.4). Direct substitution leads to $G^K(\mathbf{Z}; \mathbf{\Lambda})$ which is simply a FCF GF [46] (see Sec. 2.4 and Ch. 4),

$$
\begin{aligned}
G^K(\mathbf{Z}; \mathbf{\Lambda}) &= G^K(\mathbf{Z}; \mathbf{\Lambda})^{(\hat{1},\hat{1})} \\
&= G^K(\mathbf{Z}; \mathbf{\Lambda}; \underline{\eta}, \underline{\eta}')\big|_{\underline{\eta}=\underline{0}, \underline{\eta}'=\underline{0}}\,.
\end{aligned}
\tag{6.8}
$$

After rearranging the non-Condon GF expression (6.4) and by specifying the auxiliary parameters of position and momentum operators belonging to initial and final states, we can introduce operators up to arbitrary orders with the help of multi-variate Hermite polynomials (MHPs) (Eq. (3.3)) as it was done already for non-Condon integrals in section 3.2. The non-Condon GF expression (6.4) is rewritten as

$$
G^K(\mathbf{Z}; \mathbf{\Lambda}; \underline{\eta}, \underline{\eta}') = G^K(\mathbf{Z}; \mathbf{\Lambda})\mathcal{J}\left[\mathbf{W}_{\mathrm{NCF}}(\mathbf{Z}; \mathbf{\Lambda}), \underline{\tilde{r}}_{\mathrm{NCF}}(\mathbf{Z}; \mathbf{\Lambda}); \underline{\tilde{\eta}}_{\mathrm{NCF}}\right],
\tag{6.9}
$$

with the $8N$-dimensional collective auxiliary parameter vector (Eqs. (3.16) and (3.17)),

$$
\underline{\tilde{\eta}}_{\mathrm{NCF}} = \begin{pmatrix} \tilde{\eta}_P \\ \tilde{\eta}_Q \\ \tilde{\eta}'_P \\ \tilde{\eta}'_Q \end{pmatrix}.
\tag{6.10}
$$

Note that non-Condon GF separates into a FCF GF part ($G^K(\mathbf{Z}; \mathbf{\Lambda})$) and a non-Condon

contribution (the exponential function, $\mathcal{J}$) in Eq. (6.9).

The $8N$-dimensional square matrix $\widetilde{\mathbf{W}}_{\mathrm{NCF}}$ and vector $\underline{\tilde{r}}_{\mathrm{NCF}}$ are defined as

$$\widetilde{\mathbf{W}}_{\mathrm{NCF}}(\mathbf{Z};\mathbf{\Lambda}) =$$

$$\begin{pmatrix}
(\mathbf{I}+\mathbf{W})-\frac{1}{2}(\mathbf{I}+\mathbf{W})\widetilde{\mathbf{A}}_T^-(\mathbf{I}+\mathbf{W}) & \frac{1}{2}(\mathbf{I}+\mathbf{W})+\frac{1}{2}(\mathbf{I}+\mathbf{W})\widetilde{\mathbf{A}}_T^-(\mathbf{I}-\mathbf{W}) & -\frac{1}{2}(\mathbf{I}+\mathbf{W})\widetilde{\mathbf{A}}_T^+(\mathbf{I}+\mathbf{W}) & -\frac{i}{2}(\mathbf{I}+\mathbf{W})\widetilde{\mathbf{A}}_T^+(\mathbf{I}-\mathbf{W}) \\
\frac{1}{2}(\mathbf{I}+\mathbf{W})+\frac{1}{2}(\mathbf{I}-\mathbf{W})\widetilde{\mathbf{A}}_T^-(\mathbf{I}+\mathbf{W}) & (\mathbf{I}-\mathbf{W})+\frac{1}{2}(\mathbf{I}-\mathbf{W})\widetilde{\mathbf{A}}_T^-(\mathbf{I}-\mathbf{W}) & \frac{i}{2}(\mathbf{I}-\mathbf{W})\widetilde{\mathbf{A}}_T^+(\mathbf{I}+\mathbf{W}) & -\frac{i}{2}(\mathbf{I}-\mathbf{W})\widetilde{\mathbf{A}}_T^+(\mathbf{I}-\mathbf{W}) \\
-\frac{1}{2}(\mathbf{I}+\mathbf{W})\widetilde{\mathbf{A}}_T^+(\mathbf{I}+\mathbf{W}) & \frac{i}{2}(\mathbf{I}+\mathbf{W})\widetilde{\mathbf{A}}_T^+(\mathbf{I}-\mathbf{W}) & (\mathbf{I}+\mathbf{W})-\frac{1}{2}(\mathbf{I}+\mathbf{W})\widetilde{\mathbf{A}}_T^-(\mathbf{I}+\mathbf{W}) & -\frac{i}{2}(\mathbf{I}+\mathbf{W})-\frac{i}{2}(\mathbf{I}+\mathbf{W})\widetilde{\mathbf{A}}_T^-(\mathbf{I}-\mathbf{W}) \\
-\frac{i}{2}(\mathbf{I}-\mathbf{W})\widetilde{\mathbf{A}}_T^+(\mathbf{I}+\mathbf{W}) & -\frac{i}{2}(\mathbf{I}-\mathbf{W})\widetilde{\mathbf{A}}_T^+(\mathbf{I}-\mathbf{W}) & -\frac{i}{2}(\mathbf{I}+\mathbf{W})-\frac{i}{2}(\mathbf{I}-\mathbf{W})\widetilde{\mathbf{A}}_T^-(\mathbf{I}+\mathbf{W}) & (\mathbf{I}-\mathbf{W})+\frac{1}{2}(\mathbf{I}-\mathbf{W})\widetilde{\mathbf{A}}_T^-(\mathbf{I}-\mathbf{W})
\end{pmatrix},$$

$$\text{(6.11)}$$

and

$$\underline{\tilde{r}}_{\mathrm{NCF}}(\mathbf{Z};\mathbf{\Lambda}) = \begin{pmatrix}
\underline{r}-(\mathbf{I}+\mathbf{W})(\mathbf{I}+\mathbf{\Lambda})^{-\frac{1}{2}}\mathbf{A}^+\underline{r}_T \\
\mathrm{i}\underline{r}+\mathrm{i}(\mathbf{I}-\mathbf{W})(\mathbf{I}+\mathbf{\Lambda})^{-\frac{1}{2}}\mathbf{A}^+\underline{r}_T \\
\underline{r}-(\mathbf{I}+\mathbf{W})(\mathbf{I}+\mathbf{\Lambda})^{-\frac{1}{2}}\mathbf{A}^+\underline{r}_T \\
-\mathrm{i}\underline{r}-\mathrm{i}(\mathbf{I}-\mathbf{W})(\mathbf{I}+\mathbf{\Lambda})^{-\frac{1}{2}}\mathbf{A}^+\underline{r}_T
\end{pmatrix}, \tag{6.12}$$

where

$$\widetilde{\mathbf{A}}^\pm(\mathbf{Z};\mathbf{\Lambda}) = \mathbf{A}^+(\mathbf{Z};\mathbf{\Lambda}) \pm \mathbf{A}^-(\mathbf{Z};\mathbf{\Lambda}), \tag{6.13}$$

$$\mathbf{A}^\pm(\mathbf{Z};\mathbf{\Lambda}) = \mathbf{Z}(\mathbf{I}\pm\mathbf{Z}\mathbf{W}_T\mathbf{Z})^{-1}\mathbf{Z}, \tag{6.14}$$

$$\widetilde{\mathbf{A}}_T^\pm(\mathbf{Z};\mathbf{\Lambda}) = (\mathbf{I}+\mathbf{\Lambda})^{-\frac{1}{2}}\widetilde{\mathbf{A}}^\pm(\mathbf{Z};\mathbf{\Lambda})(\mathbf{I}+\mathbf{\Lambda})^{-\frac{1}{2}}. \tag{6.15}$$

As we have done for the non-Condon integrals in Eq. (3.21), we can express the non-Condon GF in terms of MHPs from Eq. (6.9),

$$G^K(\mathbf{Z};\mathbf{\Lambda})^{(\hat{f},\hat{g})} = \prod_{k=1}^{2N}\left[\mathrm{i}\sqrt{\tfrac{\tilde{\epsilon}_k}{2}}\right]^{\tilde{l}_k}\left[\tfrac{1}{\mathrm{i}}\sqrt{\tfrac{\hbar^2}{2\tilde{\epsilon}_k}}\right]^{\tilde{m}_k}\left[-\mathrm{i}\sqrt{\tfrac{\tilde{\epsilon}_k}{2}}\right]^{\tilde{n}_k}\left[-\tfrac{1}{\mathrm{i}}\sqrt{\tfrac{\hbar^2}{2\tilde{\epsilon}_k}}\right]^{\tilde{o}_k}$$

$$\hat{\partial}_{\underline{\tilde{\eta}}_P,\underline{\tilde{\eta}}_Q,\underline{\tilde{\eta}}'_P,\underline{\tilde{\eta}}'_Q}^{\underline{\tilde{l}},\underline{\tilde{m}},\underline{\tilde{n}},\underline{\tilde{o}}} G^K(\mathbf{Z};\mathbf{\Lambda};\underline{\eta},\underline{\eta}')\Big|_{\underline{\tilde{\eta}}_{\mathrm{NCF}}=\underline{0}}$$

$$= \prod_{k=1}^{2N}\left[\mathrm{i}\sqrt{\tfrac{\tilde{\epsilon}_k}{2}}\right]^{\tilde{l}_k}\left[\tfrac{1}{\mathrm{i}}\sqrt{\tfrac{\hbar^2}{2\tilde{\epsilon}_k}}\right]^{\tilde{m}_k}\left[-\mathrm{i}\sqrt{\tfrac{\tilde{\epsilon}_k}{2}}\right]^{\tilde{n}_k}\left[-\tfrac{1}{\mathrm{i}}\sqrt{\tfrac{\hbar^2}{2\tilde{\epsilon}_k}}\right]^{\tilde{o}_k}$$

$$\mathcal{H}_{\underline{\tilde{l}},\underline{\tilde{m}},\underline{\tilde{n}},\underline{\tilde{o}}}(\widetilde{\mathbf{W}}_{\mathrm{NCF}}^{-1}\underline{\tilde{r}}_{\mathrm{NCF}};\widetilde{\mathbf{W}}_{\mathrm{NCF}}^{-1}), \tag{6.16}$$

where the operators ($\hat{f}$ and $\hat{g}$) are identified as[4] $\hat{f} = \overline{\prod}_{\hat{Q}',\hat{P}',\hat{P},\hat{Q}}^{m',l',l,m}$ and $\hat{g} = \overline{\prod}_{\hat{Q}',\hat{P}',\hat{P},\hat{Q}}^{o',n',n,o}$, in which the collective indices are used, *i.e.* $\underline{\tilde{l}}^{\mathrm{t}} = (\underline{l}^{\mathrm{t}},\underline{l}'^{\mathrm{t}})$, $\underline{\tilde{m}}^{\mathrm{t}} = (\underline{m}^{\mathrm{t}},\underline{m}'^{\mathrm{t}})$, $\underline{\tilde{n}}^{\mathrm{t}} = (\underline{n}^{\mathrm{t}},\underline{n}'^{\mathrm{t}})$ and $\underline{\tilde{o}}^{\mathrm{t}} = (\underline{o}^{\mathrm{t}},\underline{o}'^{\mathrm{t}})$.

By evaluating Eq. (6.16) the FC/HT GF is explicitly expressed as,

$$G^K(\mathbf{Z};\mathbf{\Lambda})^{(\hat{Q}_i,\hat{1})} = \sqrt{\tfrac{\hbar^2}{2\epsilon_i}}G^K(\mathbf{Z};\mathbf{\Lambda})[\underline{r}+(\mathbf{I}-\mathbf{W})(\mathbf{I}+\mathbf{\Lambda})^{-\frac{1}{2}}\mathbf{A}^+\underline{r}_T]_i, \tag{6.17}$$

---

[4] $\hat{\partial}_{\underline{x}_1,\cdots,\underline{x}_N}^{\underline{n}_1,\cdots,\underline{n}_N} = \left(\frac{\partial^{\sum_k n_{1,k}}}{\prod_k \partial x_{1,k}^{n_{1,k}}}\right)\cdots\left(\frac{\partial^{\sum_k n_{N,k}}}{\prod_k \partial x_{N,k}^{n_{N,k}}}\right)$ and $\overline{\prod}_{\underline{x}_1,\cdots,\underline{x}_N}^{\underline{n}_1,\cdots,\underline{n}_N} = \left(\prod_k x_{1,k}^{n_{1,k}}\right)\cdots\left(\prod_k x_{N,k}^{n_{N,k}}\right)$.

and the HT GF is given explicitly by,

$$
G^K(\mathbf{Z}; \boldsymbol{\Lambda})^{(\hat{Q}_i, \hat{Q}_j)} = \frac{\hbar^2}{2} \sqrt{\frac{1}{\epsilon_i \epsilon_j}} G^K(\mathbf{Z}; \boldsymbol{\Lambda})
$$

$$
\left[[\underline{r} + (\mathbf{I} - \mathbf{W})(\mathbf{I} + \boldsymbol{\Lambda})^{-\frac{1}{2}} \mathbf{A}^+ \underline{r}_T]_i [\underline{r} + (\mathbf{I} - \mathbf{W})(\mathbf{I} + \boldsymbol{\Lambda})^{-\frac{1}{2}} \mathbf{A}^+ \underline{r}_T]_j \right.
$$

$$
\left. + \frac{1}{2} [(\mathbf{I} - \mathbf{W}) \widetilde{\mathbf{A}}_T^+ (\mathbf{I} - \mathbf{W})]_{ij} \right]. \tag{6.18}
$$

One can also determine expressions for position operators of the final electronic state, $\{\hat{Q}'_i\}$, by using the $(N + i)$-th component, instead of i-th component, of vectors or matrices in Eqs. (6.17) and (6.18) with the corresponding harmonic energy (ϵ'_i).

6.1.2. Time-dependent density matrix formalism

The method developed in the previous section for non-Condon effects is derived from the TI perspective with the aid of CSs, although it can be connected to the TCF directly via TD GF parameters (Eqs. (4.42) and (4.43)). In this section the clear link between the TD and TI formalisms for the non-Condon development in CS basis is demonstrated[5] with the quantum mechanical trace expression which is introduced in section 2.1.

It has been shown in section 2.1 that the SDF $\rho(\omega; T)$ in frequency domain at finite temperature T can be transformed into a time domain function, the TCF, as in equation (2.14). The time propagation of CSs with the corresponding vibrational Hamiltonians can be expressed as the diagonal phase space unitary operation (Eq. (2.91)),

$$
e^{-i\hat{H}t/2\hbar} |\underline{\alpha}\rangle = |\mathbf{z}(t)\underline{\alpha}\rangle, \tag{6.19}
$$

$$
e^{+i\hat{H}'t/2\hbar} |\underline{\gamma}'\rangle = |\mathbf{z}'(t)\underline{\gamma}'\rangle, \tag{6.20}
$$

where $\mathbf{z}(t)$ and $\mathbf{z}'(t)$ are defined in Eqs. (4.42) and (4.43) respectively. The thermal Boltzmann population of CSs in the initial state is expressed with the non-unitary operation (Eq. (2.92)),

$$
e^{-\beta\hat{H}/2} |\underline{\alpha}\rangle = e^{-\frac{1}{2}\underline{\alpha}^\dagger (\mathbf{I} - \boldsymbol{\Gamma}^\dagger \boldsymbol{\Gamma})\underline{\alpha}} |\boldsymbol{\Gamma}\underline{\alpha}\rangle, \tag{6.21}
$$

where $\boldsymbol{\Gamma} = (\mathbf{I} + \boldsymbol{\lambda})^{-\frac{1}{2}}$ and for the final state a similar relation holds with $\hat{H}$ being replaced by $\hat{H}'$ and $\boldsymbol{\Gamma}$ replaced by $\boldsymbol{\Gamma}' = (\mathbf{I} + \boldsymbol{\lambda}')^{-\frac{1}{2}}$. Then we can trace the spectral density function (Eq. (2.14)) in CS basis directly by inserting the initial and final state CS resolution of the identity (Eq. (2.93)) to transform the trace to a closed functional form. Instead of the specific TCF given by Eq. (2.14), herein a more general structural form for the GF corresponding to Eq. (6.3) is given as well. The extended GF is defined with the CS displacement operators (as in Eq. (6.3)) replacing $\hat{\mu}(Q)$ in Eq. (2.14),

$$
G^K = |\langle \underline{0}'|\underline{0}\rangle|^{-2} Z_{\mathrm{I,F}}^{-1} \mathrm{Tr}(\hat{D}_{\mathrm{NC}}(\underline{\eta}')^\dagger e^{\hat{H}'(-\beta - it/\hbar)} \hat{D}_{\mathrm{NC}}(\underline{\eta}) e^{\hat{H}(-\beta + it/\hbar)}), \tag{6.22}
$$

---

[5]Contribution by J. L. Stuber to Huh *et al.* [130].

where

$$Z_{\mathrm{I,F}} = \mathrm{Tr}(\mathrm{e}^{-\beta \hat{H}'} \mathrm{e}^{-\beta \hat{H}}) \,. \tag{6.23}$$

In order to have a symmetric formulation of the GF G^K as in Eq. (6.3), we split each of the exponential operators into equal contributions for time (t) and imaginary time (reciprocal temperature β) parts,

$$G^K = |\langle \underline{0}' | \underline{0} \rangle|^{-2} Z_{\mathrm{I,F}}^{-1} \mathrm{Tr} \Big(\hat{D}_{\mathrm{NC}}(\underline{\eta}')^\dagger \mathrm{e}^{\hat{H}'(-\beta - \mathrm{i}t/\hbar)/2} \mathrm{e}^{\hat{H}'(-\beta - \mathrm{i}t/\hbar)/2}$$
$$\hat{D}_{\mathrm{NC}}(\underline{\eta}) \mathrm{e}^{\hat{H}(-\beta + \mathrm{i}t/\hbar)/2} \mathrm{e}^{\hat{H}(-\beta + \mathrm{i}t/\hbar)/2} \Big) \,. \tag{6.24}$$

We, then, insert the CS resolution of the identity (Eq. (2.93)) for $|\underline{\gamma}'\rangle$ and evaluate the trace in CS phase space of $|\underline{\alpha}\rangle$,

$$G^K = |\langle \underline{0}' | \underline{0} \rangle|^{-2} Z_{\mathrm{I,F}}^{-1} \pi^{-2N} \int \mathrm{d}^2 \underline{\alpha} \int \mathrm{d}^2 \underline{\gamma}'$$

$$\langle \underline{\alpha} | \mathrm{e}^{\hat{H}(-\beta + \mathrm{i}t/\hbar)/2} \hat{D}_{\mathrm{NC}}(\underline{\eta}')^\dagger \mathrm{e}^{\hat{H}'(-\beta - \mathrm{i}t/\hbar)/2} | \underline{\gamma}' \rangle \langle \underline{\gamma}' | \mathrm{e}^{\hat{H}'(-\beta - \mathrm{i}t/\hbar)/2} \hat{D}_{\mathrm{NC}}(\underline{\eta}) \mathrm{e}^{\hat{H}(-\beta + \mathrm{i}t/\hbar)/2} | \underline{\alpha} \rangle$$

$$= |\langle \underline{0}' | \underline{0} \rangle|^{-2} Z_{\mathrm{I,F}}^{-1} \pi^{-2N} \int \mathrm{d}^2 \underline{\alpha} \int \mathrm{d}^2 \underline{\gamma}'$$

$$\exp(-\underline{\alpha}^\dagger (\mathbf{I} - \mathbf{\Gamma}^\dagger \mathbf{\Gamma}) \underline{\alpha} - (\underline{\gamma}')^\dagger (\mathbf{I} - (\mathbf{\Gamma}')^\dagger \mathbf{\Gamma}') \underline{\gamma}')$$

$$\langle \mathbf{z}'(t)^* \mathbf{\Gamma}' \underline{\gamma}' | \hat{D}_{\mathrm{NC}}(\underline{\eta}) | \mathbf{z}(t) \mathbf{\Gamma} \underline{\alpha} \rangle \langle \mathbf{z}'(t) \mathbf{\Gamma}' \underline{\gamma}' | \hat{D}_{\mathrm{NC}}(\underline{\eta}') | \mathbf{z}(t)^* \mathbf{\Gamma} \underline{\alpha} \rangle^* \,, \tag{6.25}$$

where the invariance of the trace under cyclic permutation of operators is used. After rescaling $\underline{\alpha} \to \mathbf{\Gamma} \underline{\alpha}$ and $\underline{\gamma}' \to \mathbf{\Gamma}' \underline{\gamma}'$, we see the thermal terms in this equation are precisely the thermal integral kernel K in Eq. (4.2), *i.e.*

$$Z_{\mathrm{I,F}}^{-1} \det(\mathbf{\Gamma})^{-2} \det(\mathbf{\Gamma}')^{-2} \exp\big(-\underline{\alpha}^\dagger (\mathbf{I} - (\mathbf{\Gamma}^{-1})^\dagger \mathbf{\Gamma}^{-1}) \underline{\alpha}$$
$$- (\underline{\gamma}')^\dagger (\mathbf{I} - ((\mathbf{\Gamma}')^{-1})^\dagger (\mathbf{\Gamma}')^{-1}) \underline{\gamma}' \big) = K(\mathbf{\Lambda}, \underline{\xi}) \,, \tag{6.26}$$

because $\mathbf{\Gamma}$ and $\mathbf{\Gamma}'$ are real valued matrices and $Z_{\mathrm{I,F}}^{-1} = \mathcal{N}$ in Eq. (4.14). Thus this GF expression (6.25) is identical to that of Eq. (6.3) except that the later depends on time variable t implicitly.

We note here again that Islampour and Miralinaghi [93] devised recently a TCF for internal conversion (IC) rate involving multi-promoting modes (which mediate the intramolecular transition) and vibrational mode mixing effects. They exploited second order multivariate normal moments for the momentum operator matrix elements of the promoting modes to evaluate their trace. However their TD method is not generally applicable to various transition problems and the method cannot handle nonlinear coupling problems (*cf.* Eq. (6.16)). Peng *et al.* [94, 95] also have a similar development to that of Islampour and Miralinaghi [93].

6.1.3. Franck-Condon-Herzberg-Teller sum rules

In connection with the previous work [46] and the thermal FCF section 4, we can decompose the expressions for G^K, *i.e.* Eq. (6.3) and Eq. (6.4), into terms which depend on variables

belonging to the orthogonal subspaces X and Y as well (see Sec. 2.4.2). This decomposition allows us to derive sum rules involving specific modes, via partial differentiation.

We partition G^K into the X and Y spaces, then

$$
\begin{aligned}
G^K(\mathbf{Z}; \mathbf{\Lambda}; \underline{\eta}, \underline{\eta}') = \\
\mathcal{N} R(\underline{\eta}, \underline{\eta}') \mathcal{I}_{2N-N_X}[(\mathbf{I} + \mathbf{Z}\mathbf{W}_T\mathbf{Z})_{YY}, \mathbf{Z}_{YY}\underline{b}_Y^+] \\
\mathcal{I}_{2N-N_X}[(\mathbf{I} - \mathbf{Z}\mathbf{W}_T\mathbf{Z})_{YY}, \mathbf{Z}_{YY}\underline{b}_Y^-] \\
\mathcal{I}_{N_X}[\mathbf{I}_{XX} + \mathbf{Z}_{XX}\widetilde{\mathbf{W}}_{T;XX}^+\mathbf{Z}_{XX}, \mathbf{Z}_{XX}\underline{\tilde{b}}_X^+] \\
\mathcal{I}_{N_X}[\mathbf{I}_{XX} - \mathbf{Z}_{XX}\widetilde{\mathbf{W}}_{T;XX}^-\mathbf{Z}_{XX}, \mathbf{Z}_{XX}\underline{\tilde{b}}_X^-] \,,
\end{aligned}
\tag{6.27}
$$

where

$$
(\underline{\tilde{b}}_X^\pm)^{\mathrm{t}}(\mathbf{Z}_{YY}; \mathbf{\Lambda}_{YY}; \underline{\eta}, \underline{\eta}') = (\underline{b}_X^\pm)^{\mathrm{t}} \mp (\underline{b}_Y^\pm)^{\mathrm{t}}\mathbf{Z}_{YY}((\mathbf{I} \pm \mathbf{Z}\mathbf{W}_T\mathbf{Z})_{YY})^{-1}\mathbf{Z}_{YY}\mathbf{W}_{T;YX} \,,
\tag{6.28}
$$

and the temperature dependent partitioned Doktorov matrix and vector $\widetilde{\mathbf{W}}_{T;XX}^\pm$ and $\underline{\tilde{r}}_{T;X}^+$ are listed in Eqs. (4.21) and (4.22) respectively.

We now perform the relevant partial derivatives on the partitioned form in Eq. (6.27) of G^K to derive the desired sum rules. The sum rule for one excited mode k in the fixed quantum number space X at the excitation number n is given by,

$$
\begin{aligned}
G_Y^K(\mathbf{I}_{YY}; \mathbf{\Lambda})_{k;n}^{(\hat{Q}_i, \hat{1})} = \sqrt{\tfrac{\hbar^2}{2\epsilon_i}} G_Y^K(\mathbf{I}_{YY}; \mathbf{\Lambda}) \\
\left[(r_i + \underline{c}_{iY}^{\mathrm{t}}\underline{d}_Y)\mathcal{G}(\widetilde{\mathbf{W}}_T^\pm; \underline{\tilde{r}}_T^+; k; n; 0, \tfrac{1}{2}, \tfrac{1}{2}, 0) + c_{ik}^+ \mathcal{G}(\widetilde{\mathbf{W}}_T^\pm; \underline{\tilde{r}}_T^+; k; n; 1, 1, \tfrac{1}{2}, 1)\right] \,,
\end{aligned}
\tag{6.29}
$$

for the relevant FC/HT contribution (6.17) and $\mathcal{G}$ is defined in Eq. (4.23), whereas

$$
\begin{aligned}
G_Y^K(\mathbf{I}_{YY}; \mathbf{\Lambda})_{k;n}^{(\hat{Q}_i, \hat{Q}_j)} = \tfrac{\hbar^2}{2}\sqrt{\tfrac{1}{\epsilon_i\epsilon_j}} G_Y^K(\mathbf{I}_{YY}; \mathbf{\Lambda}) \\
\Big[c_{ik}^+ c_{jk}^+ \mathcal{G}(\widetilde{\mathbf{W}}_T^\pm; \underline{\tilde{r}}_T^+; k; n; 0, \tfrac{3}{2}, \tfrac{1}{2}, 1) + c_{ik}^- c_{jk}^- \mathcal{G}(\widetilde{\mathbf{W}}_T^\pm; \underline{\tilde{r}}_T^+; k; n; 0, \tfrac{1}{2}, \tfrac{3}{2}, 1) \\
+ \{(r_i + \underline{c}_{iY}^{\mathrm{t}}\underline{d}_Y)(r_j + \underline{c}_{jY}^{\mathrm{t}}\underline{d}_Y) + \tfrac{1}{2}\underline{c}_{iY}^{\mathrm{t}}((\mathbf{I} + \mathbf{W}_T)_{YY})^{-1}\underline{c}_{jY} + \tfrac{1}{2}\underline{c}_{iY}^{\mathrm{t}}((\mathbf{I} - \mathbf{W}_T)_{YY})^{-1}\underline{c}_{jY}\} \\
\times \mathcal{G}(\widetilde{\mathbf{W}}_T^\pm; \underline{\tilde{r}}_T^+; k; n; 0, \tfrac{1}{2}, \tfrac{1}{2}, 0) \\
+ (r_i c_{jk}^+ + r_j c_{ik}^+ + \underline{c}_{iY}^{\mathrm{t}}\underline{d}_Y c_{jk}^+ + \underline{c}_{jY}^{\mathrm{t}}\underline{d}_Y c_{ik}^+)\mathcal{G}(\widetilde{\mathbf{W}}_T^\pm; \underline{\tilde{r}}_T^+; k; n; 1, 1, \tfrac{1}{2}, 1)\Big],
\end{aligned}
$$

for the HT expression (6.18). Here

$$\underline{c}_{iY}^{\mathrm{t}} = \frac{2\partial(\underline{b}_Y^+)^{\mathrm{t}}}{\mathrm{i}\partial\eta_{Q_i}}\bigg|_{\underline{\eta}=\underline{0},\underline{\eta}'=\underline{0}} = \frac{-2\partial(\underline{b}_Y^-)^{\mathrm{t}}}{\partial\eta_{Q_i}}\bigg|_{\underline{\eta}=\underline{0},\underline{\eta}'=\underline{0}}$$

$$= [(\mathbf{I} - \mathbf{W})(\mathbf{I} + \mathbf{\Lambda})^{-\frac{1}{2}}]_{iY}, \tag{6.30}$$

$$c_{ik}^+ = \frac{2\partial(\tilde{\underline{b}}_{X=k}^+)^{\mathrm{t}}}{\mathrm{i}\partial\eta_{Q_i}}\bigg|_{\underline{\eta}=\underline{0},\underline{\eta}'=\underline{0}}$$

$$= [(\mathbf{I} - \mathbf{W})(\mathbf{I} + \mathbf{\Lambda})^{-\frac{1}{2}}]_{ik} - [(\mathbf{I} - \mathbf{W})(\mathbf{I} + \mathbf{\Lambda})^{-\frac{1}{2}}]_{iY}((\mathbf{I} + \mathbf{W}_T)_{YY})^{-1}\mathbf{W}_{T;Yk}, \tag{6.31}$$

$$c_{ik}^- = \frac{-2\partial(\tilde{\underline{b}}_{X=k}^-)^{\mathrm{t}}}{\partial\eta_{Q_i}}\bigg|_{\underline{\eta}=\underline{0},\underline{\eta}'=\underline{0}}$$

$$= [(\mathbf{I} - \mathbf{W})(\mathbf{I} + \mathbf{\Lambda})^{-\frac{1}{2}}]_{ik} + [(\mathbf{I} - \mathbf{W})(\mathbf{I} + \mathbf{\Lambda})^{-\frac{1}{2}}]_{iY}((\mathbf{I} - \mathbf{W}_T)_{YY})^{-1}\mathbf{W}_{T;Yk}, \tag{6.32}$$

$$\underline{d}_Y = ((\mathbf{I} + \mathbf{W}_T)_{YY})^{-1}\underline{r}_{T;Y}, \tag{6.33}$$

are used.

Usually only the initial states are thermally excited and the temperature dependent Doktorov quantities (Eqs. (4.9)) are given precisely for this case,

$$(\mathbf{I} - \mathbf{W})(\mathbf{I} + \mathbf{\Lambda})^{-\frac{1}{2}} = 2\begin{pmatrix} \mathbf{Q}(\mathbf{I} + \boldsymbol{\lambda})^{-\frac{1}{2}} & \mathbf{R} \\ \mathbf{R}^{\mathrm{t}}(\mathbf{I} + \boldsymbol{\lambda})^{-\frac{1}{2}} & \mathbf{P} \end{pmatrix}, \tag{6.34}$$

in which the thermal factors are weighted only on the initial degrees of freedom (DOF), and $\mathbf{W}_T$ of this case can be found in Eq. (4.17).

6.1.4. Spectral density functions

By using Eqs. (6.17) and (6.18) we can construct the electronic transition dipole moment induced absorption intensity GF with FC, FC/HT and HT contributions (Eq. (2.32)), *i.e.*

$$\rho_{\mathrm{FCHTW}}(\mathbf{Z};\mathbf{\Lambda}) =$$

$$|\langle\underline{0}'|\underline{0}\rangle|^2 \left(|\underline{\mu}_0|^2 G^K(\mathbf{Z};\mathbf{\Lambda}) + 2\sum_i \underline{\mu}_0 \cdot \underline{\mu}_i' G^K(\mathbf{Z};\mathbf{\Lambda})^{(\hat{Q}_i,\hat{1})} + \sum_{i,j} \underline{\mu}_i' \cdot \underline{\mu}_j' G^K(\mathbf{Z};\mathbf{\Lambda})^{(\hat{Q}_i,\hat{Q}_j)} \right), \tag{6.35}$$

associated with the FCHT spectral profile of Eq. (2.32). Immediately we can exploit these relations within the thermal TCF formalism as described in section 6.1.2, where we obtain a simple analytic form for the exact thermal FC TCF. The Lorentzian line shaped, $L(t)$, absorption spectrum is then given as a one-dimensional Fourier transform (FT) with ω_0

corresponding to the frequency at the $0' - 0$ transition,

$$\rho_{\text{FCHTW,L}}(\omega) = \hbar^{-1} \int_{-\infty}^{\infty} \mathrm{d}t \, \rho_{\text{FCHTW}}(\mathbf{Z}(t); \mathbf{\Lambda}) L(t) \mathrm{e}^{\mathrm{i}(\omega - \omega_0)t} . \tag{6.36}$$

It should be noted here that the current development of non-Condon TCF is not restricted to linear HT expansion. The nonlinear non-Condon TCF can be evaluated by the complex MHPs in Eq. (6.16). We can partition the non-Condon TCF, as well, into irreducible representation contributions as in Eq. (4.46) for the possible speed-up of the calculation. Sum rules can similarly be determined for the spectral profile ρ_{FCHTW} as to FC developments (Ref. [46] and Sec. 4.3) via the expressions derived in the previous section. The sum rule for the absorption spectrum for some modes in Y space and all other modes in the vibrational ground state is given by[6]

$$
\begin{aligned}
\rho_{\text{FCHTW};Y}(\mathbf{I}_{YY}; \mathbf{\Lambda}) = & |\langle \underline{0}' | \underline{0} \rangle|^2 \Big(|\underline{\mu}_0|^2 G_Y^K(\mathbf{I}_Y; \mathbf{\Lambda}) \\
& + 2 \sum_i \underline{\mu}_0 \cdot \underline{\mu}_i' G_Y^K(\mathbf{I}_{YY}; \mathbf{\Lambda})^{(\hat{Q}_i, \hat{1})} \\
& + \sum_{i,j} \underline{\mu}_i' \cdot \underline{\mu}_j' G_Y^K(\mathbf{I}_{YY}; \mathbf{\Lambda})^{(\hat{Q}_i, \hat{Q}_j)} \Big) .
\end{aligned}
\tag{6.37}
$$

For a single excited mode k with excitation number n in the fixed quantum number space X, the corresponding sum rule for the absorption spectrum is then[7]

$$
\begin{aligned}
\rho_{\text{FCHTW};Y}(\mathbf{I}_{YY}; \mathbf{\Lambda})_{k;n} = & |\langle \underline{0}' | \underline{0} \rangle|^2 \Big(|\underline{\mu}_0|^2 G_Y^K(\mathbf{I}_Y; \mathbf{\Lambda})_{k;n} \\
& + 2 \sum_i \underline{\mu}_0 \cdot \underline{\mu}_i' G_Y^K(\mathbf{I}_{YY}; \mathbf{\Lambda})_{k;n}^{(\hat{Q}_i, \hat{1})} \\
& + \sum_{i,j} \underline{\mu}_i' \cdot \underline{\mu}_j' G_Y^K(\mathbf{I}_{YY}; \mathbf{\Lambda})_{k;n}^{(\hat{Q}_i, \hat{Q}_j)} \Big) .
\end{aligned}
\tag{6.38}
$$

The total sum of intensity at finite temperature has been previously determined (see *e.g.* Ref. [49]), where

$$
\begin{aligned}
\rho^{\text{total}}(T) &= |\underline{\mu}_0|^2 + \sum_{\underline{v}=\underline{0}}^{\infty} p_{\underline{v}}(T) \sum_k^N \frac{\hbar^2}{2\epsilon_k} |\underline{\mu}_k'|^2 (2v_k + 1) \\
&= |\underline{\mu}_0|^2 + \sum_k^N \frac{\hbar^2}{2\epsilon_k} |\underline{\mu}_k'|^2 \coth(\tfrac{1}{2}\beta\epsilon_k) \\
&= \rho_{\text{FCHTW}}(\mathbf{I}, \mathbf{\Lambda}(T)) .
\end{aligned}
\tag{6.39}
$$

Here $(\mathbf{I} + \mathbf{\Lambda})^{-\frac{1}{2}}$ is explicitly given at finite temperature T for only the initial state is ther-

---

[6]*cf.* Eq. (2.128) for FCFs at zero Kelvin and Eq. (4.16) for FCFs at finite temperature.
[7]*cf.* Eq. (4.20) for FCFs at finite temperature.

mally excited,

$$(\mathbf{I} + \boldsymbol{\Lambda})^{-\frac{1}{2}}(T) = \mathrm{diag}(\mathrm{e}^{-\beta(T)\epsilon_1/2}, \ldots, \mathrm{e}^{-\beta(T)\epsilon_N/2}, 1, \ldots, 1). \tag{6.40}$$

At 0 Kelvin,

$$\rho^{\mathrm{total}}(0) = |\underline{\mu}_0|^2 + \sum_k^N \frac{\hbar^2}{2\epsilon_k} |\underline{\mu_k}'|^2$$

$$= \rho_{\mathrm{FCHTW}}(\mathbf{I}, \boldsymbol{\Lambda}(T = 0)), \tag{6.41}$$

where $(\mathbf{I} + \boldsymbol{\Lambda})^{-\frac{1}{2}}(T = 0)$ is given as,

$$(\mathbf{I} + \boldsymbol{\Lambda})^{-\frac{1}{2}}(T = 0) = \mathrm{diag}(0, \ldots, 0, 1, \ldots, 1). \tag{6.42}$$

One can transform $\rho_{\mathrm{FCHTW}}(\mathbf{I}, \boldsymbol{\Lambda}(T))$ at zero Kelvin and at finite temperature into finite series sums in Eqs. (6.41) and (6.39), respectively, with the help of Doktorov matrix identities [117] in Eqs. (2.100) and (2.101). The total sum of intensity for nonlinear HT terms at finite temperature and at zero Kelvin can be evaluated easily with the MHP expression (6.16) which can be computed recursively (Eq. (3.5)) or iteratively (Eq. (3.9)). The total sum of intensity including 2-nd order HT expansion at zero Kelvin can be found in the literature (see *e.g.* Ref. [51]) in a series of summation expression. To this end it is important to mention that the non-Condon TCFs in arbitrary order (*e.g.* nonlinear HT terms) and the corresponding total intensities can be evaluated simply by the MHP expression (6.16). The corresponding prescreening strategy can be developed by exploiting the sum rules for the total intensities from the single vibronic level (SVL) GF derived in the next chapter 7. And the methods (TD and TI) developed for linear HT expansion and higher orders can also be applied for example for electronic circular dichroism (ECD) spectra with only slight modification of the prefactors. The ECD cross section has an interference term between the electronic transition dipole moment (TDM) and the magnetic TDM (see *e.g.* Refs. [54, 102] for TI approach for linear HT terms.) which are supposed to be expanded by normal coordinates like HT expansion, *i.e.* the same non-Condon GF ((6.16)) can be applied directly within the current formalism.

6.2. Integral prescreening

In this section, the integral prescreening strategies of thermally weighted FCFs of section 4.3 is extended to the non-Condon terms. The basic strategies, however, are the same as in the FC development. The integrated normalized FCHT profile is normalized to be 1

for the total intensity[8],

$$
\begin{aligned}
F_{\text{FCHT}}^{\text{tot}} = \frac{\mathcal{N}}{\rho_{\text{FCHTW}}(\mathbf{I}; \boldsymbol{\Lambda}(T))} \sum_{\underline{v}, \underline{v}' \in S} & \Big[|\underline{\mu}_0|^2 \, |\langle \underline{v}'|\underline{v}\rangle|^2 \\
& + 2 \sum_i \underline{\mu}_0 \cdot \underline{\mu}'_i \langle \underline{v}'|\hat{Q}_i|\underline{v}\rangle \langle \underline{v}|\underline{v}'\rangle \\
& + \sum_{i,j} \underline{\mu}'_i \cdot \underline{\mu}'_j \langle \underline{v}'|\hat{Q}_i|\underline{v}\rangle \langle \underline{v}|(\hat{Q}_j)|\underline{v}'\rangle \Big] e^{-\underline{v}^{\text{t}} \mathbf{B} \underline{\epsilon}} e^{-\underline{v}'^{\text{t}} \mathbf{B}' \underline{\epsilon}'},
\end{aligned}
\tag{6.43}
$$

where S is the vibrational occupation number vector (ONV) subspace. When we evaluate FCHT integrals with the ONV basis set belonging to S, then the normalized total intensity satisfies the tolerance relation for the desired tolerance $\epsilon_{\text{max}}^{\text{tol}}$,

$$
\epsilon_{\text{tot}} = 1 - F_{\text{FCHT}}^{\text{tot}} \leq \epsilon_{\text{max}}^{\text{tol}}, \tag{6.44}
$$

holds for the error ϵ_{tot} in the normalized FCHT intensity.

As for the coarse grained FCF prescreening scheme, the mode and coupling tolerance auxiliary parameters t_{m} and t_{c} are employed as well.

6.2.1. Vibrational mode coupling error

The minimum number of simultaneously excited modes are obtained for the threshold t_{c} neglecting all integrals that involve a larger number of simultaneously excited modes via Eq. (6.37). The maximum number of simultaneously excited modes (MSM) M is increased from $M = 0$ until it converges to the desired error for the coupling tolerance t_c, *i.e.*

$$
\epsilon_{\text{c}} = 1 - \sum_{m=0}^{M} F_{\text{FCHT;c}}^{(m)} = 1 - \widetilde{F}_{\text{FCHT;c}}^{(M)} < t_c, \tag{6.45}
$$

where $F_{\text{FCHT;c}}^{(m)}$ is the contribution involving precisely m simultaneously excited modes for total intensity and $\widetilde{F}_{\text{FCHT;c}}^{(M)} = \sum_{m=0}^{M} F_{\text{FCHT;c}}^{(m)}$. Each increment can be determined from the intermediate quantity,

$$
B_{\text{FCHT}}^{(m)} = \sum_{Y \in C_m^{2N}} \rho_Y(\mathbf{I}_{YY}; \boldsymbol{\Lambda}(T)), \tag{6.46}
$$

where C_m^{2N} is the set from the space Y obtained by choosing m modes for summation out of possible $2N$, via the relation

$$
F_{\text{FCHT;c}}^{(m)} = B_{\text{FCHT}}^{(m)} - \sum_{i=1}^{m} \binom{2N - m + i}{i} F_{\text{FCHT;c}}^{(m-i)}. \tag{6.47}
$$

---

[8]*cf.* Eq. (4.25) for thermal FCFs.

Note that here we use

$$
\begin{aligned}
F_{\text{FCHT;c}}^{(0)} = \frac{\mathcal{N}}{\rho_{\text{FCHTW}}(\mathbf{I}; \mathbf{\Lambda}(T))} \Big[& |\underline{\mu}_0|^2 \, |\langle \underline{0}'|\underline{0}\rangle|^2 \\
& + 2 \sum_i \underline{\mu}_0 \cdot \underline{\mu}_i' \langle \underline{0}'|\hat{Q}_i|\underline{0}\rangle \langle \underline{0}|\underline{0}'\rangle \\
& + \sum_{i,j} \underline{\mu}_i' \cdot \underline{\mu}_j' \langle \underline{0}'|\hat{Q}_i|\underline{0}\rangle \langle \underline{0}|\hat{Q}_j|\underline{0}'\rangle \Big] .
\end{aligned}
\tag{6.48}
$$

6.2.2. Vibrational mode excitation error

Here we define a mode contribution $F_{\text{FCHT;m}}^{(k)}(n)$ associated to a fixed vibrational quantum number $v_k'' = n$ for mode k while other modes are summed over,

$$
\begin{aligned}
F_{\text{FCHT;m}}^{(k)}(n) = \frac{\mathcal{N}}{\rho_{\text{FCHTW}}(\mathbf{I}; \mathbf{\Lambda}(T))} \sum_{\underline{v},\underline{v}'|v_k''=n} \Big[& |\underline{\mu}_0|^2 \, |\langle \underline{v}'|\underline{v}\rangle|^2 \\
& + 2 \sum_i \underline{\mu}_0 \cdot \underline{\mu}_i' \langle \underline{v}'|\hat{Q}_i|\underline{v}\rangle \langle \underline{v}|\underline{v}'\rangle \\
& + \sum_{i,j} \underline{\mu}_i' \cdot \underline{\mu}_j' \langle \underline{v}'|\hat{Q}_i|\underline{v}\rangle \langle \underline{v}|(\hat{Q}_j)|\underline{v}'\rangle \Big] e^{-\underline{v}^{\text{t}}\mathbf{B}\underline{\epsilon}} e^{-\underline{v}'^{\text{t}}\mathbf{B}'\underline{\epsilon}'} .
\end{aligned}
\tag{6.49}
$$

The total mode contribution of mode k can be given by Eq. (6.37) summing over the quantum numbers of all other modes while leaving the mode k at $v_k'' = 0$, *i.e.* the partial contribution $F_{\text{FCHT;m}}^{(k)}(0)$ is the contribution excluding excitations of mode k. The finite series summation for fixed quantum number Eq. (6.38) is exploited to determine the contribution $F_{\text{FCHT;m}}^{(k)}(n)$. To obtain the maximum quantum number for a specific vibrational mode, we determine a minimum quantum number $v_k''^{\max}$ satisfying

$$
\epsilon_{\text{m}}^{(k)} = \left(1 - F_{\text{FCHT};v_k''^{\max}} \right) < t_{\text{m}} ,
\tag{6.50}
$$

where

$$
F_{\text{FCHT};v_k''^{\max}} = \sum_{n=0}^{v_k''^{\max}} F_{\text{FCHT;m}}^{(k)}(n).
\tag{6.51}
$$

According to the tolerance set $(t_{\text{m}}, t_{\text{c}})$ and irreducible representations of underlying symmetry group, then the error bounds ($\epsilon_{\min}$ and $\epsilon_{\max}$) are estimated [46], satisfying the error bound condition Eq. (4.37).

6.3. Results and discussion

In this section the numerical tests of the HT developments are presented. As in chapter 4 on the thermal FCF the TI method with prescreening and the HT TCF approach are compared herein. The test example is the absorption spectrum of benzene ($1\,^1\text{A}_{\text{g}} \rightarrow 1\,^1\text{B}_{2\text{u}}$) at zero

Table 6.1.: Prescreening and error bound performance for benzene at 0 K and at finite temperatures (300 K and 500 K). For a given tolerance set, the associated error tolerance ($\epsilon_{\max}^{\text{tol}}$), prescreening stage rigorous error bounds ($\epsilon_{\max}$ and $\epsilon_{\min}$), maximum value for the maximum number of simultaneously excited modes of all irreducible representations and maximum number of simultaneously excited modes $M_{\max}^{(\gamma)}$ of each symmetry block ($M_{\max}(M_{\max}^{(a_{1g})}; M_{\max}^{(a_{2g})}; M_{\max}^{(b_{2g})}; M_{\max}^{(e_{1g})}; \boldsymbol{M}_{\max}^{(e_{2g})}; M_{\max}^{(a_{2u})}; M_{\max}^{(b_{1u})}; M_{\max}^{(b_{2u})}; M_{\max}^{(e_{1u})}; M_{\max}^{(e_{2u})})$), and the error of the integrated Herzberg-Teller profile (ϵ_{tot}) are provided; only the symmetry block e_{2g} has non-zero first derivatives of the electronic transition dipole moment with respect to the normal modes.

T	Tol. Set $(t_{\mathrm{m}}, t_{\mathrm{c}})$	$\epsilon_{\max}^{\text{tol}}$	$\epsilon_{\max}$	ϵ_{tot}	$\epsilon_{\min}$	$M_{\max}(M_{\max}^{(\gamma)})$
0 K	I$(10^{-6}, 10^{-5})$	13.0×10^{-5}	1.62×10^{-5}	1.62×10^{-5}	1.13×10^{-5}	3(2;1;2;2;**3**;1;1;2;2;3)
	II$(10^{-5}, 10^{-4})$	13.0×10^{-4}	1.47×10^{-4}	1.47×10^{-4}	0.98×10^{-4}	3(2;0;2;2;**3**;1;1;2;2;2)
300 K	I$(10^{-6}, 10^{-5})$	16.0×10^{-5}	2.67×10^{-5}	2.64×10^{-5}	1.23×10^{-5}	6(3;2;4;4;**6**;2;2;3;4;6)
	II$(10^{-5}, 10^{-4})$	16.0×10^{-4}	3.26×10^{-4}	3.22×10^{-4}	2.17×10^{-4}	6(2;2;4;4;**5**;2;2;2;3;6)
500 K	I$(10^{-6}, 10^{-5})$	16.0×10^{-5}	2.98×10^{-5}	2.86×10^{-5}	1.29×10^{-5}	8(3;2;4;4;**8**;2;2;4;6;8)
	II$(10^{-5}, 10^{-4})$	16.0×10^{-4}	3.71×10^{-4}	3.53×10^{-4}	2.16×10^{-4}	8(3;2;4;4;**7**;2;2;3;4;8)

Kelvin and at finite temperatures. In section 6.3.1 the GF developments are verified by comparing the results of the TI and TD methods. The various electronic structure results for the same system are presented in section 6.3.2 such that the analytic gradient calculations of the electronic TDM [52] are tested with the HT profile calculation of benzene.

6.3.1. (FC)HT generating function for benzene

Because the $1\,^1A_g \rightarrow 1\,^1B_{2u}$ absorption spectrum of benzene has been exhaustively studied experimentally and theoretically (see *e.g.* Ref. [36]), the benzene absorption spectrum is suitable to test and verify methodological the developments for non-Condon effects. A detailed discussion of the spectrum including its peak assignments, which can be found elsewhere (see *e.g.* Refs. [36, 52]), is omitted in this discussion because the theoretical development and the validation of it is the major purpose of the current work. Instead we overlaid the experimental UV absorption spectrum of Fischer [2] to compare it with the computed FC profile at 300 K in Fig. 6.1(c). The overlay is made according to the energy scale. The experimental spectrum height is rescaled to have the same 6_0^1 peak height of the computed one. The ingredients (optimized molecular structures, harmonic force fields, electronic TDMs and its first derivatives) for the FCHT vibronic structure calculation of the absorption spectrum of benzene are taken from Ref. [36] (CASSCF/DZV). As shown in Fig. 6.1(c) the main feature of the spectrum is the band ν_6 (belonging to e_{2g} the so-called false origin) and a progression in the breathing mode ν_1 (belonging to a_{1g}), *i.e.* $6_0^1 1_0^n$. The experimental wavenumbers [194] are $\tilde{\nu}_6 = 521$ cm^{-1} and $\tilde{\nu}_1 = 923$ cm^{-1}, and the theoretical harmonic wavenumbers of Berger *et al.* [36] are $\tilde{\nu}_6 = 575$ cm^{-1} and $\tilde{\nu}_1 = 963$ cm^{-1} which are bigger than experimental ones due to the harmonic approximation.

We exploit the molecular symmetry of benzene (D_{6h}) for the ground state ($1\,^1A_g$) and the first excited state ($1\,^1B_{2u}$) of benzene in the TI prescreening calculations and the corresponding vibronic structure calculations. For the TCF approach, the molecular point group symmetry is not exploited even though it is straightforward to use molecular symmetry (Eq. (4.46)).

In the evaluation of Eq. (6.36), corresponding to the FT of the Lorentzian weighted TCF,
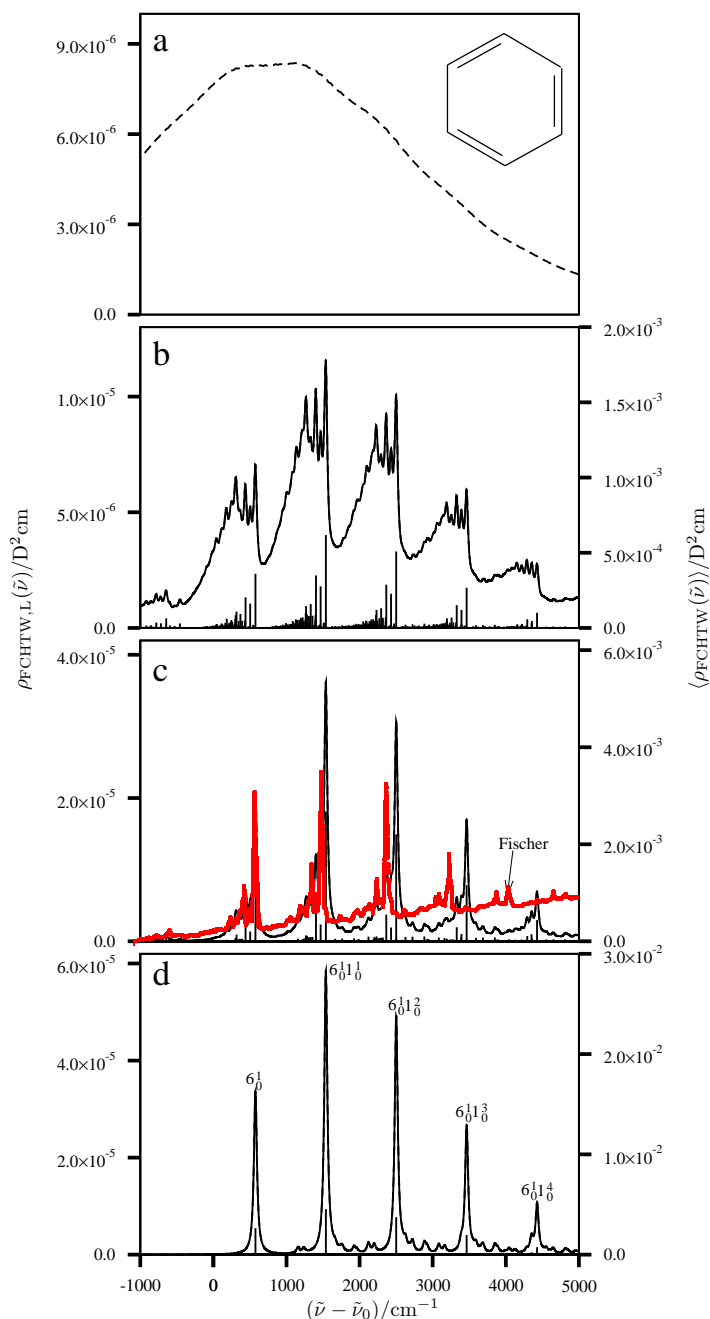
Figure 6.1.: Calculated HT profiles for the $1\,^1A_g \rightarrow 1\,^1B_{2u}$ absorption spectrum of benzene at (a) 1000 K , (b) 500 K with tolerance set I, (c) 300 K with tolerance set I and (d) 0 K with tolerance set I. Tolerance set descriptions are provided in Table 6.1. Each line in the stick spectra [right axis, $\langle \rho_{\text{FCHTW}}(\tilde{\nu}) \rangle$] represents the averaged FCHT weighted density of states in a wavenumber interval $\Delta\tilde{\nu} = 1\,\text{cm}^{-1}$. The $\langle \rho_{\text{FCHTW}}(\tilde{\nu}) \rangle$ of all intervals sums to $(1 - \epsilon_{\text{tot}})/\Delta\tilde{\nu}$ for a given temperature. The stick representations have additionally been convoluted with Lorentzian line shapes with full width at half maximum (half-width) of $50\,\text{cm}^{-1}$ [solid, left axis, $\rho_{\text{FCHTW,L}}(\tilde{\nu})$] and compared to the results obtained from the TCF approach [dashed, left axis, $\rho_{\text{FCHTW,L}}(\tilde{\nu})$]. Differences are, however, barely visible on the current scale. Here $\tilde{\nu}_0$ corresponds to the wavenumber of the $0' - 0$ transition for this UV absorption band. The experimental UV absorption spectrum of Fischer [2] is additionally compared with the FC profile at 300 K in (c).

the FFTW [178] library (version 3.1.2) for the fast Fourier transform (FFT) is used with a grid size of 2^{16}, a time increment of $\Delta t = 0.51$ fs, and a time interval [-16.7 ps, 16.7 ps]. The time reversal symmetry relation of the TCF, $\rho_{\text{FCHTW}}(\mathbf{Z}(-t); \tilde{\mathbf{\Gamma}}) = \rho_{\text{FCHTW}}(\mathbf{Z}(t); \tilde{\mathbf{\Gamma}})^*$ is also exploited. The real part of the FT is taken for the FCHT profile. In Fig. 6.1 the frequency and the wavenumber representation relation $\rho_{\text{FCHTW,L}}(\tilde{\nu}) = hc_0\rho_{\text{FCHTW,L}}(\omega)$ is exploited.

All calculations have been performed by the development version of hotFCHT [36, 46, 129–131] in which the method developed in current HT work was implemented. It takes about 40 hours for the TI calculation at 500 K with prescreening tolerance set I (Table 6.1) and 12 minutes for the corresponding TCF calculation on a 64 bit single processor machine. For the TI calculation all possible vibrational quantum number combinations (about 544 million FCHT integrals) are generated within the prescreening bound conditions and the FC and HT integrals[9] are evaluated with recurrence relations of Eqs. (2.103) and (2.104). Those codes are not optimized and further efficient improvements are certainly possible.

In Table 6.1 the prescreening bound condition with various tolerance sets $(t_{\text{m}}, t_{\text{c}})$ at 0 K and at finite temperatures (300 K and 500 K) are summarized. According to the prescreening conditions the HT profiles are computed and the error of the integrated normalized HT profiles (ϵ_{tot}) are reported in the table. The prescreening calculations of all tolerance sets satisfy the error bound condition (Eq. (4.37)). In each tolerance set calculations at different temperatures show the trend that ϵ_{tot}s are closer to their upper bounds ϵ_{max}s in this benzene example. Only the symmetry block e_{2g} of benzene contains the non-zero first derivative of the electronic TDM, so that the prescreening conditions (maximum excitation quantum number of modes (MQM) and MSM) of other symmetry blocks are identical to those of the FC case [46, 129]. For this absorption the electronic TDM at the equilibrium molecular structure of the ground state ($\underline{\mu}_0 = \underline{0}$) vanishes, so that only ρ_{HT} (Eq. (2.31)) contributes to the $1\,^1A_g \to 1\,^1B_{2u}$ absorption profile of benzene. The MSM $M_{\text{max}}^{(\gamma)}$ of each symmetry block is presented in the table. The bold font is assigned for the numbers of the symmetry block e_{2g} to distinguish them from the numbers belonging to the other symmetry blocks. As the tolerance condition gets tighter and temperature increases, the $M_{\text{max}}^{(\gamma)}$s of each symmetry block become bigger and the corresponding absorption profile computations become more expensive. In Fig. 6.1 one can find the stick spectra $\langle \rho_{\text{FCHTW}}(\tilde{\nu}) \rangle$, representing the averaged FCHT weighted density of states in a wavenumber interval $\Delta\tilde{\nu} = 1$ cm^{-1}, with the tolerance set I in Table 6.1 at raising temperature conditions from 0 K to 500 K. The stick representations have additionally been convoluted with Lorentzian line shapes with full width at half maximum (FWHM) of 50 cm^{-1}, $\rho_{\text{FCHTW,L}}(\tilde{\nu})$ in solid line, and compared to the results obtained from the TCF approach $\rho_{\text{FCHTW,L}}(\tilde{\nu})$ in dashed line. Differences (about 0.001 %) are, however, barely visible on the current scale. The agreement of the TI and TD approaches (the two independent approaches) and the error bound condition (Eq. (4.37)) show the validity of our developments and the total sum rules in closed forms (Eqs. (6.39) and (6.41)). The UV absorption band at 1000 K obtained with the TCF method is presented additionally. It would take too much time to finish the TI calculation for the featureless blurred curve (Fig. 6.1a).

As shown in Fig. 6.2, only up to 5 simultaneously excited modes (out of the final state alone) are sufficient at 0 K to reach a coupling error below 0.1%. At higher temperatures,

---

[9]With the second quantized expression of position operator.
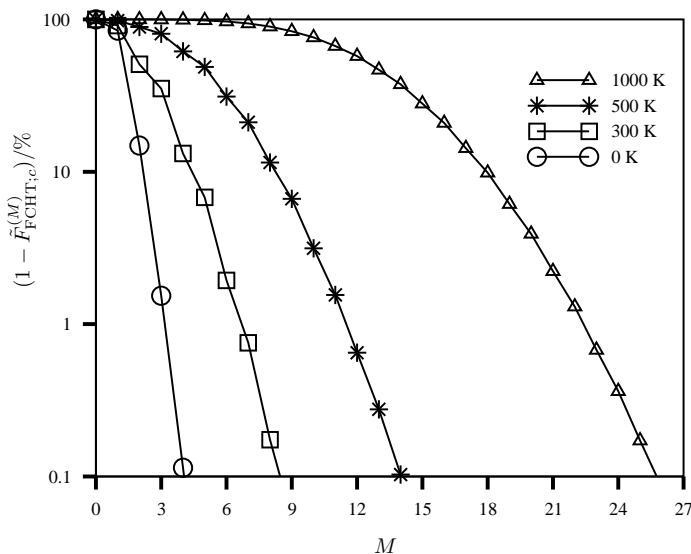
Figure 6.2.: Dependence of the coupling error $\epsilon_c = 1 - \widetilde{F}_{\mathrm{FCHT;c}}^{(M)}$ on the largest number of simultaneously excited modes M for the HT contribution to the $1\,^1A_g \to 1\,^1B_{2u}$ UV absorption spectrum of benzene. The coupling error is shown on a logarithmic scale for temperatures of 0 K, 300 K, 500 K and 1000 K. Lines are drawn only to guide the eye.

however, up to 9, 15 and 26 simultaneously excited modes out of a total 60 modes, composed of 30 initial and 30 final state modes, are necessary to reach a similar threshold for ϵ_c at 300 K, 500 K and 1000 K, respectively. In Fig. 6.2 M is different from M_{max} in Table 6.1, these are identical only when C_1 symmetry is used and $t_m = 10^{-12}$ is employed the calculation. In contrast to the FC coupling error diagrams (Figs. 4.2 and 4.4) of the previous thermal prescreening section, the data points are not smoothly linked to each other (the curves drawn to guide the eye are not smooth) at low temperatures (0 K and 300 K). When we look close at the HT inducing symmetry block e_{2g}, Fig. 6.3, it becomes more clear that the data points are not smoothly linked to each other at all temperatures. The detailed prescreening data are available in appendix C.

6.3.2. (FC)HT profile of benzene for various electronic structure methods

The FCHT GF method is used with various electronic structure calculations to test the recently developed analytic gradient method for electronic TDM exploiting geometric gradients of a generic linear response function by Coriani *et al.* [52]. Hartree-Fock (HF) and density functional theory (DFT) methods are used to compute the gradients of the electronic TDM for the FC-forbidden one-photon absorption process of benzene at zero Kelvin. The quality of the computed first derivatives of the electronic TDM with respect to normal coordinates of the initial state was tested with the TCF development in this chapter and the results were presented in Ref. [52]. The computed one-photon absorption cross sections (in pm^2) with various electronic structure methods are displayed in Fig. 6.4 for HF/TZVP, camB3LYP/TZVP and B3LYP/TZVP. The plotted spectra are generated with the TD ap-
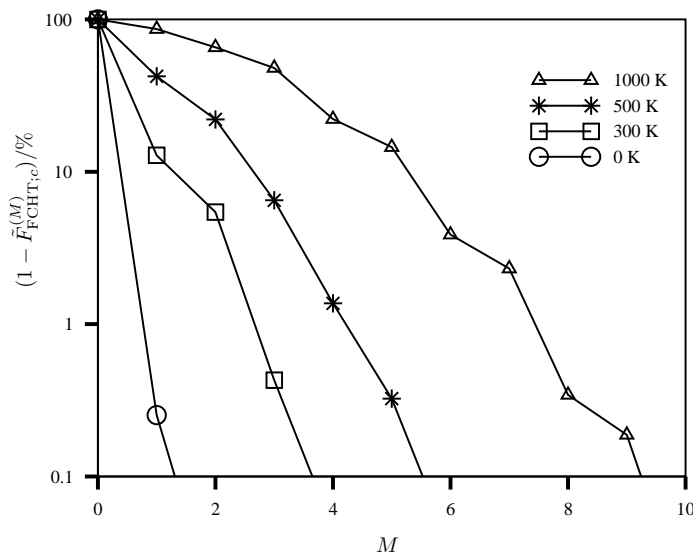
Figure 6.3.: Dependence of the coupling error $\epsilon_{\rm c} = 1 - \widetilde{F}_{\rm FCHT;c}^{(M)}$ on the largest number of simultaneously excited modes M for the HT contribution to the $1\,^1{\rm A}_{\rm g} \rightarrow 1\,^1{\rm B}_{\rm 2u}$ UV absorption spectrum of benzene symmetric block $e_{\rm 2g}$. The coupling error is shown on a logarithmic scale for temperatures of 0 K, 300 K, 500 K and 1000 K. Lines are drawn only to guide the eye.

proach implemented in hotFCHT. In the evaluation of the FT of the Lorentzian weighted TCF (see Eq. (6.36)) the FFTW library (version 3.1.2) is used with a grid size of 2^{15}, a time increment of $\Delta t = 1.0$ fs, and a time interval [-16.384 ps, 16.384 ps]. For the detailed discussion of the quality of the electronic structure methods and peak assignments one is referred to the work of Coriani *et al.* [52][10]. Herein it is just mentioned that the HT development of this thesis has been tested successfully. The analytic gradient method for HT terms is implemented in the linear-scaling development version of the electronic structure program DALTON [195–197] and nonlinear HT terms can be obtained by finite differences of the analytic first derivatives. The joint development in vibronic and electronic structure impacts on theoretical vibronic spectroscopy by pursuing linear and nonlinear HT terms (see Eq. (2.24)).

6.4. Chapter summary and conclusion

The current work is a complementary development to the previous FC prescreening [46,129] and TCF [129] methods including the linear HT and nonlinear HT terms. It has potential to be extended to vibronic couplings and anharmonic oscillators. The present development underlines that the FC/HT contribution and vibrational mode mixing HT contributions are not negligible even though the contributions do not appear in the total sum rules (Eqs. (6.39) and (6.41)). One may argue that the $1\,^1{\rm A}_{\rm g} \rightarrow 1\,^1{\rm B}_{\rm 2u}$ absorption spectrum of benzene is not a good example to verify our FC/HT contribution formalism, as the electronic transition

---

[10]J. Huh has contributed to this work only by computing the HT intensity profile of benzene with the FCHT TCF developed by himself.
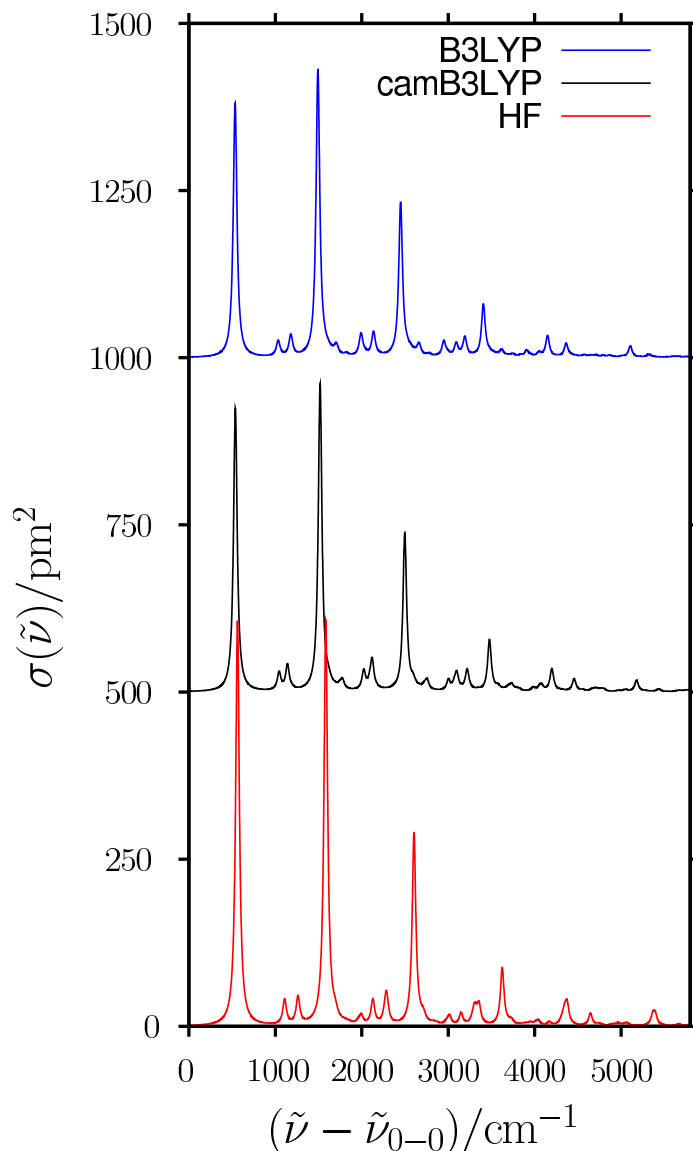
**Figure 6.4.:** Calculated absorption cross-sections $\sigma(\tilde{\nu}) = \frac{4\pi^2}{3}\left(\frac{\alpha_0}{e_0^2}\right)\tilde{\nu}\rho_{\text{FCHTW,L}}(\tilde{\nu})$ in pm^2 at zero Kelvin. The spectra with HF/TZVP, camB3LYP/TZVP and B3LYP/TZVP electronic structure calculations are plotted from bottom to top respectively. The spectra are generated by the time-dependent picture of the HT generating function. The cross section of the B3LYP and camB3LYP hybrid density functionals are shifted by 1000 pm^2 and 500 pm^2 respectively for graphical purpose. A Lorentzian lineshape function FWHM of 50 cm^{-1} is convoluted. $\tilde{\nu}_{0-0} = 38086$cm^{-1} was used to weight the HT spectral density function for the wavenumber-dependent absorption cross section. The figure is reproduced with permission from *J. Chem. Theory Comput.* 6, 1028. Copyright 2010 American Chemical Society."

dipole moment at the equilibrium molecular structure of the ground state ($\underline{\mu}_0$) is zero. But it should be noticed that our HT GF (Eq. (6.18)) is derived from the FC/HT GF (Eq. (6.17)) and the TCF method and TI approach with prescreening strategy agree well. Together with the successful error bound conditions the validity of the formalism has been tested successfully. The vibrational mode interferences in the HT contribution, which do not appear explicitly in the total sum rules that are separable in the vibrational modes (Eqs. (6.39) and (6.41)), play an important role in the prescreening sum rules (Eqs. (6.37) and (6.38)) and the TCF (Eq. (6.36)). Especially in the evaluation of the TCF, if the interplay of the vibrational mode contributions are ignored, the proper spectrum cannot be obtained. We have also tested an artificial case in benzene $\underline{\mu}_0 \neq \underline{0}$ for the total intensity sum rule (see Sec. 6.1.4) to verify our HT GF development. For a detailed discussion of the FC/HT interference term to the absorption band in TI approach, we refer to the recent work of Santoro *et al.* [49] and earlier studies [108, 198, 199]. The method developed for the non-Condon effects will in future be applied to the nonlinear HT and weak FC transition with various electronic structure calculations. For example the experimental fluorescence spectra of jet-cooled benzene [200] shows lines which cannot be explained with the linear HT theory, thus one should go beyond the linear HT expansion of the electronic TDM for this example. The HT GF, herein, is derived explicitly but the non-Condon GF can also be expressed as MHPs with additional dimension for position and momentum operators. Then the HT GF can be exploited for finer-grained integral prescreening and nonlinear (non-Condon) TCFs.

In this chapter, the methods for inclusion of non-Condon effects were explained, discussed and tested for real systems. We extended the FC thermal GF to the non-Condon effects via the CS phase displacement operators, which allows to use a similar mathematical frameworks as the FC prescreening strategy and FC thermal TCF in chapter 4. The link between TI and TD approach has been shown via the TD trace formalism in section 6.1.2. The GF methods developed so far in this thesis (Chs.3-6) are closely related and the non-Condon GF is the most general GF including the FC thermal GFs. This method is further developed for other purposes, anharmonicity, resonance Raman (rR) and SVL transition, in the following chapter.

7. Single vibronic levels

In previous chapters, we have developed generating functions (GFs) for the one-photon absorption (OPA) process. This technique takes the thermal (Chs. 4 and 5) and the non-Condon (Ch. 6) effects into account. By using the GFs, we have devised the Franck-Condon (FC) and non-Condon integral prescreening strategies for the time-independent (TI) approach. Similarly the time-correlation functions (TCFs) are developed for the time-dependent (TD) approach.

So far we have assumed the initial states to be in a Boltzmann-distributed ensemble of vibrational states at finite temperature or a vibrationless state at zero Kelvin for the OPA process. Those kind of initial vibrational states for GFs can be introduced by simple GF parameter assignments[1]. The Boltzmann weighted coherent states (CSs) (Eq. (2.92)) are used in the case of a thermally averaged ensemble of vibrational states. However, for optical processes such as the single vibronic level (SVL) fluorescence (see *e.g.* Refs. [9, 11, 34]) and the resonance Raman (rR) scattering we have to consider specific vibronic levels[2].

In SVL fluorescence, a vibronic level which is not necessarily the vibrational ground state[3] in the excited electronic state is populated by tuning the corresponding laser wavelength [9, 11] (see Fig. 2.1). The vibronic state on the excited electronic potential energy surface (PES) is called the SVL. The spectral density function (SDF) of SVL fluorescence is identical to the OPA one in Eq. (2.1) but with the reversed initial and final electronic states and a given fixed initial vibronic state (SVL), which is not included in the summation over vibronic levels. The fluorescence from a vibrationally excited vibronic state shows often vibrationally well-resolved spectra, unlike the normal absorption or emission spectra at finite temperature [9, 11]. The initial and the final vibronic levels belonging to the ground electronic states for the rR amplitude (2.5) appear in rR scattering process (see Sec. 2.1).

We have already used a mathematical set up in the coarse-grained integral prescreening steps [46] (Chs. 4 and 6) that has a fixed quantum number for one vibrational mode. This was, however, not tailored for generating arbitrary SVLs. Therein we only considered a one-dimensional fixed quantum number space X (see the integral space partitioning section 2.4.2) which corresponds to the SVLs in terms of fixed quantum number of the vibrational mode, *i.e.* the single vibrational mode excitation (*e.g.* $|v, 0, \cdots, 0\rangle$). In other words, we can generate the one-dimensional fixed quantum number space X (Eq. (4.20) and Sec. 6.1.3) in the prescreening steps (see Sec. 4.2.2) but we have not used the space X for the SVL TCF in the TD approach, although by virtue of the developments in reported the previous chapters. For the coarse-grained integral prescreening of the SVL transition, however, we have to consider at least two-dimensional X spaces. Even for the usual absorption and emission processes, if we want to have the fine-grained integral prescreening strategy,

---

[1] *e.g.* $\underline{z} = \underline{0}$ for the vibrationl ground state.

[2] These vibronic levels are not summed-over in the Fermi's golden rule (FGR) expression (see *e.g.* Eq. (2.1) for OPA), *i.e.* those are expressed in the fixed quantum levels during the optical processes.

[3] *e.g.* $|v, 0, \cdots, 0\rangle$

we need to consider multi-dimensional X spaces. When non-Condon effects should be considered, the problem becomes even more difficult. The purpose of this chapter is thus to modify the GFs developed in the previous chapters. The possible modifications could be applicable to the rR, SVL, fine-grained integral prescreening and anharmonic FC transitions with the SVLs either in the TI integral prescreening or TD TCF approaches.

There were efforts (see *e.g.* Refs. [34,65,72,73]) to generate SVLs particularly suited for the rR excitation profile computation. But most of the applications are restricted to the single vibrational mode excited states[4], Condon approximation and limited Duschinsky effects. We develop herein an arbitrary SVL transition GFs with the help of multi-variate Hermite polynomials (MHPs) including the thermal and non-Condon effects. This development is similar to the previous chapter developments in terms of the non-Condon effects (see Chs. 3 and 6). The TCF for the thermally averaged rR intensity including arbitrary order of non-Condon effects is developed in the form of the overlap integral of two rR amplitude GFs in different time domains. The novelty of our GF approach is that it can provide both TI and TD methods, including arbitrary order of non-Condon effects and arbitrary SVLs. We can evaluate TCFs or sum rules for arbitrary SVLs and non-Condon operators with the help of MHPs.

This chapter is organized as follows: In the methodology section 7.1, we develop a GF having fixed quantum number occupation number vector (ONV) spaces (see Sec. 2.4.2 for the integral space partitioning). The analytic form of the GF is derived via the coherent-Fock (cF) state (2.81) which is a mixture of harmonic eigenstates and CSs. The development is formulated for the rR profile GFs in section 7.2, SVL transitions in section 7.3 and anharmonic FC/non-Condon transitions in section 7.4. Those sections contain only methods, but numerical tests have not been made yet. The chapter is concluded in section 7.5.

7.1. Methodology

In the previous chapters 4 and 6 we had at most a one-dimensional fixed quantum number space X for the coarse-grained integral prescreening strategies [46] (see Sec. 2.4.2). One can in principle extend the method in sections 4.2.2 and 6.1.3, which separates the fixed quantum number space X from the Gaussian integral of the GFs, to be applicable also to more than one-dimensional X spaces. But this method is not computationally feasible for multi-dimensional X spaces and non-Condon operators, because the Taylor expansion of multi-dimensional Gaussian function and the subsequent collection of terms in the same orders are not easy. Instead, in this section, we introduce the arbitrary dimensions in X space by exploiting the MHP technique (Ch. 3) to generate the arbitrary SVLs. The GF that we want to have for an arbitrary number of fixed quantum numbers both in the initial and the final vibronic states would be in the following occupation representation[5] with thermally weighted Y space ($K_{YY} = K(\mathbf{\Lambda}_{YY}; \underline{\xi}_Y)$, see Eq. (4.2)), namely

---

[4] *e.g.* $|v, 0 \cdots, 0\rangle$.
[5] *cf.* Eq. (6.1) for empty X space GF.

$$G_{\text{cF}}^{K_{YY}}(\widetilde{\mathbf{Z}}_{\text{cF}}, \mathbf{Z}_{YY}; \mathbf{\Lambda}_{YY}; \underline{\tilde{v}}_{\text{KB}}, \underline{\tilde{v}}_{\text{BK}})^{(\hat{f}, \hat{g})}$$

$$= \mathcal{N}_{YY} |\langle \underline{0}' | \underline{0} \rangle|^{-2} \sum_{\underline{v}_Y, \underline{v}_Y' = \underline{0}}^{\infty} \langle \underline{v}_{\text{B}_X}; \underline{v}_Y | (\hat{g})^* | \underline{v}_{\text{K}_X}'; \underline{v}_Y' \rangle \langle \underline{v}_{\text{B}_X}'; \underline{v}_Y' | \hat{f} | \underline{v}_{\text{K}_X}; \underline{v}_Y \rangle$$

$$\overline{\prod}_{\underline{z}_Y, \underline{z}_Y'}^{2\underline{v}_Y, 2\underline{v}_Y'} e^{-(\underline{v}_Y^{\text{t}} \mathbf{B}_{YY} \underline{\epsilon}_Y + \underline{v}_Y'^{\text{t}} \mathbf{B}_{YY}' \underline{\epsilon}_Y')} \overline{\prod}_{\underline{z}_{\text{K}_X}, \underline{z}_{\text{B}_X}, \underline{z}_{\text{B}_X}', \underline{z}_{\text{K}_X}'}^{\underline{v}_{\text{K}_X}, \underline{v}_{\text{B}_X}, \underline{v}_{\text{B}_X}', \underline{v}_{\text{K}_X}'}, \tag{7.1}$$

where $\underline{v}_{\text{B}_X}$ and $\underline{v}_{\text{K}_X}$ are N_X-dimensional ONVs and $\underline{v}_{\text{B}_X}'$ and $\underline{v}_{\text{K}_X}'$ are N_X'-dimensional ONVs [6]. $\mathcal{N}_{YY} = 1/\text{Tr}(-\underline{\beta}_Y \cdot \hat{\underline{h}}_Y)$ is a normalizing factor corresponding to the thermal integral kernel K_{YY} (see Sec. 4.1). The collective ONVs are additionally defined,

$$\underline{\tilde{v}}_{\text{KB}} = \begin{pmatrix} \underline{v}_{\text{K}_X} \\ \underline{v}_{\text{B}_X} \end{pmatrix}, \quad \underline{\tilde{v}}_{\text{BK}} = \begin{pmatrix} \underline{v}_{\text{B}_X} \\ \underline{v}_{\text{K}_X} \end{pmatrix}, \tag{7.2}$$

and the block-diagonal GF parameter matrix is also defined as

$$\widetilde{\mathbf{Z}}_{\text{cF}} = \text{bldiag}(\mathbf{z}_{\text{K}}, \mathbf{z}_{\text{B}}', \mathbf{z}_{\text{B}}, \mathbf{z}_{\text{K}}'), \tag{7.3}$$

with the block matrices $\mathbf{z}_{\text{K}} = \text{diag}(\underline{z}_{\text{K}})$, $\mathbf{z}_{\text{B}}' = \text{diag}(\underline{z}_{\text{B}}')$, $\mathbf{z}_{\text{B}} = \text{diag}(\underline{z}_{\text{B}})$ and $\mathbf{z}_{\text{K}}' = \text{diag}(\underline{z}_{\text{K}}')$ corresponding to the ONVs $\underline{v}_{\text{K}_X}$, $\underline{v}_{\text{B}_X}'$, $\underline{v}_{\text{B}_X}$ and $\underline{v}_{\text{K}_X}'$, respectively. In the OPA SDF (2.1) we have $\underline{v}_{\text{B}_X} = \underline{v}_{\text{K}_X}$ and $\underline{v}_{\text{B}_X}' = \underline{v}_{\text{K}_X}'$, but for the generality of the development and for the rR GFs we make these vibrational ONVs independent of each other. In section 7.3 the constraints are recovered for the SVL transition to the GF (7.1).

We express the functional form of the GF (7.1) by exploiting the cF state (2.81), which can be generated by taking partial derivatives of the CSs, *i.e.*

$$G_{\text{cF}}^{K_{YY}}(\widetilde{\mathbf{Z}}_{\text{cF}}, \mathbf{Z}_{YY}; \mathbf{\Lambda}_{YY}; \underline{\tilde{v}}_{\text{KB}}, \underline{\tilde{v}}_{\text{BK}})^{(\hat{f}, \hat{g})}$$

$$= \prod_{k=1}^{2N} \left[i \sqrt{\tfrac{\tilde{\epsilon}_k}{2}} \right]^{\tilde{l}_k} \left[\tfrac{1}{i} \sqrt{\tfrac{\hbar^2}{2\tilde{\epsilon}_k}} \right]^{\tilde{m}_k} \left[-i \sqrt{\tfrac{\tilde{\epsilon}_k}{2}} \right]^{\tilde{n}_k} \left[-\tfrac{1}{i} \sqrt{\tfrac{\hbar^2}{2\tilde{\epsilon}_k}} \right]^{\tilde{o}_k}$$

$$\left(\hat{\partial}_{\tilde{\underline{\eta}}_P, \tilde{\underline{\eta}}_Q, \tilde{\underline{\eta}}_P', \tilde{\underline{\eta}}_Q'}^{\tilde{\underline{l}}, \tilde{\underline{m}}, \tilde{\underline{n}}, \tilde{\underline{o}}} \right) \left(\widetilde{\prod}_{\underline{v}_{\text{B}_X}, \underline{v}_{\text{K}_X}}^{-\frac{1}{2}, -\frac{1}{2}} \hat{\partial}_{\underline{\alpha}_{\text{B}_X}^*, \underline{\alpha}_{\text{K}_X}}^{\underline{v}_{\text{B}_X}, \underline{v}_{\text{K}_X}} \right) \left(\widetilde{\prod}_{\underline{v}_{\text{B}_X}', \underline{v}_{\text{K}_X}'}^{-\frac{1}{2}, -\frac{1}{2}} \hat{\partial}_{\underline{\gamma}_{\text{K}_X}', \underline{\gamma}_{\text{B}_X}'^*}^{\underline{v}_{\text{B}_X}', \underline{v}_{\text{K}_X}'} \right)$$

$$\left. G_{\text{cF}}^{K_{YY}}(\widetilde{\mathbf{Z}}_{\text{cF}}, \mathbf{Z}_{YY}; \mathbf{\Lambda}_{YY}; \underline{\tilde{\xi}}_{\text{BK}}, \underline{\tilde{\xi}}_{\text{KB}}; \underline{\eta}, \underline{\eta}') \right|_{\underline{\tilde{\xi}}_{\text{KB}}, \underline{\tilde{\xi}}_{\text{BK}}, \tilde{\underline{\eta}}_{\text{NCF}} = \underline{0}}, \tag{7.4}$$

where [7]

$$\underline{\tilde{\xi}}_{\text{KB}} = \begin{pmatrix} \underline{\alpha}_{\text{K}_X} \\ \underline{\gamma}_{\text{B}_X}^* \end{pmatrix}, \quad \underline{\tilde{\xi}}_{\text{BK}} = \begin{pmatrix} \underline{\alpha}_{\text{B}_X} \\ \underline{\gamma}_{\text{K}_X}^* \end{pmatrix}, \tag{7.5}$$

---

[6] B and K stand for "Bra" and "Ket" respectively, and $\overline{\prod}_{\underline{x}_1, \cdots, \underline{x}_N}^{\underline{n}_1, \cdots, \underline{n}_N} = \left(\prod_k x_{1,k}^{n_{1,k}} \right) \cdots \left(\prod_k x_{N,k}^{n_{N,k}} \right)$.

[7] $\hat{\partial}_{\underline{x}_1, \cdots, \underline{x}_N}^{\underline{n}_1, \cdots, \underline{n}_N} = \left(\frac{\partial^{\sum_k n_{1,k}}}{\prod_k \partial x_{1,k}^{n_{1,k}}} \right) \cdots \left(\frac{\partial^{\sum_k n_{N,k}}}{\prod_k \partial x_{N,k}^{n_{N,k}}} \right)$ and $\widetilde{\prod}_{\underline{x}_1, \cdots, \underline{x}_N}^{\underline{n}_1, \cdots, \underline{n}_N} = \left(\prod_k (x_{1,k}!)^{n_{1,k}} \right) \cdots \left(\prod_k (x_{N,k}!)^{n_{N,k}} \right)$.

and the operators ($\hat{f}$ and $\hat{g}$) are identified as $\hat{f} = \overline{\overline{\prod}}_{\hat{\underline{Q}}',\hat{\underline{P}}',\underline{\hat{P}},\underline{\hat{Q}}}^{\underline{m}',\underline{l}',\underline{l},\underline{m}}$ and $\hat{g} = \overline{\overline{\prod}}_{\hat{\underline{Q}}',\hat{\underline{P}}',\underline{\hat{P}},\underline{\hat{Q}}}^{\underline{o}',\underline{n}',\underline{n},\underline{o}}$. In Eq. (7.4) we have inserted the CS displacement operators ($\hat{D}_{\mathrm{NC}}$, Eq. (3.15)) to produce non-Condon operators with the corresponding partial derivatives. The collective vectors are used additionally $\tilde{\underline{l}}^{\mathrm{t}} = (\underline{l}^{\mathrm{t}}, \underline{l}'^{\mathrm{t}})$, $\tilde{\underline{m}}^{\mathrm{t}} = (\underline{m}^{\mathrm{t}}, \underline{m}'^{\mathrm{t}})$, $\tilde{\underline{n}}^{\mathrm{t}} = (\underline{n}^{\mathrm{t}}, \underline{n}'^{\mathrm{t}})$ and $\tilde{\underline{o}}^{\mathrm{t}} = (\underline{o}^{\mathrm{t}}, \underline{o}'^{\mathrm{t}})$. The integral form of the CS-based GF, $G_{\mathrm{cF}}^{K_{YY}}(\mathbf{Z}_{XX}, \mathbf{Z}_{YY}; \mathbf{\Lambda}_{YY}; \tilde{\underline{\xi}}_{\mathrm{KB}}, \tilde{\underline{\xi}}_{\mathrm{BK}}; \underline{\eta}, \underline{\eta}')$ is, then, given as [8]

$$
G_{\mathrm{cF}}^{K_{YY}}(\widetilde{\mathbf{Z}}_{\mathrm{cF}}, \mathbf{Z}_{XX}, \mathbf{Z}_{YY}; \mathbf{\Lambda}_{YY}; \tilde{\underline{\xi}}_{\mathrm{KB}}, \tilde{\underline{\xi}}_{\mathrm{BK}}; \underline{\eta}, \underline{\eta}')
$$
$$
= \pi^{-(N_Y + N_Y')} |\langle \underline{0}'|\underline{0}\rangle|^{-2} \exp(\tfrac{1}{2}|\tilde{\underline{\xi}}_{\mathrm{KB}}|^2 + \tfrac{1}{2}|\tilde{\underline{\xi}}_{\mathrm{BK}}|^2)
$$
$$
\int \mathrm{d}^2\underline{\alpha}_Y \mathrm{d}^2\underline{\gamma}_Y' K(\mathbf{\Lambda}_{YY}; \underline{\xi}_Y)
$$
$$
\langle \mathbf{z}_{\mathrm{B}}'^{*}\underline{\gamma_{\mathrm{B}}}'_X; \mathbf{z}_{YY}'^{*}\underline{\gamma}_Y'|\hat{D}_{\mathrm{NC}}(\underline{\eta})|\mathbf{z}_{\mathrm{K}}\underline{\alpha_{\mathrm{K}}}_X; \mathbf{z}_{YY}\underline{\alpha}_Y\rangle \langle \mathbf{z}_{\mathrm{K}}'\underline{\gamma_{\mathrm{K}}}'_X; \mathbf{z}_{YY}'\underline{\gamma}_Y'|\hat{D}_{\mathrm{NC}}(\underline{\eta}')|\mathbf{z}_{\mathrm{B}}^{*}\underline{\alpha_{\mathrm{B}}}_X; \mathbf{z}_{YY}^{*}\underline{\alpha}_Y\rangle^{*}.
$$
(7.6)

Then the resulting expression after integration is in a separated form with the FC contribution, the non-Condon part[9] and the SVL and non-Condon contribution, of the vibrational modes belonging to the space Y, Y and X, respectively,

$$
G_{\mathrm{cF}}^{K_{YY}}(\widetilde{\mathbf{Z}}_{\mathrm{cF}}, \mathbf{Z}_{YY}; \mathbf{\Lambda}_{YY}; \tilde{\underline{\xi}}_{\mathrm{KB}}, \tilde{\underline{\xi}}_{\mathrm{BK}}; \underline{\eta}, \underline{\eta}') =
$$
$$
G^{K_{YY}}(\mathbf{Z}_{YY}; \mathbf{\Lambda}_{YY}) \mathcal{J}[\widetilde{\mathbf{W}}_{\mathrm{NCF};YY}(\mathbf{Z}_{YY}; \mathbf{\Lambda}_{YY}), \tilde{\underline{r}}_{\mathrm{NCF};Y}(\mathbf{Z}_{YY}; \mathbf{\Lambda}_{YY}); \tilde{\underline{\eta}}_{\mathrm{NCF};Y}]
$$
$$
\mathcal{J}[\widetilde{\mathbf{Z}}_{\mathrm{cF}}\widetilde{\mathbf{W}}_{\mathrm{cF}}(\mathbf{Z}_{YY}; \mathbf{\Lambda}_{YY})\widetilde{\mathbf{Z}}_{\mathrm{cF}}, \widetilde{\mathbf{Z}}_{\mathrm{cF}}\tilde{\underline{b}}_{\mathrm{cF}}(\mathbf{Z}_{YY}; \mathbf{\Lambda}_{YY}; \underline{\eta}, \underline{\eta}'); \tilde{\underline{\xi}}_{\mathrm{cF}}],
$$
(7.7)

with the collective vectors and matrices,

$$
\tilde{\underline{\xi}}_{\mathrm{cF}} = \begin{pmatrix} \underline{\xi}_{\mathrm{KB}} \\ \underline{\xi}_{\mathrm{BK}}^{*} \end{pmatrix},
$$
(7.8)

$$
\widetilde{\mathbf{W}}_{\mathrm{cF}}(\mathbf{Z}_{YY}; \mathbf{\Lambda}_{YY}) = \frac{1}{2} \begin{pmatrix} (\widetilde{\mathbf{W}}_{T;XX}^{+} + \widetilde{\mathbf{W}}_{T;XX}^{-}) & (\widetilde{\mathbf{W}}_{T;XX}^{+} - \widetilde{\mathbf{W}}_{T;XX}^{-}) \\ (\widetilde{\mathbf{W}}_{T;XX}^{+} - \widetilde{\mathbf{W}}_{T;XX}^{-}) & (\widetilde{\mathbf{W}}_{T;XX}^{+} + \widetilde{\mathbf{W}}_{T;XX}^{-}) \end{pmatrix},
$$
(7.9)

$$
\tilde{\underline{b}}_{\mathrm{cF}}(\mathbf{Z}_{YY}; \mathbf{\Lambda}_{YY}; \underline{\eta}, \underline{\eta}') = \begin{pmatrix} \tilde{\underline{b}}_X^{+} - \mathrm{i}\tilde{\underline{b}}_X^{-} \\ \tilde{\underline{b}}_X^{+} + \mathrm{i}\tilde{\underline{b}}_X^{-} \end{pmatrix},
$$
(7.10)

where the components of $\widetilde{\mathbf{W}}_{\mathrm{cF}}$ and $\tilde{\underline{b}}_{\mathrm{cF}}$ are defined in Eqs. (4.21) and (6.28) respectively.

We can evaluate the cF GF with Eq. (7.4). When we can rearrange Eq. (7.7) to be expressed in terms of MHPs, it will be easy to automatize the calculation. The arrangement is straightforward but lengthy. Herein we present thus only explicitly the FC cF GF, in a simple form, as a special case ignoring the non-Condon operators, *i.e.*

---

[8]*cf.* Eq. (6.3)
[9]$\mathcal{J}[\mathbf{A}, \underline{b}; \underline{x}] = \exp(-\frac{1}{2}\underline{x}^{\mathrm{t}}\mathbf{A}\underline{x} + \underline{b}^{\mathrm{t}}\underline{x})$.

$$\left. G_{\mathrm{cF}}^{K_{YY}}(\widetilde{\mathbf{Z}}_{\mathrm{cF}}, \mathbf{Z}_{YY}; \mathbf{\Lambda}_{YY}; \underline{\tilde{\xi}}_{\mathrm{KB}}, \underline{\tilde{\xi}}_{\mathrm{BK}}; \underline{\eta}, \underline{\eta}') \right|_{\underline{\eta},\underline{\eta}'=\underline{0}} = G_{\mathrm{cF}}^{K_{YY}}(\widetilde{\mathbf{Z}}_{\mathrm{cF}}, \mathbf{Z}_{YY}; \mathbf{\Lambda}_{YY}; \underline{\tilde{\xi}}_{\mathrm{KB}}, \underline{\tilde{\xi}}_{\mathrm{BK}})$$

$$= G^{K_{YY}}(\mathbf{Z}_{YY}; \mathbf{\Lambda}_{YY}) \mathcal{J}[\widetilde{\mathbf{Z}}_{\mathrm{cF}} \widetilde{\mathbf{W}}_{\mathrm{cF}}(\mathbf{Z}_{YY}; \mathbf{\Lambda}_{YY}) \widetilde{\mathbf{Z}}_{\mathrm{cF}}, \widetilde{\mathbf{Z}}_{\mathrm{cF}} \underline{\tilde{r}}_{\mathrm{cF}}(\mathbf{Z}_{YY}; \mathbf{\Lambda}_{YY}); \underline{\tilde{\xi}}_{\mathrm{cF}}], \quad (7.11)$$

where

$$\underline{\tilde{r}}_{\mathrm{cF}}(\mathbf{Z}_{YY}; \mathbf{\Lambda}_{YY}) = \begin{pmatrix} \underline{\tilde{r}}_{T;X}^{+} \\ \underline{\tilde{r}}_{T;X}^{+} \end{pmatrix}, \tag{7.12}$$

and the vector component is defined in Eq. (4.22). Eq. (7.11) can be rearranged to give the FC cF GF in MHPs, *i.e.*

$$G_{\mathrm{cF}}^{K_{YY}}(\widetilde{\mathbf{Z}}_{\mathrm{cF}}, \mathbf{Z}_{YY}; \mathbf{\Lambda}_{YY}; \underline{\tilde{v}}_{\mathrm{KB}}, \underline{\tilde{v}}_{\mathrm{BK}})$$

$$= \left(\widetilde{\prod}_{\underline{v}_{\mathrm{B}_X}, \underline{v}_{\mathrm{K}_X}}^{-\frac{1}{2}, -\frac{1}{2}} \hat{\partial}_{\underline{\alpha}_{\mathrm{B}_X}^{*}, \underline{\alpha}_{\mathrm{K}_X}}^{v_{\mathrm{B}_X}, v_{\mathrm{K}_X}} \right) \left(\widetilde{\prod}_{\underline{v}'_{\mathrm{B}_X}, \underline{v}'_{\mathrm{K}_X}}^{-\frac{1}{2}, -\frac{1}{2}} \hat{\partial}_{\underline{\gamma}_{\mathrm{K}_X}', \underline{\gamma}_{\mathrm{B}_X}'^{*}}^{v'_{\mathrm{B}_X}, v'_{\mathrm{K}_X}} \right)$$

$$G_{\mathrm{cF}}^{K_{YY}}(\widetilde{\mathbf{Z}}_{\mathrm{cF}}, \mathbf{Z}_{YY}; \mathbf{\Lambda}_{YY}; \underline{\tilde{\xi}}_{\mathrm{BK}}, \underline{\tilde{\xi}}_{\mathrm{KB}}) \Big|_{\underline{\tilde{\xi}}_{\mathrm{KB}}, \underline{\tilde{\xi}}_{\mathrm{BK}}=\underline{0}}$$

$$= \left(\widetilde{\prod}_{\underline{v}_{\mathrm{B}_X}, \underline{v}_{\mathrm{K}_X}}^{-\frac{1}{2}, -\frac{1}{2}} \right) \left(\widetilde{\prod}_{\underline{v}'_{\mathrm{B}_X}, \underline{v}'_{\mathrm{K}_X}}^{-\frac{1}{2}, -\frac{1}{2}} \right)$$

$$G^{K_{YY}}(\mathbf{Z}_{YY}; \mathbf{\Lambda}_{YY}) \mathcal{H}_{\underline{\tilde{v}}_{\mathrm{KB}}, \underline{\tilde{v}}_{\mathrm{BK}}}\left(\left(\widetilde{\mathbf{Z}}_{\mathrm{cF}} \widetilde{\mathbf{W}}_{\mathrm{cF}} \widetilde{\mathbf{Z}}_{\mathrm{cF}} \right)^{-1} \underline{\tilde{r}}_{\mathrm{cF}}; \left(\widetilde{\mathbf{Z}}_{\mathrm{cF}} \widetilde{\mathbf{W}}_{\mathrm{cF}} \widetilde{\mathbf{Z}}_{\mathrm{cF}} \right)^{-1} \right), \quad (7.13)$$

which can be evaluated recursively (Eq. (3.5)) or iteratively (Eq. (3.9)). We can introduce an arbitrary number of fixed quantum numbers in the GFs as in Eq. (7.1) exploiting the equations (7.7) and (7.11) for non-Condon and Condon processes respectively in combination with the partial derivatives Eq. (7.4). With the cF GF (7.7) we try to make GFs for the rR (Sec. 7.2), the SVL transition (Sec. 7.3) and the anharmonic OPA transition (Sec. 7.4) in the following sections.

7.2. Application to resonance Raman scattering

We can express the rR amplitude TCF (χ_α) of Eq. (2.18) in harmonic approximation with the cF GF Eq. (7.7). In the TCF for the rR excitation profile we have no fixed quantum numbers in the excited electronic state and all vibrational quantum numbers in the ground electronic state are fixed, *i.e.* $(N_X = N, N_Y = 0)$ and $(N'_X = 0, N'_Y = N)$[10]. We can express the TCF the scalar products of transition dipole moment (TDM) and polarization vectors ($\mu^{\mathrm{S}}(\underline{Q})$ and $\mu^{\mathrm{L}}(\underline{Q})$ in Eq. (2.4)) as like the Herzberg-Teller (HT) linear approximation (Eq. (2.24)), *i.e.*

---

[10]such that X represents ground electronic states and Y represents excited electronic states in this section.

$$\chi_\alpha(\tau; \underline{v}_i, \underline{v}_f) \simeq |\langle \underline{0}'|\underline{0}\rangle|^2 \Big((\mu_0^{\mathrm{S}})^\dagger \mu_0^{\mathrm{L}} G_{\mathrm{cF}}^{K_{YY}} (\widetilde{\mathbf{I}}_{\mathrm{cF}}, \mathbf{z}'(\tau); \mathbf{\Lambda}_{YY}; \underline{\widetilde{v}}_{\mathrm{KB}}, \underline{\widetilde{v}}_{\mathrm{BK}})$$

$$+ \sum_i (\mu_i'^{\mathrm{S}})^\dagger \mu_0^{\mathrm{L}} G_{\mathrm{cF}}^{K_{YY}} (\widetilde{\mathbf{I}}_{\mathrm{cF}}, \mathbf{z}'(\tau); \mathbf{\Lambda}_{YY}; \underline{\widetilde{v}}_{\mathrm{KB}}, \underline{\widetilde{v}}_{\mathrm{BK}})^{(\hat{Q}_i, \hat{1})}$$

$$+ \sum_i (\mu_0^{\mathrm{S}})^\dagger \mu_i'^{\mathrm{L}} G_{\mathrm{cF}}^{K_{YY}} (\widetilde{\mathbf{I}}_{\mathrm{cF}}, \mathbf{z}'(\tau); \mathbf{\Lambda}_{YY}; \underline{\widetilde{v}}_{\mathrm{KB}}, \underline{\widetilde{v}}_{\mathrm{BK}})^{(\hat{1}, \hat{Q}_i)}$$

$$+ \sum_{i,j} (\mu_i'^{\mathrm{S}})^\dagger \mu_j'^{\mathrm{L}} G_{\mathrm{cF}}^{K_{YY}} (\widetilde{\mathbf{I}}_{\mathrm{cF}}, \mathbf{z}'(\tau); \mathbf{\Lambda}_{YY}; \underline{\widetilde{v}}_{\mathrm{KB}}, \underline{\widetilde{v}}_{\mathrm{BK}})^{(\hat{Q}_i, \hat{Q}_j)} \Big),$$

$$(7.14)$$

with proper set up for GF parameters $\mathbf{Z}_{YY}(\tau) = \mathbf{z}'(\tau)$ as in Eq. (4.43) for the TCF of the vibronic absorption profiles in Eq. (4.41) and $\widetilde{\mathbf{I}}_{\mathrm{cF}} = \mathrm{bldiag}(\mathbf{I}_{XX}, \mathbf{I}_{XX})$. There were other GF approaches (see *e.g.* Refs. [72] and [73]) including the Duschinsky effects proposed that are similar to the current developments, but the approaches have limitations for the dimension of X and for including thermal effects in a closed formula within the Condon approximation. The current approach can handle an arbitrary SVLs and non-Condon (linear and nonlinear HT terms in rR scattering cross section) effects. We can obtain a closed form, with the help of the CS formalism, for the rR intensity TCF (2.23) , namely the 3-point-TCF, *i.e.*

$$G_{\mathrm{rR}}^K(\widetilde{\mathbf{Z}}_{\mathrm{cF}}(t), \mathbf{Z}_{YY}(\tau), \mathbf{Z}_{YY}(\tau'); \mathbf{\Lambda}_{YY}, \widetilde{\mathbf{\Lambda}}_{\mathrm{cF}}; \underline{\eta_1}, \underline{\eta_1}', \underline{\eta_2}, \underline{\eta_2}')$$

$$= \pi^{-2N} \int \mathrm{d}^2 \underline{\alpha_{\mathrm{K}}} \mathrm{d}^2 \underline{\alpha_{\mathrm{B}}} K(\widetilde{\mathbf{\Lambda}}_{\mathrm{cF}}; \underline{\tilde{\xi}}_{\mathrm{cF}}) \exp(-|\underline{\tilde{\xi}}_{\mathrm{cF}}|^2)$$

$$G_{\mathrm{cF}}^{K_{YY}}(\widetilde{\mathbf{Z}}_{\mathrm{cF}}(t), \mathbf{Z}_{YY}(\tau); \mathbf{\Lambda}_{YY}; \underline{\tilde{\xi}}_{\mathrm{KB}}, \underline{\tilde{\xi}}_{\mathrm{BK}}; \underline{\eta_1}, \underline{\eta_1}')$$

$$G_{\mathrm{cF}}^{K_{YY}}(\widetilde{\mathbf{Z}}_{\mathrm{cF}}^*(t), \mathbf{Z}_{YY}(\tau'); \mathbf{\Lambda}_{YY}; \underline{\tilde{\xi}}_{\mathrm{KB}}, \underline{\tilde{\xi}}_{\mathrm{BK}}; \underline{\eta_2}, \underline{\eta_2}')^*, \qquad (7.15)$$

which is in the form of an overlap between two rR amplitude GFs , in different time domains (τ and τ'), where the thermal parameter matrix $\widetilde{\mathbf{\Lambda}}_{\mathrm{cF}} = \mathrm{bldiag}(\mathbf{\Lambda}_{XX}, \mathbf{\Lambda}_{XX})^{\frac{1}{2}}$ is used. It is worth to note here that we suggest a closed integral form of the rR cross section in harmonic approximation including Duschinsky and thermal effects in a functional analogy to the Förster-type energy transfer processes (see *e.g.* Ref. [8]) which is in a form of convolution between the absorption and the emission spectra. We can transform the integration into a $2N$-dimensional Gaussian integral ($\mathcal{I}_{2N}$, Eq. (2.122)) which is not like equation (2.121) a product of two separated Gaussian integrals, because the integral variables can not be separated into the real and imaginary parts, and we obtain the Gaussian integral

$$
\begin{aligned}
&G_{\mathrm{rR}}^{K}(\widetilde{\mathbf{Z}}_{\mathrm{cF}}(t), \mathbf{Z}_{YY}(\tau), \mathbf{Z}_{YY}(\tau'); \mathbf{\Lambda}_{YY}, \widetilde{\mathbf{\Lambda}}_{\mathrm{cF}}; \underline{\eta_1}, \underline{\eta_1}', \underline{\eta_2}, \underline{\eta_2}') \\
&= G^{K_{YY}}(\mathbf{Z}_{YY}(\tau); \mathbf{\Lambda}_{YY}) G^{K_{YY}}(\mathbf{Z}_{YY}(\tau'); \mathbf{\Lambda}_{YY})^* \\
&\mathcal{J}[\widetilde{\mathbf{W}}_{\mathrm{NCF};YY}(\mathbf{Z}_{YY}(\tau); \mathbf{\Lambda}_{YY}), \underline{\tilde{r}}_{\mathrm{NCF};Y}(\mathbf{Z}_{YY}(\tau); \mathbf{\Lambda}_{YY}); \underline{\tilde{\eta}_1}_{\mathrm{NCF};Y}] \\
&\mathcal{J}[\widetilde{\mathbf{W}}_{\mathrm{NCF};YY}(\mathbf{Z}_{YY}(\tau'); \mathbf{\Lambda}_{YY}), \underline{\tilde{r}}_{\mathrm{NCF};Y}(\mathbf{Z}_{YY}(\tau'); \mathbf{\Lambda}_{YY}); \underline{\tilde{\eta}_2}_{\mathrm{NCF};Y}]^* \\
&\mathcal{N}_{\mathrm{cF}} \mathcal{I}_{2N}[\mathbf{I} - \widetilde{\mathbf{Z}}_{\mathrm{rR}}(t) \widetilde{\mathbf{W}}_{\mathrm{rR}}(\mathbf{Z}_{YY}(\tau), \mathbf{Z}_{YY}(\tau'); \mathbf{\Lambda}_{YY}, \widetilde{\mathbf{\Lambda}}_{\mathrm{cF}}) \widetilde{\mathbf{Z}}_{\mathrm{rR}}(t) \\
&, \tfrac{1}{2} \widetilde{\mathbf{Z}}_{\mathrm{rR}}(t) \underline{\tilde{b}}_{\mathrm{rR}}(\mathbf{Z}_{YY}(\tau), \mathbf{Z}_{YY}(\tau'); \mathbf{\Lambda}_{YY}, \mathbf{\Lambda}_{\mathrm{cF}})],
\end{aligned}
\tag{7.16}
$$

where the $4N$-dimensional square matrix and vector are defined as

$$
\widetilde{\mathbf{W}}_{\mathrm{rR}}(\mathbf{Z}_{YY}(\tau), \mathbf{Z}_{YY}(\tau'); \mathbf{\Lambda}_{YY}, \widetilde{\mathbf{\Lambda}}_{\mathrm{cF}}) =
$$

$$
\frac{1}{2} \begin{pmatrix} \left(\widetilde{\mathbf{W}}_{\mathrm{cF};T}(\mathbf{Z}_{YY}(\tau); \mathbf{\Lambda}_{YY}) + \widetilde{\mathbf{W}}_{\mathrm{cF};T}(\mathbf{Z}_{YY}(\tau'); \mathbf{\Lambda}_{YY})^*\right) & \mathrm{i}\left(\widetilde{\mathbf{W}}_{\mathrm{cF};T}(\mathbf{Z}_{YY}(\tau); \mathbf{\Lambda}_{YY}) - \widetilde{\mathbf{W}}_{\mathrm{cF};T}(\mathbf{Z}_{YY}(\tau'); \mathbf{\Lambda}_{YY})^*\right) \\ \mathrm{i}\left(\widetilde{\mathbf{W}}_{\mathrm{cF};T}(\mathbf{Z}_{YY}(\tau); \mathbf{\Lambda}_{YY}) - \widetilde{\mathbf{W}}_{\mathrm{cF};T}(\mathbf{Z}_{YY}(\tau'); \mathbf{\Lambda}_{YY})^*\right) & -\left(\widetilde{\mathbf{W}}_{\mathrm{cF};T}(\mathbf{Z}_{YY}(\tau); \mathbf{\Lambda}_{YY}) + \widetilde{\mathbf{W}}_{\mathrm{cF};T}(\mathbf{Z}_{YY}(\tau'); \mathbf{\Lambda}_{YY})^*\right) \end{pmatrix},
\tag{7.17}
$$

$$
\begin{aligned}
&\underline{\tilde{b}}_{\mathrm{rR}}(\mathbf{Z}_{YY}(\tau), \mathbf{Z}_{YY}(\tau'); \mathbf{\Lambda}_{YY}, \widetilde{\mathbf{\Lambda}}_{\mathrm{cF}}; \underline{\eta_1}, \underline{\eta_1}', \underline{\eta_2}, \underline{\eta_2}') \\
&= \begin{pmatrix} \underline{\tilde{b}}_{\mathrm{cF};T}(\mathbf{Z}_{YY}(\tau); \mathbf{\Lambda}_{YY}; \underline{\eta_1}, \underline{\eta_1}') + \underline{\tilde{b}}_{\mathrm{cF};T}(\mathbf{Z}_{YY}(\tau'); \mathbf{\Lambda}_{YY}; \underline{\eta_2}, \underline{\eta_2}')^* \\ \mathrm{i}\left(\underline{\tilde{b}}_{\mathrm{cF};T}(\mathbf{Z}_{YY}(\tau); \mathbf{\Lambda}_{YY}; \underline{\eta_1}, \underline{\eta_1}') - \underline{\tilde{b}}_{\mathrm{cF};T}(\mathbf{Z}_{YY}(\tau'); \mathbf{\Lambda}_{YY}; \underline{\eta_2}, \underline{\eta_2}')^*\right) \end{pmatrix},
\end{aligned}
\tag{7.18}
$$

and

$$
\widetilde{\mathbf{Z}}_{\mathrm{rR}} = \mathrm{bldiag}(\widetilde{\mathbf{Z}}_{\mathrm{cF}}, \widetilde{\mathbf{Z}}_{\mathrm{cF}})^{\frac{1}{2}}.
\tag{7.19}
$$

The thermally weighted quantities used are

$$
\widetilde{\mathbf{W}}_{\mathrm{cF};T} = (\mathbf{I} + \mathbf{\Lambda}_{\mathrm{cF}})^{-\frac{1}{2}} \widetilde{\mathbf{W}}_{\mathrm{cF}} (\mathbf{I} + \mathbf{\Lambda}_{\mathrm{cF}})^{-\frac{1}{2}},
\tag{7.20}
$$

$$
\underline{\tilde{b}}_{\mathrm{cF};T} = (\mathbf{I} + \mathbf{\Lambda}_{\mathrm{cF}})^{-\frac{1}{2}} \underline{\tilde{b}}_{\mathrm{cF}}.
\tag{7.21}
$$

$\mathcal{N}_{\mathrm{cF}} = 1/\mathrm{Tr}(\exp(-\underline{\beta} \cdot \underline{\hat{h}}))$ is a normalizing factor for the thermal integral kernel, with the N-dimensional vibrational Hamiltonian ($\hat{H} = \sum_i^N \hat{h}_i$).

In Condon approximation, the expression (Eq. (7.1)) is simplified as

$$
\begin{aligned}
&G_{\mathrm{rR}}^{K}(\widetilde{\mathbf{Z}}_{\mathrm{cF}}(t), \mathbf{Z}_{YY}(\tau), \mathbf{Z}_{YY}(\tau'); \mathbf{\Lambda}_{YY}, \widetilde{\mathbf{\Lambda}}_{\mathrm{cF}}) \\
&= G^{K_{YY}}(\mathbf{Z}_{YY}(\tau); \mathbf{\Lambda}_{YY}) G^{K_{YY}}(\mathbf{Z}_{YY}(\tau'); \mathbf{\Lambda}_{YY})^* \\
&\mathcal{N}_{\mathrm{cF}} \mathcal{I}_{2N}[\mathbf{I} - \widetilde{\mathbf{Z}}_{\mathrm{rR}}(t) \widetilde{\mathbf{W}}_{\mathrm{rR}}(\mathbf{Z}_{YY}(\tau), \mathbf{Z}_{YY}(\tau'); \mathbf{\Lambda}_{YY}, \widetilde{\mathbf{\Lambda}}_{\mathrm{cF}}) \widetilde{\mathbf{Z}}_{\mathrm{rR}}(t) \\
&, \tfrac{1}{2} \widetilde{\mathbf{Z}}_{\mathrm{rR}}(t) \underline{\tilde{r}}_{\mathrm{rR}}(\mathbf{Z}_{YY}(\tau), \mathbf{Z}_{YY}(\tau'); \mathbf{\Lambda}_{YY}, \mathbf{\Lambda}_{\mathrm{cF}})],
\end{aligned}
\tag{7.22}
$$

where

$$
\begin{aligned}
&\tilde{\underline{b}}_{\mathrm{rR}}(\mathbf{Z}_{YY}(\tau), \mathbf{Z}_{YY}(\tau'); \mathbf{\Lambda}_{YY}, \widetilde{\mathbf{\Lambda}}_{\mathrm{cF}}; \underline{\eta_1}, \underline{\eta_1}', \underline{\eta_2}, \underline{\eta_2}')\Big|_{\underline{\eta_1}, \underline{\eta_1}', \underline{\eta_2}, \underline{\eta_2}'=\underline{0}} \\
&= \tilde{\underline{r}}_{\mathrm{rR}}(\mathbf{Z}_{YY}(\tau), \mathbf{Z}_{YY}(\tau'); \mathbf{\Lambda}_{YY}, \widetilde{\mathbf{\Lambda}}_{\mathrm{cF}}) \\
&= \begin{pmatrix} \tilde{\underline{r}}_{\mathrm{cF};T}(\mathbf{Z}_{YY}(\tau); \mathbf{\Lambda}_{YY}) + \tilde{\underline{r}}_{\mathrm{cF};T}(\mathbf{Z}_{YY}(\tau'); \mathbf{\Lambda}_{YY}) \\ \mathrm{i}\Big(\tilde{\underline{r}}_{\mathrm{cF};T}(\mathbf{Z}_{YY}(\tau); \mathbf{\Lambda}_{YY}) - \tilde{\underline{r}}_{\mathrm{cF};T}(\mathbf{Z}_{YY}(\tau'); \mathbf{\Lambda}_{YY})\Big) \end{pmatrix}.
\end{aligned} \tag{7.23}
$$

$G_{\mathrm{rR}}^{K}(t, \tau, \tau')$[11] is a 3-point-TCF in an analytic closed form for rR intensity including Duschinsky, thermal and non-Condon effects (Albrecht B and C terms [60]). The evaluation is straightforward with the help of MHP technique (Sec. 3) for non-Condon operators. G_{rR}^{K} provides not only the TCFs but also the sum rule for the Raman intensity [69] by setting $\mathbf{Z}_{\mathrm{rR}}(t)$ to the identity matrix which can lead to possible prescreening strategies for the rR intensity profile. In the rR calculation the peaks are identified by computing the individual scattering amplitude from the amplitude TCF in Eq. (7.14). If we know the individual contributions from the sum rule, we can avoid the efforts to compute many scattering amplitudes that have negligible impact on the profile.

The explicit expressions for the rR amplitude and intensity in Condon approximation are given in appendix D where only the vibrational modes in initial state are allowed to be thermally excited at finite temperature.

7.3. Application to single vibronic level transition

It is straightforward to derive the GF of the SVL transition from the cF GF in Eq. (7.4). Herein we introduce constraints $\underline{v}_{\mathrm{B}X} = \underline{v}_{\mathrm{K}X}$ and $\underline{v}_{\mathrm{B}X}' = \underline{v}_{\mathrm{K}X}'$ which will reduce the dimension of the corresponding MHPs to half, *i.e.*

$$
\begin{aligned}
&G_{\mathrm{SVL}}^{K_{YY}}(\mathbf{Z}_{XX}, \mathbf{Z}_{YY}; \mathbf{\Lambda}_{YY}; \underline{\xi}_X; \underline{\eta}, \underline{\eta}') = G^{K_{YY}}(\mathbf{Z}_{YY}; \mathbf{\Lambda}_{YY}) \\
&\mathcal{J}[\widetilde{\mathbf{W}}_{\mathrm{NCF};YY}(\mathbf{Z}_{YY}; \mathbf{\Lambda}_{YY}), \tilde{\underline{r}}_{\mathrm{NCF};Y}; \underline{\tilde{\eta}}_{\mathrm{NCF};Y}] \\
&\mathcal{J}[2\mathbf{Z}_{XX}\widetilde{\mathbf{W}}_{T;XX}^{+}(\mathbf{Z}_{YY}; \mathbf{\Lambda}_{YY})\mathbf{Z}_{XX}, 2\mathbf{Z}_{XX}(\tilde{\underline{b}}_X^{+})^{\mathrm{t}}(\mathbf{Z}_{YY}; \mathbf{\Lambda}_{YY}; \underline{\eta}, \underline{\eta}'); \underline{\xi}_X],
\end{aligned} \tag{7.24}
$$

where we have assumed that the generating variables are real numbers without loosing generality, *i.e.*

$$
\underline{\alpha}_{\mathrm{K}X} = \underline{\alpha}_{\mathrm{B}X}^{*} = \underline{\alpha}_X \in \mathbb{R}, \tag{7.25}
$$

$$
\underline{\gamma}_{\mathrm{B}X}^{'*} = \underline{\gamma}_{\mathrm{K}X}' = \underline{\gamma}_X' \in \mathbb{R}. \tag{7.26}
$$

In the SVL transition the ONV of the initial vibronic state is in the fixed quantum number space X, but also some of the final vibrational modes have fixed quantum numbers for possible prescreening applications, *i.e.* $N_X = N$, $N_Y = 0$, $0 \leq N_X' \leq N$ and $N_Y' = N - N_X'$. In Condon approximation the expression is further simplified as

---

[11]Eqs. (7.16) and (7.22) for non-Condon and Condon approximations respectively.

$$G_{\text{SVL}}^{K_{YY}}(\mathbf{Z}_{XX}, \mathbf{Z}_{YY}; \mathbf{\Lambda}_{YY}; \underline{\xi}_X) = G^{K_{YY}}(\mathbf{Z}_{YY}; \mathbf{\Lambda}_{YY})$$

$$\mathcal{J}[2\mathbf{Z}_{XX}\widetilde{\mathbf{W}}_{T;XX}^+(\mathbf{Z}_{YY}; \mathbf{\Lambda}_{YY})\mathbf{Z}_{XX}, 2\mathbf{Z}_{XX}(\underline{\tilde{r}}_{T;X}^+)^{\text{t}}(\mathbf{Z}_{YY}; \mathbf{\Lambda}_{YY}); \underline{\xi}_X]. \tag{7.27}$$

We can also have a similar MHP expression in Eq. (7.13) for the FC SVL GF

$$G_{\text{SVL}}^{K_{YY}}(\mathbf{Z}_{XX}, \mathbf{Z}_{YY}; \mathbf{\Lambda}_{YY}; \underline{\tilde{v}}_X)$$

$$= \left(\widetilde{\prod}_{\underline{\tilde{v}}_X}^{-\frac{1}{2}}\right) G^{K_{YY}}(\mathbf{Z}_{YY}; \mathbf{\Lambda}_{YY})$$

$$\mathcal{H}_{\underline{\tilde{v}}_X}\left((2\mathbf{Z}_{XX}\widetilde{\mathbf{W}}_{T;XX}^+\mathbf{Z}_{XX})^{-1}\underline{\tilde{r}}_{T;X}^+; (2\mathbf{Z}_{XX}\widetilde{\mathbf{W}}_{T;XX}^+\mathbf{Z}_{XX})^{-1}\right). \tag{7.28}$$

We can obtain the SVL transition TCF from the GF (7.28) with the TD GF parameter $\mathbf{Z}_{YY} = \mathbf{z}'(t)$ in Eq. (4.43). The resulting expression is not given in a closed form, but we can evaluate the TCF with the MHPs caring complex numbers from the TD GF parameters. Additionally we can also apply the SVL transition GF to fine-grained integral prescreening strategies directly with the integral space partitioned expressions (7.24) and (7.27) for multi-dimensional X spaces.

The explicit expression for the SVL transition in Condon approximation is given in appendix D, where only the vibrational modes in initial state are allowed to be thermally excited at finite temperature.

7.4. Application to anharmonic transition

FC or non-FC transition moments computed on the approximated harmonic PESs are not sufficient to describe transitions involving for example torsional motions and large amplitude motions (see *e.g.* Ref. [150]). In this case we need to start from the full rovibrational Hamiltonian such as the Watson [201] or Meyer-Günthard [202] molecular Hamiltonian, which include momentum and position operator coupling terms as well as the anharmonic potential energy terms.

There are many approaches for propagating wavepackets on general potential energy surfaces in time domain to compute vibronic spectra, for instance the Gaussian wavepacket approach [137,203], the multi-configurational time dependent Hartree (MCTDH) method [204, 205] and the coupled CS method [206]. In these approaches, the initial wavepacket evolves on the final PES which provides the time correlation functions. The corresponding Fourier transform (FT) is the vibrational spectrum in frequency domain (see Chs. 4 and 6 for our harmonic developments). However, one of the major demands for computational approaches is the peak assignment and (exact) excitation energy levels, which can not be given directly by the TD approaches.

In TI approaches one has to obtain the vibrational anharmonic eigenfunctions from the molecular Hamiltonian by perturbation methods (see *e.g.* Refs. [36, 123, 207–211]) or by diagonalizing it in a given finite basis set for instance harmonic oscillators and (complex) Gaussians. The anharmonic transition amplitudes can then be calculated by perturbation methods and basis set expansion approaches, respectively.

In all approaches the TI method for FC transitions between anharmonic vibrational states is computationally expensive because of the multitude of overlap integrals to be evaluated. The situation is even worse, if we need to consider the Duschinsky mode mixing effects (Sec. 2.2). There were some approaches proposed (see *e.g.* Refs.(see *e.g.* Refs. [22, 106, 183, 212–214])) to avoid the mode mixing problem by expanding the wavefunctions with a one-center basis set. However, the one-center basis set expansion of the anharmonic vibrational wavefunctions usually requires a larger number of basis functions than the two-reference point expansion approach inducing the Duschinsky rotation between the two basis sets.

The vibrational self-consistent field (VSCF) and vibrational configuration interaction (VCI), which are analogous to the Hartree-Fock and configuration interaction (CI) methods, respectively, in the electronic structure theory, are widely used to describe the anharmonic vibrational wavefunctions with harmonic oscillator eigenfunctions [215–218]. VSCF and VCI wavefunctions, expanded via the harmonic oscillator eigenfunctions, were used to compute the anharmonic Franck-Condon factors (FCFs) of at most three atomic systems [53, 106, 218] . In the work of Huh *et al.* [53] we computed the potodetachment-photoelectron spectra of HS_2^- and DS_2^- to their neutral ground and first excited states by computing the FC profiles based on VCI wavefunctions from the Watson molecular Hamiltonian [201] expanded in terms of displaced Gaussians [219]. In this method we only need to compute many Gaussian overlap integrals (of the type $\langle \underline{0}' | \underline{0} \rangle$, Eq. (2.102)) including the Duschinsky rotations. One trick exploited was to prescreen the overlap integrals according to the displacements of the two displaced Gaussians, and then to store all important Gaussian overlap integrals at least for the three atomic systems to speed up the calculations. Luis and coworkers [220–223] have set up linear equations, for anharmonic FC integrals and matrix elements of the potential energy difference operator, which lower the computational cost by introducing the Duschinsky relation in the potential energy operator not in the wavefunctions but they considered only a simple diagonal kinetic energy operator.

Lucas [148] proposed a method for evaluation of FCFs in nonlinear Duschinsky relation (Sec. 2.2). Nonlinear Duschinsky effects were treated perturbatively by Lucas for the (momentum-position coupled) non-Condon operators. We can easily handle this perturbation approach with the non-Condon integral evaluation scheme developed in section 3.2.

Luckhaus [150] developed an approach which treats reaction path problems with large curvature. Therein the author solved the vibrational eigenfunction problem for a two-dimensional model system by diagonalizing the Hamiltonian in non-orthogonal harmonic oscillator basis sets along the grid points on the reaction path. In this approach one has to compute the non-Condon integrals for matrix elements of the Hamiltonian as well as the FC integrals for the overlap integrals for the non-orthogonal harmonic basis set in the Duschinsky relation (Ch. 3). If the reaction path and non-orthogonal basis set approach should be extended to larger systems, the developments of this thesis will be highly beneficial for this method.

The simplest approach would be to introduce the anharmonicity in the potential energy surfaces only for a few vibrational modes neglecting the kinetic energy rovibrational part. Even for the simplest model Hamiltonians it is a computationally difficult task to compute the FCFs including the mode mixing effects due to the extremely large number of integrals to be evaluated. We present herein the simple anharmonic-harmonic block approach to treat systems that have many harmonic degrees of freedom (DOF) but a small number

of anharmonic DOF which are still much more computationally expensive than the harmonic transitions. We further assume that the anharmonic and harmonic DOF are separable but the normal coordinates of two electronic states are related by the Duschinsky equation (Sec. 2.2). The anharmonic partition of the vibrational wavefunctions are expanded by a finite number of the harmonic oscillator eigenstates as a basis set and the harmonic basis sets of two electronic states are related in the Duschinsky relation. The important contribution of our development in this section is that it can provide the possible prescreening strategies and TCFs with the the non-Condon effects for anharmonic transitions. The GF developed in this section is in the form of linear combination of the cF GFs in section 7.1.

The anharmonic DOF is denoted as X and the harmonic ones as Y like in the partitioning scheme in chapter 2 for the fixed and the active vibrational spaces, respectively. The n-th vibrationally excited anharmonic wavefunction of the initial electronic state, with the associated harmonic eigenstate $|\underline{v}_Y\rangle$, $|\Psi_{n;\underline{v}_Y}\rangle$ is defined as,

$$
\begin{aligned}
|\Psi_{n;\underline{v}_Y}\rangle &= \sum_{\{\underline{v}_{K_X}\}} c_{\underline{v}_{K_X};n} |\underline{v}_{K_X}\rangle \otimes |\underline{v}_Y\rangle \\
&= \sum_{\{\underline{v}_{K_X}\}} c_{\underline{v}_{K_X};n} |\underline{v}_{K_X}; \underline{v}_Y\rangle,
\end{aligned}
\tag{7.29}
$$

where the finite number of N_X^A anharmonic expansion coefficients for finite basis set ($\{\underline{v}_{K_X}\}$) satisfy the normalization condition,

$$
\sum_{\{\underline{v}_{K_X}\}} |c_{\underline{v}_{K_X};n}|^2 = 1,
\tag{7.30}
$$

and the final state is expressed in the same manner,

$$
|\Psi'_{m;\underline{v}'_Y}\rangle = \sum_{\{\underline{v}'_{K_X}\}} c'_{\underline{v}'_{K_X};m} |\underline{v}'_{K_X}; \underline{v}'_Y\rangle,
\tag{7.31}
$$

$$
\sum_{\{\underline{v}'_{K_X}\}} |c'_{\underline{v}'_{K_X};m}|^2 = 1.
\tag{7.32}
$$

The FCFs of the vibronic transition from the n-th vibrationally excited wavefunction is summed to unity in any complete basis set expansion but it should be close to unity in a proper finite basis set expansion, *i.e.*

$$
\begin{aligned}
1 &= \langle \Psi_{n;\underline{v}_Y} | \Psi_{n;\underline{v}_Y}\rangle \\
&\simeq \sum_{\{\underline{v}_{K_X}\},\{\underline{v}_{B_X}\},\{\underline{v}'_{K_X}\},\{\underline{v}'_{B_X}\}} \sum_{m=0}^{(N_X^A)'-1} c'_{\underline{v}'_{K_X};m} c'^{*}_{\underline{v}'_{B_X};m} c^{*}_{\underline{v}_{B_X};n} c_{\underline{v}_{K_X};n} \\
&\quad \times \sum_{\underline{v}'_Y=\underline{0}}^{\infty} \langle \underline{v}_{B_X}; \underline{v}_Y | \underline{v}'_{K_X}; \underline{v}'_Y\rangle \langle \underline{v}'_{B_X}; \underline{v}'_Y | \underline{v}_{K_X}; \underline{v}_Y\rangle,
\end{aligned}
\tag{7.33}
$$

where $(N_X^A)'$ is the finite number of final vibronic levels, which equals the number of har-

monic basis functions.

From Eq. (7.33) and (7.1) we have the anharmonic transition GF G_A which contains the anharmonic transition information associated with the GF parameters,

$$
\begin{aligned}
&G_A(\widetilde{\mathbf{Z}}_{\mathrm{cF}}, \mathbf{Z}_{YY}; \underline{c_n}, \underline{c_m}'; \widetilde{\underline{\xi}}_{\mathrm{KB}}, \widetilde{\underline{\xi}}_{\mathrm{BK}}; \underline{\eta}, \underline{\eta}') \\
&= \sum_{\{\underline{v}_{\mathrm{K}_X}\}, \{\underline{v}_{\mathrm{B}_X}\}, \{\underline{v}_{\mathrm{K}_X'}\}, \{\underline{v}_{\mathrm{B}_X'}\}} c'_{\underline{v}_{\mathrm{K}_X'};m} c'^{*}_{\underline{v}_{\mathrm{B}_X'};m} c^{*}_{\underline{v}_{\mathrm{B}_X};n} c_{\underline{v}_{\mathrm{K}_X};n} G^{K_{YY}}_{\mathrm{cF}}(\widetilde{\mathbf{Z}}_{\mathrm{cF}}, \mathbf{Z}_{YY}; \mathbf{0}_{YY}; \widetilde{\underline{\xi}}_{\mathrm{KB}}, \widetilde{\underline{\xi}}_{\mathrm{BK}}; \underline{\eta}, \underline{\eta}'),
\end{aligned}
$$

$$(7.34)$$

where the cF GF in Eq. (7.7) is used for the possible non-Condon transition. The anharmonic transition GF is evaluated to have specific SVLs and non-Condon operators with Eq. (7.4), *i.e.*

$$
\begin{aligned}
&G_A(\widetilde{\mathbf{Z}}_{\mathrm{cF}}, \mathbf{Z}_{YY}; \underline{c_n}, \underline{c_m}'; \widetilde{\underline{v}}_{\mathrm{KB}}, \widetilde{\underline{v}}_{\mathrm{BK}})^{(\hat{f}, \hat{g})} \\
&= \sum_{\{\underline{v}_{\mathrm{K}_X}\}, \{\underline{v}_{\mathrm{B}_X}\}, \{\underline{v}_{\mathrm{K}_X'}\}, \{\underline{v}_{\mathrm{B}_X'}\}} c'_{\underline{v}_{\mathrm{K}_X'};m} c'^{*}_{\underline{v}_{\mathrm{B}_X'};m} c^{*}_{\underline{v}_{\mathrm{B}_X};n} c_{\underline{v}_{\mathrm{K}_X};n} \\
&\left(\widetilde{\prod_{\underline{v}_{\mathrm{B}_X}, \underline{v}_{\mathrm{K}_X}}}^{-\frac{1}{2}, -\frac{1}{2}} \hat{\partial}^{\underline{v}_{\mathrm{B}_X}, \underline{v}_{\mathrm{K}_X}}_{\underline{\alpha}_{\mathrm{B}_X}^{*}, \underline{\alpha}_{\mathrm{K}_X}} \right) \left(\widetilde{\prod_{\underline{v}_{\mathrm{B}_X'}, \underline{v}_{\mathrm{K}_X'}}}^{-\frac{1}{2}, -\frac{1}{2}} \hat{\partial}^{\underline{v}_{\mathrm{B}_X'}, \underline{v}_{\mathrm{K}_X'}}_{\underline{\gamma}_{\mathrm{K}_X'}', \underline{\gamma}_{\mathrm{B}_X'}'^{*}} \right) \\
&\prod_{k=1}^{2N} \left[\mathrm{i}\sqrt{\frac{\tilde{\epsilon}_k}{2}} \right]^{\tilde{l}_k} \left[\frac{1}{\mathrm{i}} \sqrt{\frac{\hbar^2}{2\tilde{\epsilon}_k}} \right]^{\tilde{m}_k} \left[-\mathrm{i}\sqrt{\frac{\tilde{\epsilon}_k}{2}} \right]^{\tilde{n}_k} \left[-\frac{1}{\mathrm{i}} \sqrt{\frac{\hbar^2}{2\tilde{\epsilon}_k}} \right]^{\tilde{o}_k} \left(\hat{\partial}^{\tilde{l}, \tilde{m}, \tilde{n}, \tilde{o}}_{\tilde{\eta}_P, \tilde{\eta}_Q, \tilde{\eta}_P', \tilde{\eta}_Q'} \right) \\
&G^{K_{YY}}_{\mathrm{cF}}(\widetilde{\mathbf{Z}}_{\mathrm{cF}}, \mathbf{Z}_{YY}; \mathbf{0}_{YY}; \widetilde{\underline{\xi}}_{\mathrm{BK}}, \widetilde{\underline{\xi}}_{\mathrm{KB}}; \underline{\eta}, \underline{\eta}') \Big|_{\widetilde{\underline{\xi}}_{\mathrm{KB}}, \widetilde{\underline{\xi}}_{\mathrm{BK}}, \tilde{\eta}_{\mathrm{NCF}}=\underline{0}}.
\end{aligned}
$$

$$(7.35)$$

We can devise prescreening strategies for an anharmonic transition from n-th vibrationally excited initial state to the m-th vibrationally excited final state with the GF including non-Condon effects. The TCF can also be evaluated by the GF with the TD GF parameters $\mathbf{Z}_{YY}(t)$ in Eqs. (4.42) and (4.43). In this development we assume the transition from a single vibronic initial state to manifold final vibronic states but it can easily be generalized for the thermally averaged initial vibronic states.

The explicit expression for the anharmonic transition in Condon approximation is given in appendix D where only the vibrational modes in initial state are allowed to be thermally excited at finite temperature.

7.5. Chapter summary and conclusion

In this chapter we have developed GFs for the rR scattering and intensity profile (Sec. 7.2), the SVL transition (Sec. 7.3) and the anharmonic FC/non-Condon transition (Sec. 7.4). Those GFs are built upon the cF GF, see section 7.1. These can introduce arbitrary SVLs via the corresponding partial derivatives.

The rR developments in section 7.2 differ from other works [17, 56, 61, 64, 66, 67, 72, 73, 75, 109]. The difference appears in the TCFs from the GFs. We can introduce non-Condon and thermal effects to our CS GF approach within the Duschinsky linear transform approximation. We emphasize herein that we can relatively easily include the non-Condon

effects and the arbitrary SVLs at the same time by the MHP technique. We have derived the analytic expression for the 3-point TCF for the rR intensity profile within the Duschinsky approximation including the non-Condon and thermal effects.

The SVL transition GF is shown to be only a special case of the cF GF in section 7.1. It has constraints on identical vibrational ONVs in the ket and bra vibronic states. As a result, the SVL transition GF is simplified to a reduced dimensional form. From this development, we can obtain the SVL transition TCF, the integral prescreening strategy for the SVL transition, and the fine-grained FC/non-Condon prescreening strategies of multi-dimensional fixed quantum number space X.

As a last development, section 7.4 of this chapter, we have applied the cF GF of section 7.1 to one anharmonic transition problem that can be approximated with a few anharmonic DOF, whereas the remaining DOF are treated harmonically. With the developments we can construct the FC/non-Condon TCFs and integral prescreening conditions from the anharmonic GF. We have made the GF with a separation ansatz of anharmonic and harmonic DOF, and the benefit of the GF decreases as the number of anharmonic DOF grows.

We have exploited the MHP technique in chapter 3 to modify the FCF GF (Ch. 4) and the non-Condon GF (Ch. 6) for SVLs. From the development of this chapter, we can now have GFs including thermal effects, arbitrary non-Condon effects and arbitrary SVLs in the Duschinsky oscillator basis. As special applications to the cF GF, SVL transition, rR scattering and anharmonic transitions are introduced. But the GF approach can possibly contribute to the vibronic coupling, multi-photon transition, general anharmonic problems which could have intrinsic harmonic structures. The application is shown to be not only restricted to molecular transitions but it could be any quantum mechanical process involving harmonic oscillators.

8. Conclusion and outlook

One of the fundamental goals of molecular science is to obtain a perfect control of molecular processes with optical techniques and molecular design abilities. For this purpose a detailed understanding on the dynamics of vibrational and electronic (vibronic) degrees of freedom (DOF) is necessary, because the interplay of vibronic DOF plays a major role in many molecular processes, which could be either radiative (*e.g.* one-photon absorption (OPA), one-photon emission (OPE) and resonance Raman (rR) scattering) or non-radiative (*e.g.* electron transfer (ET), internal conversion (IC), inter-system crossing (ISC) and conduction of molecular junction), see figure 1.1.

Usually, polyatomic systems of interest are relatively large (more than 100 atoms, especially biomolecules) such that the corresponding description and analysis of the dynamics are challenging. Molecular spectra, which contain information about the molecular processes, are typically highly congested, such that the dynamics of the individual vibrational DOF can not directly be disentangled. We need theoretical analysis tools for the complex molecular system to study the individual mode contributions to the molecular processes . Computational difficulties arise for complex systems in evaluating a tremendously large number of multi-dimensional Franck-Condon (FC) integrals. The density of states (DOS) or the number of FC integrals at a transition energy grows steeply with increasing number of vibrational DOF, vibrational excitation energy and temperature [112].

Even in a harmonic approximation for the Born-Oppenheimer (BO) potential energy surface (PES) the computation of FC integrals is still a challenging problem especially for large molecular systems, due to the inseparable multi-dimensional integrals originated by the Duschinsky mode mixing effects (Ref. [107] and Sec. 2.2). There have been attempts (see *e.g.* Refs. [115–121] for the most recent works) to improve the computational efficiency of the FC integral evaluation schemes including the Duschinsky mode mixing effects. Fast evaluation of the FC integrals is essential for tackling large systems. We have suggested an iterative FC integral evaluation scheme exploiting the Magnus expansion for multi-variate Hermite polynomials (MHPs) [176] in chapter 3. The integral evaluation scheme in terms of the MHPs with the Magnus expansion can be expressed as summations of one-dimensional Hermite polynomials, which appears in a simpler form (smaller number of summations) than the existing summation scheme for the multiple products of one-dimensional Hermite polynomials (see *e.g.* Refs. [120, 121]).

It was pointed out, however, that only a small portion of the Franck-Condon factors (FCFs) contributes to the total FC profiles significantly (see *e.g.* Refs. [44–46]). The idea can be used in an *ad hoc* way by limiting for instance the vibrational excitation in each mode by some predefined numbers. For example, one could arbitrarily restrict the number of FC integrals to be evaluated by allowing only up to 10 vibrationally excited quanta for every vibrational DOF. In this example we need to compute 11^{2N} FC integrals for the N-dimensional harmonic oscillator system. Unfortunately, in this brute-force way the computational complexity still increases drastically and becomes infeasible. Instead, if we
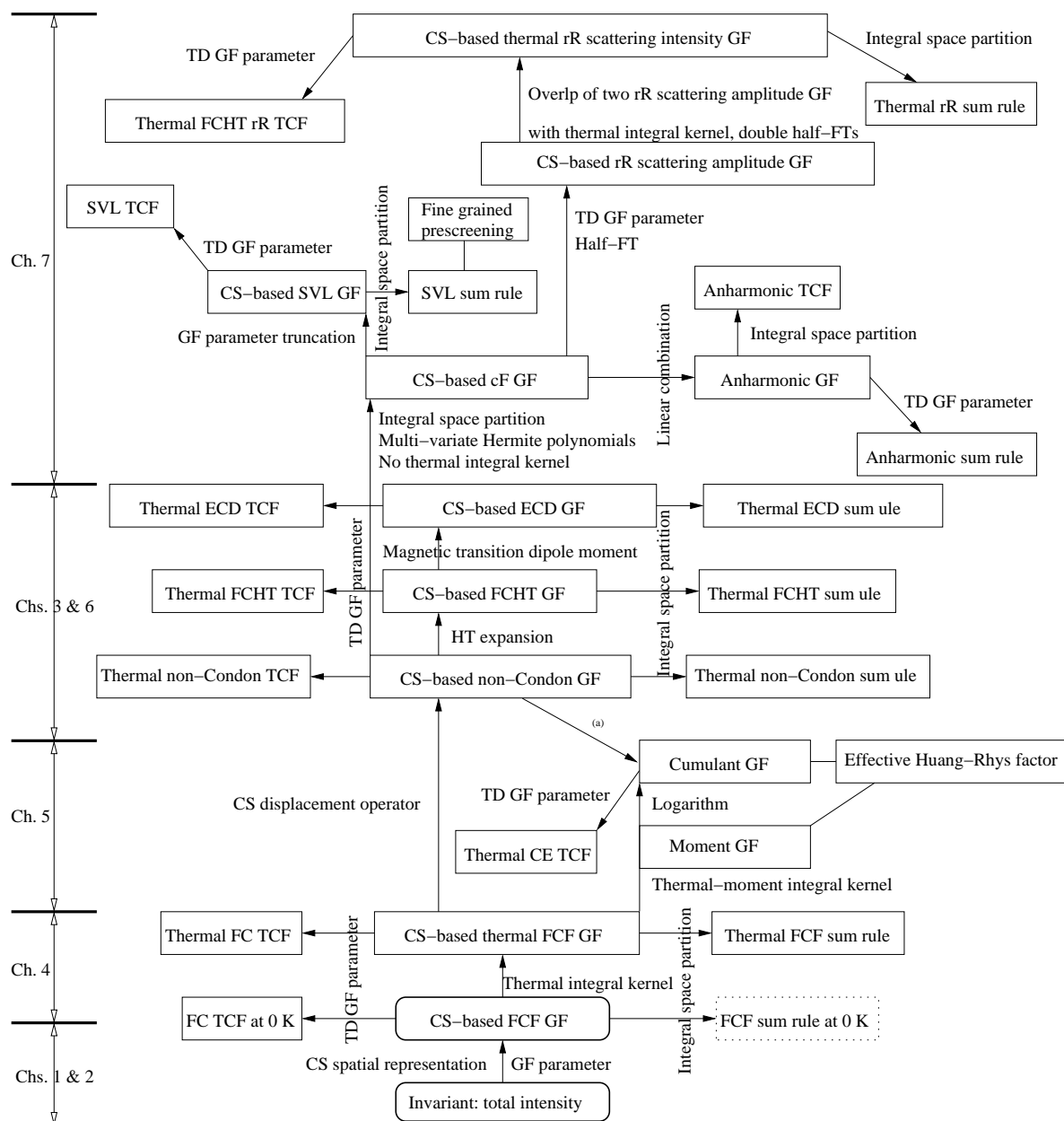
Figure 8.1.: Summary of the CS-based GF developments for various molecular vibronic transitions. The round boxes refer to the fundamental quantities. The dotted box represents the work not in a part of this thesis. The solid square boxes indicate the developments within the thesis. The arrows indicate the functional transformations. The properties of the GF are shown in a box that are inherited from the previous (lower) boxes, otherwise details are mentioned on the arrows. The single solid lines without arrows imply only one of many usages for the corresponding functions to mention their importance. The corresponding chapters for the developments are indicated on the left side of the diagram. (a) It is straightforward to obtain the mean value including the non-Condon effects but for the higher order statistical quantities a numerical algorithm has to be developed.

can construct the most important FC intensity profiles, say 99 % of the total FC intensity, with a small fraction of FCFs of the total FCF, the computation of FC intensity profiles becomes feasible even for complex systems. For this purpose we must address the issue of knowing which sets of FCFs contribute to the total FC intensity for about 99 % without having all FCFs at hand. Jankowiak *et al.* [46] exploited this simple idea by modifying the Doktorov and coworkers' initial idea of CS-based GF [29]. Exploiting the modified GF Jankowiak *et al.* developed a coarse-grained integral prescreening strategy for the FC intensity profiles at zero Kelvin. The starting point of this thesis was precisely this zero Kelvin time-independent (TI) FC development. Throughout the thesis, we have extended and modified the method to include temperature and non-Condon effects which are important in molecular transition processes (see diagram 8.1). In diagram 8.1 we summarize the developments in this thesis and show the relations between the developments described herein. Based on the fundamental developments (the round boxes at the bottom of the diagram) the GF approaches have been extended (following the arrows in the diagram) to account for thermal effects, non-Condon effects and single vibronic level (SVL) transitions.

The theoretical description of most of the molecular vibronic transitions[1] involving the Duschinsky rotated harmonic oscillators boils down to a common mathematical problem, *i.e.* the MHPs evaluation (see diagram 8.2 and Ch. 3). The calculation of the MHPs appears as a computationally hard problem (Ch. 3). Nevertheless, translation of the molecular transition problem in harmonic approximation to an equivalent MHP evaluation problem enables us to analyze various transition processes by the same mathematical tool. An analogous transformation for the Ermakov invariant for dissipative systems (see *e.g.* Refs. [224–229]) can be given as an example for a similar reduction to a simpler computational problem. The various equations of motion, *e.g.* the Langevin and the Fokker-Planck equations, for dissipative systems which are in different forms converge to the invariant quantity at the end.

In the following paragraph we summarize the developments in this thesis according to the diagram 8.1 sequencing from bottom to top. The GF approaches are described briefly in the quantum mechanical trace formalism. Then the conclusion and outlook of this dissertation follows.

Summary of developments   An invariant quantity for a quantum mechanical problem is a powerful tool to understand the system (see *e.g.* Refs. [24–29, 224]). The invariance constraints the system dynamics. We can extract useful data about the quantum mechanical processes from the invariant functional, *i.e.* herein the GF which is characterized by its GF parameters (see Ref. [46] and Sec. 2.4), with proper modifications or mathematical manipulations to the functional (see the bottom of Fig. 8.1). The GF appears to be an analogous tool like the partition function ($\mathrm{Tr}(\exp(-\beta \hat{H}))$), which is invariant and from which we can obtain thermodynamic quantities. Analogously the GF can provide the quantity of interest by (proper) operations on itself, *e.g.* partial derivatives with respect to the GF parameters for intensity sum rules (see Chs. 4 and 6).

To illustrate the invariant GF idea, we consider the FC transition probabilities from an

---

[1]FC and non-Condon integral evaluation, integral prescreening strategy, rR excitation profile, SVL transition and non-Condon transition, time-correlation function (TCF) evaluation
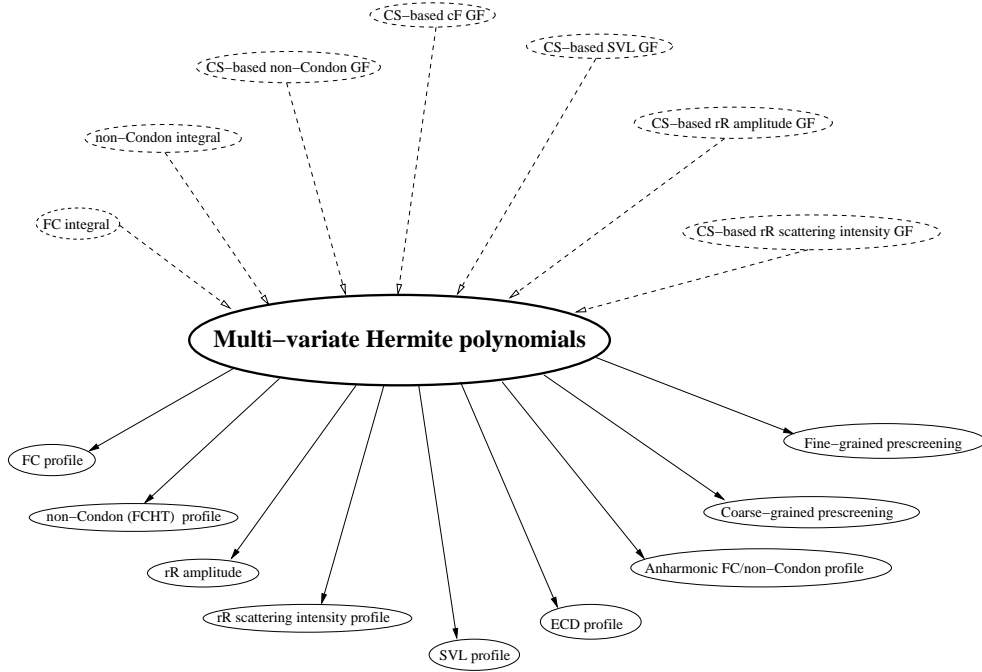
Figure 8.2.: Most of the working equations in this thesis are translated into the MHP evaluation problem. The functions in dashed-ellipse are cast into MHPs and the corresponding output can be obtained after the MHP evaluation.

initial state to a manifold of other states that have to be summed to unity, *i.e.*

$$\text{Tr}(\hat{\rho}) = 1, \tag{8.1}$$

where the density operator $\hat{\rho}$ can be defined for instance via thermally averaged initial vibronic states ($\hat{\rho} = \sum_{\underline{v}} p_{\underline{v}}(T)|\underline{v}\rangle\langle\underline{v}|$), where the $p_{\underline{v}}(T)$ is a thermal distribution of initial vibronic state ($|\underline{v}\rangle$) at a finite temperature (T). This simple sum rule (8.1) can be traced by an arbitrary complete basis set resulting in an infinite summation of FCFs, which converges to unity (*e.g.* for the final vibronic states $|\underline{v}'\rangle$, $\sum_{\underline{v}} p_{\underline{v}}(T)|\langle\underline{v}'|\underline{v}\rangle|^2 = 1$). The FCF sum rule equation itself, however, is not powerful enough, because it tells us only, if the total intensity is conserved with respect to any complete basis set expansion. We invoke, instead, the Dirac δ-distribution operators to resolve the FCFs by vibronic transition energies,

$$\int_{-\infty}^{\infty} \text{d}\omega \text{Tr}\Big(\delta(\omega_1 - \hat{H}'/\hbar)\delta(\omega_2 - \hat{H}/\hbar)\hat{\rho}\Big) = 1, \tag{8.2}$$

where $\omega = \omega_1 - \omega_2$ is the vibronic transition frequency, and $\hat{H}$ and $\hat{H}'$ are the vibrational Hamiltonians of the initial and final states respectively (Sec. 2.2). The integrand in Eq. (8.2), the quantum mechanical trace, is simply the FC spectral density function (SDF) with Dirac δ-distribution at finite temperature, *i.e.* $\varrho_{\text{FCW}}(\omega) = \text{Tr}(\delta(\omega_1 - \hat{H}'/\hbar)\delta(\omega_2 - \hat{H}/\hbar)\hat{\rho})$, which is transition frequency (ω)-resolved (Sec. 2.1). By introducing CSs both for initial and final

vibrational states and replacing the δ-distribution operator with the GF parameters[2], we can make the CS-based FCF GF (Sec. 6.1.2). Exploiting the resulting GFs Jankowiak *et al.* [46] developed the FC integral prescreening strategy at zero Kelvin and herein we have developed the thermal FC integral prescreening method (Ch. 4) for TI FC profile calculations.

We have introduced the thermal effects to the CS-based GF via the thermal integral kernel (Sec. 4.1). The important feature of this thermal development is that the individual vibrational DOF can have different finite temperatures so that we can control the vibrational excitation pattern with the individual temperatures, not only via the GF parameters (Eq. (4.4)). At finite temperature the initial vibrational state can be considered as the thermally averaged effective single vibrational initial state in the GF. As a result the thermal prescreening strategies (Sec. 4.3) can inherit the prescreening strategies at zero Kelvin [46]. This CS-based thermal FCF GF generalizes the corresponding zero Kelvin development to the development at finite temperature.

Recalling where the GF parameters are coming from[3], it is clear that we can transform the same FCF GF into a TCF and the FCF sum rule according to the GF parameter values (Ch. 4). In chapter 4, we develop the time-dependent (TD) approach (TCF) from the TI perspective. The TCF method is adopted typically for its simplicity and fast evaluation besides the disadvantage of no immediate peak assignment ability (see *e.g.* Refs. [17, 33, 34, 37, 38, 40, 40–42, 48, 55, 56, 61, 64, 66, 67, 72, 73, 75, 79, 81, 84, 86, 87, 93–95, 109, 137, 138]). Up to now (before this thesis) the TD and TI approaches for absorption or emission profile calculations were (practically) considered as independent approaches [18], even if the formalisms are mutually transformable (Sec. 2.1). The TD approach exploits the Fourier transformed representation of the δ-distribution ($\delta(\omega - \overline{\omega}) = \int_{-\infty}^{\infty} \mathrm{d}t\, \mathrm{e}^{\mathrm{i}(\omega - \overline{\omega})t}$) in Eq. (8.2), *i.e.*

$$\varrho_{\mathrm{FCW}}(\omega) = \hbar^{-1} \int_{-\infty}^{\infty} \mathrm{d}t \mathrm{Tr}\Big(\exp(-\mathrm{i}\hat{H}'t/\hbar) \exp(\mathrm{i}\hat{H}t/\hbar)\hat{\rho} \Big) \mathrm{e}^{\mathrm{i}(\omega - \omega_0)t}. \qquad (8.3)$$

By assigning the TD phase parameter values (Eqs. (4.42) and (4.43)) to the GF parameters we can obtain the TCF (corresponding to $\mathrm{Tr}(\exp(-\mathrm{i}\hat{H}'t/\hbar) \exp(\mathrm{i}\hat{H}t/\hbar)\hat{\rho})$ in Eq. (8.3)) simply from the CS-based FCF GF. Then the corresponding Fourier transform (FT) is the FC profile (Sec. 4.4). We emphasize herein that we can use the same GF for the (TI) integral prescreening and (TD) TCF approaches. The validity of the TI and the TD approaches has been confirmed by their mutual agreement (Sec. 4.5). We can judge the quality of the prescreening level from the comparison between the two approaches (Secs. 4.5 and 6.3). It is interesting to note that the TCF value at $t = 0$ is simply the sum rule functional value. When the time evolves ($t \neq 0$) the complex TCF values carry the vibrational transition information of the system. One last thing to be mentioned for the current TCF approach is that we can try to assign the peaks indirectly (even in the TD method) by freezing some vibrational DOF in the TCF evaluation via controlling the GF parameters. This feature is possible because we have made a link between the TI and the TD approaches with the identical GF (Sec. 4.4) via the GF parameters.

In the evaluation of TCFs (see *e.g.* Sec. 4.4) for fast Fourier transform (FFT), a good

---

[2]because we know all eigenfunctions and eigenvalues of the harmonic systems, the δ-distribution can simply be represented by GF parameters.

[3]Dirac δ-distribution.

guess on the relevant time step and length is required, which are corresponding to the highest frequency and the resolution in frequency domain, respectively. For the efficient computation of the TCF we have to choose the time scaling parameters carefully because a large number of TCF evaluation involving inverse complex matrix calculations (Eq. (4.10)) can slow down the computation of the FC intensity profile significantly. If we know the important energy window before the FC integral calculation, even for the TI approach with the prescreening technique, we can devise additional efficient computational ways for the FC intensity profile. Therefore it is desirable to know an approximate spectral shape which is available with cheap computational cost. In chapter 5 we have constructed the FC transition SDF as a probability density function (PDF) characterized by the statistical quantities (cumulants) such as mean, variance, skewness and kurtosis (see Eq. (5.18)). As emphasized above and through out this thesis the FCF GF contains all information about the FC process. We have realized the cumulant expansion (CE) idea by introducing the thermal-moment integral kernel (Eq. (5.4)) augmented in the thermal integral kernel (Eq. (4.2)) into the logarithm of FCF GF (Eq. (4.2)). The FCF cumulant GF has an auxiliary parameter to generate the cumulants of the vibronic transition energy. To compute the cumulants of higher orders, we develop an efficient numerical algorithm for the partial derivatives of an inverse matrix up to arbitrary orders (Sec. 5.1.1).

A mean value of an individual vibrational mode can be interpreted as an effective Huang-Rhys factor (HRF) in electron transfer theory, which includes the molecular structural changes, the potential energy distortion, the Duschinsky mode mixing and the temperature effects, resulting the separable individual mode contribution to the Franck-Condon processes (Sec. 5.3.2). This effective (temperature-dependent) electron-phonon coupling constant (HRF) is useful to study the temperature effects on the electron transfer theory for large systems to verify the individual vibrational mode contributions. In section 5.3.2 we were able to show that the Duschinsky mode coupling can induce thermal energy transfer from low to high frequency vibrational modes with this method. We could also interface the cumulant GF with the TCF via the TD GF parameters (Sec. 5.1.2). Moreover we were able to use the CE for the fast estimation of the TCF by expanding the TD function with the corresponding Taylor series in terms of the cumulants (Sec. 5.1.2). It reduces the effort to evaluate the inverse complex matrix by estimating it with the Taylor expansion to certain orders[4] to avoid the inverse matrix calculation at each time step. We exploit the thermal-moment integral kernel to obtain the moments of vibrationally excited quanta of individual vibrational modes (Sec. 5.2). The moment GF approach is introduced for the reason that it is necessary to keep the vibrational mode indices for the multi-dimensional partial derivatives during the moment calculation. We have developed a book keeping algorithm for the moments of the vibrational quanta in the FC process, but the method can possibly extended also to the non-Condon processes with the non-Condon GFs developed in chapter 6.

The important contributions of this thesis are introducing the TCF approach and the non-Condon effects to the GF approach [46]. The former can simply be adopted to the CS-based GFs by assigning the TD GF parameters. We have taken the non-Condon effects into account with the CS displacement operator (Sec. 3.2). With the help of the phase displacement operator we have used the same mathematical machinery of the FCF GF for the non-Condon GF. The phase displacement operator introduces auxiliary phase parameters for momentum

---

[4]2-nd order in this thesis.

and position operators to be used for non-Condon operators extracted by partial derivatives with respect to the auxiliary parameters. In section 3.2 we have developed the non-Condon integral evaluation scheme such that we have transformed the non-Condon integrals into MHPs not like the existing linear combination of FC integral approaches [36, 49].

In chapter 6 we have considered the non-Condon effects as the linear Herzberg-Teller (HT) approximation (Eq. (2.24)) and we invoke the HT expansion to the CS-based FCHT GF. The extension to the nonlinear problems (including momentum-position operator coupling terms) and the fine-grained prescreening strategies are possible by constructing collective matrices and vectors for the MHPs which require the additional dimensionality for the operators (see *e.g.* Eq. (6.16)). We can also deduce the TCF and the prescreening strategies from the CS-based GF. With the complex MHP evaluation we can evaluate the TCFs including arbitrary polynomial non-Condon operators (Eq. (6.4)). The non-Condon GF can be applied to the electronic circular dichroism (ECD) with the electric and magnetic transition dipole moment (TDM) coupling terms [102].

We have suggested the GF approach for SVLs in chapter 7. The SVLs are involved in the rR scattering excitation profile and the SVL fluorescence spectrum. The rR scattering and the SVL transition (Secs. 7.2 and 7.3) GFs are related to $\text{Tr}((\omega - \hat{H}'/\hbar + i\Gamma/2)^{-1}|\underline{v}_i\rangle\langle\underline{v}_j|)$ and $\text{Tr}(\delta(\omega - \hat{H}'/\hbar)|\underline{v}\rangle\langle\underline{v}|)$, respectively. The major difference between the two traces is the later has the identical SVLs ($|\underline{v}\rangle\langle\underline{v}|$) in the ket- and bra- states while the former has different SVLs ($|\underline{v}_i\rangle\langle\underline{v}_j|$). We can evaluate the rR excitation profile with the half-FT[5] and the SVL trace with the full FT in the TCF approach (Sec. 2.1). The rR TCF is similar to that of SVL transition but rR scattering usually involves two different SVLs in the initial electronic state.

The GFs are made via the coherent-Fock (cF) state which is a mixture of occupation number vector (ONV) and coherent phase vector states (Sec. 7.1). The cF states are obtained by taking partial derivatives with respect to the CS phase parameters belonging to the non-integral space (Sec. 2.3). With the help of MHP technique exploited in the previous chapters the automatized generation of SVLs is possible and the inclusion of the non-Condon effects is possible as well by using the CS displacement operators additionally. With the SVL transition GF we are able to develop a fine-grained prescreening strategy for the multi-dimensional fixed quantum number space X either for the FC or the non-Condon process. We can also exploit the SVL transition GF as the TCF via the TD GF parameters (Eqs. (4.42) and (4.43)). With the SVL GF, non-Boltzmann distributed thermal distributions such as thermo-coherent distributions (see *e.g.* Refs. [84, 230]) could be made.

We can obtain the rR scattering intensity GF at finite temperature and at zero Kelvin including non-Condon effects in an integral form by tracing over the two SVL space for the overlap of two rR amplitude GF with the thermal integral kernel (Sec. 7.2). As for the absorption process, the GF can be used as the TCF and the sum rules for the prescreening strategies. It is worth to note that we have suggested the closed integral form of rR cross section in harmonic approximation including the Duschinsky and thermal effects in a functional analogy to the Förster-type energy transfer processes (see *e.g.* Ref. [8]) which is in a form of convolution between the absorption and the emission spectra.

Additionally we have applied the cF GF to an anharmonic (FC/non-Condon) transition problem which has a few anharmonic DOF and the rest of harmonic DOF so that we can

---

[5] $\frac{1}{\omega - \overline{\omega} + i\Gamma/2} = -i \int_0^\infty \mathrm{d}t\, \mathrm{e}^{i(\omega - \overline{\omega})t - \frac{\Gamma}{2}t}$, which is a special case of the Laplace transform.

benefit from the harmonic GF machinery (Sec. 7.4). The anharmonic GF is expanded by the CS-based cF GFs with the corresponding anharmonic expansion coefficients. With the integral space partitioning we can develop sum rules for the anharmonic transition as in the harmonic cases and we can construct the TCF as well.

Conclusion and outlook   The developments in this thesis are generally applicable to transition problems in the harmonic approximation (see Fig. 8.2). With slight modifications the same approach can be exploited for other problems such as mass spectroscopy (see *e.g.* Ref. [231]), non-equilibrium FC processes in molecular junction (see *e.g.* Ref. [232]) and the Förster-type energy transfer processes (see *e.g.* Ref. [8]). The IC process requires the matrix elements of momentum operators which can easily be handled by the non-Condon developments (Ch. 6). The non-Condon developments can be applied to the vibronic coupling effects (see *e.g.* Refs. [50, 80, 88, 96].) for instance spin-orbit coupling (see *e.g.* Ref. [96]), Jahn-Teller effects (see *e.g.* Ref [2]), nonadiabatic electron transfer (see *e.g.* Ref. [233]) and dissipation with environmental effects (see *e.g.* Ref. [8]). The rR developments in this thesis could be extended for the surface enhancement effects, *i.e.* the surface enhanced Raman scattering (SERS) (see *e.g.* Refs. [234–237].) and the surface enhanced Raman optical activity (SEROA) (see *e.g.* Ref. [238].) with the non-Condon effects and the finite temperature effects if we can make a proper description on the metal surfaces with for example jellium model (see *e.g.* Ref. [239]). The extension to the general anharmonic problem, however, has to be made because the harmonic approximation is very crude in many cases. As mentioned in the anharmonic section (Sec. 7.4), the non-Condon development and the matrix element evaluation procedure are suitable to the anharmonic problems possibly with the reaction path approach [150] of Luckhaus. Our CS-based TCF could be used for propagating wavepackets in time domain on the general anharmonic surfaces (see *e.g.* Refs. [137, 203–206]) via the complex MHP evaluation.

   To this end, we remark that a unified description of vibronic transitions in frequency and time domains, presented in this thesis, facilitates various theoretical applications and experimental analyses for large molecular systems.

9. Zusammenfassung

Eines der grundlegenden Ziele molekularer Wissenschaften ist die perfekte Kontrolle molekularer Prozesse. Molekulare Maschinen und künstliche Lichtsammelsysteme sind wichtige Beispiele, die diesem Ziel entsprechen. Zu diesem Zweck ist eine genaue Kenntnis der Dynamik von vibratorischen und elektronischen (vibronischen) Freiheitsgraden nötig, da das Zusammenspiel vibronischer Freiheitsgrade eine bedeutende Rolle in vielen molekularen Prozessen spielt, die entweder strahlender (z. B. Absorption, Emission und Raman-Resonanzstreuung) oder strahlungsloser Art (z. B. Elektronentransfer, interne Konversion, Übergänge zwischen Systemen und Leitung molekularer Verbindungen) sein können (siehe Abb. 1.1).

Normalerweise sind die betrachteten polyatomischen Systeme relativ groß (mehr als 100 Atome, insbesondere bei Biomolekülen), was die entsprechenden Analysen der Systeme zu einer Herausforderung. Die Analysen großer molekularer Systeme sind typischerweise nicht einfach, weil die Spektren der dazugehörigen Molekularübergänge überfüllt sind, wir aber die Dynamik der einzelnen Vibrationsfreiheitsgrade für die Feinkontrolle oder die künstliche Gestaltung eines erweiterten Molekülsystems benötigen.

Um die Beiträge der einzelnen Schwingungen zu den molekularen Prozessen zu studieren, müssen Ansätze für die theoretische Analyse komplexer molekularer Systeme bereitstehen. Darüberhinaus können in der Berechnung komplexer Systeme Schwierigkeiten in der Auswertung einer gewaltig großen Zahl mehrdimensionaler Franck-Condon(FC)-Integrale auftreten. Es ist nötig, die Franck-Condon-Faktoren (FCF) als Wahrscheinlichkeiten vibronischer Übergänge in der Condon-Näherung zu ermitteln, um FC-vibronische Prozesse theoretisch zu beschreiben.

Die Zustandsdichte oder die Zahl von FC-Integralen bei einer Übergangsenergie steigt mit zunehmender Zahl von Schwingungsfreiheitsgraden, wachsender Anregungsenergie und steigender Temperatur steil an [112].

Sogar in der harmonischen Näherung der Born-Oppenheimer(BO)schen Potentialhyperfläche ist die Berechnung der FC-Integrale besonders für große Molekülsysteme wegen der untrennbaren mehrdimensionalen Integrale als Folge der Duschinskymischung verschiedener Schwingungsfreiheitsgrade (Ref. [107] und Abschn. 2.2) immer noch eine schwierige Aufgabe. Es gab Versuche (s. z. B. Refs. [115–121] für die aktuellsten Arbeiten), die Effizienz der Berechnungsvorschriften von FC-Integralen einschließlich der Duschinsky-Effekte zu verbessern. Die schnelle Berechnung von FC-Integralen ist zur Behandlung großer Systeme überaus wichtig. Wir haben eine iterative Berechnungsvorschrift für FC-Integrale vorgeschlagen, um die Magnus-Entwicklung für multi-variate Hermite-Polynome auszunutzen (MHPs) [176] (siehe Kapitel 3). Die Berechnungsvorschrift über MHP mit der Magnus-Entwicklung kann als Summation eindimensionaler Hermite-Polynome ausgedrückt werden, wodurch eine einfachere Form als durch die bisherige Methode (mehrere Produkte eindinmensionaler Hermite-Polynome) erreicht wird (s. z. B. Refs. [120, 121]).

Es wurde jedoch darauf hingewiesen, dass nur ein kleiner Teil der FCF signifikant zu den

Gesamt-FC-Profilen beiträgt (s. z. B. Refs. [44–46]). Die Idee kann ad hoc verwendet werden, indem man beispielsweise die Anregung in jeder Normalschwingung auf festgelegte Zahlen begrenzt.

Zum Beispiel könnte man die Zahl der zu berechnenden FC-Integrale eingrenzen, indem man höchstens 10 Schwingungsanregungsquanten für jeden Schwingungsfreiheitsgrad zulässt. In diesem Fall müssen wir für ein N-dimensionales harmonisches Oszillatorsystem 11^{2N} FC-Integrale berechnen. Unglücklicherweise steigt die Komplexität der Rechnung immer noch drastisch an und eine Berechnung wird unpraktikabel. Wir könnten stattdessen versuchen, den größten Teil des FC-Intensitätsprofils anzunähern, zum Beispiel 99 % der gesamten FC-Intensität, mit Hilfe von ausgesuchten FCFs. Dadurch wird die Berechnung der FC-Intensitätsprofile selbst für komplexe Systeme möglich. In diesem Fall müssen wir uns dem Problem widmen, einen Teil der FCFs zu kennen, die etwa 99 % der Gesamt-FC-Intensität ausmachen, ohne alle FCFs verfügbar zu haben. Jankowiak *et al.* [46] nutzten diese einfache Idee aus, indem sie die ursprüngliche Idee Doktorovs und seiner Koautoren von erzeugenden Funktionen [29] modifizierten. Mithilfe dieser erzeugenden Funktion entwickelten Jankowiak *et al.* eine Strategie zu einer grobkörnigen Integralvorauswahl für die FC-Intensitätsprofile am Temperaturnullpunkt. Der Ausgangspunkt dieser Dissertation war gerade diese zeitunabhängige FC-Entwicklung für 0 K. Im Laufe der Dissertation haben wir diese Methode erweitert und modifiziert, um Temperatur- und Nicht-Condon-Effekte einzubeziehen, welche in Molekülübergangsprozessen wichtig sind. In Diagramm 8.1 fassen wir die methodischen Entwicklungen in dieser Arbeit zusammen und zeigen die Beziehungen der darin beschriebenen Entwicklungen auf.

Die theoretische Beschreibung der meisten vibronischen molekularen Übergänge mit Duschinsky-rotierten harmonischen Oszillatoren läuft auf ein bekanntes mathematisches Problem hinaus, die Auswertung von MHP (s. Diagramm 8.2 und Kap. 3). Die Berechnung der MHP scheint hinsichtlich des Rechenaufwandes ein schwieriges Problem zu sein (Kap. 3). Dennoch erlaubt uns die Übersetzung des Problems der molekularen Übergänge in harmonischer Näherung in ein äquivalentes MHP-Auswertungsproblem, die verschiedenen Übergangsprozesse mit derselben mathematischen Methode zu analysieren. Eine analoge Transformation für die Ermakov Invariante in dissipativen Systemen (s. z. B. Refs. [224–229]) kann als Beispiel für eine ähnliche Reduzierung zu einem einfacher berechenbaren Problem angegeben werden. Die unterschiedlichen Bewegungsgleichungen für dissipative Systeme, z. B. die Langevin- und die Fokker-Planck-Gleichungen, die sich in verschiedenen Formen befinden, konvergieren letztendlich auf diese invariante Größe.

Im folgenden Absatz fassen wir die Entwicklungen in dieser Arbeit zusammen. Die Ansätze mit erzeugenden Funktionen werden kurz im quantenmechanischen Spurformalismus beschrieben. Danach folgen die Schlusfolgerungen und Ausblicke dieser Dissertation.

Zusammenfassung der Entwicklungen Eine invariante Größe in einem quantenmechanischen Problem ist ein mächtiges Werkzeug zum Verständnis des Systems [224]. Die Invarianz schränkt die Dynamik des Systems ein. Mit den richtigen Modifikationen oder mathematischen Manipulationen am Funktional (s. unterer Teil der Abb. 8.1) können wir nützliche Daten über die quantenmechanischen Prozesse aus dem invarianten Funktional gewinnen, in diesem Fall aus der erzeugenden Funktion, die durch ihre Parameter charakterisiert wird (s. Ref. [46] und Abschn. 2.4). Die erzeugende Funktion scheint eine der Zustandssumme analoge Funktion zu sein ($\mathrm{Tr}(\exp(-\beta \hat{H}))$), welche invariant ist und

uns erlaubt, thermodynamische Größen zu berechnen. In analoger Weise erlaubt die erzeugende Funktion die Berechnung relevanter Größen durch (entsprechende) Operationen, z. B. partielle Ableitungen nach den Parametern der erzeugenden Funktion für die Summenregeln der Intensität (s. Kap. 4 und 6).

Um den Gedanken der invarianten erzeugenden Funktion zu verdeutlichen, betrachten wir die FC-Übergangswahrscheinlichkeiten von einem anfänglichen Zustand zu einer Vielzahl anderer Zustände, die zu eins summiert werden müssen, d. h. $\text{Tr}(\hat{\rho}) = 1$, wobei der Dichteoperator $\hat{\rho}$ beispielsweise über thermisch gemittelte vibronische Anfangszustände ($\hat{\rho} = \sum_{\underline{v}} p_{\underline{v}}(T)|\underline{v}\rangle\langle\underline{v}|$) definiert sein kann, mit einer thermischen Verteilungsfunktion $p_{\underline{v}}(T)$ des vibronischen Anfangszustands ($|\underline{v}\rangle$) bei einer endlichen Temperatur (T). Diese einfache Summenregel kann durch Spurbildung mit einer beliebigen vollständigen Basismenge befolgt werden, was in einer unendlichen Summe von FCFs resultiert, die gegen die Einheit konvergiert (z. B. für die vibronischen Endzustände $|\underline{v}'\rangle$, $\sum_{\underline{v}} p_{\underline{v}}(T)|\langle\underline{v}'|\underline{v}\rangle|^2 = 1$). Die Gleichung der FCF-Summenregel ist jedoch nicht stark genug, da sie uns nur mitteilt, dass die Gesamtintensität hinsichtlich Entwicklung in einer beliebigen Basis erhalten bleibt. Wir greifen daher stattdessen auf die Diracschen δ-Distributionsoperatoren zurück, um die FCF mittels vibronischer Übergangsenergien aufzulösen, sodass $\int_{-\infty}^{\infty} d\omega \text{Tr}^M(\delta(\omega_1 - \hat{H}'/\hbar)\delta(\omega_2 - \hat{H}/\hbar)\hat{\rho}) = 1$, wobei $\omega = \omega_1 - \omega_2$ die vibronische Übergangsfrequenz ist und $\hat{H}$ und $\hat{H}'$ die vibronischen Hamilton-Operatoren des Anfangs- bzw. Endzustandes sind (Abschn. 2.2). Der Integrand, die quantenmechanische Spur, ist einfach die spektrale FC-Dichtefunktion mit der Diracschen δ-Distribution bei endlichen Temperaturen, d. h. $\varrho_{\text{FCW}}(\omega) = \text{Tr}(\delta(\omega_1 - \hat{H}'/\hbar)\delta(\omega_2 - \hat{H}/\hbar)\hat{\rho})$, welches nach der Übergangsfrequenz (ω) aufgelöst ist (Abschn. 2.1). Durch Einführen kohärenter Zustände sowohl für Anfangs- und Endzustände und Ersetzen des δ-Distributionsoperators mit den Parametern der erzeugenden Funktion können wir die erzeugende Funktion der FCF erhalten (Abschn. 6.1.2). Unter Ausnutzung der resultierenden erzeugenden Funktion entwickelten Jankowiak *et al.* [46] die Strategie der FC-Integralvorauswahl bei Null Kelvin, wovon ausgehend wir die Methode zur thermischen FC-Integralvorauswahl (Kap. 4 für zeitunabhängige FC-Profile entwickelt haben.

Wir haben die thermischen Effekte durch den thermischen Integranden in die kohärenzzustandsbasierte erzeugende Funktion eingeführt (Abschn. 4.1). Die wichtige Eigenschaft dieser thermischen Entwicklung ist, dass die individuellen Schwingungsfreiheitsgrade verschiedene endliche Temperaturen haben können, sodass wir das Schwingungsanregungsmuster mit den individuellen Temperaturen kontrollieren können, nicht nur über die Parameter der erzeugenden Funktion (Gl. (4.4)). Bei endlicher Temperatur kann der anfängliche Schwingungszustand als thermisch gemittelter, effektiver Schwingungsgrundzustand betrachtet werden, und nicht als Menge thermisch angeregter Vibrationszustände in der erzeugenden Funktion. Aus diesem Grund können die Strategien zur thermischen Vorauswahl (Abschn. 4.3) die der Vorauswahl beim Temperaturnullpunkt beerben [46]. Diese thermische erzeugenden Funktion der FCFs verallgemeinert die korrespondierende Entwicklung für 0 K zu einer Entwicklung bei endlicher Temperatur.

Bedenkt man die Herkunft der Parameter der erzeugenden Funktion (Diracsche δ-Distribution), so ist klar, dass wir dieselbe erzeugenden Funktion der FCFs in eine Zeitkorrelationsfunktion und in die FCF-Summenregel gemäß der Werte der Parameter der erzeugenden Funktion (Kap. 4) transformieren können. In Kapitel 4 entwickeln wir die zeitabhängige Herangehensweise aus der zeitunabhängigen Perspektive. Die Methode der Zeitkorrela-

tionsfunktion wird typischerweise wegen ihrer Einfachheit und schnellen Berechenbarkeit verwendet, sieht man vom Nachteil der fehlenden Möglichkeit der Signalzuordnung ab (s. z. B. Refs. [17,33,34,37,38,40,40–42,48,55,56,61,64,66,67,72,73,75,79,81,84,86,87,93–95, 109,137,138]). Bis zu diesem Zeitpunkt (vor dieser Arbeit) wurden die zeitabhängigen und zeitunabhängigen Herangehensweisen für die Berechnung der Profile für Absorption und Emission (praktisch) als unabhängige Verfahren betrachtet [18], obwohl die Formalismen sogar ineinander transformiert werden können (Abschn. 2.1). Die zeitabhängige Herangehensweise nutzt die fouriertransformierte Darstellung der δ-Distribution, d. h. $\varrho_{\mathrm{FCW}}(\omega) = \hbar^{-1} \int_{-\infty}^{\infty} dt \mathrm{Tr}(\exp(-\mathrm{i}\hat{H}'t/\hbar)\exp(\mathrm{i}\hat{H}t/\hbar)\hat{\rho})\mathrm{e}^{\mathrm{i}(\omega-\omega_0)t}$. Indem wir die zeitabhängigen Phasenparameterwerte (Gl. (4.42) und (4.43)) den Parametern der erzeugenden Funktion zuordnen, erhalten wir die zu $(\mathrm{Tr}(\exp(-\mathrm{i}\hat{H}'t/\hbar)\exp(\mathrm{i}\hat{H}t/\hbar)\hat{\rho}))$ korrespondierende Zeitkorrelationsfunktion einfach aus der erzeugenden Funktion der FCFs. Die korrespondierende FT ergibt dann das FC-Profil (Abschn. 4.4). Wir betonen dabei, dass wir dieselbe erzeugende Funktion für die Integralvorauswahl und die Ansätze für die Zeitkorrelationsfunktion verwenden können. Die Gültigkeit der zeitabhängigen und zeitunabhängigen Herangehensweisen wurde durch ihren Vergleich überprüft (Abschn. 4.5). Wir können die Qualität der Vorauswahl aus dem Vergleich zwischen den beiden Methoden beurteilen (Abschn. 4.5 und 6.3). Es ist interessant festzuhalten, dass der Wert der Zeitkorrelationsfunktion bei $t = 0$ einfach der Wert der Summenregel ist. Wenn sich die Zeit verändert ($t \neq 0$), beinhaltet die komplexe Zeitkorrelationsfunktion Informationen über Vibrationsübergänge des Systems. Ferner ist zur derzeitigen Methode der Zeitkorrelationsfunktion anzumerken, dass wir versuchen können, die Signale indirekt zuzuweisen (sogar beim zeitabhängigen Verfahren), indem wir mittels Kontrolle der Parameter der erzeugenden Funktion einige Schwingungsfreiheitsgrade bei der Auswertung der Zeitkorrelationsfunktion einfrieren. Dies ist möglich, da wir über ihre Parameter mit der identischen erzeugenden Funktion eine Verbindung zwischen den zeitunabhängigen und zeitabhängigen Methoden geschaffen haben.

In der Auswertung von Zeitkorrelationsfunktionen (s. z. B. Abschn. 4.4) für die schnelle Fourier Transformations (FFT) wird eine gute Annahme über die Anzahl und Länge der Zeitschritte benötigt, welche jeweils zur höchsten Frequenz bzw. zur Auflösung in der Frequenzdomäne korrespondieren. Um die Zeitkorrelationsfunktion effizient zu berechnen, müssen wir die Zeitskalierungsparameter sorgfältig wählen, da eine große Zahl von Auswertungen von Zeitkorrelationsfunktionen mit inverser komplexer Matrixberechnung (Gl. (4.10)) die Berechnung der FC-Intensitätsprofile signifikant verlangsamen kann. Ist uns beim zeitunabhängigen Verfahren mit Vorauswahl das relevante Energiefenster vor der Berechnung der FC-Integrale bekannt, können wir zusätzliche effiziente Rechenverfahren für die FC-Intensitätsprofile finden. Daher ist es erstrebenswert, eine ungefähre spektrale Form zu kennen, die mit geringem Rechenaufwand verfügbar ist. In Kapitel 5 haben wir die spektrale FC-Übergangsdichtefunktion als durch statistische Größen (Kumulanten) wie Mittelwert, Varianz, Schiefe und Kurtosis (s. Gl. (5.18)) charakterisierte Wahrscheinlichkeitsdichtefunktion beschrieben. Wie oben und im weiteren Verlauf dieser Arbeit betont wird, enthalten die FCFs alle Informationen zum FC-Prozess. Wir haben den Gedanken der Kumulantenerweiterung umgesetzt durch Einführen eines Integralkerns zum thermischen Moment (Gl. (5.4)), der im thermischen Integralkern (Gl. (4.2)) zum Logarithmus der erzeugenden Funktion der FCFs (Gl. (4.2)) erweitert wird. Die erzeugende Funktion für FCF-Kumulanten hat einen Hilfsparameter zur Erzeugung der Kumulanten der vibronischen Übergangsenergie. Um die Kumulanten höherer Ordnung zu berechnen, entwickeln

wir einen effizienten numerischen Algorithmus für die partiellen Ableitungen einer inversen Matrix bis zu einer beliebigen Ordnung (Abschn. 5.1.1).

Ein Mittelwert einer einzelnen Normalschwingung kann als effektiver Huang-Rhys-Faktor (HRF) in der Theorie des Elektronentransfers interpretiert werden, der molekulare Strukturänderungen, die Verzerrung der potentiellen Energie, die Duschinsky-Rotationen und Temperatureffekte beinhaltet, was zum Beitrag der separablen Einzelmoden zu FC-Prozessen (Abschn. 5.3.2) führt. Diese effektive (temperaturabhängige) Elektron-Phonon-Kopplungskonstante (HRF) ist nützlich, um die Temperatureffekte auf die Elektronentransfertheorie für große Systeme zur Bestätigung der Beiträge einzelner Normalschwingungen zu studieren. In Abschnitt 5.3.2 waren wir durch diese Methode in der Lage zu zeigen, dass die Kopplung der Duschinsky-Rotationen den thermischen Elektronentransfer von nieder- zu hochfrequenten Normalschwingungen induzieren kann. Wir könnten ebenso die Kumulantenerzeugende über die Parameter der zeitabhängigen erzeugenden Funktion an die Zeitkorrelationsfunktion koppeln (Abschn. 5.1.2).

Die wichtigen Beiträge dieser Arbeit sind die Einführung der Methode der Zeitkorrelationsfunktion und der Nicht-Condon-Effekte zum Verfahren der erzeugenden Funktion [46]. Ersteres kann einfach durch Setzen der Parameter der zeitabhängigen erzeugenden Funktion in die auf kohärenten Zuständen basierende erzeugende Funktion eingeführt werden. Die Nicht-Condon-Effekte wurden mittels des Verschiebungsoperators berücksichtigt (Abschn. 3.2). Mithilfe des Phasenverschiebungsoperators haben wir denselben mathematischen Apparat der erzeugenden Funktion der FCFs für die erzeugende Funktion im Nicht-Condon-Fall verwendet. Der Phasenverschiebungsoperator führt Hilfsphasenparameter für Impuls- und Ortsoperatoren ein, die für die durch partielle Ableitungen nach den Hilfsparametern erhaltenen Nicht-Condon-Operatoren verwendet werden sollen: In Abschn. 3.2 haben wir das Auswertungsverfahren für Nicht-Condon-Integrale in der Weise entwickelt, dass wir diese Integrale in MHP transformiert haben, die der existierenden Linearkombination der FC-Integral-Verfahren nicht gleichen [36, 49].

In Kapitel 6 haben wir Nicht-Condon-Effekte in der linearen Herzberg-Teller(HT)-Näherung (Gl. (2.24)) betrachtet und greifen für die HT-Erweiterung auf die auf kohärenten Zuständen basierende erzeugende Funktion zurück. Die Erweiterung auf nichtlineare Probleme (einschließlich Orts-Impulsoperator-Kopplungstermen) und die feinkörnigen Vorauswahl-Strategien werden durch Aufstellen gemeinsamer Matrizen und Vektoren für die MHP ermöglicht (s. z. B. Gl. (6.16)). Wir können auch die Zeitkorrelationsfunktion und die Vorauswahl-Strategien aus der erzeugenden Funktion, die auf kohärenten Zuständen basiert, ableiten. Mit der Berechnung der komplexen MHP können wir die Zeitkorrelationsfunktion einschließlich beliebiger Nicht-Condon-Polynome auswerten (Gl. (6.4)). Die erzeugende Funktion für den Nicht-Condon-Fall kann auf den elektronischen Circulardichroismus mit seinen Kopplungstermen für das elektrische und magnetische Übergangsdipolmoment angewendet werden [102].

Wir haben die Methode der erzeugenden Funktionen für einzelne vibronische Level in Kapitel 7 vorgeschlagen. Die einzelnen vibronischen Level sind am Anregungsprofil der Resonanz-Raman-Streuung und dem Fluoreszenzspektrum des vibronischen Einzelzustands beteiligt. Die erzeugenden Funktionen der Resonanz-Raman-Streuung und der vibronischen Übergange ausgehend aus einem einzelnen vibronischen Zustand (Abschn. 7.2 und 7.3) sind verknüpft mit $\mathrm{Tr}((\omega - \hat{H}'/\hbar + \mathrm{i}\Gamma/2)^{-1} \, |\underline{v}_i\rangle\langle\underline{v}_j|)$ bzw. $\mathrm{Tr}(\delta(\omega - \hat{H}'/\hbar)|\underline{v}\rangle\langle\underline{v}|)$. Der größte Unterschied zwischen den beiden Spuren ist die Tatsache, dass die vibronischen

Einzelzustände in den Ket- und Bra-Zuständen in der ersten Spur identisch ($|\underline{v}\rangle\langle\underline{v}|$), in der zweiten aber verschieden sind ($|\underline{v}_i\rangle\langle\underline{v}_j|$). Wir können zwar die Resonanz-Raman-Anregungsprofile mit der half-FT (einem Spezialfall der Laplacetransformation) und die Spur des vibronischen Einzelzustands mit der vollen FT mit der Methode der Zeitkorrelationsfunktion berechnen, doch lassen sie sich bei der zeitunabhängigen Herangehensweise direkt auswerten (Abschn. 2.1). Die Zeitkorrelationsfunktion für Resonanz-Raman-Prozesse ähnelt der des vibronischen Einzelzustandsübergangs, aber Resonanz-Raman-streuung beinhält normalerweise zwei verschiedene vibronische Einzelzustände im elektronischen Ausgangszustand.

Die erzeugenden Funktionen werden mittels des kohärenten Fockzustandes, der eine Mischung von Besetzungszahlvektor- und kohärenten Phasenvektorzuständen (Abschn. 7.1) ist, beschrieben. Die kohärenten Fockzustände werden erhalten, indem man partielle Ableitungen nach den nicht zum Integralraum gehörenden Phasenparametern des kohärenten Zustandes bildet (Abschn. 2.3). Mithilfe der in den vorausgegangenen Kapiteln ausgenutzten MHP-Technik ist die automatische Berechnung zur Erzeugung von vibronischen Einzelzuständen möglich, danach lassen sich die Nicht-Condon-Effekte ebenso wie die Verschiebungsoperatoren des kohärenten Zustandes einführen. Mit der erzeugenden Funktion des vibronischen Einzelzustands sind wir in der Lage, feinkörnige Vorauswahl-Strategien des mehrdimensionalen, festen Quantenzahlenraumes X entweder für den FC- oder den Nicht-Condon-Prozess zu erstellen. Wir können außerdem die erzeugende Funktion des vibronischen Einzelzustandsübergangs über die Parameter der zeitabhängigen Erzeugendenfunktion als Zeitkorrelationsfunktion ausnutzen (Gl. (4.42) und (4.43)). Mit der Erzeugendenfunktion des vibronischen Einzelzustands könnten auch thermische Verteilungen, die nicht der Boltzmannverteilung genügen, wie die thermo-kohärente Verteilung erzeugt werden (s. z. B. Refs. [84, 230]).

Wir können die erzeugende Funktion der Intensität der Resonanz-Raman-Streuung bei endlicher Temperatur und bei Null Kelvin einschließlich der Nicht-Condon-Effekte in einer Integralform erhalten, indem wir die Spur über die zwei vibronischen Einzelzustandsräume für die Überlappung der erzeugenden Funktionen der Resonanz-Raman-Amplitude mit dem thermischen Integralkern (Abschn. 7.2) bilden. Wie beim Absorptionsprozess kann die erzeugende Funktion als Zeitkorrelationsfunktion und für die Summenregel bei den Vorauswahl-Strategien verwendet werden. Es soll hier hervorgehoben werden, dass wir die geschlossene Integralform des Wirkungsquerschnitts der Resonanz-Raman-Streuung in harmonischer Näherung einschließlich der Duschinsky- und thermischen Effekte in funktioneller Analogie zu den Försterartigen Energietransferprozessen vorgeschlagen haben (s. z. B. Ref. [8]), welche die Form einer Faltung zwischen den Absorptions- und Emissionsspektren hat.

Zusätzlich haben wir die mittels des kohärenten Fockzustandes beschriebene erzeugende Funktion auf ein anharmonisches Übergangsproblem angewendet, das einige anharmonische und ansonsten mehrere harmonische Freiheitsgrade besitzt, sodass wir auf die Vorteile des Apparats der harmonischen erzeugenden Funktionen zurückgreifen können (Abschn. 7.4). Die anharmonische erzeugende Funktion wird durch die auf kohärenten Fockzuständen basierenden Erzeugungsfunktionen mit den entsprechenden anharmonischen Entwicklungskoeffizienten erweitert. Mit der Aufteilung des Integrationsraumes können wir die Summenregel für den anharmonischen Übergang gerade wie für den harmonischen aufstellen und außerdem die Zeitkorrelationsfunktion konstruieren.

Schlußfolgerungen und Ausblicke Die Entwicklungen in dieser Arbeit sind im Allgemeinen auf Übergangsprobleme in harmonischer Näherung anwendbar (s. Abb. 8.2). Mit leichten Modifikationen kann dasselbe Verfahren für andere Probleme wie Massenspektroskopie (s. z. B. Ref. [231]), FC-Prozesse in molekularen Verbindungen im Nicht-Gleichgewicht (s. z. B. Ref. [232]) und die Försterartigen Energietransferprozesse (s. z. B. Ref. [8]) eingesetzt werden. Der innere Umwandlungsprozess benötigt die Matrixelemente von Impulsoperatoren, die einfach per Nicht-Condon-Entwicklung behandelt werden können (Kap. 6). Die Nicht-Condon-Entwicklungen können auf vibronische Kopplungseffekte angewendet werden (s. z. B. Refs. [50, 80, 88, 96]), beispielsweise die Spin-Bahn-Kopplung (s. z. B. Ref. [96]), Jahn-Teller-Effekte (s. z. B. Ref. [2]), der nichtadiabatische Elektronentransfer (s. z. B. Ref. [233]) und die Dissipation mit Umgebungseffekten (s. z. B. Ref. [8]). Die Resonanz-Raman-Entwicklungen in dieser Arbeit könnten für Oberflächenverstärkungseffekte, d. h. surface enhanced Raman scattering (SERS) (s. z. B. Refs. [234–237]) und surface enhanced Raman optical activity (SEROA) (s. z. B. Ref. [238]) mit Nicht-Condon-Effekten und Effekten endlicher Temperatur erweitert werden, sofern wir eine korrekte Beschreibung auf metallischen Oberflächen mit beispielsweise dem Jellium-Modell (s. z. B. Ref. [239]) erreichen. Die Erweiterung auf allgemeine anharmonische Probleme muss erfolgen, da die harmonische Näherung in vielen Fällen sehr grob ist. Wie im anharmonischen Abschnitt (Abschn. 7.4) erwähnt wurde, sind die Nicht-Condon-Entwicklung und die Prozedur zur Berechnung von Matrixelementen für anharmonische Probleme geeignet, möglicherweise mit der Reaktionspfadmethode [150] von Luckhaus kombiniert zu werden. Unsere Zeitkorrelationsfunktion könnte über die Auswertung komplexer MHP für die Propagation von Wellenpaketen in der Zeitdomäne auf allgemeinen anharmonischen Potentialhyperflächen (s. z. B. Refs. [137, 203–206]) verwendet werden.

Eine vereinigte Beschreibung vibronischer Übergänge in Frequenz- und Zeitdomäne, wie sie in dieser Arbeit vorgestellt wurde, vereinfacht verschiedene theoretische Anwendungen und experimentelle Analysen für große molekulare Systeme.

A. Supplementary data for chapter 4

A.1. General remarks

In this appendix we report maximum quantum numbers $v_k^{'\max}$ (final state) and $v_k^{\max}$ (initial state) in each harmonic mode k determined via Eq. (4.20) in this thesis, together with the various wavemunber windows for each irreducible representation γ, the number of the evaluated integrals and the mode coupling error ϵ_c (see Figures 4.2 and 4.4). For each molecule the irreducible representation and the numbering of the vibrational modes are reported as in the previous work cited in this thesis [Jankowiak, Stuber and Berger, *J. Chem. Phys.*, **127**, 234101 (2007)].
Maximum mode excitation numbers in each normal mode are given in following form:

$$\langle \underline{v}_{\max}^{(\gamma)'} | \underline{v}_{\max}^{(\gamma)} \rangle$$

$\underline{v}_{\max}^{(\gamma)'}$ and $\underline{v}_{\max}^{(\gamma)}$ are vectors containing the maximum quantum numbers of the various normal modes of each irreducible representation γ for the final and initial electronic states respectively. The vectors are sorted according to the number of vibrational mode (in ascending order), which are given in subsection of each molecule, for each irreducible representation.
The wavenumber windows for each irreducible representation γ are given as $[\tilde{\nu}_{\min}^{(\gamma)}, \tilde{\nu}_{\max}^{(\gamma)}]$ in cm^{-1}. The windows are determined by the maximum mode coupling numbers and maximum mode excitation numbers for each irreducible representation γ as the following relations,

$$-\tilde{\nu}_{\min}^{(\gamma)} = \max_{\underline{s} \in C_{M^{(\gamma)}}^{N^{(\gamma)}}} \left(\sum_{k=s_1}^{s_{M^{(\gamma)}}} v_{\max,k}^{(\gamma)} \tilde{\nu}_k \right)$$

and

$$\tilde{\nu}_{\max}^{(\gamma)} = \max_{\underline{s} \in C_{M^{(\gamma)}}^{N^{(\gamma)}}} \left(\sum_{k=s_1}^{s_{M^{(\gamma)}}} v_{\max,k}^{(\gamma)'} \tilde{\nu}_k' \right)$$

where $C_{M^{(\gamma)}}^{N^{(\gamma)}}$ is the index set choosing $M^{(\gamma)}$ modes out of $N^{(\gamma)}$ for initial or final state of irreducible representation γ. When $M^{(\gamma)}$ exceeds $N^{(\gamma)}$, we have set $\underline{s}$ to $\underline{v}_{\max}^{(\gamma)}$ or $\underline{v}_{\max}^{(\gamma)'}$ accordingly. In our program hotFCHT, we have set the wavenumbers to the nearest graining point $(-[\tilde{\nu}_{\min}^{(\gamma)}/\Delta\tilde{\nu}] * \Delta\tilde{\nu}$ or $[\tilde{\nu}_{\max}^{(\gamma)}/\Delta\tilde{\nu}] * \Delta\tilde{\nu})$ with graining $\Delta\tilde{\nu} = 10$ cm^{-1}.
The number of integrals that is to be evaluated according to the prescreening conditions are reported for the various irreducible representations and wavenumber windows.
For the calculation of mode coupling error ϵ_c, we set the mode coupling threshold t_c as 10^{-12}, and set the mode excitation threshold $t_m = 0.0$. We report the results only up to $\epsilon_c \simeq 0.005\%$ for the mode coupling error due to the numerical precision and the sensitivity to the selection of CODATA sets for the conversion of units.
The increments $F_{\text{FC;c}}^{(m^{(\gamma)})}$ (see Eq. (4.29) in this thesis) are computed for each irreducible representation γ and subsequently folded (convoluted) to form the total increments $F_{\text{FC;c}}^{(m)}$, from which we obtain $\widetilde{F}_{\text{FC;c}}^{(M)}$ and finally (via Eq. (4.27) in this thesis) ϵ_c.

A.2. Formic acid

- Harmonic vibrational wavenumbers of the initial electronic state in cm^{-1}:

  1. a′(from $\tilde{\nu}_1$ to $\tilde{\nu}_7$)
  3765.2386 3088.1826 1825.1799 1416.9512 1326.4684
  1137.0490 629.7144

  2. a″(from $\tilde{\nu}_8$ to $\tilde{\nu}_9$)
  1062.7001 677.5835

- Harmonic vibrational wavenumbers of the final electronic state in cm^{-1}:

  1. a′(from $\tilde{\nu}'_1$ to $\tilde{\nu}'_7$)
  3629.9472 3064.9143 1566.4602 1399.6554 1215.3420
  1190.9077 496.2845

  2. a″(from $\tilde{\nu}'_8$ to $\tilde{\nu}'_9$)
  1033.6951 717.3864

A.2.1. Maximum mode excitation numbers

- a′

  0 K

Tol. set	Max. quantum numbers	$[\tilde{\nu}_{\min}^{(a')},\tilde{\nu}_{\max}^{(a')}]$	# of integrals
I	< 2 2 8 3 4 3 4 | 0 0 0 0 0 0 0 >	[0.00, 38554.46]	27792
II	< 2 2 7 3 3 2 4 | 0 0 0 0 0 0 0 >	[0.00, 32199.94]	10104
III	< 1 1 6 2 2 2 2 | 0 0 0 0 0 0 0 >	[0.00, 18892.93]	1084

  300 K

Tol. set	Max. quantum numbers	$[\tilde{\nu}_{\min}^{(a')},\tilde{\nu}_{\max}^{(a')}]$	# of integrals
I	< 2 2 8 4 4 3 5 | 0 0 1 1 1 2 3 >	[−8731.84, 42435.54]	1339196
II	< 2 2 7 3 3 2 4 | 0 0 1 1 1 1 3 >	[−7594.79, 34581.75]	200785
III	< 1 1 6 2 2 2 3 | 0 0 0 1 1 1 2 >	[−5139.90, 21323.62]	14931

  1000 K

Tol. set	Max. quantum numbers	$[\tilde{\nu}_{\min}^{(a')},\tilde{\nu}_{\max}^{(a')}]$	# of integrals
III	< 2 1 7 4 4 4 8 | 1 1 2 3 3 4 7 >	[−27690.24, 40483.93]	60445788

- a″

  0 K

Tol. set	Max. quantum numbers	$[\tilde{\nu}_{\min}^{(a'')},\tilde{\nu}_{\max}^{(a'')}]$	# of integrals
I	< 2 2 | 0 0 >	[0.00, 3502.16]	9
II	< 1 2 | 0 0 >	[0.00, 2468.47]	6
III	< 0 1 | 0 0 >	[0.00, 717.39]	2

  300 K

Tol. set	Max. quantum numbers	$[\tilde{\nu}_{\min}^{(a'')},\tilde{\nu}_{\max}^{(a'')}]$	# of integrals
I	< 2 3 | 2 3 >	[−4158.15, 4219.55]	144
II	< 2 2 | 1 2 >	[−2417.87, 3502.16]	54
III	< 1 2 | 1 2 >	[−2417.87, 2468.47]	20

  1000 K

Tol. set	Max. quantum numbers	$[\tilde{\nu}_{\min}^{(a'')},\tilde{\nu}_{\max}^{(a'')}]$	# of integrals

III $< 4\,7\,|\,4\,7 >$ $[-8993.88, 9156.49]$ 1600

A.2.2. Mode coupling error

M	$\epsilon_\text{c}/\% = (1 - \widetilde{F}_{\text{FC;c}}^{(M)})/\%$		
	$T = 0$ K(%)	$T = 300$ K(%)	$T = 1000$ K(%)
0	78.50	80.61	96.60
1	20.25	28.02	86.80
2	3.61	10.87	75.93
3	0.41	2.51	54.73
4	0.03	0.55	40.23
5	0.00	0.09	22.48
6		0.01	12.82
7		0.00	5.53
8			2.26
9			0.73
10			0.20
11			0.04
12			0.01
13			0.00

A.3. Anthracene

- Harmonic vibrational wavenumbers of the initial electronic state in cm^{-1}:

1. $\mathrm{a_g}$(from $\tilde{\nu}_1$ to $\tilde{\nu}_{12}$)
3067.9748 3044.8144 3036.9660 1530.2636 1459.5709
1369.1946 1239.8467 1149.6155 991.7868 735.3180
619.9167 383.7560

2. $\mathrm{b_{1g}}$(from $\tilde{\nu}_{13}$ to $\tilde{\nu}_{23}$)
3056.1237 3039.4771 1600.7036 1561.1451 1364.6309
1249.2842 1168.0443 1085.0601 897.1103 517.3005
382.4764

3. $\mathrm{b_{2g}}$(from $\tilde{\nu}_{24}$ to $\tilde{\nu}_{27}$)
921.8861 737.2308 461.2524 224.7566

4. $\mathrm{b_{3g}}$(from $\tilde{\nu}_{28}$ to $\tilde{\nu}_{33}$)
946.1364 852.0268 807.8076 696.2309 549.1235
253.1248

5. $\mathrm{a_u}$(from $\tilde{\nu}_{34}$ to $\tilde{\nu}_{38}$)
946.9771 821.6030 692.7847 474.9120 114.9426

6. $\mathrm{b_{1u}}$(from $\tilde{\nu}_{39}$ to $\tilde{\nu}_{44}$)
923.4842 853.3592 709.1380 453.8243 367.9794
87.0330

7. $\mathrm{b_{2u}}$(from $\tilde{\nu}_{45}$ to $\tilde{\nu}_{55}$)
3056.3758 3040.2103 3035.1222 1604.1604 1431.3884
1290.0584 1245.0921 1132.2622 886.8443 637.6725
227.6664

8. $\mathrm{b_{3u}}$(from $\tilde{\nu}_{56}$ to $\tilde{\nu}_{66}$)
3067.6168 3043.4896 1517.3260 1428.9232 1357.9155
1322.2589 1145.5196 1117.1321 987.1214 790.0827
596.0896

- Harmonic vibrational wavenumbers of the final electronic state in cm^{-1}:

1. $\mathrm{a_g}$(from $\tilde{\nu}'_1$ to $\tilde{\nu}'_{12}$)
3074.6924 3049.5882 3036.8257 1526.6846 1469.0538
1355.6525 1218.4629 1144.4341 1008.5096 723.7630
585.8853 379.0983

2. $\mathrm{b_{1g}}$(from $\tilde{\nu}'_{13}$ to $\tilde{\nu}'_{23}$)
3060.3080 3045.2855 1496.6960 1463.9727 1365.1563
1243.3561 1166.6021 1046.6257 885.4103 508.3649
373.7143

3. $\mathrm{b_{2g}}$(from $\tilde{\nu}'_{24}$ to $\tilde{\nu}'_{27}$)
837.0218 689.9723 406.7704 220.9519

4. $\mathrm{b_{3g}}$(from $\tilde{\nu}'_{28}$ to $\tilde{\nu}'_{33}$)
866.4218 809.0660 716.3337 474.9560 296.4920
188.6317

5. a_u(from $\tilde{\nu}'_{34}$ to $\tilde{\nu}'_{38}$)
864.6336 773.0836 495.8657 462.7943 105.6943

6. b_{1u}(from $\tilde{\nu}'_{39}$ to $\tilde{\nu}'_{44}$)
832.9560 793.0119 685.7976 387.7267 301.2646
80.7003

7. b_{2u}(from $\tilde{\nu}'_{45}$ to $\tilde{\nu}'_{55}$)
3060.6666 3045.9702 3035.5527 1537.2677 1407.3867
1257.2842 1238.7458 1083.1173 877.0652 641.9751
225.1369

8. b_{3u}(from $\tilde{\nu}'_{56}$ to $\tilde{\nu}'_{66}$)
3074.1325 3048.4088 1509.2821 1421.5496 1381.1242
1305.0277 1170.0600 1133.1663 1006.4406 791.1413
579.4029

A.3.1. Maximum mode excitation numbers

- a_g

0 K

Tol. set	Max. quantum numbers	$[\tilde{\nu}_{\min}^{(a_g)},\tilde{\nu}_{\max}^{(a_g)}]$	# of integrals
I	$< 1\,1\,1\,4\,4\,6\,2\,3\,2\,2\,3\,5\,\|\,0\,0\,0\,0\,0\,0\,0\,0\,0\,0\,0\,0 >$	[0.00, 29674.45]	447452
II	$< 1\,0\,0\,3\,3\,5\,2\,3\,2\,2\,2\,4\,\|\,0\,0\,0\,0\,0\,0\,0\,0\,0\,0\,0\,0 >$	[0.00, 22273.47]	42604
III	$< 0\,0\,0\,3\,2\,4\,1\,2\,1\,1\,1\,3\,\|\,0\,0\,0\,0\,0\,0\,0\,0\,0\,0\,0\,0 >$	[0.00, 15229.64]	2389

100 K

Tol. set	Max. quantum numbers	$[\tilde{\nu}_{\min}^{(a_g)},\tilde{\nu}_{\max}^{(a_g)}]$	# of integrals
I	$< 1\,1\,1\,4\,4\,6\,2\,3\,2\,2\,3\,5\,\|\,0\,0\,0\,0\,0\,0\,0\,0\,0\,1\,1\,2 >$	[−2122.75, 29674.45]	1177589
II	$< 1\,0\,0\,3\,3\,5\,2\,3\,2\,2\,2\,4\,\|\,0\,0\,0\,0\,0\,0\,0\,0\,0\,0\,1\,1 >$	[−1003.67, 22273.47]	70326
III	$< 0\,0\,0\,3\,2\,4\,1\,2\,1\,1\,1\,3\,\|\,0\,0\,0\,0\,0\,0\,0\,0\,0\,0\,0\,1 >$	[−383.76, 15229.64]	3151

300 K

Tol. set	Max. quantum numbers	$[\tilde{\nu}_{\min}^{(a_g)},\tilde{\nu}_{\max}^{(a_g)}]$	# of integrals
II	$< 1\,0\,0\,3\,3\,5\,2\,3\,2\,2\,3\,7\,\|\,0\,0\,0\,1\,1\,1\,1\,1\,1\,2\,3\,5 >$	[−11997.66, 29381.11]	77641163
III	$< 0\,0\,0\,3\,2\,4\,1\,2\,1\,2\,2\,5\,\|\,0\,0\,0\,0\,0\,1\,1\,1\,1\,1\,2\,3 >$	[−7141.55, 18572.66]	508664

500 K

Tol. set	Max. quantum numbers	$[\tilde{\nu}_{\min}^{(a_g)},\tilde{\nu}_{\max}^{(a_g)}]$	# of integrals
III	$< 0\,0\,0\,3\,3\,4\,2\,2\,2\,3\,3\,8\,\|\,0\,0\,0\,1\,1\,1\,1\,2\,2\,3\,3\,6 >$	[−16249.92, 28114.37]	341185395

- b_{1g}

0 K

Tol. set	Max. quantum numbers	$[\tilde{\nu}_{\min}^{(b_{1g})},\tilde{\nu}_{\max}^{(b_{1g})}]$	# of integrals
I	$< 1\,1\,2\,2\,1\,1\,1\,2\,2\,2\,2\,\|\,0\,0\,0\,0\,0\,0\,0\,0\,0\,0\,0 >$	[0.00, 6105.59]	148
II	$< 0\,0\,2\,2\,1\,1\,1\,2\,1\,1\,1\,\|\,0\,0\,0\,0\,0\,0\,0\,0\,0\,0\,0 >$	[0.00, 5921.34]	76
III	$< 0\,0\,0\,1\,0\,0\,0\,1\,0\,0\,0\,\|\,0\,0\,0\,0\,0\,0\,0\,0\,0\,0\,0 >$	[0.00, 2510.60]	4

100 K

Tol. set	Max. quantum numbers	$[\tilde{\nu}_{\min}^{(b_{1g})},\tilde{\nu}_{\max}^{(b_{1g})}]$	# of integrals
I	$< 1\,1\,2\,2\,1\,1\,1\,2\,2\,2\,2\,\|\,0\,0\,0\,0\,0\,0\,0\,0\,0\,1\,2 >$	[−1282.25, 12026.93]	5013
II	$< 0\,0\,2\,2\,1\,1\,1\,2\,1\,1\,1\,\|\,0\,0\,0\,0\,0\,0\,0\,0\,0\,1\,1 >$	[−899.78, 5921.34]	103
III	$< 0\,0\,0\,1\,0\,0\,0\,1\,0\,0\,1\,\|\,0\,0\,0\,0\,0\,0\,0\,0\,0\,0\,1 >$	[−382.48, 2510.60]	11

300 K

Tol. set	Max. quantum numbers	$[\tilde{\nu}_{\min}^{(\mathrm{b_{1g}})},\tilde{\nu}_{\max}^{(\mathrm{b_{1g}})}]$	# of integrals
II	$<\ 0\ 0\ 2\ 2\ 1\ 1\ 1\ 2\ 2\ 3\ 5\ \mid\ 0\ 0\ 1\ 1\ 1\ 1\ 1\ 1\ 2\ 3\ 5\ >$	$[-9784.98, 13179.08]$	931984
III	$<\ 0\ 0\ 1\ 1\ 1\ 1\ 1\ 1\ 1\ 2\ 3\ \mid\ 0\ 0\ 0\ 0\ 1\ 1\ 1\ 1\ 1\ 2\ 3\ >$	$[-4929.39, 5569.18]$	7523

500 K

Tol. set	Max. quantum numbers	$[\tilde{\nu}_{\min}^{(\mathrm{b_{1g}})},\tilde{\nu}_{\max}^{(\mathrm{b_{1g}})}]$	# of integrals
III	$<\ 0\ 0\ 1\ 1\ 1\ 1\ 2\ 2\ 2\ 4\ 6\ \mid\ 0\ 0\ 1\ 1\ 1\ 1\ 2\ 2\ 2\ 4\ 6\ >$	$[-15190.97, 14798.85]$	17892000

- $\mathrm{b_{2g}}$

0 K

Tol. set	Max. quantum numbers	$[\tilde{\nu}_{\min}^{(\mathrm{b_{2g}})},\tilde{\nu}_{\max}^{(\mathrm{b_{2g}})}]$	# of integrals
I	$<\ 2\ 2\ 3\ 2\ \mid\ 0\ 0\ 0\ 0\ >$	$[0.00, 4274.30]$	84
II	$<\ 2\ 2\ 2\ 1\ \mid\ 0\ 0\ 0\ 0\ >$	$[0.00, 3053.99]$	26
III	$<\ 2\ 1\ 2\ 0\ \mid\ 0\ 0\ 0\ 0\ >$	$[0.00, 2487.58]$	14

100 K

Tol. set	Max. quantum numbers	$[\tilde{\nu}_{\min}^{(\mathrm{b_{2g}})},\tilde{\nu}_{\max}^{(\mathrm{b_{2g}})}]$	# of integrals
I	$<\ 2\ 2\ 3\ 3\ \mid\ 0\ 1\ 1\ 3\ >$	$[-1872.75, 4937.16]$	1053
II	$<\ 2\ 2\ 2\ 2\ \mid\ 0\ 0\ 1\ 2\ >$	$[-910.77, 4309.43]$	342
III	$<\ 2\ 1\ 2\ 2\ \mid\ 0\ 0\ 1\ 2\ >$	$[-910.77, 2487.58]$	52

300 K

Tol. set	Max. quantum numbers	$[\tilde{\nu}_{\min}^{(\mathrm{b_{2g}})},\tilde{\nu}_{\max}^{(\mathrm{b_{2g}})}]$	# of integrals
II	$<\ 2\ 2\ 4\ 8\ \mid\ 2\ 2\ 4\ 8\ >$	$[-6961.30, 6448.68]$	102585
III	$<\ 2\ 2\ 3\ 6\ \mid\ 1\ 1\ 3\ 6\ >$	$[-4391.41, 5600.01]$	21744

500 K

Tol. set	Max. quantum numbers	$[\tilde{\nu}_{\min}^{(\mathrm{b_{2g}})},\tilde{\nu}_{\max}^{(\mathrm{b_{2g}})}]$	# of integrals
III	$<\ 2\ 3\ 5\ 10\ \mid\ 2\ 3\ 5\ 10\ >$	$[-8609.29, 7987.33]$	537264

- $\mathrm{b_{3g}}$

0 K

Tol. set	Max. quantum numbers	$[\tilde{\nu}_{\min}^{(\mathrm{b_{3g}})},\tilde{\nu}_{\max}^{(\mathrm{b_{3g}})}]$	# of integrals
I	$<\ 2\ 2\ 3\ 4\ 8\ 9\ \mid\ 0\ 0\ 0\ 0\ 0\ 0\ >$	$[0.00, 8153.60]$	6456
II	$<\ 2\ 1\ 2\ 2\ 6\ 7\ \mid\ 0\ 0\ 0\ 0\ 0\ 0\ >$	$[0.00, 6264.88]$	1744
III	$<\ 1\ 1\ 2\ 2\ 4\ 5\ \mid\ 0\ 0\ 0\ 0\ 0\ 0\ >$	$[0.00, 3568.55]$	352

100 K

Tol. set	Max. quantum numbers	$[\tilde{\nu}_{\min}^{(\mathrm{b_{3g}})},\tilde{\nu}_{\max}^{(\mathrm{b_{3g}})}]$	# of integrals
I	$<\ 2\ 2\ 3\ 4\ 8\ 10\ \mid\ 0\ 0\ 0\ 1\ 1\ 3\ >$	$[-2004.73, 8307.08]$	20090
II	$<\ 2\ 1\ 2\ 2\ 6\ 7\ \mid\ 0\ 0\ 0\ 0\ 1\ 2\ >$	$[-1055.37, 6264.88]$	4248
III	$<\ 1\ 1\ 2\ 2\ 4\ 5\ \mid\ 0\ 0\ 0\ 0\ 0\ 1\ >$	$[-253.12, 3568.55]$	455

300 K

Tol. set	Max. quantum numbers	$[\tilde{\nu}_{\min}^{(\mathrm{b_{3g}})},\tilde{\nu}_{\max}^{(\mathrm{b_{3g}})}]$	# of integrals
II	$<\ 2\ 2\ 3\ 4\ 8\ 11\ \mid\ 2\ 2\ 2\ 2\ 3\ 7\ >$	$[-10023.65, 11846.69]$	7834000
III	$<\ 1\ 1\ 2\ 3\ 5\ 8\ \mid\ 1\ 1\ 1\ 2\ 2\ 5\ >$	$[-6362.30, 7524.54]$	224945

500 K

Tol. set	Max. quantum numbers	$[\tilde{\nu}_{\min}^{(\mathrm{b_{3g}})},\tilde{\nu}_{\max}^{(\mathrm{b_{3g}})}]$	# of integrals
III	$<\ 2\ 3\ 3\ 4\ 7\ 11\ \mid\ 2\ 2\ 2\ 3\ 4\ 9\ >$	$[-11775.25, 12359.26]$	36790704

- a_u

  0 K

Tol. set	Max. quantum numbers	$[\tilde{\nu}_{\min}^{(a_u)}, \tilde{\nu}_{\max}^{(a_u)}]$	# of integrals
I	$< 2\ 2\ 4\ 2\ 2\ \|\ 0\ 0\ 0\ 0\ 0 >$	$[0.00, 5258.90]$	197
II	$< 2\ 2\ 4\ 2\ 2\ \|\ 0\ 0\ 0\ 0\ 0 >$	$[0.00, 3712.73]$	69
III	$< 1\ 1\ 2\ 1\ 1\ \|\ 0\ 0\ 0\ 0\ 0 >$	$[0.00, 1856.37]$	21

  100 K

Tol. set	Max. quantum numbers	$[\tilde{\nu}_{\min}^{(a_u)}, \tilde{\nu}_{\max}^{(a_u)}]$	# of integrals
I	$< 2\ 2\ 4\ 2\ 7\ \|\ 0\ 0\ 1\ 1\ 6 >$	$[-1857.35, 6924.35]$	14288
II	$< 2\ 2\ 4\ 2\ 5\ \|\ 0\ 0\ 0\ 1\ 5 >$	$[-1049.62, 6184.49]$	3188
III	$< 1\ 1\ 2\ 1\ 4\ \|\ 0\ 0\ 0\ 1\ 4 >$	$[-934.68, 3092.24]$	678

  300 K

Tol. set	Max. quantum numbers	$[\tilde{\nu}_{\min}^{(a_u)}, \tilde{\nu}_{\max}^{(a_u)}]$	# of integrals
II	$< 2\ 2\ 4\ 4\ 16\ \|\ 2\ 2\ 2\ 4\ 16 >$	$[-8661.46, 8801.18]$	3877511
III	$< 1\ 2\ 3\ 3\ 12\ \|\ 1\ 1\ 2\ 3\ 12 >$	$[-5958.20, 6555.11]$	284832

  500 K

Tol. set	Max. quantum numbers	$[\tilde{\nu}_{\min}^{(a_u)}, \tilde{\nu}_{\max}^{(a_u)}]$	# of integrals
III	$< 2\ 3\ 4\ 5\ 21\ \|\ 2\ 2\ 3\ 5\ 20 >$	$[-10288.93, 10565.53]$	24088320

- b_{1u}

  0 K

Tol. set	Max. quantum numbers	$[\tilde{\nu}_{\min}^{(b_{1u})}, \tilde{\nu}_{\max}^{(b_{1u})}]$	# of integrals
I	$< 2\ 2\ 2\ 4\ 4\ 2\ \|\ 0\ 0\ 0\ 0\ 0\ 0 >$	$[0.00, 4802.84]$	473
II	$< 2\ 2\ 2\ 2\ 2\ 2\ \|\ 0\ 0\ 0\ 0\ 0\ 0 >$	$[0.00, 3251.94]$	73
III	$< 2\ 0\ 1\ 2\ 2\ 1\ \|\ 0\ 0\ 0\ 0\ 0\ 0 >$	$[0.00, 2441.37]$	34

  100 K

Tol. set	Max. quantum numbers	$[\tilde{\nu}_{\min}^{(b_{1u})}, \tilde{\nu}_{\max}^{(b_{1u})}]$	# of integrals
I	$< 2\ 2\ 2\ 4\ 4\ 9\ \|\ 0\ 0\ 1\ 1\ 2\ 9 >$	$[-2682.22, 7379.50]$	103320
II	$< 2\ 2\ 2\ 2\ 3\ 7\ \|\ 0\ 0\ 0\ 1\ 1\ 7 >$	$[-1431.03, 5527.32]$	8973
III	$< 2\ 0\ 1\ 2\ 2\ 5\ \|\ 0\ 0\ 0\ 1\ 1\ 5 >$	$[-1256.97, 3729.69]$	2307

  300 K

Tol. set	Max. quantum numbers	$[\tilde{\nu}_{\min}^{(b_{1u})}, \tilde{\nu}_{\max}^{(b_{1u})}]$	# of integrals
II	$< 2\ 2\ 2\ 4\ 6\ 22\ \|\ 2\ 2\ 2\ 4\ 5\ 22 >$	$[-10541.88, 9757.43]$	119774634
III	$< 2\ 1\ 2\ 3\ 4\ 16\ \|\ 1\ 1\ 2\ 3\ 3\ 16 >$	$[-7053.06, 7489.96]$	5195308

  500 K

Tol. set	Max. quantum numbers	$[\tilde{\nu}_{\min}^{(b_{1u})}, \tilde{\nu}_{\max}^{(b_{1u})}]$	# of integrals
III	$< 2\ 2\ 3\ 5\ 7\ 27\ \|\ 2\ 2\ 3\ 5\ 6\ 27 >$	$[-12507.99, 11535.72]$	1557855504

- b$_{2u}$

0 K

Tol. set	Max. quantum numbers	$[\tilde{\nu}_{\min}^{(b_{2u})},\tilde{\nu}_{\max}^{(b_{2u})}]$	# of integrals
I	$<$ 1 1 0 2 2 1 2 2 2 1 2 $\mid$ 0 0 0 0 0 0 0 0 0 0 0 $>$	[0.00, 6135.20]	131
II	$<$ 0 0 0 1 1 1 2 2 1 1 1 $\mid$ 0 0 0 0 0 0 0 0 0 0 0 $>$	[0.00, 4643.73]	54
III	$<$ 0 0 0 1 0 0 0 1 0 0 0 $\mid$ 0 0 0 0 0 0 0 0 0 0 0 $>$	[0.00, 2620.39]	4

100 K

Tol. set	Max. quantum numbers	$[\tilde{\nu}_{\min}^{(b_{2u})},\tilde{\nu}_{\max}^{(b_{2u})}]$	# of integrals
I	$<$ 1 1 0 2 2 1 2 2 2 1 3 $\mid$ 0 0 0 0 0 0 0 0 0 1 3 $>$	[−1320.67, 11995.95]	5571
II	$<$ 0 0 0 1 1 1 2 2 1 1 2 $\mid$ 0 0 0 0 0 0 0 0 0 1 2 $>$	[−1093.01, 6180.99]	418
III	$<$ 0 0 0 1 0 0 0 1 0 0 2 $\mid$ 0 0 0 0 0 0 0 0 0 0 2 $>$	[−455.33, 2620.39]	20

300 K

Tol. set	Max. quantum numbers	$[\tilde{\nu}_{\min}^{(b_{2u})},\tilde{\nu}_{\max}^{(b_{2u})}]$	# of integrals
II	$<$ 0 0 0 1 1 1 2 2 2 3 8 $\mid$ 0 0 0 1 1 1 1 1 2 3 8 $>$	[−9833.64, 11662.14]	888980
III	$<$ 0 0 0 1 1 1 1 1 1 2 6 $\mid$ 0 0 0 0 1 1 1 1 1 2 6 $>$	[−5362.79, 5579.43]	12618

500 K

Tol. set	Max. quantum numbers	$[\tilde{\nu}_{\min}^{(b_{2u})},\tilde{\nu}_{\max}^{(b_{2u})}]$	# of integrals
III	$<$ 0 0 0 1 1 1 1 2 2 3 10 $\mid$ 0 0 0 1 1 1 1 2 2 3 10 $>$	[−13798.59, 13538.34]	8411337

- b$_{3u}$

0 K

Tol. set	Max. quantum numbers	$[\tilde{\nu}_{\min}^{(b_{3u})},\tilde{\nu}_{\max}^{(b_{3u})}]$	# of integrals
I	$<$ 1 1 2 1 2 2 2 1 2 1 2 $\mid$ 0 0 0 0 0 0 0 0 0 0 0 $>$	[0.00, 9141.11]	738
II	$<$ 0 0 1 1 2 2 1 1 1 1 2 $\mid$ 0 0 0 0 0 0 0 0 0 0 0 $>$	[0.00, 5372.30]	76
III	$<$ 0 0 0 0 1 1 1 0 1 0 0 $\mid$ 0 0 0 0 0 0 0 0 0 0 0 $>$	[0.00, 2686.15]	11

100 K

Tol. set	Max. quantum numbers	$[\tilde{\nu}_{\min}^{(b_{3u})},\tilde{\nu}_{\max}^{(b_{3u})}]$	# of integrals
I	$<$ 1 1 2 1 2 2 2 1 2 1 2 $\mid$ 0 0 0 0 0 0 0 0 0 1 1 $>$	[−1386.17, 9141.11]	1052
II	$<$ 0 0 1 1 2 2 1 1 1 1 2 $\mid$ 0 0 0 0 0 0 0 0 0 0 1 $>$	[−596.09, 5372.30]	89
III	$<$ 0 0 0 0 1 1 1 0 1 0 0 $\mid$ 0 0 0 0 0 0 0 0 0 0 0 $>$	[0.00, 2686.15]	11

300 K

Tol. set	Max. quantum numbers	$[\tilde{\nu}_{\min}^{(b_{3u})},\tilde{\nu}_{\max}^{(b_{3u})}]$	# of integrals
II	$<$ 0 0 1 1 2 2 2 1 2 2 3 $\mid$ 0 0 1 1 1 1 1 1 1 2 3 $>$	[−6314.68, 9725.31]	20098
III	$<$ 0 0 1 1 1 1 1 1 1 1 2 $\mid$ 0 0 0 1 1 1 1 1 1 1 2 $>$	[−5301.28, 5616.98]	4729

500 K

Tol. set	Max. quantum numbers	$[\tilde{\nu}_{\min}^{(b_{3u})},\tilde{\nu}_{\max}^{(b_{3u})}]$	# of integrals
III	$<$ 0 0 1 1 2 1 2 2 2 3 4 $\mid$ 0 0 1 1 1 1 2 2 2 3 4 $>$	[−12771.48, 14072.62]	1058422

A.3.2. Mode coupling error

M	$\epsilon_{\mathrm{c}}/\% = (1 - \widetilde{F}_{\mathrm{FC;c}}^{(M)})/\%$			
	$T = 0$ K(%)	$T = 100$ K(%)	$T = 300$ K(%)	$T = 500$ K(%)
0	81.82	90.72	99.84	100.00
1	45.93	72.40	99.50	100.00
2	18.11	51.10	98.20	99.99
3	5.51	30.67	95.95	99.97
4	1.31	15.99	91.41	99.90
5	0.24	7.23	84.91	99.76
6	0.04	2.81	75.77	99.42
7	0.00	0.96	64.92	98.85
8		0.28	52.98	97.73
9		0.07	41.10	96.07
10		0.02	30.27	93.38
11		0.00	21.09	89.79
12			13.96	84.82
13			8.72	78.81
14			5.19	71.55
15			2.91	63.55
16			1.56	54.94
17			0.79	46.28
18			0.38	37.85
19			0.18	30.08
20			0.08	23.19
21			0.03	17.34
22			0.01	12.57
23			0.00	8.84
24				6.02
25				3.98
26				2.55
27				1.58
28				0.95
29				0.56
30				0.32
31				0.17
32				0.09
33				0.05
34				0.03
35				0.01
36				0.01
37				0.00

B. Supplementary data for chapter 5

B.1. General remarks

In this appendix we report vertical transition, peak maximum, cumulants of vibronic transition energies, corresponding to figures 5.1 and 5.2. Cumulans are computed via and the method described in Sec. 5.1.1 of this thesis. We added a variance of a Gaussian line shape function ($4.51E+04$ $(hc_0\mathrm{cm}^{-1})^2$) to the second order cumulants to include the line shape to the statistics. And we provide equilibrium structures of (modified) bacteriochlorophyll and harmonic wavenumbers which are used for the calculations in section 5.3.2 and figure 1.2. The relevant data for figures 5.3, 5.4 and 5.6 are also provided in this appendix.

B.2. Formic acid

n	$\langle E^n_{\epsilon',\epsilon}\rangle^{\mathrm{c}}/(hc_0\mathrm{cm}^{-1})^{\mathrm{n}}$	
	$T = 0$ K	$T = 1000$ K
1	2.4197E+03	2.4130E+03
2	4.1926E+06	5.3965E+06
3	8.6790E+09	1.0320E+10
4	2.5221E+13	3.5786E+13
5	1.0062E+17	1.4515E+17
6	4.8832E+20	7.6078E+20
7	2.6660E+24	4.4214E+24
8	1.6154E+28	2.9387E+28
Vertical transition energy/$(hc_0\mathrm{cm}^{-1})$	2.3286E+03	2.3286E+03

B.3. Anthracene

n	$\langle E^n_{\epsilon',\epsilon}\rangle^{\mathrm{c}}/(hc_0\mathrm{cm}^{-1})^{\mathrm{n}}$	
	$T = 0$ K	$T = 500$ K
1	1.7657E+03	1.4946E+03
2	2.2815E+06	2.5229E+06
3	3.1553E+09	3.1617E+09
4	4.9080E+12	5.2116E+12
5	8.8569E+15	9.2295E+15
6	2.0027E+19	2.1892E+19
7	5.8643E+22	6.4247E+22
8	2.1280E+26	2.3674E+26
Vertical transition energy/$(hc_0\mathrm{cm}^{-1})$	1.5957E+03	1.5957E+03

B.4. Bacteriochlorophyll

- Harmonic vibrational wavenumbers of the initial electronic state in cm^{-1}:

  a(from $\tilde{\nu}_{162}$ to $\tilde{\nu}_1$)
  21.4557 25.2760 28.9246 35.9083 36.9274 55.0378 64.8232 78.6292 101.4081 110.1421 117.8279 129.2884 132.0941 141.7461 167.2401 171.5542 175.7069 186.0948 190.6627 216.3728 221.1104 232.5598 242.3415 251.1938 272.4438 285.1315 293.2799 319.4423 333.5508 343.0773 350.1340 375.3155 378.7104 408.4328 422.9386 433.6818 439.7590 444.4470 484.1491 524.9598 527.2614 543.5474 559.2862 572.1327 581.9131 612.2568 620.5894 634.8125 642.1622 655.1760 656.9652 675.5145 678.9407 688.1909 717.9663 720.0682 732.7538 735.4780 739.9762 742.7562 746.3043 762.0798 771.6862 777.8221 785.0985 808.5506 818.1191 820.2261 837.1350 840.6778 849.3824 859.0087 876.4723 884.1983 886.3528 911.6225

935.0293 937.2806 945.3227 948.6115 954.2098 956.4429 986.5676 990.0052 993.8284 1012.8991 1026.2299 1033.8934 1044.3209 1072.2985 1096.0683 1103.9634 1132.8693 1134.7095 1142.5179 1147.8039 1150.2906 1150.8844 1160.4601 1168.1541 1174.6808 1184.8494 1193.6330 1212.2979 1220.2899 1227.5304 1246.6922 1254.1699 1262.7627 1274.4224 1287.2967 1298.5147 1318.5625 1324.4651 1339.2505 1361.9833 1366.7085 1380.9141 1403.8590 1423.5844 1437.9237 1441.5442 1446.0721 1452.4917 1456.0822 1460.4679 1466.6235 1477.9717 1477.9926 1492.3057 1498.9438 1509.2878 1520.1494 1538.3528 1550.2263 1562.6400 1571.4999 1610.0767 1648.0236 1674.9175 1684.6337 1702.1374 2861.5879 3010.7520 3013.5222 3015.0308 3026.5882 3036.0644 3052.4533 3062.5547 3074.0909 3132.9584 3151.1517 3168.9883 3170.4017 3208.6810 3224.2968 3234.1183 3262.0423 3263.7019 3283.8211 3658.0584

- Harmonic vibrational wavenumbers of the final electronic state in cm^{-1}:

  a(from $\tilde{\nu}'_{162}$ to $\tilde{\nu}'_1$)
  24.1874 26.9493 28.1876 34.1241 42.3549 45.4448 59.7211 74.7635 86.5382 107.2859 118.0977 127.6239 131.6449 140.7447 165.8894 169.8607 172.0188 182.4159 187.5042 214.9788 220.1778 240.7945 247.6741 251.1979 272.3135 285.8508 300.4375 311.5338 336.6297 341.5927 355.7712 373.7130 382.8051 407.6117 431.4515 436.2209 441.4128 450.5279 485.5725 535.1172 552.5416 554.9939 565.6402 574.7885 597.1107 618.8413 626.0233 635.1243 647.7105 657.0271 662.0390 681.5670 683.4574 691.4158 723.1445 732.5825 739.4243 743.7289 743.9494 749.6568 762.9512 791.3647 813.0276 818.7360 820.4121 828.8282 840.7354 845.5062 861.3969 862.3159 877.4312 882.0767 886.4929 891.8679 892.1326 911.6777 936.8690 938.4925 948.4734 953.0589 958.2847 964.3568 988.5890 996.9944 1003.1644 1009.5575 1020.0180 1024.6730 1048.3166 1078.1472 1090.9059 1113.2551 1140.7534 1148.7002 1152.0833 1156.3096 1161.4099 1164.5131 1166.3020 1170.3287 1180.0757 1188.7186 1197.6781 1216.9217 1227.1321 1247.8446 1256.8131 1266.8484 1272.8347 1278.0447 1288.9878 1306.7606 1333.3498 1336.6701 1345.5470 1361.0684 1371.3230 1398.2680 1413.3843 1429.7560 1444.4840 1445.4825 1450.2790 1454.7084 1456.3188 1461.1588 1469.0316 1478.2566 1495.3556 1502.3581 1505.2608 1517.8413 1551.0598 1560.2710 1564.3924 1570.3108 1574.7650 1603.7168 1640.9509 1697.1686 1732.1366 1762.3276 2898.5810 3028.8494 3035.8380 3038.0599 3044.9258 3057.8497 3063.4126 3066.0358 3084.8592 3144.9878 3168.8037 3181.6048 3184.4366 3222.8470 3237.2230 3242.5729 3267.1586 3268.8032 3289.5138 3648.6472

- Equilibrium structure of initial state:

Atom	x/Å	y/Å	z/Å
C	-0.434498854852	-2.992831300387	-0.994103540802
N	-0.009467710721	-2.064288379190	-0.070579215362
C	0.493763232230	-2.738656770068	0.939796945149
N	0.410885417668	-4.072402934786	0.707580306356
C	-0.181986811386	-4.250741242313	-0.528476940408
Mg	-0.053998117393	0.151635987704	-0.144093317610
N	1.938804465600	0.481968071483	-0.872801132227
C	2.232792598342	0.547939302586	-2.191180214269
C	3.737277895993	0.632837853258	-2.398711043726
C	4.278669510770	0.582690323602	-0.986386706220
C	3.089526772676	0.522591424747	-0.103578992636
C	1.337503464580	0.552072411320	-3.242093558435
C	-0.083309191632	0.530412606218	-3.194664398762
C	-0.985250798797	0.587172481089	-4.321758675582
C	-2.281621820826	0.552451611674	-3.782913326106
C	-2.151544103423	0.480990370251	-2.386146312018
N	-0.809508270416	0.458073320356	-2.044427433816
C	-3.222880741458	0.445450956127	-1.446446254848
C	-3.170279501131	0.436844813936	-0.072010491604
C	-4.420118691099	0.386539895897	0.803334127554
C	-3.873640028443	0.669231631642	2.213824961248
C	-2.371101799635	0.526980506490	2.030331055067
N	-2.048774261585	0.443327298832	0.698554656402
C	-1.436563928910	0.532778833308	3.031056884035
C	-0.031210084025	0.509101560464	2.827255660360
C	0.732547923376	0.589676727449	4.013906098101
C	-0.173399147446	0.657925211219	5.140322048425
C	-1.621412583032	0.638753343921	4.537693498982
N	0.736470518920	0.452782775242	1.731529098898
C	2.049659771243	0.514627571610	2.181820377892
C	2.080025654341	0.589816052326	3.598213702439
C	3.144719755327	0.522514047456	1.272362019769
O	0.048911772579	0.718503534201	6.344608644967
C	-0.631934175286	0.663433419304	-5.710999424125
O	-1.414393884188	0.693148093357	-6.660576222774
H	-4.114004101626	1.686844725087	2.540565424908
H	-4.871492191282	-0.609651550302	0.745650565830
H	-3.203066400592	0.588923409834	-4.343386758380
H	0.458110771733	0.696307940568	-5.921066786207
H	4.106190711491	-0.193952311085	-3.012612427492
C	5.572258586092	0.587755001004	-0.648123205426
H	2.969354794469	0.658713664737	4.206509727466
H	-2.173665906520	-0.200230766272	4.975678624539
H	-0.360832890192	-5.225902567758	-0.945923157378
H	0.729496353472	-4.797322476842	1.328530714143
H	0.918077482330	-2.302789197488	1.829933464530
H	-0.887080928512	-2.686236301828	-1.922185559456
H	-4.215170180060	0.445175264573	-1.885667853648
H	1.777706499418	0.609703242031	-4.230224889374
H	4.130561281940	0.569921251407	1.720015408259
H	-5.178258262203	1.102883516671	0.481342299161
H	4.015813950010	1.561254312523	-2.906647014966
H	-2.138516248005	1.552965518617	4.850292599873
H	-4.264788809356	-0.009316133017	2.974812058519
H	5.896780688009	0.549508416469	0.384591503685
H	6.351078098613	0.633358557154	-1.400866597535

- Equilibrium structure of final state:

Atom	x/Å	y/Å	z/Å
C	-0.464765173796	-3.017840623633	-1.045255432584
N	-0.012106100103	-2.132948476621	-0.088725406280
C	0.484538265696	-2.862082357245	0.890707433228
N	0.369579638324	-4.179567646169	0.604402016111
C	-0.235484039177	-4.296602303081	-0.630360702484
Mg	-0.040440457336	0.055275000151	-0.128994320982
N	1.961164707501	0.452231443488	-0.866521218987
C	2.253465813231	0.525126867411	-2.177585234408
C	3.751072436489	0.638683982532	-2.393977439861
C	4.290265247161	0.623437454132	-0.979431038307
C	3.099913374371	0.534427992150	-0.102966846205
C	1.336457642831	0.526625948073	-3.222976250263
C	-0.066174337164	0.505688215924	-3.158175524127
C	-0.977223156103	0.590898930700	-4.287866413884
C	-2.251446545482	0.567912133179	-3.763594596221
C	-2.124955860590	0.471782206105	-2.345532859347
N	-0.793615165390	0.423247443197	-2.007925438376
C	-3.199359825707	0.456637257431	-1.439388466409
C	-3.168879120420	0.445531309613	-0.052214928242
C	-4.428382208744	0.497757088284	0.802776119190
C	-3.877187393652	0.604008021202	2.238654841419
C	-2.377046815970	0.492461972457	2.037276418478
N	-2.058894136006	0.403999313162	0.713785291589
C	-1.422416878793	0.523227459100	3.032164604518
C	-0.032200650075	0.510632096202	2.817283190114
C	0.739104996322	0.655703042191	4.000526514973
C	-0.181434150927	0.744056163406	5.138128512796
C	-1.622791412784	0.663639746872	4.534504307157
N	0.736751763547	0.431259409942	1.722704270743
C	2.040223860681	0.546015523211	2.164676286954
C	2.065140184113	0.678121198347	3.596788669762
C	3.136061721567	0.563434275650	1.282892596219
O	0.053689982995	0.853445290833	6.323088862598
C	-0.631002124807	0.691444168043	-5.700068555497
O	-1.439469582918	0.735339306486	-6.609029787095
H	-4.132529082090	1.556942551865	2.709747361233
H	-5.025444980548	-0.406041875619	0.656398738219
H	-3.172842896684	0.627315547877	-4.322237227969
H	0.452005502531	0.727393580742	-5.931635194842
H	4.132375746649	-0.192732190585	-2.993457595021
C	5.575126668246	0.675339978083	-0.623279675542
H	2.951982852412	0.793854591637	4.200888680691
H	-2.150668536554	-0.181117976132	4.988186306810
H	-0.439218128423	-5.250107709802	-1.084436574640
H	0.676182459962	-4.938300735898	1.191864265170
H	0.925535880757	-2.479119351820	1.796288649718
H	-0.918845080323	-2.672356035480	-1.958288928005
H	-4.184130608916	0.498586315029	-1.891020389269
H	1.766512905864	0.593850048851	-4.214521375648
H	4.113678723698	0.652999275775	1.740046766164
H	-5.059600467848	1.344884435600	0.528571181440
H	4.008024847843	1.561545362192	-2.921591463272
H	-2.172448470662	1.567408686737	4.815939489059
H	-4.252351199772	-0.182917089396	2.896467909392
H	5.886933247237	0.660156016189	0.413469067298
H	6.363314304585	0.737272903551	-1.363668012035

- Fig. 5.3
  Reorganization energy $(\frac{1}{2}\underline{\delta}^{\mathrm{t}}\mathrm{diag}(\underline{\epsilon}')\underline{\delta})$=1.0794E+03 $hc_0\mathrm{cm}^{-1}$

Temperature	Cumulants	With Duschinsky rotation	Without Duschinsky rotation
0 K	Mean/cm^{-1}	1.5376E+03	1.0925E+03
	Variance/(cm^{-1})^2	2.9747E+06	1.4364E+06
100 K	Mean/cm^{-1}	1.8719E+03	1.0945E+03
	Variance/(cm^{-1})^2	4.1002E+06	1.4475E+06
200 K	Mean/cm^{-1}	2.4059E+03	1.0922E+03
	Variance/(cm^{-1})^2	6.4085E+06	1.4730E+06
300 K	Mean/cm^{-1}	2.9790E+03	1.1021E+03
	Variance/(cm^{-1})^2	9.4091E+06	1.5125E+06

• Mean excitation energies of individual vibrational modes

n	$\epsilon'_n \langle v'_n \rangle / (hc_0 \mathrm{cm}^{-1})$								
	Displaced-Distorted-Rotated				Displaced-Distorted				Displaced
	T=0 K	T=100 K	T=200 K	T=300 K	T=0 K	T=100 K	T=200 K	T=300 K	$\frac{1}{2}\epsilon'_n \delta_n^2$
162	1.5286E+00	6.6919E+01	1.4359E+02	2.2049E+02	1.1303E+00	6.8491E+01	1.4709E+02	2.2591E+02	1.0433E+00
161	6.6743E+00	6.7477E+01	1.4059E+02	2.1400E+02	6.2762E+00	6.7848E+01	1.4170E+02	2.1582E+02	6.2485E+00
160	1.9896E+00	5.6616E+01	1.2409E+02	1.9195E+02	5.1148E-01	5.5143E+01	1.2241E+02	1.9000E+02	5.0679E-01
159	8.8038E-01	5.1424E+01	1.1687E+02	1.8281E+02	8.2872E-01	5.1345E+01	1.1675E+02	1.8264E+02	8.0656E-01
158	3.5437E+01	8.9743E+01	1.6249E+02	2.3606E+02	3.2954E+01	9.3931E+01	1.7346E+02	2.5362E+02	3.2755E+01
157	1.2459E+01	5.4406E+01	1.1550E+02	1.7780E+02	8.6561E+00	4.0021E+01	9.0021E+01	1.4123E+02	7.2078E+00
156	9.1676E+00	5.6654E+01	1.2807E+02	2.0093E+02	7.3831E+00	5.7006E+01	1.3073E+02	2.0575E+02	7.2835E+00
155	4.7360E+00	4.2196E+01	1.0699E+02	1.7406E+02	3.7860E+00	3.9438E+01	1.0221E+02	1.6722E+02	3.7385E+00
154	4.9826E+00	3.9446E+01	1.0387E+02	1.7132E+02	3.5450E+00	3.0085E+01	8.5130E+01	1.4345E+02	2.9999E+00
153	1.7002E+01	4.4860E+01	1.0611E+02	1.7170E+02	1.6564E+01	4.4240E+01	1.0537E+02	1.7078E+02	1.6546E+01
152	2.8010E+00	3.0047E+01	9.2756E+01	1.6047E+02	2.2914E+00	2.8841E+01	9.0812E+01	1.5776E+02	2.2912E+00
151	3.0413E+00	2.6311E+01	8.5473E+01	1.5047E+02	2.6706E+00	2.6198E+01	8.5835E+01	1.5125E+02	2.6653E+00
150	5.0483E+00	2.8412E+01	8.8482E+01	1.5463E+02	4.8366E+00	2.7975E+01	8.7820E+01	1.5372E+02	4.8362E+00
149	1.4369E+00	2.2731E+01	8.1333E+01	1.4674E+02	8.8933E-01	2.1940E+01	8.0302E+01	1.4547E+02	8.8756E-01
148	9.4070E-01	1.7046E+01	7.0862E+01	1.3371E+02	3.3676E-01	1.6775E+01	7.1523E+01	1.3519E+02	3.3403E-01
147	3.2511E+00	1.9262E+01	7.3474E+01	1.3700E+02	2.7767E+00	1.8502E+01	7.2526E+01	1.3582E+02	2.7726E+00
146	4.3164E+00	1.9848E+01	7.3385E+01	1.3645E+02	3.9881E+00	1.8912E+01	7.1738E+01	1.3408E+02	3.9688E+00
145	8.0960E+00	2.2385E+01	7.4934E+01	1.3785E+02	7.5051E+00	2.0066E+01	6.9577E+01	1.2962E+02	7.4159E+00
144	1.3695E+01	2.8096E+01	8.1642E+01	1.4586E+02	1.3355E+01	2.7195E+01	7.9984E+01	1.4346E+02	1.3352E+01
143	2.5560E+00	1.3222E+01	6.1686E+01	1.2316E+02	1.6805E+00	1.1684E+01	5.9125E+01	1.1963E+02	1.6783E+00
142	3.4015E+00	1.0122E+01	5.7251E+01	1.1785E+02	2.2527E+00	9.7661E+00	5.6582E+01	1.1687E+02	2.2428E+00
141	7.0873E+00	9.3840E+00	5.5539E+01	1.1667E+02	3.8039E-01	9.1773E+00	5.6048E+01	1.1788E+02	3.0749E-01
140	1.0311E+00	9.5083E+00	5.4938E+01	1.1586E+02	4.5797E-02	7.8658E+00	5.2569E+01	1.1280E+02	1.6462E-02
139	4.5947E+00	1.2267E+01	5.5914E+01	1.1538E+02	4.2838E+00	1.1239E+01	5.3611E+01	1.1183E+02	4.2838E+00
138	7.2195E-01	6.8235E+00	4.6979E+01	1.0439E+02	2.8447E-05	5.5132E+00	4.4650E+01	1.0109E+02	1.2865E-05
137	1.7627E+01	2.3073E+01	6.1258E+01	1.1759E+02	1.7314E+01	2.2119E+01	5.9492E+01	1.1503E+02	1.7314E+01
136	1.2109E+01	1.7103E+01	5.5112E+01	1.1217E+02	1.1753E+01	1.6238E+01	5.3223E+01	1.0927E+02	1.1709E+01
135	9.6168E-01	4.4559E+00	3.6647E+01	8.8308E+01	6.9384E-01	3.8708E+00	3.5495E+01	8.6602E+01	6.4490E-01
134	2.6137E+00	5.9865E+00	3.7390E+01	8.9532E+01	2.2722E+00	5.0683E+00	3.5876E+01	8.7467E+01	2.2651E+00
133	1.3231E+00	4.6956E+00	3.5602E+01	8.7399E+01	6.8694E-01	3.1582E+00	3.2318E+01	8.2351E+01	6.8533E-01
132	3.0348E+00	5.9757E+00	3.6047E+01	8.7686E+01	2.4656E+00	4.7896E+00	3.3639E+01	8.4050E+01	2.4429E+00
131	5.5202E-01	2.9396E+00	2.9308E+01	7.7533E+01	7.6106E-02	1.7718E+00	2.7002E+01	7.4086E+01	7.4395E-02
130	1.0636E+00	3.1925E+00	2.9332E+01	7.7651E+01	1.2422E-02	1.6663E+00	2.6883E+01	7.4365E+01	1.3532E-03
129	4.8131E-01	1.8556E+00	2.3948E+01	6.8530E+01	2.4544E-01	1.3919E+00	2.3040E+01	6.7167E+01	2.4503E-01
128	1.2807E+00	2.7648E+00	2.4616E+01	6.9623E+01	4.5611E-01	1.4407E+00	2.2077E+01	6.5823E+01	4.1327E-01
127	4.8515E+00	6.2127E+00	2.6169E+01	6.8914E+01	4.5295E+00	5.3820E+00	2.4685E+01	6.6815E+01	4.5258E+00
126	4.3395E+00	5.3019E+00	2.4391E+01	6.6293E+01	4.1003E+00	4.8906E+00	2.3585E+01	6.5066E+01	4.0988E+00
125	1.0547E+00	2.1423E+00	2.1574E+01	6.4130E+01	3.7894E-01	1.1329E+00	1.9580E+01	6.1039E+01	3.5814E-01
124	4.0745E+00	4.7401E+00	1.9950E+01	5.7629E+01	3.8800E+00	4.3386E+00	1.9269E+01	5.6686E+01	3.8789E+00
123	6.8511E-01	1.1992E+00	1.3722E+01	4.8193E+01	2.6304E-01	4.3455E-01	1.0021E+01	3.9595E+01	1.9269E-03
122	5.9958E+00	6.6215E+00	1.8143E+01	5.1084E+01	5.5433E+00	5.8336E+00	1.8512E+01	5.4077E+01	5.1810E+00
121	8.7235E+00	9.7494E+00	2.1150E+01	5.3523E+01	8.4982E+00	8.7803E+00	2.1305E+01	5.6666E+01	8.1335E+00
120	8.8986E-01	1.2956E+00	1.4311E+01	5.0662E+01	2.3406E-01	4.6141E-01	1.1808E+01	4.5320E+01	9.5701E-03
119	7.4580E-01	1.0342E+00	1.0658E+01	4.0808E+01	1.9823E-02	1.7281E-01	9.5514E+00	3.9531E+01	1.6741E-02
118	3.6459E-01	3.9909E+00	1.3380E+01	4.3303E+01	3.9156E-01	5.2966E-01	9.6131E+00	3.9446E+01	2.9233E-01
117	9.8473E-01	3.4355E+00	1.3705E+01	4.2909E+01	1.0715E-01	1.8916E-01	7.3137E+00	3.3351E+01	1.0592E-01
116	3.9710E-01	6.0631E-01	8.4400E+00	3.5918E+01	9.5475E-02	1.8903E-01	7.8435E+00	3.5182E+01	1.8090E-02
115	4.1902E+00	5.7965E+00	1.4648E+01	4.2054E+01	3.3680E+00	3.4366E+00	1.0037E+01	3.5125E+01	3.3679E+00
114	1.1308E-01	2.3026E-01	6.7678E+00	3.1772E+01	1.3704E-02	7.6637E-02	6.4616E+00	3.1225E+01	1.7198E-03
113	1.7688E+00	5.5234E+00	1.6287E+01	4.4892E+01	4.5973E-01	5.1266E-01	6.4103E+00	3.0117E+01	4.5842E-01
112	2.2764E+01	2.3490E+01	3.0357E+01	5.5086E+01	2.2357E+01	2.2409E+01	2.8275E+01	5.1974E+01	2.2347E+01
111	4.5441E-01	6.1844E-01	6.1486E+00	2.8829E+01	4.8835E-02	8.9816E-02	5.3751E+00	2.7839E+01	3.5278E-02
110	1.3163E-01	1.9016E-01	5.4318E+00	2.7724E+01	3.1639E-02	7.0757E-02	5.2416E+00	2.7426E+01	2.4128E-02
109	4.5266E-01	5.7464E-01	5.6151E+00	2.7241E+01	2.6282E-02	6.0923E-02	4.9551E+00	2.6491E+01	2.2504E-02
108	5.5630E+00	6.6338E+00	1.2539E+01	3.3951E+01	4.3322E+00	4.3558E+00	8.4876E+00	2.8207E+01	4.3229E+00
107	1.2947E+00	1.6273E+00	5.8716E+00	2.5035E+01	9.9869E-01	1.0161E+00	4.5889E+00	2.2691E+01	9.8022E-01
106	1.5269E+01	1.6031E+01	2.0888E+01	4.0651E+01	1.4728E+01	1.4752E+01	1.8915E+01	3.8895E+01	1.4598E+01
105	6.1307E-01	7.4426E-01	4.6971E+00	2.3641E+01	2.5583E-01	2.7546E-01	4.0963E+00	2.3079E+01	2.1473E-01
104	4.3203E-01	5.0418E-01	4.6674E+00	2.4518E+01	1.4058E-01	1.5945E-01	3.9071E+00	2.2664E+01	1.1618E-01
103	3.8585E+01	3.9688E+01	4.5260E+01	6.5654E+01	3.7405E+01	3.7422E+01	4.1006E+01	5.9300E+01	3.7389E+01
102	8.5422E-01	1.3378E+00	5.5644E+00	2.4594E+01	4.3764E-01	4.5421E-01	4.0102E+00	2.2338E+01	3.4481E-01
101	1.0070E+01	1.2117E+01	1.8016E+01	3.7289E+01	8.6331E+00	8.6440E+00	1.1584E+01	2.8082E+01	8.5742E+00
100	2.2959E+01	2.3353E+01	2.6483E+01	4.2009E+01	2.2339E+01	2.2346E+01	2.4767E+01	3.9523E+01	2.2333E+01
99	2.3357E+00	2.4378E+00	5.9810E+00	2.4290E+01	4.2173E-01	4.3191E-01	3.3205E+00	1.9852E+01	6.1425E-02
98	7.3802E+00	7.7887E+00	1.1283E+01	2.8082E+01	4.2556E+00	4.2698E+00	7.6918E+00	2.6098E+01	3.1393E+00
97	1.9740E+00	2.1609E+00	5.7104E+00	2.3673E+01	1.1794E-01	1.1920E-01	4.4177E+00	2.2224E+01	1.2163E-01
96	3.9439E+00	3.9735E+00	6.6220E+00	2.2133E+01	1.1819E-01	1.2289E-01	2.1097E+00	1.5304E+01	1.1819E-01
95	9.7265E-02	1.5705E-01	2.1215E+00	1.4988E+01	2.1655E-02	2.5821E-02	1.9027E+00	1.4658E+01	1.7233E-02
94	9.4830E-01	2.3035E+00	5.8941E+00	2.0180E+01	8.7369E-01	8.8035E-01	3.2779E+00	1.8269E+01	3.0135E-01
93	1.5277E+00	1.6212E+00	4.2618E+00	1.9636E+01	2.2157E-01	2.2406E-01	1.6918E+00	1.2693E+01	5.8603E-02
92	1.6704E+00	1.7893E+00	4.4679E+00	1.9865E+01	1.0233E+00	1.0298E+00	3.4375E+00	1.8578E+01	2.5838E-02
91	1.3736E+01	1.4837E+01	1.8089E+01	3.1572E+01	1.3547E+01	1.3553E+01	1.5694E+01	2.9780E+01	1.2944E+01
90	1.5767E-01	1.7154E-01	1.7570E+00	1.3326E+01	2.4689E-01	2.5070E-01	2.0878E+00	1.4897E+01	2.7050E-02
89	2.4683E+00	5.3563E+00	1.1718E+01	2.8194E+01	8.1402E-02	8.4379E-02	1.7138E+00	1.3613E+01	1.3794E-02
88	1.0940E+00	1.1343E+00	3.3048E+00	1.7354E+01	2.1253E-02	2.1253E-02	1.5629E+00	1.3053E+01	7.9007E-04
87	6.5489E+00	6.9978E+00	9.0672E+00	2.0197E+01	5.8346E+00	5.8365E+00	7.1297E+00	1.7492E+01	5.8346E+00
86	1.3648E+00	3.6475E+00	7.8971E+00	2.0563E+01	3.0590E-01	3.0720E-01	1.4122E+00	1.0883E+01	3.0585E-01
85	1.0929E+00	1.3793E+00	2.8590E+00	1.2760E+01	8.7151E-01	8.7286E-01	1.9979E+00	1.1583E+01	8.6830E-01
84	6.5603E+00	1.2002E+01	2.1872E+01	4.0237E+01	2.3178E+00	2.3189E+00	3.3501E+00	1.2453E+01	2.3178E+00
83	4.4519E-01	5.9511E-01	1.9330E+00	1.1519E+01	1.1007E-01	1.1125E-01	1.1722E+00	1.0458E+01	9.4244E-02
82	6.3307E-01	8.3430E-01	2.1051E+00	1.1362E+01	3.7177E-01	3.7281E-01	1.3735E+00	1.0338E+01	3.6742E-01
81	2.0547E-01	2.2469E-01	1.2748E+00	1.0345E+01	4.5561E-02	4.6580E-02	1.0376E+00	9.9671E+00	2.9191E-02
80	1.0319E+01	1.1152E+01	1.3201E+01	2.2290E+01	9.6172E+00	9.6178E+00	1.0394E+01	1.8104E+01	9.6103E+00

79	3.6292E+01	7.0593E+01	1.2765E+02	1.9354E+02	1.0406E+01	1.0407E+01	1.1232E+01	1.9272E+01	1.0379E+01
78	2.9797E-01	3.4771E-01	1.2878E+00	9.5608E+00	7.8495E-02	7.9149E-02	8.8895E-01	8.8519E+00	3.4767E-02
77	3.4891E+00	3.8738E+00	5.2133E+00	1.2606E+01	2.0091E+00	2.0095E+00	2.6375E+00	9.4204E+00	1.9414E+00
76	4.5033E+00	7.9687E+00	1.3866E+01	2.6373E+01	1.8784E+00	1.8787E+00	2.4792E+00	9.0940E+00	1.8318E+00
75	3.7368E+00	4.0620E+00	5.2297E+00	1.2641E+01	7.4670E-02	7.5151E-02	7.7669E-01	8.0969E+00	4.0456E-02
74	1.2551E+01	1.5732E+01	2.1470E+01	3.3294E+01	9.8684E+00	9.8687E+00	1.0441E+01	1.6919E+01	9.8646E+00
73	5.0346E+00	5.9899E+00	7.7058E+00	1.4806E+01	4.4178E+00	4.4180E+00	4.8994E+00	1.0754E+01	4.4098E+00
72	2.3014E+00	2.7285E+00	3.8876E+00	1.0124E+01	1.3529E+00	1.3531E+00	1.7636E+00	7.0694E+00	1.3468E+00
71	1.0455E+00	1.1334E+00	1.6428E+00	6.9629E+00	6.2230E-01	6.2244E-01	1.0183E+00	6.2382E+00	6.0275E-01
70	2.9131E+01	2.9442E+01	3.0309E+01	3.5552E+01	2.8326E+01	2.8326E+01	2.8656E+01	3.3332E+01	2.8312E+01
69	2.5414E+00	6.3335E+00	1.1576E+01	2.0947E+01	9.8375E-01	9.8383E-01	1.2933E+00	5.7960E+00	9.7538E-01
68	1.4772E+01	1.5009E+01	1.5729E+01	2.0785E+01	1.4310E+01	1.4310E+01	1.4609E+01	1.9015E+01	1.4306E+01
67	4.7900E-01	5.1503E-01	9.3252E-01	5.6073E+00	3.0144E-02	3.0219E-02	3.2485E-01	4.6963E+00	2.2270E-02
66	7.0035E-01	7.8589E-01	1.3211E+00	6.0964E+00	1.0300E-01	1.0306E-01	3.7811E-01	4.5657E+00	1.0280E-01
65	1.1646E+01	1.1701E+01	1.2135E+01	1.6568E+01	1.1495E+01	1.1495E+01	1.1827E+01	1.6562E+01	1.1300E+01
64	2.6436E-01	2.8966E-01	6.2719E-01	5.0882E+00	8.8927E-02	8.9002E-02	3.8493E-01	4.7823E+00	3.7293E-02
63	7.5926E+00	7.6452E+00	8.0183E+00	1.2228E+01	7.2731E+00	7.2731E+00	7.5354E+00	1.1607E+01	7.2721E+00
62	5.0251E+00	1.7222E+01	3.3347E+01	5.3488E+01	4.7081E+00	4.7086E+00	7.2316E+00	4.7053E+00	4.6462E-01
61	2.0721E+00	2.3710E+00	3.1332E+00	7.4926E+00	1.1574E+00	1.1574E+00	1.3936E+00	5.2191E+00	1.1542E+00
60	1.6637E+00	1.8786E+00	2.4961E+00	6.6368E+00	9.2781E-01	9.2785E-01	1.1513E+00	4.8508E+00	9.2438E-01
59	5.7012E+00	5.8627E+00	6.3930E+00	1.0357E+01	5.2026E+00	5.2026E+00	5.4011E+00	8.8463E+00	5.1982E+00
58	2.4627E+00	2.6274E+00	3.0881E+00	6.7671E+00	2.0443E+00	2.0443E+00	2.2237E+00	5.4590E+00	2.0443E+00
57	2.3756E+00	2.4681E+00	2.8209E+00	6.3595E+00	1.2552E+00	1.2552E+00	1.4474E+00	4.8515E+00	1.0997E+00
56	3.0309E+00	3.1072E+00	3.3878E+00	6.5262E+00	2.6250E+00	2.6250E+00	2.7851E+00	5.8145E+00	2.6044E+00
55	6.6730E+00	6.7556E+00	7.0301E+00	9.9835E+00	6.0063E+00	6.0064E+00	6.1385E+00	8.8200E+00	5.9951E+00
54	1.3643E+00	1.4957E+00	1.8620E+00	4.9976E+00	9.3083E-01	9.3085E-01	1.0753E+00	3.9208E+00	9.1075E-01
53	9.7062E-01	1.0596E+00	1.3661E+00	4.4597E+00	6.6348E-01	6.6350E-01	8.1777E-01	3.7928E+00	5.4986E-01
52	2.7677E+00	6.0981E+00	1.0552E+01	1.7522E+01	1.1032E+00	1.1032E+00	1.2257E+00	3.7942E+00	1.1026E+00
51	2.1575E+00	2.2129E+00	2.4498E+00	5.1306E+00	1.5414E+00	1.5414E+00	1.6560E+00	4.1264E+00	1.5283E+00
50	9.1423E-01	9.6789E-01	1.1929E+00	3.6708E+00	4.1401E-01	4.1401E-01	5.1527E-01	2.8095E+00	3.7255E-01
49	5.2052E+00	5.2731E+00	5.5102E+00	7.9227E+00	4.7914E+00	4.7914E+00	4.8887E+00	7.1257E+00	4.7633E+00
48	1.8502E+01	1.8606E+01	1.8887E+01	2.1268E+01	1.7887E+01	1.7887E+01	1.7975E+01	2.0076E+01	1.7880E+01
47	4.2557E+00	6.4378E+00	9.3436E+00	1.4138E+01	3.2185E+00	3.2185E+00	3.2941E+00	5.2033E+00	3.2183E+00
46	3.1892E+01	3.2021E+01	3.2327E+01	3.4478E+01	3.1412E+01	3.1412E+01	3.1486E+01	3.3367E+01	3.1408E+01
45	2.8862E+00	2.9475E+00	3.1756E+00	5.1696E+00	2.3407E+00	2.3407E+00	2.4086E+00	4.2027E+00	2.2862E+00
44	1.4802E+00	1.6196E+00	1.9340E+00	3.7825E+00	7.1474E+00	7.1474E+00	7.6516E-01	2.2481E+00	6.9647E-01
43	6.9179E+00	6.9642E+00	7.1401E+00	9.0123E+00	6.2812E+00	6.2812E+00	6.3400E+00	7.9867E+00	6.1618E+00
42	1.6719E+01	1.6918E+01	1.7290E+01	1.9057E+01	1.6112E+01	1.6112E+01	1.6156E+01	1.7519E+01	1.6112E+01
41	3.0812E+00	4.2051E+00	5.7000E+00	8.5766E+00	2.2743E+00	2.2743E+00	2.3196E+00	3.7129E+00	2.2716E+00
40	3.0058E+00	3.6129E+00	4.5256E+00	6.8426E+00	2.4180E+00	2.4180E+00	2.4600E+00	3.7874E+00	2.4171E+00
39	2.8313E+00	3.5491E+00	4.6366E+00	7.1006E+00	2.1932E+00	2.1932E+00	2.2400E+00	3.6665E+00	2.1442E+00
38	3.3376E+00	3.4422E+00	3.6314E+00	5.1227E+00	3.1565E+00	3.1565E+00	3.1976E+00	4.5082E+00	3.1565E+00
37	2.9691E-01	5.1639E-01	8.7555E-01	2.5146E+00	5.9398E-02	5.9399E-02	9.9377E-02	1.3873E+00	5.9317E-02
36	6.6493E+00	6.6745E+00	6.7757E+00	8.1938E+00	5.9423E+00	5.9423E+00	5.9808E+00	7.2385E+00	5.9414E+00
35	5.2463E+00	5.3776E+00	5.6285E+00	7.0416E+00	3.4646E-01	3.4646E-01	3.8212E-01	1.5817E+00	3.4645E-01
34	2.0317E+01	2.0340E+01	2.0443E+01	2.1742E+01	1.8153E+01	1.8153E+01	1.8189E+01	1.9403E+01	1.8102E+01
33	2.7698E+00	2.8220E+00	2.9796E+00	4.2639E+00	7.0742E-03	7.0748E-03	3.8241E-02	1.1422E+00	5.1300E-03
32	1.0175E+02	1.0186E+02	1.0212E+02	1.0363E+02	1.0056E+02	1.0056E+02	1.0059E+02	1.0174E+02	1.0053E+02
31	6.9376E-01	1.2992E+00	2.1045E+00	3.9649E+00	1.7543E-01	1.7543E-01	2.0466E-01	1.2667E+00	1.6332E-01
30	5.4998E+01	5.5020E+01	5.5110E+01	5.6300E+01	5.4360E+01	5.4360E+01	5.4387E+01	5.5418E+01	5.4203E+01
29	9.4946E+00	9.5543E+00	9.7134E+00	1.0872E+01	8.6748E+00	8.6748E+00	8.6972E+00	9.5965E+00	8.6585E+00
28	3.9669E+00	4.0044E+00	4.1142E+00	5.2005E+00	3.3167E+00	3.3167E+00	3.3372E+00	4.1873E+00	3.3162E+00
27	3.2115E+00	3.2146E+00	3.2242E+01	3.3265E+01	3.1923E+01	3.1923E+01	3.1948E+01	3.2905E+01	3.1757E+01
26	6.5837E-01	7.2453E-01	8.3396E-01	1.7562E+00	3.5437E-01	3.5437E-01	3.7375E-01	1.1943E+00	3.5267E-01
25	1.1790E+00	1.2280E+00	1.3358E+00	2.1687E+00	8.0774E-01	8.0774E-01	8.2270E-01	1.5186E+00	8.0146E-01
24	1.4657E+02	1.4665E+02	1.4682E+02	1.4766E+02	1.4604E+02	1.4604E+02	1.4606E+02	1.4665E+02	1.4604E+02
23	7.2130E+00	1.1388E+01	1.6914E+01	2.3111E+01	5.1844E+00	5.1844E+00	5.1937E+00	5.7105E+00	5.1611E+00
22	3.1537E+01	3.2076E+01	3.3317E+01	3.5320E+01	2.9682E+01	2.9682E+01	2.9692E+01	3.0245E+01	2.9194E+01
21	4.0635E+01	4.3919E+01	4.8785E+01	5.4433E+01	3.7624E+01	3.7624E+01	3.7633E+01	3.8127E+01	3.7092E+01
20	1.3083E+00	1.3584E+00	1.4918E+00	1.6497E+00	9.7663E-01	9.7663E-01	9.7663E-01	9.7981E-01	8.5707E-01
19	2.2769E+00	3.1647E+00	4.5386E+00	6.0560E+00	2.0358E-01	2.0358E-01	2.0358E-01	2.0520E-01	1.7638E-01
18	9.5198E-01	1.9952E+00	3.3756E+00	4.8059E+00	2.9509E-02	2.9509E-02	2.9510E-02	3.1016E-02	2.2441E-02
17	5.2130E+01	6.4303E+01	8.6177E+01	1.1227E+02	2.0805E-01	2.0805E-01	2.0806E-01	2.0965E-01	1.6408E-01
16	2.2820E+02	3.7170E+02	6.1486E+02	8.6868E+02	7.2262E+01	7.2262E+01	7.2262E+01	7.2264E+01	7.2180E+01
15	1.2953E+00	1.5826E+00	2.0367E+00	2.5385E+00	5.9021E-02	5.9021E-02	5.9022E-02	6.0473E-02	1.9941E-02
14	4.1620E-01	4.5802E-01	5.1790E-01	5.9141E-01	1.4146E-02	1.4146E-02	1.4147E-02	1.5490E-02	4.3093E-03
13	5.2598E+01	8.0329E+01	1.2759E+02	1.7706E+02	1.3979E+01	1.3979E+01	1.3979E+01	1.3980E+01	1.3978E+01
12	1.7863E+01	2.1251E+01	2.6972E+01	3.3159E+01	1.6722E+00	1.6722E+00	1.6722E+00	1.6734E+00	1.6628E+00
11	1.0895E+00	1.4949E+00	2.0595E+00	2.6909E+00	3.2533E-02	3.2533E-02	3.2534E-02	3.3471E-02	2.0986E-02
10	3.3116E+00	3.8834E+00	4.8297E+00	5.9911E+00	6.0156E-02	6.0156E-02	6.0156E-02	6.1022E-02	3.5435E-02
9	2.7830E-01	2.9782E-01	3.3423E-01	3.8642E-01	2.4949E-02	2.4949E-02	2.4949E-02	2.5742E-02	1.5052E-02
8	3.2798E+00	3.5837E+00	4.1482E+00	4.9433E+00	3.0141E-02	3.0141E-02	3.0141E-02	3.0940E-02	1.1314E-02
7	1.1833E+00	1.6569E+00	2.3442E+00	3.1163E+00	3.8065E-02	3.8065E-02	3.8065E-02	3.8733E-02	2.2429E-02
6	4.5364E+00	5.2792E+00	6.4668E+00	7.9676E+00	1.1272E-01	1.1272E-01	1.1272E-01	1.1334E-01	9.9760E-02
5	1.0631E+00	1.2009E+00	1.4227E+00	1.7125E+00	4.8622E-02	4.8622E-02	4.8622E-02	4.9218E-02	4.3097E-02
4	1.8577E+00	2.0520E+00	2.3122E+00	2.6139E+00	4.5335E-02	4.5335E-02	4.5335E-02	4.5859E-02	4.3329E-02
3	2.3662E+00	3.7314E+00	5.5148E+00	7.3632E+00	1.2645E-02	1.2645E-02	1.2645E-02	1.3166E-02	1.0652E-02
2	2.7259E+00	5.1069E+00	8.2086E+00	1.1394E+01	1.3210E-01	1.3210E-01	1.3210E-01	1.3258E-01	1.2963E-01
1	4.1941E+00	6.1100E+00	8.5934E+00	1.1157E+01	9.4186E-01	9.4186E-01	9.4186E-01	9.4195E-01	9.3581E-01

- Fig. 5.6

Displacements	State	Modes	T=0 K (cm^{-1})	T=100 K (cm^{-1})	T=200 K (cm^{-1})	T=300 K (cm^{-1})
$\underline{\delta} = (0,0)^{\mathrm{t}}$	initial	993 cm^{-1}	0	6.1968E-04	7.8506E-01	8.5589E+00
		65 cm^{-1}	0	4.1997E+01	1.0903E+02	1.7770E+02
	final	997 cm^{-1}	9.1548E+00	2.2745E+01	4.5221E+01	7.5223E+01
		60 cm^{-1}	7.9080E-01	3.8405E+01	9.8445E+01	1.5996E+02
$\underline{\delta} = (1,1)^{\mathrm{t}}$	initial	993 cm^{-1}	0	6.1968E-04	7.8506E-01	8.5589E+00
		65 cm^{-1}	0	4.1997E+01	1.0903E+02	1.7770E+02
	final	997 cm^{-1}	1.9535E+01	3.3125E+01	5.5601E+01	8.5603E+01
		60 cm^{-1}	7.8621E+00	4.5477E+01	1.0552E+02	1.6703E+02

C. Supplementary data for chapter 6

C.1. General remarks

In this appendix we report maximum quantum numbers $v_k^{'\mathrm{max}}$ (final state) and v_k^{max} (initial state) in each harmonic mode k determined via Eq. (6.49) in this thesis, together with the various wavenumber windows for each irreducible representation γ, the number of the evaluated integrals and the mode coupling error ϵ_c (see Figures 6.2 and 6.3). For benzene the irreducible representation and the numbering of the vibrational modes are reported as in the work cited in this thesis [Berger, Fischer and Klessinger, *J. Phys. Chem. A*, **102**, 7157 (1998)].

Maximum mode excitation numbers in each normal mode are given in following form:

$$\langle \underline{v}_{\mathrm{max}}^{(\gamma)'} | \underline{v}_{\mathrm{max}}^{(\gamma)} \rangle$$

$\underline{v}_{\mathrm{max}}^{(\gamma)'}$ and $\underline{v}_{\mathrm{max}}^{(\gamma)}$ are vectors containing the maximum quantum numbers of the various normal modes of each irreducible representation γ for the final and initial electronic states respectively. The vectors are sorted according to the number of vibrational mode (in ascending order), which are given in subsection of each molecule, for each irreducible representation.

The wavenumber windows for each irreducible representation γ are given as $[\tilde{\nu}_{\mathrm{min}}^{(\gamma)}, \tilde{\nu}_{\mathrm{max}}^{(\gamma)}]$ in cm^{-1}. The windows are determined by the maximum mode coupling numbers and maximum mode excitation numbers for each irreducible representation γ as the following relations,

$$-\tilde{\nu}_{\mathrm{min}}^{(\gamma)} = \max_{\underline{s} \in C_{M^{(\gamma)}}^{N^{(\gamma)}}} \left(\sum_{k=s_1}^{s_{M^{(\gamma)}}} v_{\mathrm{max},k}^{(\gamma)} \tilde{\nu}_k \right)$$

and

$$\tilde{\nu}_{\mathrm{max}}^{(\gamma)} = \max_{\underline{s} \in C_{M^{(\gamma)}}^{N^{(\gamma)}}} \left(\sum_{k=s_1}^{s_{M^{(\gamma)}}} v_{\mathrm{max},k}^{(\gamma)'} \tilde{\nu}_k' \right)$$

where $C_{M^{(\gamma)}}^{N^{(\gamma)}}$ is the index set choosing $M^{(\gamma)}$ modes out of $N^{(\gamma)}$ for initial or final state of irreducible representation γ. When $M^{(\gamma)}$ exceeds $N^{(\gamma)}$, we have set $\underline{s}$ to $\underline{v}_{\mathrm{max}}^{(\gamma)}$ or $\underline{v}_{\mathrm{max}}^{(\gamma)'}$ accordingly. In our program hotFCHT, we have set the wavenumbers to the nearest graining point $(-[\tilde{\nu}_{\mathrm{min}}^{(\gamma)}/\Delta\tilde{\nu}] * \Delta\tilde{\nu}$ or $[\tilde{\nu}_{\mathrm{max}}^{(\gamma)}/\Delta\tilde{\nu}] * \Delta\tilde{\nu})$ with graining $\Delta\tilde{\nu} = 1$ cm^{-1}.

The number of integrals that is to be evaluated according to the prescreening conditions are reported for the various irreducible representations and wavenumber windows.

For the calculation of mode coupling error ϵ_c, we set the mode coupling threshold t_c as 10^{-12}, and set the mode excitation threshold $t_m = 0.0$. We report the results only up to $\epsilon_c \simeq 0.005\%$ for the mode coupling error due to the numerical precision and the sensitivity to the selection of CODATA sets for the conversion of units. The increments $F_{\mathrm{FCHT;c}}^{(m^{(\gamma)})}$ (see Eq. (6.45) in this thesis) are computed for each irreducible representation γ and subsequently folded (convoluted) to form the total increments $F_{\mathrm{FCHT;c}}^{(m)}$, from which we obtain $\widetilde{F}_{\mathrm{FCHT;c}}^{(M)}$ and finally (see Eq. (6.45) in this thesis) ϵ_c. We report, additionally, $\widetilde{F}_{\mathrm{FCHT;c}}^{(M)}$ for the symmetry block $_{\mathrm{e2g}}$ of benzene which contains the non-zero first derivative of the electronic transition dipole moment.

C.2. Benzene

- Harmonic vibrational wavenumbers of the initial electronic state in cm^{-1}:

    1. $\mathrm{a}_{1\mathrm{g}}$(from $\tilde{\nu}_1$ to $\tilde{\nu}_2$)
    3398.9256 1033.0985

    2. $\mathrm{a}_{2\mathrm{g}}(\tilde{\nu}_3)$
    1481.7300

    3. $\mathrm{b}_{2\mathrm{g}}$(from $\tilde{\nu}_4$ to $\tilde{\nu}_5$)
    1022.0643 712.6271

    4. $\mathrm{e}_{1\mathrm{g}}$(from $\tilde{\nu}_6$ to $\tilde{\nu}_7$)
    869.5370 869.5370

    5. $\mathrm{e}_{2\mathrm{g}}$(from $\tilde{\nu}_8$ to $\tilde{\nu}_{15}$)
    3369.2220 3369.222 1730.1965 1730.1964 1263.3599
    1263.3599 646.1398 646.1398

    6. $\mathrm{a}_{2\mathrm{u}}(\tilde{\nu}_{16})$
    705.3327

    7. $\mathrm{b}_{1\mathrm{u}}$(from $\tilde{\nu}_{17}$ to $\tilde{\nu}_{18}$)
    3358.8251 1086.1432

    8. $\mathrm{b}_{2\mathrm{u}}$(from $\tilde{\nu}_{19}$ to $\tilde{\nu}_{24}$)
    1611.6583 1611.6583 1104.9068 1104.9068 1332.6123
    1168.7674

    9. $\mathrm{e}_{1\mathrm{u}}$(from $\tilde{\nu}_{25}$ to $\tilde{\nu}_{26}$)
    3387.7258 3387.7258

    10. $\mathrm{e}_{2\mathrm{u}}$(from $\tilde{\nu}_{27}$ to $\tilde{\nu}_{30}$)
    990.7565 990.7565 426.6068 426.6068

- Harmonic vibrational wavenumbers of the final electronic state in cm^{-1}:

    1. $\mathrm{a}_{1\mathrm{g}}$(from $\tilde{\nu}_1'$ to $\tilde{\nu}_2'$)
    3417.7683 963.1593

    2. $\mathrm{a}_{2\mathrm{g}}(\tilde{\nu}_3')$
    1457.6221

    3. $\mathrm{b}_{2\mathrm{g}}$(from $\tilde{\nu}_4'$ to $\tilde{\nu}_5'$)
    693.6713 482.2731

    4. $\mathrm{e}_{1\mathrm{g}}$(from $\tilde{\nu}_6'$ to $\tilde{\nu}_7'$)
    593.2363 593.2363

    5. $\mathrm{e}_{2\mathrm{g}}$(from $\tilde{\nu}_8'$ to $\tilde{\nu}_{15}'$)
    3389.0368 3389.0368 1665.3003 1665.3003 1236.7103
    1236.7103 575.1367 575.1367

    6. $\mathrm{a}_{2\mathrm{u}}(\tilde{\nu}_{16}')$
    522.9955

7. b_{1u}(from $\tilde{\nu}'_{17}$ to $\tilde{\nu}'_{18}$)
3381.1447 1056.0267

8. b_{2u}(from $\tilde{\nu}'_{19}$ to $\tilde{\nu}'_{24}$)
1532.9517 1532.9517 960.6835 960.6835 1854.6937
1253.8107

9. e_{1u}(from $\tilde{\nu}'_{25}$ to $\tilde{\nu}'_{26}$)
3404.0649 3404.0649

10. e_{2u}(from $\tilde{\nu}'_{27}$ to $\tilde{\nu}'_{30}$)
674.4727 674.4727 291.7207 291.7207

C.2.1. Electronic transition dipole moment

- Electronic transition dipole moment (in D):
  $\underline{\mu}_0 = (0.0, 0.0, 0.0)^{\text{t}}$

- First derivatives of electronic transition dipole moment of symmetry group e_{2g} (in $D/(\text{Å} * \sqrt{u})$):
  $\underline{\mu}'_{\nu_8} = (0.00000, 0.30540, 0.00000)^{\text{t}}$
  $\underline{\mu}'_{\nu_9} = (0.30540, 0.00000, 0.00000)^{\text{t}}$
  $\underline{\mu}'_{\nu_{10}} = (0.00000, -0.17945, 0.00000)^{\text{t}}$
  $\underline{\mu}'_{\nu_{11}} = (0.17945, 0.00000, 0.00000)^{\text{t}}$
  $\underline{\mu}'_{\nu_{12}} = (0.00000, -0.11900, 0.00000)^{\text{t}}$
  $\underline{\mu}'_{\nu_{13}} = (0.11900, 0.00000, 0.00000)^{\text{t}}$
  $\underline{\mu}'_{\nu_{14}} = (0.57095, 0.00000, 0.00000)^{\text{t}}$
  $\underline{\mu}'_{\nu_{15}} = (0.00000, -0.57095, 0.00000)^{\text{t}}$

C.2.2. Maximum mode excitation numbers

- a_{1g}

0 K

Tol. set	Max. quantum numbers	$[\tilde{\nu}_{\min}^{(a_{1g})}, \tilde{\nu}_{\max}^{(a_{1g})}]$	# of integrals
I	< 2 10 | 0 0 >	[0.00, 16467.13]	33
II	< 2 9 | 0 0 >	[0.00, 15503.97]	30

300 K

Tol. set	Max. quantum numbers	$[\tilde{\nu}_{\min}^{(a_{1g})}, \tilde{\nu}_{\max}^{(a_{1g})}]$	# of integrals
I	< 2 10 | 0 2 >	[−2066.20, 16467.13]	99
II	< 2 9 | 0 2 >	[−2066.20, 15503.97]	54

500 K

Tol. set	Max. quantum numbers	$[\tilde{\nu}_{\min}^{(a_{1g})}, \tilde{\nu}_{\max}^{(a_{1g})}]$	# of integrals
I	< 2 11 | 1 4 >	[−7531.32, 17430.29]	272
II	< 2 10 | 1 3 >	[−7531.32, 17430.29]	204

- a_{2g}

  0 K

Tol. set	Max. quantum numbers	$[\tilde{\nu}_{\min}^{(a_{2g})}, \tilde{\nu}_{\max}^{(a_{2g})}]$	# of integrals
I	$< 2 \mid 0 >$	$[0.00, 2915.24]$	3
II	$< 0 \mid 0 >$	$[0.00, 0.00]$	1

  300 K

Tol. set	Max. quantum numbers	$[\tilde{\nu}_{\min}^{(a_{2g})}, \tilde{\nu}_{\max}^{(a_{2g})}]$	# of integrals
I	$< 2 \mid 1 >$	$[-1481.73, 2915.24]$	6
II	$< 2 \mid 1 >$	$[-1481.73, 2915.24]$	6

  500 K

Tol. set	Max. quantum numbers	$[\tilde{\nu}_{\min}^{(a_{2g})}, \tilde{\nu}_{\max}^{(a_{2g})}]$	# of integrals
I	$< 3 \mid 3 >$	$[-4445.19, 4372.87]$	16
II	$< 2 \mid 2 >$	$[-4445.19, 4372.87]$	9

- b_{2g}

  0 K

Tol. set	Max. quantum numbers	$[\tilde{\nu}_{\min}^{(b_{2g})}, \tilde{\nu}_{\max}^{(b_{2g})}]$	# of integrals
I	$< 6\,6 \mid 0\,0 >$	$[0.00, 7055.67]$	49
II	$< 6\,6 \mid 0\,0 >$	$[0.00, 7055.67]$	49

  300 K

Tol. set	Max. quantum numbers	$[\tilde{\nu}_{\min}^{(b_{2g})}, \tilde{\nu}_{\max}^{(b_{2g})}]$	# of integrals
I	$< 7\,8 \mid 2\,4 >$	$[-4894.64, 8713.88]$	1080
II	$< 6\,6 \mid 2\,3 >$	$[-4182.01, 7055.67]$	588

  500 K

Tol. set	Max. quantum numbers	$[\tilde{\nu}_{\min}^{(b_{2g})}, \tilde{\nu}_{\max}^{(b_{2g})}]$	# of integrals
I	$< 8\,10 \mid 4\,6 >$	$[-8364.02, 10372.10]$	3465
II	$< 6\,8 \mid 3\,5 >$	$[-8364.02, 10372.10]$	1512

- e_{1g}

  0 K

Tol. set	Max. quantum numbers	$[\tilde{\nu}_{\min}^{(e_{1g})}, \tilde{\nu}_{\max}^{(e_{1g})}]$	# of integrals
I	$< 6\,6 \mid 0\,0 >$	$[0.00, 7118.84]$	49
II	$< 6\,6 \mid 0\,0 >$	$[0.00, 7118.84]$	49

  300 K

Tol. set	Max. quantum numbers	$[\tilde{\nu}_{\min}^{(e_{1g})}, \tilde{\nu}_{\max}^{(e_{1g})}]$	# of integrals
I	$< 7\,7 \mid 3\,3 >$	$[-5217.22, 8305.31]$	1024
II	$< 6\,6 \mid 2\,2 >$	$[-3478.15, 7118.84]$	441

  500 K

Tol. set	Max. quantum numbers	$[\tilde{\nu}_{\min}^{(e_{1g})}, \tilde{\nu}_{\max}^{(e_{1g})}]$	# of integrals
I	$< 9\,9 \mid 5\,5 >$	$[-8695.37, 10678.25]$	3600
II	$< 7\,7 \mid 4\,4 >$	$[-8695.37, 10678.25]$	16

- e_{2g}

0 K

Tol. set	Max. quantum numbers	$[\tilde{\nu}_{\min}^{(\mathrm{e_{2g}})},\tilde{\nu}_{\max}^{(\mathrm{e_{2g}})}]$	# of integrals
I	$< 2\,2\,3\,3\,3\,3\,5\,5\,|\,0\,0\,0\,0\,0\,0\,0\,0 >$	$[0.00, 18552.05]$	2150
II	$< 1\,1\,2\,2\,2\,2\,4\,4\,|\,0\,0\,0\,0\,0\,0\,0\,0 >$	$[0.00, 10108.67]$	732

300 K

Tol. set	Max. quantum numbers	$[\tilde{\nu}_{\min}^{(\mathrm{e_{2g}})},\tilde{\nu}_{\max}^{(\mathrm{e_{2g}})}]$	# of integrals
I	$< 2\,2\,3\,3\,3\,3\,6\,6\,|\,0\,0\,1\,1\,2\,2\,4\,4 >$	$[-13682.95, 30968.21]$	2111504
II	$< 1\,1\,2\,2\,2\,2\,5\,5\,|\,0\,0\,1\,1\,1\,1\,4\,4 >$	$[-9892.87, 16314.96]$	116539

500 K

Tol. set	Max. quantum numbers	$[\tilde{\nu}_{\min}^{(\mathrm{e_{2g}})},\tilde{\nu}_{\max}^{(\mathrm{e_{2g}})}]$	# of integrals
I	$< 2\,2\,3\,3\,4\,4\,9\,9\,|\,1\,1\,2\,2\,3\,3\,8\,8 >$	$[-31577.63, 43794.09]$	468744712
II	$< 1\,1\,3\,3\,3\,3\,8\,8\,|\,1\,1\,2\,2\,3\,3\,7\,7 >$	$[-31577.63, 43794.09]$	47153622

- a_{2u}

  0 K

Tol. set	Max. quantum numbers	$[\tilde{\nu}_{\min}^{(\mathrm{a_{2u}})},\tilde{\nu}_{\max}^{(\mathrm{a_{2u}})}]$	# of integrals
I	$< 6\,|\,0 >$	$[0.00, 3137.97]$	7
II	$< 4\,|\,0 >$	$[0.00, 2091.98]$	5

  300 K

Tol. set	Max. quantum numbers	$[\tilde{\nu}_{\min}^{(\mathrm{a_{2u}})},\tilde{\nu}_{\max}^{(\mathrm{a_{2u}})}]$	# of integrals
I	$< 7\,|\,4 >$	$[-2821.33, 3660.97]$	40
II	$< 5\,|\,3 >$	$[-2116.00, 2614.98]$	24

  500 K

Tol. set	Max. quantum numbers	$[\tilde{\nu}_{\min}^{(\mathrm{a_{2u}})},\tilde{\nu}_{\max}^{(\mathrm{a_{2u}})}]$	# of integrals
I	$< 9\,|\,6 >$	$[-4232.00, 4706.96]$	70
II	$< 7\,|\,5 >$	$[-4232.00, 4706.96]$	48

- b_{1u}

  0 K

Tol. set	Max. quantum numbers	$[\tilde{\nu}_{\min}^{(\mathrm{b_{1u}})},\tilde{\nu}_{\max}^{(\mathrm{b_{1u}})}]$	# of integrals
I	$< 2\,2\,|\,0\,0 >$	$[0.00, 6762.29]$	5
II	$< 0\,2\,|\,0\,0 >$	$[0.00, 2112.05]$	3

  300 K

Tol. set	Max. quantum numbers	$[\tilde{\nu}_{\min}^{(\mathrm{b_{1u}})},\tilde{\nu}_{\max}^{(\mathrm{b_{1u}})}]$	# of integrals
I	$< 2\,3\,|\,0\,2 >$	$[-2172.29, 9930.37]$	24
II	$< 0\,2\,|\,0\,2 >$	$[-2172.29, 2112.05]$	9

  500 K

Tol. set	Max. quantum numbers	$[\tilde{\nu}_{\min}^{(\mathrm{b_{1u}})},\tilde{\nu}_{\max}^{(\mathrm{b_{1u}})}]$	# of integrals
I	$< 2\,4\,|\,1\,4 >$	$[-7703.40, 10986.40]$	54
II	$< 1\,3\,|\,1\,3 >$	$[-7703.40, 10986.40]$	31

- b_{2u}

  0 K

Tol. set	Max. quantum numbers	$[\tilde{\nu}_{\min}^{(b_{2u})},\tilde{\nu}_{\max}^{(b_{2u})}]$	# of integrals
I	$<\,6\,2\,|\,0\,0\,>$	$[0.00,\,13635.78]$	21
II	$<\,6\,1\,|\,0\,0\,>$	$[0.00,\,12381.97]$	14

  300 K

Tol. set	Max. quantum numbers	$[\tilde{\nu}_{\min}^{(b_{2u})},\tilde{\nu}_{\max}^{(b_{2u})}]$	# of integrals
I	$<\,7\,2\,|\,2\,2\,>$	$[-5002.76,\,15490.48]$	160
II	$<\,6\,2\,|\,1\,2\,>$	$[-3670.15,\,13635.78]$	50

  500 K

Tol. set	Max. quantum numbers	$[\tilde{\nu}_{\min}^{(b_{2u})},\tilde{\nu}_{\max}^{(b_{2u})}]$	# of integrals
I	$<\,8\,3\,|\,3\,4\,>$	$[-8672.91,\,18598.98]$	720
II	$<\,6\,3\,|\,3\,3\,>$	$[-8672.91,\,18598.98]$	286

- e_{1u}

  0 K

Tol. set	Max. quantum numbers	$[\tilde{\nu}_{\min}^{(e_{1u})},\tilde{\nu}_{\max}^{(e_{1u})}]$	# of integrals
I	$<\,2\,2\,2\,2\,4\,4\,|\,0\,0\,0\,0\,0\,0\,>$	$[0.00,\,13616.26]$	121
II	$<\,1\,1\,2\,2\,4\,4\,|\,0\,0\,0\,0\,0\,0\,>$	$[0.00,\,7685.47]$	92

  300 K

Tol. set	Max. quantum numbers	$[\tilde{\nu}_{\min}^{(e_{1u})},\tilde{\nu}_{\max}^{(e_{1u})}]$	# of integrals
I	$<\,2\,2\,2\,2\,4\,4\,|\,0\,0\,1\,1\,2\,2\,>$	$[-7642.94,\,21301.73]$	5748
II	$<\,1\,1\,2\,2\,4\,4\,|\,0\,0\,1\,1\,2\,2\,>$	$[-6031.29,\,11089.53]$	1063

  500 K

Tol. set	Max. quantum numbers	$[\tilde{\nu}_{\min}^{(e_{1u})},\tilde{\nu}_{\max}^{(e_{1u})}]$	# of integrals
I	$<\,2\,2\,3\,3\,5\,5\,|\,1\,1\,2\,2\,4\,4\,>$	$[-22061.34,\,32420.80]$	495896
II	$<\,1\,1\,2\,2\,4\,4\,|\,1\,1\,2\,2\,3\,3\,>$	$[-22061.34,\,32420.80]$	11949

- e_{2u}

  0 K

Tol. set	Max. quantum numbers	$[\tilde{\nu}_{\min}^{(e_{2u})},\tilde{\nu}_{\max}^{(e_{2u})}]$	# of integrals
I	$<\,6\,6\,6\,6\,|\,0\,0\,0\,0\,>$	$[0.00,\,9844.00]$	1105
II	$<\,6\,6\,6\,6\,|\,0\,0\,0\,0\,>$	$[0.00,\,8093.67]$	241

  300 K

Tol. set	Max. quantum numbers	$[\tilde{\nu}_{\min}^{(e_{2u})},\tilde{\nu}_{\max}^{(e_{2u})}]$	# of integrals
I	$<\,7\,7\,10\,10\,|\,2\,2\,6\,6\,>$	$[-9082.31,\,15277.03]$	1425984
II	$<\,6\,6\,8\,8\,|\,2\,2\,5\,5\,>$	$[-8229.09,\,12761.20]$	598596

  500 K

Tol. set	Max. quantum numbers	$[\tilde{\nu}_{\min}^{(e_{2u})},\tilde{\nu}_{\max}^{(e_{2u})}]$	# of integrals
I	$<\,8\,8\,15\,15\,|\,4\,4\,11\,11\,>$	$[-17311.40,\,19543.18]$	74649600
II	$<\,7\,7\,12\,12\,|\,4\,4\,9\,9\,>$	$[-17311.40,\,19543.18]$	27040000

C.2.3. Mode coupling error

- Total (Fig. 6.2)

M	$\epsilon_{\mathrm{c}}/\% = (1 - \widetilde{F}_{\mathrm{FCHT;c}}^{(M)})/\%$			
	$T = 0$ K(%)	$T = 300$ K(%)	$T = 500$ K(%)	$T = 1000$ K(%)
0	100.00	100.00	100.00	100.00
1	84.38	91.12	98.16	99.99
2	14.85	50.76	89.14	99.94
3	1.53	35.14	80.54	99.80
4	0.11	13.17	61.63	99.37
5	0.01	6.79	48.72	98.53
6	0.00	1.94	31.18	96.80
7		0.75	21.12	93.99
8		0.17	11.50	89.69
9		0.05	6.65	83.59
10		0.01	3.14	76.21
11			1.56	66.84
12			0.65	57.44
13			0.28	46.71
14			0.10	37.49
15			0.04	28.01
16			0.01	20.89
17			0.00	14.27
18				9.85
19				6.14
20				3.91
21				2.22
22				1.30
23				0.68
24				0.36
25				0.17
26				0.09
27				0.04
28				0.02
29				0.01
30				0.00

- For e_{2g} (Fig. 6.3)

M	$\epsilon_{\mathrm{c}}/\% = (1 - \widetilde{F}_{\mathrm{FCHT;c}}^{(M)})/\%$			
	$T = 0$ K(%)	$T = 300$ K(%)	$T = 500$ K(%)	$T = 1000$ K(%)
0	100.00	100.00	100.00	100.00
1	0.25	12.82	42.30	86.37
2	0.01	5.43	22.05	65.54
3	0.00	0.43	6.49	48.02
4		0.05	1.37	22.16
5		0.00	0.32	14.51
6			0.03	3.86
7			0.01	2.32
8			0.00	0.34
9				0.19
10				0.01
11				0.01
12				0.00

D. Explicit expressions for chapter 7

D.1. General remarks

In this appendix we present explicit expressions for the developments of chapter 7, as for a special case of thermally averaged initial state because the expressions in Ch. 7 are general expressions allowing for individual temperatures for each mode. Herein, only the initial state is thermally excited and all vibrational modes are at a finite temperature T and non-Condon effects are ignored. The N-dimensional space X belongs to the initial state and the N-dimensional space Y does to the final state in this appendix.

D.2. Resonance Raman scattering

- Amplitude
  The first (Condon) term of resonance Raman (rR) amplitude in Eq. (7.14) is given as follows,

$$G_{\mathrm{cF}}^{K_{YY}}(\widetilde{\mathbf{I}}_{\mathrm{cF}}, \mathbf{z}'(\tau); \mathbf{\Lambda}_{YY}; \underline{\widetilde{v}}_{\mathrm{KB}}, \underline{\widetilde{v}}_{\mathrm{BK}}) = G_{\mathrm{cF}}^{K_{YY}}(\mathbf{I}, \mathbf{z}'(\tau); \mathbf{0}; \underline{\widetilde{v}}_{\mathrm{KB}}, \underline{\widetilde{v}}_{\mathrm{BK}}), \tag{D.1}$$

where we do not have thermal excitation ($\mathbf{\Lambda}_{YY} = \mathbf{0}$, an N-dimensional square zero matrix) for single vibronic levels ($\underline{\widetilde{v}}_{\mathrm{KB}}, \underline{\widetilde{v}}_{\mathrm{BK}}$). $\mathbf{z}'(\tau)$ is given in Eq. (4.43). The explicit expression is then given by

$$\begin{aligned} &G_{\mathrm{cF}}^{K_{YY}}(\mathbf{I}, \mathbf{z}'(\tau); \mathbf{0}; \underline{\widetilde{v}}_{\mathrm{KB}}, \underline{\widetilde{v}}_{\mathrm{BK}}) \\ &= \left(\widetilde{\prod}_{\underline{v}_{\mathrm{B}_X}, \underline{v}_{\mathrm{K}_X}}^{-\frac{1}{2}, -\frac{1}{2}}\right)\left(\widetilde{\prod}_{\underline{v}_{\mathrm{B}_X}', \underline{v}_{\mathrm{K}_X}'}^{-\frac{1}{2}, -\frac{1}{2}}\right) G_Y(\mathbf{z}'(\tau)) \mathcal{H}_{\underline{\widetilde{v}}_{\mathrm{KB}}, \underline{\widetilde{v}}_{\mathrm{BK}}}(\widetilde{\mathbf{W}}_{\mathrm{cF}}^{-1}\underline{\widetilde{r}}_{\mathrm{cF}}; \widetilde{\mathbf{W}}_{\mathrm{cF}}^{-1}). \end{aligned} \tag{D.2}$$

Precisely the first part is expressed with determinant and exponential functions

$$\begin{aligned} G_Y(\mathbf{z}'(\tau)) = {}&\det(\mathbf{I} + \mathbf{z}'(\tau)\mathbf{W}_{YY}\mathbf{z}'(\tau))^{-1/2} \det(\mathbf{I} - \mathbf{z}'(\tau)\mathbf{W}_{YY}\mathbf{z}'(\tau))^{-1/2} \\ &\exp(\underline{r}_Y^{\mathrm{t}}\mathbf{z}'(\tau)(\mathbf{I} + \mathbf{z}'(\tau)\mathbf{W}_{YY}\mathbf{z}'(\tau))^{-1}\mathbf{z}'(\tau)\underline{r}_Y), \end{aligned} \tag{D.3}$$

with the Doktorov matrices and vectors in Eq. (2.98),

$$\mathbf{W}_{YY} = \mathbf{I} - 2\mathbf{P}, \quad \underline{r}_Y = \sqrt{2}(\mathbf{I} - \mathbf{P})\underline{\delta}. \tag{D.4}$$

For the multi-variate Hermite polynomial (MHP) part, the parameters are given as follows,

$$\widetilde{\mathbf{W}}_{\mathrm{cF}}(\mathbf{z}'(\tau); \mathbf{0}) = \frac{1}{2}\begin{pmatrix} (\widetilde{\mathbf{W}}_{XX}^+ + \widetilde{\mathbf{W}}_{XX}^-)(\mathbf{z}'(\tau)) & (\widetilde{\mathbf{W}}_{XX}^+ - \widetilde{\mathbf{W}}_{XX}^-)(\mathbf{z}'(\tau)) \\ (\widetilde{\mathbf{W}}_{XX}^+ - \widetilde{\mathbf{W}}_{XX}^-)(\mathbf{z}'(\tau)) & (\widetilde{\mathbf{W}}_{XX}^+ + \widetilde{\mathbf{W}}_{XX}^-)(\mathbf{z}'(\tau)) \end{pmatrix}, \tag{D.5}$$

$$\underline{\widetilde{r}}_{\mathrm{cF}}(\mathbf{z}'(\tau); \mathbf{0}_{YY}) = \begin{pmatrix} \underline{\widetilde{r}}_X^+(\mathbf{z}'(\tau)) \\ \underline{\widetilde{r}}_X^+(\mathbf{z}'(\tau)) \end{pmatrix}, \tag{D.6}$$

with the quantities in Eqs. (2.130) and (2.131) in which

$$\mathbf{W}_{XX} = \mathbf{I} - 2\mathbf{Q}, \quad \mathbf{W}_{XY} = -2\mathbf{R}, \quad \mathbf{W}_{YX} = -2\mathbf{R}^{\mathrm{t}}, \tag{D.7}$$

$$\underline{r}_X = -\sqrt{2}\mathbf{R}\underline{\delta}, \tag{D.8}$$

are used.

- Intensity
  The explicit rR intensity time-correlation function (TCF) expression of Eq. (7.22) in Condon approxi-

mation is given for the thermally averaged initial state, *i.e.*

$$G_{\mathrm{rR}}^{K}(\mathrm{bldiag}(\mathbf{z}(t),\mathbf{z}(t)),\mathbf{z}'(\tau),\mathbf{z}'(\tau');\mathbf{0},\mathrm{bldiag}(\boldsymbol{\lambda},\boldsymbol{\lambda})^{\frac{1}{2}})$$

$$= \frac{1}{\mathrm{Tr}(\exp(-\beta\hat{H}))} G_{Y}(\mathbf{z}'(\tau)) G_{Y}(\mathbf{z}'(\tau))^{*}$$

$$\mathcal{I}_{2N}\Big[\mathbf{I} - \mathrm{bldiag}\Big(\mathbf{z}(t),\mathbf{z}(t),\mathbf{z}(t),\mathbf{z}(t)\Big)\widetilde{\mathbf{W}}_{\mathrm{rR}}\left(\mathbf{z}'(\tau),\mathbf{z}'(\tau');\mathbf{0},\mathrm{bldiag}(\boldsymbol{\lambda},\boldsymbol{\lambda})^{\frac{1}{2}}\right)\mathrm{bldiag}\Big(\mathbf{z}(t),\mathbf{z}(t),\mathbf{z}(t),\mathbf{z}(t)\Big)$$

$$,\tfrac{1}{2}\mathrm{bldiag}\Big(\mathbf{z}(t),\mathbf{z}(t),\mathbf{z}(t),\mathbf{z}(t)\Big)\underline{\tilde{r}}_{\mathrm{rR}}\left(\mathbf{z}'(\tau),\mathbf{z}'(\tau');\mathbf{0},\mathrm{bldiag}(\boldsymbol{\lambda},\boldsymbol{\lambda})^{\frac{1}{2}}\right)\Big], \tag{D.9}$$

where $\mathcal{I}_{2N}$ is the Gaussian integral defined in Eq. (2.122), and $\widetilde{\mathbf{W}}_{\mathrm{rR}}(\mathbf{z}'(\tau),\mathbf{z}'(\tau');\mathbf{0},\mathrm{bldiag}(\boldsymbol{\lambda},\boldsymbol{\lambda})^{\frac{1}{2}})$ and $\underline{\tilde{r}}_{\mathrm{rR}}(\mathbf{z}'(\tau),\mathbf{z}'(\tau');\mathbf{0},\mathrm{bldiag}(\boldsymbol{\lambda},\boldsymbol{\lambda})^{\frac{1}{2}})$ can be found in Eq. (7.17) and Eq. (7.23), respectively.

D.3. Single vibronic level transition

In this section we present the explicit expression for Eq. (7.28) of non-thermally excited final state, *i.e.*

$$G_{\mathrm{SVL}}^{K_{YY}}(\mathbf{z},\mathbf{z}';\mathbf{0};\underline{\tilde{v}}_{X})$$

$$= \left(\widetilde{\prod}_{\underline{\tilde{v}}_{X}}^{-\frac{1}{2}}\right) G_{Y}(\mathbf{z}')\mathcal{H}_{\underline{\tilde{v}}_{X}}\left((2\mathbf{z}\widetilde{\mathbf{W}}_{XX}^{+}\mathbf{z})^{-1}\underline{\tilde{r}}_{X}^{+};(2\mathbf{z}\widetilde{\mathbf{W}}_{XX}^{+}\mathbf{z})^{-1}\right), \tag{D.10}$$

where the quantities $(\widetilde{\mathbf{W}}_{XX}^{+},\underline{\tilde{r}}_{X}^{+})$ defined in Eqs. (2.130) and (2.131) are used with Eqs. (D.7) and (D.8).

D.4. Anharmonic transition

Eq. (7.35) can be evaluated with Eq. (D.2) in Condon approximation, *i.e.*

$$G_{\mathrm{A}}(\mathbf{I},\mathbf{z}';\underline{c_{n}},\underline{c_{m}}';\underline{\tilde{v}}_{\mathrm{KB}},\underline{\tilde{v}}_{\mathrm{BK}})$$

$$= \sum_{\{v_{\mathrm{K}_{X}}\},\{v_{\mathrm{B}_{X}}\},\{v_{\mathrm{K}'_{X}}\},\{v_{\mathrm{B}'_{X}}\}} c'_{v_{\mathrm{K}'_{X}};m} c'^{*}_{v_{\mathrm{B}'_{X}};m} c^{*}_{v_{\mathrm{B}_{X}};n} c_{v_{\mathrm{K}_{X}};n}$$

$$\left(\widetilde{\prod}_{\underline{v_{\mathrm{B}_{X}}},\underline{v_{\mathrm{K}_{X}}}}^{-\frac{1}{2},-\frac{1}{2}}\right)\left(\widetilde{\prod}_{\underline{v_{\mathrm{B}'_{X}}},\underline{v_{\mathrm{K}'_{X}}}}^{-\frac{1}{2},-\frac{1}{2}}\right) G_{Y}(\mathbf{z}')\mathcal{H}_{\underline{\tilde{v}}_{\mathrm{KB}},\underline{\tilde{v}}_{\mathrm{BK}}}(\widetilde{\mathbf{W}}_{\mathrm{cF}}^{-1}\underline{\tilde{r}}_{\mathrm{cF}};\widetilde{\mathbf{W}}_{\mathrm{cF}}^{-1}). \tag{D.11}$$

E. Bibliography

[1] E. B. Wilson, J. C. Decius, and P. C. Cross. *Molecular vibrations*. Dover, New York, 1980.

[2] G. Fischer. *Vibronic Coupling*. Academic Press Inc., London, 1984.

[3] D. P. Craig and T. Thirunamachandran. *Molecular quantum electrodynamics: an introduction to radiation – molecule interactions*. Dover Publications, Inc., New York, 1984.

[4] M. Klessinger and J. Michl. *Excited States and Photochemistry of Organic Molecules*. VCH, New York, 1995.

[5] S. Mukamel. *Principles of Nonlinear Optical Spectroscopy*. Oxford University Press, New York, 1995.

[6] D. A. Long. *The Raman effect*. John Wiley & Sons Ltd, Chichester, 2002.

[7] S. Stenholm. *Foundations of laser spectroscopy*. Dover, New York, 2005.

[8] V. May and O. Kühn. *Charge and energy transfer dynamics in molecular systems*. WILEY-VCH Verlag GmbH & Co. KGaA, Weinheim, 2nd edition, 2003.

[9] J. M. Hollas. *High resolution spectroscopy*. John Wiley & Sons, Ltd, Chichester, 2nd edition, 1998.

[10] W. Demtröder. *Laser spectroscopy*. Springer-Verlag, Berlin Heidelberg New York, 3rd edition, 2003.

[11] J. M. Hollas. *Modern spectroscopy*. John Wiley & Sons, Ltd, Chichester, 4th edition, 2004.

[12] Marc Dierksen and Stefan Grimme. Density functional calculations of the vibronic structure of electronic absorption spectra. *J. Chem. Phys.*, 120(8):3544–3554, 2004.

[13] P. Hohenberg and W. Kohn. Inhomogenous electron gas. *Phys. Rev. B*, 136:864–871, 1964.

[14] W. Kohn and L. J. Sham. Self-consistent equations including exchange and correlation effects. *Phys. Rev.*, 140:1133–1138, 1965.

[15] C. Lee, W. Yang, and R. G. Parr. Development of the Colle-Salvetti correlation-energy formula into a functional of the electron-density. *Phys. Rev. B*, 37:785–789, 1988.

[16] Erich Runge and E. K. U. Gross. Density-functional theory for time-dependent systems. *Phys. Rev. Lett.*, 52(12):997, Mar 1984.

[17] A. B. Myers. 'Time-dependent' resonance Raman theory. *J. Raman Spectros.*, 28:389, 1997.

[18] R. Improta, A. Lami, V. Barone, and F. Santoro. Time-dependent and time-independent approaches for the computation of absorption spectra of uracil derivatives in solution. *Int. J. Quant. Chem.*, 110:624, 2010.

[19] C. W. Müller, J. J. Newby, C.-P. Liu, C. P. Rodrigo, and T. S. Zwier. Duschinsky mixing between four non-totally symmetric normal coordinates in the $S_1 - S_0$ vibronic structure of (*E*)-phenylvinylacetylene: a quantitative analysis. *Phys. Chem. Chem. Phys.*, 12:2331, 2010.

[20] P. Atkins. *Molecular quantum mechanics*. Oxford University Press, Oxford, 4th edition, 2005.

[21] G. Orlandi and W. Siebrand. Theory of vibronic intensity borrowing. Comparison of Herzberg-Teller and Born-Oppenheimer coupling. *J. Chem. Phys.*, 58:4513–4525, 1973.

[22] L.S. Cederbaum and W. Domcke. A many-body approach to the vibratioanl structure in molecular electronic spectra. i. theory. *J. Chem. Phys.*, 64(2):603–611, 1976.

[23] E. J. Heller. Quantum corrections to classical photodissociation models. *J. Chem. Phys.*, 68:2066, 1978.

[24] E. V. Doktorov, I. A. Malkin, and V. I. Man'ko. Dynamical symmetrie of vibronic transitions in polyatomic molecules and the Franck-Condon principle. *J. Mol. Spectrosc.*, 56:1–20, 1975.

[25] E. V. Doktorov, I. A. Malkin, and V. I. Man'ko. Dynamical symmetry of vibronic transitions with degenerate vibrations and the Franck-Condon factors. *J. Phys. B*, 9:507–514, 1976.

[26] E. V. Doktorov, I. A. Malkin, and V. I. Man'ko. Dynamical symmetry of vibronic transitions in poly-atomic molecules and the Franck-Condon principle. *J. Mol. Spectrosc.*, 64:302–326, 1977.

[27] E. V. Doktorov, I. A. Malkin, and V. I. Man'ko. The Franck-Condon principle and sum rules for vibronic transitions in polyatomic molecules. *Chem. Phys. Lett.*, 46(1):183–187, 1977.

[28] E. V. Doktorov, I. A. Malkin, and V. I. Man'ko. The Franck-Condon principle for nuclear gamma transitions in polyatomic molecules. *Sov. Phys. JETP*, 49(4):638–645, 1979.

[29] E. V. Doktorov, I. A. Malkin, and V. I. Man'ko. The dushinsky effect and sum rules for vibronic transi-tions in polyatomic molecules. *J. Mol. Spectrosc.*, 77:178–194, 1979.

[30] N. Heider and S. F. Fischer. Multimode effects in molecular spectra involving vibronic coupled excited states with application to pyrazine. *Chem. Phys.*, 88:209, 1984.

[31] R. Islampour and S. Mukamel. Spectral lineshapes of molecular clusters. *Chem. Phys. Lett.*, 239:107, 1984.

[32] R. Islampour and S. Mukamel. Line broadening in rigid and nonrigid clusters and molecular electronic spectra. The spectral density formalism. *J. Chem. Phys.*, 80:5487, 1984.

[33] S. Mukamel, S. Abe, Y. J. Yan, and R Islampour. Generating function for electronic spectra of polyatomic molecules. *J. Phys. Chem.*, 89:201, 1985.

[34] Y. J. Yan and S. Mukamel. Eigenstate-free, Green function, calculation of molecular absorption and fluorescence line shapes. *J. Chem. Phys.*, 85:5908, 1986.

[35] R. Islampour. Electronic spectral line shape of a polyatomic molecule. *Chem. Phys.*, 133:425, 1989.

[36] R. Berger, C. Fischer, and M. Klessinger. Calculation of the vibronic fine structure in electronic spectra at higher temperatures. 1. benzene and pyrazine. *J. Phys. Chem. A*, 102:7157–7167, 1998.

[37] H. Wadi and E. Pollak. Theory of laser cooling of polyatomic molecules in an electronically excited state. *J. Chem. Phys.*, 110:11890, 1999.

[38] Y. J. Shiu, M. Hayashi, A. M. Mebel, Y.-T. Chen, and S. H. Lin. Computational formulas for symmetry-forbidden vibronic spectra and their application to $n - \pi^*$ transition in neat acetone. *J. Chem. Phys.*, 115:4080, 2001.

[39] J. K. G. Watson. Calculated vibrational intensities in the $\tilde{A} - \tilde{X}$ electronic transition of acetylene. *J. Mol. Spec.*, 207:276, 2001.

[40] Y. He and E. Pollak. Theory of cooling of room temperature benzene upon photo-excitation to the S_1 state. *J. Phys. Chem. A*, 105:10961, 2001.

[41] R. Ianconescu and E. Pollak. Photoinduced cooling of polyatomic molecules in an electronically excited state in the presence of Dushinskii rotations. *J. Phys. Chem. A*, 108, 2004.

[42] S. Banerjee and G. Gangopadhyay. Laser cooling vibrational degrees of freedom of a molecular system. *J. Chem. Phys.*, 123:114304, 2005.

[43] M. Dierksen and S. Grimme. An efficent approach for the calculation of Franck-Condon integrals of large molecules. *J. Chem. Phys.*, 122(24):244101, 2005.

[44] Fabrizio Santoro, Roberto Improta, Alessandro Lami, Julien Bloino, and Vincenzo Barone. Effective method to compute Franck-Condon integrals for optical spectra of large molecules in solution. *J. Chem. Phys.*, 126(8):084509, 2007.

[45] Fabrizio Santoro, Alessandro Lami, Roberto Improta, and Vincenzo Barone. Effective method to com-pute vibrationally resolved optical spectra of large molecules at finite temperature in the gas phase and in solution. *J. Chem. Phys.*, 126, 2007.

[46] H.-C. Jankowiak, J. L. Stuber, and R. Berger. Vibronic transitions in large molecular systems: Rigorous prescreening conditions for Franck-Condon factors. *J. Chem. Phys.*, 127:234101, 2007.

[47] V. Hizhnyakov and I. Tehver. Effects of mode-mixing and non-Condon interaction in the vibronic spectra of multimode systems. *J. Lumin.*, 128:1001, 2008.

[48] J. Tatchen and E. Pollak. Ab initio spectroscopy and photoinduced cooling of the trans-stilbene molecule. *J. Chem. Phys.*, 128:164303, 2008.

[49] F. Santoro, A. Lami, R. Improta, J. Bloino, and V. Barone. Effective method for the computation of optical spectra of large molecules at finite temperature including the Duschinsky and Herzberg-Teller effect: The Q_x band of porphyrin as a case study. *J. Chem. Phys.*, 128:224311, 2008.

[50] M. S. Schuurman and D. R. Yarkony. A mehtod to reduce the size of the vibronic basis employed in the simulation of spectra using the multimode vibronic coupling approximation. *J. Chem. Phys.*, 128:044119, 2008.

[51] V. Barone, J. Bloino, M. Biczysko, and F. Santoro. Fully integrated approach to compute vibrationally resolved optical spectra: from small molecules to macrosystems. *J. Chem. Theory Comput.*, 5:540, 2009.

[52] S. Coriani, T. Kjærgaard, P. Jøgensen, K. Ruud, J. Huh, and R. Berger. An atomic-orbital based Lagrangian approach for calculating geometric gradients of linear response properties. *J. Chem. Theory Comp.*, 6:1028, 2010.

[53] J. Huh, M. neff, G. Rauhut, and R. Berger. Franck-Condon profiles in photodetachment-photoelectron spectra of HS_2^- and DS_2^- based on vibrational configuration interaction wavefunctions. *Mol. Phys.*, 108:409, 2010.

[54] J. Bloino, M. Biczysko, F. Santoro, and V. Barone. General approach to compute vibrationally resolved one-photon electron spectra. *J. Chem. Theory Comput.*, 6:1256, 2010.

[55] S. Mukamel. On the semicalssical calculation of molecular absorption and fluorescence spectra. *J. Chem. Phys.*, 77:173, 1982.

[56] D. J. Tannor, M. Blanco, and E. J. Heller. Simplification of the resonance fluorescence spectrum by detuning from absorption features. *J. Phys. Chem.*, 88:6240, 1984.

[57] K. Gustav and M. Storch. Vibronic spectral behavior of molecules. xiii. theoretical contribution to the vibronic coupling and the Duschinsky effect on the $S_1 \leftarrow S_0$ absorption and the $S_1 \rightarrow S_0$, $S_2 \rightarrow S_1$, and $S_2 \rightarrow S_0$ fluorescence of azulene. *Inter. J. Quantum Chem.*, 38:25–39, 1990.

[58] G. N. Patwari, S. Wategaonkar, and M. D. Prasad. Franck-Condon spectral calculations on trans-hydroquinone. *Chem. Phys. Lett.*, 344:229, 2001.

[59] Q. Peng, Y. Yi, Z. Shuai, and J. Shao. Toward quantitative prediction of molecular fluorescence quantum efficiency: Role of Duschinsky rotation. *J. Am. Chem. Soc.*, 129, 2007.

[60] A. C. Albrecht. On the theory of Raman intensities. *J. Chem. Phys.*, 34:1476, 1961.

[61] S. Y. Lee and E. J. Heller. Time-dependent theory of Raman scattering. *J. Chem. Phys.*, 71:4777, 1979.

[62] S. Hassing and O. S. Mortensen. The role of vibronic coupling and Duschinsky effect in resonance Raman scattering. *J. Mol. Spectros.*, 87:1, 1981.

[63] P. M. Champion and A. C. Albrecht. Resonance Raman scattering: the multimode problem and transform methods. *Ann. Rev. Phys. Chem.*, 33:353, 1982.

[64] D. J. Tannor and E. J. Heller. Polyatomic Raman scattering for general harmonic potentials. *J. Chem. Phys.*, 77:202, 1982.

[65] A. B. Myers, R. A. Nathies, D. J. Tannor, and E. J. Heller. Excited state geometry changes from preresonance Raman intensities: isoprene and hexatriene. *J. Chem. Phys.*, 77:3857, 1982.

[66] E. J. Heller, R. Sundberg, and D. Tannor. Simple aspects of Raman scattering. *J. Phys. Chem.*, 86:1822, 1982.

[67] C. K. Chan and J. B. Page. Temperature effects in the time-correlator theory of resonance Raman scattering. *J. Chem. Phys.*, 79:5234, 1983.

[68] B. R. Stallard, P. M. Champion, P. R. Callis, and A. C. Albrecht. Advances in calculating Raman excitation profiles by means of the transform theory. *J. Chem. Phys.*, 78:712, 1983.

[69] R. A. Harris, R. Mathies, and A. Myers. A simple sum rule in Raman theory. *Chem. Phys. Lett.*, 94:327, 1983.

[70] C. Svendsen, O. S. Mortensen, and R. J. H. Clark. Transform methods in resonance Raman scattering based on Heller theory. *Chem. Phys.*, 187:349, 1994.

[71] C. Svendsen, O. S. Mortensen, and N. E. Henriksen. Calculation of optical absorption and resonance Raman correlators using time-dependent recursion relationships. *Chem. Phys. Lett.*, 260:627, 1996.

[72] R. Islampour, M. Hayashi, and S. H. Lin. On the calculation of resonance Raman spectra. *J. Raman Spectros.*, 28:331, 1997.

[73] R. Islampour, M. Dehestani, and S. H. Lin. Calculation of resonance Raman excitation profiles. *Mol. Phys.*, 98:101, 2000.

[74] J. Neugebauer and B. A. Hess. Resonance Raman spectra of uracil based on Kramers-Kronig relations using time-dependent density functional calculations and multireference perturbation theory. *J. Chem. Phys.*, 120:11564, 2004.

[75] T. Petrenko and F. Neese. Analysis and prediction of absorption band shapes, fluorescence band shapes, resonance Raman intensities, and excitation profiles using the time-dependent theory of electronic spectroscopy. *J. Chem. Phys.*, 127:164319, 2007.

[76] K. Kiewisch, J. Neugebauer, and M. Reiher. Selective calculation of high-intensity vibrations in molecular resonance Raman spectra. *J. Chem. Phys.*, 129:204103, 2008.

[77] A. Lami and F. Santoro. A Fermi golden rule, Liouville-space approach to the study of intramolecular electron transfer rate in solution. *J. Chem. Phys.*, 106:94, 1997.

[78] R. Islampour, R. G. Alden, G. Y. C. Wu, and S. H. Lin. Effect of temperature, energy gap, and distortion of potential surfaces on photoinduced intramolecular electron transfer. *J. Phys. Chem.*, 97:6793, 1993.

[79] J. Tang. Electron-transfer reactions involving non-linear spin-boson interaction. *Chem. Phys.*, 188:143, 1994.

[80] A. Peluso, F. Santoro, and Giuseppe del Re. Vibronic coupling in electronic transitions with significant duschinky effect. *Int. J. Quant. Chem.*, 63:233–244, 1997.

[81] E. Pollak and L. Pilmak. Control of thermal photoinduced electron transfer reactions in the activated and activationless regimes. *J. Chem. Phys.*, 115:1867, 2001.

[82] G. M. Sando, K. G. Spears, J. T. Hupp, and P. T. Ruhoff. Large electron transfer rate effects from the Duschinsky mixing vibrations. *J. Phys. Chem. A*, 105:5317, 2001.

[83] B. Segev. Fermi's golden rule in the Wigner representation. *J. Opt. B: Quantum Semiclass. Opt.*, 5:S381, 2003.

[84] S. Banerjee and G. Gangopadhyay. On the quantum theory of electron transfer: Effect of potential surfaces of the reactants and products. *J. Chem. Phys.*, 126:034102, 2007.

[85] P. O. J. Scherer and M. Tachiya. Computer simulation studies of electron transfer parameters for cyanoanthracene/n,n-dimethylaniline solutions. *J. Chem. Phys.*, 118:4149, 2003.

[86] J. Tang, M. T. Lee, and S. H. Lin. Effects of the Duschinsky mode-mixing mechanism on temperature dependence of electron transfer processes. *J. Chem. Phys.*, 119:7188, 2003.

[87] K. K. Liang, A. M. Mebel, S. H. Lin, M. Hayashi, H. L. Selzle, E. W. Schlag, and M. Tachiya. Influence of distortion and Duschinsky effects on Marcus-type theories of electron transfer rate. *Phys. Chem. Chem. Phys.*, 5:4656, 2003.

[88] P. O. J. Scherer and S. F. Fischer. Quantum chemical analysis of the excited state dynamics of hydrated electrons. *Chem. Phys. Lett.*, 421:427, 2006.

[89] N. Lin, X. Zhao, A. Rizzo, and Y. Luo. Vibronic induced one- and two-photon absorption in a charge-transfer stilbene derivate. *J. Chem. Phys.*, 126:244509, 2007.

[90] S. H. Lin. Rate of interconversion of electronic and vibrational energy. *J. Chem. Phys.*, 44:3759–3767, 1966.

[91] A. M. Mebel, M. Hayashi, K. K. Liang, and S. H. Lin. Ab initio calculations of vibronic spectra and dynamics for small polyatomic molecules: role of Duschinsky effect. *J. Phys. Chem. A*, 103:10674, 1999.

[92] S. Kallush, B. Segev, A. V. Sergeev, and E. J. Heller. Surface jumping: Franck-Condon factors and Condon points in phase space. *J. Phys. Chem. A*, 106:6006, 2002.

[93] R. Islampour and M. Miralinaghi. Dynamics of radiationless transitions: effects of displacement-distortion-rotation of potential energy surfaces on internal conversion decay rate constants. *J. Phys. Chem. A*, 111:9454, 2007.

[94] Q. Peng, Y. Yi, Z. Shuai, and J. Shao. Ecited state radiationless decay process with Duschinsky rotation effect: Formalism and implementation. *J. Chem. Phys.*, 126, 2007.

[95] Q. Peng, Y. Niu, C. Deng, and Z. Shuai. Vibration correlation function formalism of radiative and non-radiative rates for complex molecules. *Chem. Phys.*, 370, 2010.

[96] A. Toniolo and M. Persico. Efficient calculation of Franck-Condon factors and vibronic couplings in polyatomics. *J. Comput. Chem.*, 22:968–975, 2001.

[97] R. J. Glauber. Coherent and incoherent states of the radiation field. *Phys. Rev.*, 131:2766–2788, 1963.

[98] I. A. Malkin, V. I. Man'ko, and D. A. Trifonov. Coherent states and transition probabilities in a time-dependent electromagnetic field. *Phys. Rev. D.*, 2:1371–1385, 1970.

[99] M. Born and R. Oppenheimer. Zur Quantentheorie der Molekeln. *Ann. Phys.*, 84:457–463, 1927.

[100] D. R. Yarkony. Diabolical conical intersections. *Rev. Mod. Phys.*, 68, 1996.

[101] C. Eckart. Some studies concerning rotating axes and polyatomic molecules. *Phys. Rev.*, 47:552–558, 1935.

[102] F. Santoro and V. Barone. Computational approach to the study of the lineshape of absorption and electronic circular dichroism spectra. *Int. J. Quant. Chem.*, 110:476, 2010.

[103] P. A. M. Dirac. The quantum theory of the emission and absorption of radiation. *Proc. Roy. Soc. (London) A*, 114(767):243–265, 1927.

[104] E. Fermi. *Nuclear Physics*. University of Chicago Press., Chicago, 1950.

[105] R. Islampour and S. H. Lin. On the theory of photoinduced intramolecular electron transfer. *J. Phys. Chem.*, 95:10261, 1991.

[106] Valerie Rodriguez-Garcia, K. Yagi, K. Hirao, S. Iwata, and S. Hirata. Franck-Condon factors based on anharmonic vibrational wave functions of polyatomic molecules. *J. Chem. Phys.*, 125(20):014109, 2006.

[107] F. Duschinsky. Zur Deutung der Elektronenspektren mehratomiger Moleküle. *Acta Physicochim. URSS*, 7:551–566, 1937.

[108] G. J. Small. Herzberg-Teller vibronic coupling and the Duschinsky effect. *J. Chem. Phys.*, 54:3300–3306, 1971.

[109] D. L. Tonks and J. B. Page. General theory of vibrational mode mixing and frequency shifts in resonance Raman scattering. *Chem. Phys. Lett.*, 79:247, 1981.

[110] Gerald M. Sando and Kenneth G. Spears. Ab initio computation of the Duschinsky mixing of vibrations and nonlinear effects. *J. Chem. Phys. A*, 105(22):5326–5333, 2001.

[111] C. T. Chang, J. P. Sethna, A. N. Pasupathy, J. Park, D. C. Ralph, and P. L. McEuen. Phonons and conduction in molecular quantum dots: Density functional calculations of Franck-Condon emission rates for bifullerenes in external fields. *Phys. Rev. B*, 76, 2007.

[112] R. Berger and M. Klessinger. Algorithms for exact counting of transition energy levels at different temperatures. *J. Comput. Chem.*, 18:1312–1319, 1997.

[113] G. Herzberg and E. Teller. Schwingungsstruktur der Elektronenübergänge bei mehratomigen Molekülen. *Z. Phys. Chem. B*, 21:410–446, 1933.

[114] T. E. Sharp and H. M. Rosenstock. Franck-Condon factors for polyatomic molecules. *J. Chem. Phys.*, 41:3453–3463, 1964.

[115] P.-Å. Malmqvist and N. Forsberg. Franck-Condon factors for multidimensional harmonic oscillators. *Chem. Phys.*, 228:227–240, 1998.

[116] R. Islampour, M. Dehestani, and S. H. Lin. A new expression for multidimensional Franck-Condon integrals. *J. Mol. Spectrosc.*, 194:179–184, 1999.

[117] J. Liang and H. Li. Calculation of the multimode Franck-Condon factors based on the coherent state method. *Mol. Phys.*, 103(24):3337–3342, 2005.

[118] J. Liang, H. Zheng, X. Zhang, R. Li, and Z. Cui. Exact evaluation of the multidimensional Franck-Condon integrals based on the contour integral method. *Mol. Phys.*, 105:1903, 2007.

[119] R. Borrelli and A. Peluso. Perturbative calculation of Franck-Condon integrals: New hints for a rational implementation. *J. Chem. Phys.*, 129, 2008.

[120] J.-L Chang. A new method to calculate Franck-Condon factors of multidimensional harmonic oscillators including Duschinsky effect. *J. Chem. Phys.*, 128:174111, 2008.

[121] J. Liang, C. Liu, C. Wang, and Z. Cui. An algebraic formula to calculate the three-dimensional Franck-Condon factors including the Duschinsky effect. *Mol. Phys.*, 107:2601, 2009.

[122] D. S. Yang, M. Z. Zgierski, A. Bérces, P. A. Hackett, P. N. Roy, A. Martinez, T. Carrington, D. R. Salahub, R. Fournier, T. Pang, and C. Chen. Vibrational and geometric structures of Nb_3C_2 and $Nb_3C_2^+$ from pulsed field ionization-zero electron kinetic energy photoelectron spectra and density functional calculations. *J. Chem. Phys.*, 105:10663–10671, 1996.

[123] K. M. Ervin, T. M. Ramond, G. E. Davico, R. L. Schwartz, S. M. Casey, and W. C. Lineberger. Naphthyl radical: Negative ion photoelectron spectroscopy, Franck-Condon simulation and thermochemistry. *J. Phys. Chem. A*, 105:10822–10831, 2001.

[124] A. Hazra and M. Nooijen. Derivation and efficent implementation of a recursion formula to calculate harmonic Franck-Condon factors for polyatomic molecules. *Inter. J. Quantum Chem.*, 95:643–657, 2003.

[125] I. A. Malkin, V. I. Man'ko, and D. A. Trifonov. Linear adiabatic invariants and coherent states. *J. Math. Phys.*, 14:576–582, 1973.

[126] R. P. Feynman and A. R. Hibbs. *Quantum mechanics and path integrals*. McGraw-Hill, New York, 1965.

[127] E. J. Heller. Photofragmentation of symmetric triatomic molecules: Time dependent picture. *J. Chem. Phys.*, 68:3891, 1978.

[128] W. W. Parson, Z. T. Chu, and A. Warshel. Reorganization energy of the initial electron-transfer step in photosynthetic bacterial reaction centers. *Biophys. J.*, 74:182, 1998.

[129] J. Huh, H.-C. Jankowiak, J. L. Stuber, and R. Berger. Vibronic transitions in large molecular systems: Prescreening conditions for Franck-Condon factors at finite temperature and the thermal time-correlation function. to be published.

[130] J. Huh, J. L. Stuber, and R. Berger. Vibronic transitions in large molecular systems: The thermal time-correlation function and rigorous prescreening of Herzberg-Teller terms. to be published.

[131] J. Huh, J. L. Stuber, and R. Berger. Vibronic transitions in large molecular systems: Time-independent cumulant expansion for Franck-Condon profiles at finite temperature and at zero kelvin. to be published.

[132] J. Huh and R. Berger. Application of time-independent cumulant expansion to calculation of Franck-Condon profiles for large molecular systems. *Faraday Discuss.*, accepted.

[133] C. S. Withers. A simple expression for the multivariate Hermite polynomials. *Stat. Probab. Lett.*, 47:165–169, 2000.

[134] R. Willink. Normal moments and Hermite polynomials. *Stat. Probab. Lett.*, 271:271, 2005.

[135] R. P. Feynman. *Statistical mechanics: a set of lectures*. Addison-Wesley, Redwood City, 1972.

[136] H. M. Lu and B. Page. General theory of simultaneous mode mixing and non-Condon effects in resonance Raman scattering. *Chem. Phys. Lett.*, 131:87, 1986.

[137] E. J. Heller. Photofragmentation of symmetric triatomic molecules: Time dependent picture. *J. Chem. Phys.*, 68:3891, 1978.

[138] A. Warshel, P. S. Stern, and S. Mukamel. Semiclassical calculation of electronic spectra of supercooled anharmonic molecules. *J. Chem. Phys.*, 78:7498–7500, 1983.

[139] G. Orlandi and W. Siebrand. Mechanisms of vibronic intensity borrowing. *Chem. Phys. Lett.*, 15:465–468, 1972.

[140] H. M. Pickett and H. L. Strauss. Conformational structure, energy, and inversion rates of cyclohexane and som related oxanes. *J. Am. Chem. Soc.*, 92:7281–7290, 1970.

[141] P. R. Bunker. *Molecular Symmetry and Spectroscopy*. NRC Research Press, Ottawa, 2nd edition, 1998.

[142] J. T. Hougen and J. K. G. Watson. Anomalous rotational line intensities in electronic transitions of polyatomic molecules: Axis-switching. *Can. J. Phys.*, 43:298–320, 1965.

[143] J. K. G. Watson. The a'' vibrations of singlet propynal. *Can. J. Chem.*, 71:1556, 1993.

[144] K. N. Kudin and A. Y. Dymarsky. Eckart axis conditions and the minimization of the root-mean-square deviation: Two closely related problems. *J. Chem. Phys.*, 122:224105, 2005.

[145] A. Y. Dymarsky and K. N. Kudin. Computation of the pseudorotation matrix to satisfy the Eckart axis conditions. *J. Chem. Phys.*, 122:124103, 2005.

[146] İ. Özkan. Franck-Condon principle for polyatomic molecules: axis-switching effects and transformation of normal coordinates. *J. Mol. Spectrosc.*, 139:147, 1990.

[147] A. Warshel and M. Karplus. Vibrational structure of electronic transitions in conjugated molecules. *Chem. Phys. Lett.*, 17:7–14, 1972.

[148] N. J. D. Lucas. The Franck-Condon principal for polyatomic molecules. *J. Phys. B*, 6:155–163, 1973.

[149] D. W. Kohn, E. S. J. Robles, C. F. Logan, and P. Chen. Photoelectron spectrum , ionization potential, and heat of formation of CCl_2. *J. Phys. Chem.*, 97(19):4936–4940, 1993.

[150] D. Luckhaus. Large curvature tunnelling on the reaction path. *Phys. Chem. Chem. Phys.*, 10:6215, 2008.

[151] H. Fan. Operator ordering in quantum optics theory and the development of Dirac's symbolic method. *J. Opt. B: Quantum Semiclass. Opt.*, 5:R147, 2003.

[152] E. J. Heller. Time-dependent approach to semiclassical dynamics. *J. Chem. Phys.*, 62:1544, 1975.

[153] S. Sivakumar. Studies on nonlinear coherent states. *J. Opt. B: Quantum Semiclass. Opt.*, 2:R61, 2000.

[154] J. Zinn-Justin. *Path integrals in quantum mechanics*. Oxford University Press, USA, illustrated edition, 2005.

[155] P. Chen. Photoelectron spectroscopy of reactive intermediates. In C. Y. Ng, T. Bear, and I. Powis, editors, *Unimolecular and Bimolecular Reaction Dynamics*. John Willey & Sons Ttd., 1994.

[156] R. Botter, V. H. Dibeler, J. A. Walker, and H. M. Rosenstock. Experimental and theoretical studies of photoionization-efficiency curves for C_2H_2 and C_2D_2. *J. Chem. Phys.*, 44:1271–1278, 1966.

[157] V. I. Baranov, L. A. Gribov, and B. K. Novosadov. Calculation of vibronic spectra of ployatomic molecules in the Franck-Condon and Herzberg-Teller approximations. *J. Mol. Struct.*, 70:1–29, 1981.

[158] J. Weber and G. Hohlneicher. Franck-Condon factors for polyatomic molecules. *Mol. Phys.*, 101(13):2125–2144, 2003.

[159] J. Liang and H. Li. Franck-Condon simulation of the photoelectron spectrum of SO_2^- including Duschinsky effects. *Chem. Phys.*, 314:317–322, 2005.

[160] M. Lee and M. S. Kim. Mass-analyzed threshold ionization study of vinyl choride cation in the first excited elctronic state using vacuum ultraviolet radiation in the 107-102.8 nm range. *J. Phys. Chem. A*, 110:9377–9382, 2006.

[161] H. Kupka and P. H. Cribb. Multidimensional Franck-Condon integrals and Duschinsky mixing effects. *J. Chem. Phys.*, 85:1303–1315, 1986.

[162] R. Borrelli and A. Peluso. Dynamics of radiationless transitions in large molecualr systems: A Franck-Condon-based method accountimg for displacements and rotations of all the normal coordinates. *J. Chem. Phys.*, 119:8437–8448, 2003.

[163] R. Borrelli and A. Peluso. The vibrational progression of the $n \rightarrow v$ elctronic transition of ethylene: A test case for the computation of Franck-Condon factors of highly flexible photoexcited molecules. *J. Chem. Phys.*, 125:194308, 2006.

[164] P. M. Johnson, Haifeng Xu, and T. J. Sears. The calculation of vibrational intensities in forbidden electronic transitions. *J. Chem. Phys.*, 125:164330, 2006.

[165] H. Xu, P. M. Johnson, and T. J. Sears. Photoinduced rydberg ionization spectroscopy of the $\tilde{B}$ state of benzonitrile cation. *J. Chem. Phys.*, 125:164331, 2006.

[166] M. Yamaguchi, T. Momose, and T. Shida. Vibrational analysis and calculation of Franck-Condon factors for the vinoxy radical $\tilde{X}(^2a'')$ and $\tilde{B}(^2a'')$ states. *J. Chem. Phys.*, 93:4211–4222, 1990.

[167] D. Gruner and P. Brumer. Efficient evaluation of harmonic polyatomic Franck-Condon factors. *Chem. Phys. Lett.*, 138:310–314, 1987.

[168] P. T. Ruhoff and M. A. Ratner. Algorithm for computing Franck-Condon overlap integrals. *Inter. J. Quantum Chem.*, 77:383–392, 2000.

[169] H. Hwang and P. J. Rossky. Harmonic model description of the Franck-Condon density for a betaine dye molecule. *J. Phys. Chem. A*, 108:2607–2616, 2004.

[170] S. Schumm, M. Gerhards, and K. Kleinermanns. Franck-Condon simulation of the $S_1 \rightarrow S_0$ spectrum of phenol. *J. Phys. Chem. A*, 104:10648–10655, 2000.

[171] D. Spangenberg, P. Imhof, and K. Kleinermanns. The S_1 state geometry of phenol determined by simultaneous Franck-Condon and rotational fits. *Phys. Chem. Chem. Phys.*, 5:2505–2514, 2003.

[172] P. Imhof, D. Krügler, R. Brause, and K. Kleinermans. Geometry change of simple aromatics upon electronic excitation obtained from Franck-Condon fits of dispersed fluorescence spectra. *J. Chem. Phys.*, 121(6):2598–2610, 2004.

[173] O. Castaños, R. López-Peña, and R. Lemus. A new approach to obtain the non-Condon factors in closed form for two one-dimensional harmonic oscillators. *J. Mol. Spec.*, 241:51, 2007.

[174] P. Bałuk, A. Kawski, M. Kalas, and Ch. Jung. Zur Schwingungsfeinstruktur der Shpolskii-Spektren von Naphthalin in n-Pentan bei 77 K (Fluoreszenz, $S_0 \rightarrow S_1$- und $S_0 \rightarrow S_2$-absorption). *Z. Naturforsch.*, 36a:705–712, 1981.

[175] F. Metz. Theory of intramolecular radiationless transitions i. discussion of Franck-Condon factors of large polyatomic molecules over the whole energy region. *Chem. Phys.*, 18, 1976.

[176] R. Kan. From moments of sum to moments of product. *J. Multivar. Anal.*, 99:542–554, 2008.

[177] K. S. Miller. Derivatives of noninteger order. *Math. Magaz.*, 68:183, 1995.

[178] Matteo Frigo and Steven G. Johnson. The design and implementation of FFTW3. *Proceedings of the IEEE*, 93(2):216–231, 2005. Special issue on "Program Generation, Optimization, and Platform Adaptation".

[179] S. Leach, M. Schwell, D. Talbi, G. Berthier, K. Hottmann, H.-W. Jochims, and H. Baumgärtel. He i photoelectron spectroscopy of four isototologues of formicacid: HCOOH, HCOOD, DCOOH and DCOOD. *Chem. Phys.*, 286:15–43, 2003.

[180] E. Rudberg and T. Brinck. Computation of Franck-Condon factors for many-atom systems: simulated photoelectron spectra of formic acid isotopologues. *Chem. Phys.*, 302:217–228, 2004.

[181] J. Ferguson, L. W. Reeves, and W. G. Schneider. Vapor absorption spectra and oscillator strengths of naphthalene, anthracene, and pyrene. *Can. J. Chem.*, 35:1117, 1957.

[182] W. Hongwei. *FFT Basics and Case Study using Multi-Instrument*. Virtins Technology, www.virtins.com, rev01 edition, 2009.

[183] L. S. Cederbaum and W. Domcke. Theoretical aspects of ionization potentials and photoelectron spectroscopy:a Green's function approach. *Adv. Chem. Phys.*, 36:205–344, 1977.

[184] K. Kladko and P. Fulde. On the properties of cumulant expansions. *Int. J. Quant. Chem.*, 66:377, 1998.

[185] K. B. Petersen and M. S. Pedersen. *The Matrix Cookbook*. Technical University of Denmark, 2008.

[186] M. N. Berberan-santos. Expressing a probability density function in terms of another PDF: A generalized Gram-Charlier expansion. *J. Math. Chem.*, 42:585, 2006.

[187] S. Blinnikov and R. Moessner. Expansions for nearly Gaussian distributions. *Astron. Astrophys. Suppl. Ser.*, 130:193, 1998.

[188] M. Hardy. Combinatorics of partial derivatives. *Electro. J. Combinat.*, 13:R1, 2006.

[189] R. A. Marcus. On the theory of oxidation-reduction reactions involving electron transfer. i. *J. Chem. Phys.*, 24, 1956.

[190] TURBOMOLE V5.7 2004, a development of University of Karlsruhe and Forschungszentrum Karlsruhe GmbH, 1989-2007, TURBOMOLE GmbH, since 2007; available from http://www.turbomole.com.

[191] K. F. Freed. Influence of frequency shifts on electron transfer processes. *J. Phys. Chem. B*, 107:10341, 2003.

[192] S. Jang and M. D. Newton. Closed-form expressions of quantum electron transfer rate based on the stationary-phase approximation. *J. Phys. Chem. B*, 110:18996, 2006.

[193] K. Umesaki and H. Kikuchi. A line-shape function in terms of changes in both molecular structure and force constants: A Gaussian approximation. *J. Chem. Phys.*, 124:074304, 2006.

[194] J. H. Callomon, T. M. Dunn, and I. M. Mills. Rotational analysis of the 2600 Å absorption system of benzene. *Trans. R. Soc. London*, 259:499–532, 1966.

[195] S. Coriani, S. Høst, B. Jansík, L. Thøgersen, J. Olsen, P. Jørgensen, S. Reine, F. Pawłowski, T. Helgaker, and P. Sałek. Linear-scaling implementation of molecular response theory in self-consistent field electronic-structure theory. *J. Chem. Phys.*, 126, 2007.

[196] C. Angeli, K. L. Bak, V. Bakken, O. Christiansen, R. Cimiraglia, S. Coriani, P. Dahle, E. K. Dalskov, T. Enevoldsen, B. Fernandez, C. Hättig, K. Hald, A. Halkier, H. Heiberg, T. Helgaker, H. Hettema, H. J. Å. Jensen, D. Jonsson, P. Jørgensen, S. Kirpekar, W. Klopper, R. Kobayashi, H. Koch, A. Ligabue, O. B. Lutnaes, K. V. Mikkelsen, P. Norman, J. Olsen, M. J. Packer, T. B. Pedersen, Z. Rinkevicius, E. Rudberg, T. A. Ruden, K. Ruud, P. Salek, A. Sanchez de Meras, T. Saue, S. P. A. Sauer, B. Schimmelpfennig, K. O. Sylvester-Hvid, P. R. Taylor, O. Vahtras, D. J. Wilson, and H. Ågren. Dalton, a molecular electronic structure program, release 2.0, 2005.

[197] P. Sałek, S. Høst, L. Thøgersen, P. Jørgensen, P. Manninen, J. Olsen, B. Jansík, S. Reine, F. Pawłowski, E. Tellgren, T. Helgaker, and S. Coriani. Linear-scaling implementation of molecular electronic self-consistent field theory. *J. Chem. Phys.*, 126, 2007.

[198] D. P. Craig and G. J. Small. Totally symmetric vibronic perturbations and the phenanthrene 3400-Å spectrum. *J. Chem. Phys.*, 50, 1969.

[199] K. P. Geigle, J. Wolf, and G. Hohlneicher. Franck-Condon/Herzberg-Teller interferences in the ^1L_b transitions of pyrene and chrysene. *J. Photochem. Photobiol. A*, 105, 1997.

[200] T. A. Stephenson, P. L. Radloff, and S. A. Rice. $^1B_{2u} \leftrightarrow {}^1A_{1g}$ spectroscopy of jet-cooled benzene: Single vibronic level fluorescence studies. *J. Chem. Phys.*, 81:1060–1072, 1984.

[201] James K. G. Watson. Simplification of the molecular vibration-rotation Hamiltonian. *Mol. Phys.*, 15(5):479–490, 1968.

[202] R. Meyer and Hs. H. Günthard. General internal motion of molecules, classical and quantum-mechanical Hamiltonian. *J. Chem. Phys.*, 49, 1968.

[203] M. J. Davis and E. J. Heller. Semiclassical Gaussian basis set method for molecular vibrational wave functions. *J. Chem. Phys.*, 71:3383, 1979.

[204] G. A. Worth, H.-D. Meyer, and L. S. Cederbaum. Relaxation of a system with a conical intersection coupled to a bath: A benchmark 24-dimensional wave packet study treating the environment explicitly. *J. Chem. Phys.*, 109(9):3518–3529, 1998.

[205] A. Raab, G. A. Worth, H.-D. Meyer, and L. S. Cederbaum. Molecular dynamics of pyrazine after excitation to the S_2 electronic state using a realistic 24-mode model Hamiltonian. *J. Chem. Phys.*, 110(2):936–946, 1999.

[206] D. V. Shalashilin and M. S. Child. Real time quantum propagation on a monte carlo trajectory guided grids of coupled coherent states: 26D simulation of pyrazine absorption spectrum. *J. Chem. Phys.*, 121:3563, 2004.

[207] Elmer Hutchisson. Band spectrum intensities for symmetrical molecules. *Phys. Rev.*, 36:410–420, 1930.

[208] Elmer Hutchisson. Band spectrum intensities for symmetrical molecules. ii. *Phys. Rev.*, 37:45–50, 1931.

[209] M. Storch and K. Gustav. Comparative-study of the properties of approximated anharmonic vibration functions and their suitability in the treatment of radiative and non-radiative processes. *Z. Phys. Chem. L*, 270(5):1041–1046, 1989.

[210] F.-T. Chau, J. M. Dyke, E. P. F Lee, and D. C. Wang. Franck-Condon analysis of photoelectron and electronic spectra of small molecules. *J. Electron Spectrosc. Relat. Phenom.*, 97:33–47, 1998.

[211] Wolfgang Eisfeld. Calculation of the vibrationally resolved electronic absorption spectrum of the propargyl radical (H_2CCCH). *J. Phys. Chem. A*, 110(11):3903–3910, 2006.

[212] W. Domcke, L.S. Cederbaum, H. Köppel, and W. von Niessen. A comparison of different approaches to the calculation of Franck-Condon factors for polyatomic molecules. *Mol. Phys.*, 34(6):1759–1770, 1977.

[213] Anirban Hazra, Hannah H. Chang, and Marcel Nooijen. First principles simulations of the UV absorption spectrum of ethylene using the vertical Franck-Condon approach. *J. Chem. Phys.*, 121(5):2125–2136, 2004.

[214] A. Hazra and M. Nooijen. Comparison of Franck-Condon and vibronic coupling approaches for simulating electronic spectra: The case of the lowest band of tethylene. *Phys. Chem. Chem. Phys.*, 7:1759–1771, 2005.

[215] J. M. Bowman. Selfconsistent field energies and wavefunctions for coupled oscillators. *J. Chem. Phys.*, 68, 1978.

[216] J.M. Bowman. The self-consistent-field approach to polyatomic vibrations. *Acc. Chem. Res*, 19:202–208, 1986.

[217] K. M. Christoffel and J. M. Bowman. Investigations of self-consistent field, scf ci and virtual state-configuration interaction vibrational energies for a model three-mode system. *Chem. Phys. Lett.*, 85, 1982.

[218] J. M. Bowman, X. Huang, L. B. Harding, and S. Carter. The determination of molecular properties from multimode with an application to the calculation of Franck-Condon factors for photoionization of CF_3 to CF_3^+. *Mol. Phys.*, 104(1):33–45, 2006.

[219] I. Hamilton and J. Light. On distributed Gaussian bases for simple model multidimensional vibrational problems. *J. Chem. Phys.*, 84:306, 1986.

[220] J. M. Luis, D. M. Bishop, and B. Kirtman. A different approach for calculating Franck-Condon factors including anharmonicity. *J. Chem. Phys.*, 120:813–822, 2004.

[221] J. M. Luis, B. Kirtman, and O. Christiansen. A variational approach for calculating Franck-Condon factors including mode-mode anharmonic coupling. *J. Chem. Phys.*, 125:154114, 2006.

[222] J. M. Luis, M. Torrent-Sucarrat, M. Sol'a, D. M. Bishop, and B. Kirtman. Calculation of Franck-Condon factors including anharmonicity: Simulation of the $C_2H_4^+ \tilde{X}^2 b_{3u} \rightarrow C_2H_4 \tilde{X}^1 a_g$ band in the photoelectron spectrum of ethylene. *J. Chem. Phys.*, 122:184104, 2005.

[223] S. Bonness, B. Kirtman, M. Huix, A. J. Sanchez, and J. M. Luis. Simulation of photoelectron spectra fully included: Application to the $\tilde{X}^2 A_2 \leftarrow \tilde{X}^1 A_1$ band of furan. *J. Chem. Phys.*, 125:014311, 2006.

[224] D. Schuch. On the complex relations between equations describing the dynamics of wave and particle aspects. *Int. J. Quant. Chem.*, 42:663, 1992.

[225] D. Schuch. Effective description of the dissipative interaction between simple model-systems and their environment. *Int. J. Quant. Chem.*, 72:537, 1998.

[226] D. Schuch. On the relation between the Wigner function and an exact dynamical invariant. *Phys. Lett.*, 338:225, 2005.

[227] D. Schuch and M. Moshinsky. Connection between quantum-mechanical and classical time evolution via a dynamical invariant. *Phys. Rev. A*, 73:062111, 2006.

[228] D. Schuch. Connection between quantum mechanical and classical time evolution of dissipative systems via a dynamical invariant. *J. Math. Phys.*, 48:122701, 2007.

[229] D. Schuch. Riccati and Ermakov equations in time-dependent and time-independent quantum systems. *SIGMA*, 4:043, 2008.

[230] G. Lachs. Theoretical aspects of mixtures of thermal and coherent radiation. *Phys. Rev.*, 138:B1012, 1965.

[231] J. Roithová, D. Schröder, J. Loos, H. Schwarz, H.-C. Jankowiak, R. Berger, R. Thissen, and O. Dutuit. Revision of the second ionization energy of toluene. *J. Chem. Phys.*, 122:094306, 2005.

[232] J. S. Seldenthuis, H. S. J. van der Zant, M. A. Ratner, and J. M. Thijssen. Vibrational excitations in weakly coupled single-molecule junctions: A computational analysis. *ACS NANO*, 2:1445, 2008.

[233] S. F. Fischer. A mixed adiabaticdiabatic representation for the vibronic coupling problem of polyatomic molecules. *Chem. Phys. Lett.*, 91:367, 1982.

[234] J. R. Lombardi, R. L. Birke, T. Lu, and J. Xu. Charge-transfer theory of surface enhanced Raman spectroscopy: Herzberg-Teller contributions. *J. Chem. Phys.*, 84:4174, 1986.

[235] J. R. Lombardi and R. L. Birke. Time-dependent picture of the charge-transfer contributions to surface enhanced Raman spectroscopy. *J. Chem. Phys.*, 126:244709, 2007.

[236] J. R. Lombardi and R. L. Birke. A unified approach to surface-enhanced Raman scattering. *J. Phys. Chem. C*, 112:5605–5617, 2008.

[237] J. R. Lombardi and R. L. Birke. A unified view of surface-enhanced Raman scattering. *Acc. Chem. Res.*, 42:734–742, 2009.

[238] L. Jensen, J. Autschbach, M. Krykunov, and G. C. Schatz. Resonance vibrational Raman optical activity: A time-dependent density functional theory approach. *J. Chem. Phys.*, 127:134101, 2007.

[239] R. I. G. Hughes. Theoretical practice: the bohm-pines quartet. *Perspectives on Science*, 14, 2006.

F. Acknowledgements

G. Curriculum Vitae

Joonsuk Huh

Born in Seoul, Korea on 19.10.1978
Nationality: the Republic of Korea

Education

[03/1997-12/1999] Undergraduate Student, Department of Chemistry,
Pohang University of Science and Technology (POSTECH), Korea

[06/2000-08/2002] Army

[08/2002-08/2003] Undergraduate student, Department of Chemistry, POSTECH, Korea,
thesis title: *Theoretical study of the structure and thermodynamic quantities of the water dimmer*
(B. Sc. in chemistry and minor in physics with *Cum Laude*, supervisor: Prof. Dr. KwangSoo Kim)

[10/2004-09/2006] Master student, Computational Science and Engineering (CSE),
Technischen Universität München (TUM), Germany,
thesis title: *Vibronic coupling in the reaction center of bacterial photosynthesis*
(M. Sc. in computational science with *Passed with Merit*,
supervisors: Prof. Dr. Sighart F. Fischer and Prof. Dr. Philipp O. J. Scherer)

[01/2007-02/2011] Graduate student (supervisor: Prof. Dr. Robert Berger),
Frankfurt Institute for Advanced Studies (FIAS),
Johann Wolfgang Goethe-Universität, Frankfurt am Main, Germany

Scholarship

[08/2004-08/2006] Korea Science and Engineering Foundation (KOSEF)
[01/2007-12/2010] Frankfurt International Graduate School for Science (FIGSS)